AD290094

PROCEEDINGS

of

THE EIGHTH SAGAMORE ORDNANCE MATERIALS RESEARCH CONFERENCE

MECHANISMS OPERATING IN METALS AT ELEVATED TEMPERATURES

Conducted at
Sagamore Conference Center
Racquette Lake, New York
August 22, 23, 24, and 25, 1961

Contract No. DA-30-069-ORD-3298

Sponsored by
THE ORDNANCE MATERIALS RESEARCH OFFICE
of the
U. S. ARMY

Arrangements by
SYRACUSE UNIVERSITY RESEARCH INSTITUTE

TABLE OF CONTENTS

UF524.2 S3 St1961

PREFACE

The papers assembled in this report were presented at the Eighth Sagamore Ordnance Materials Research Conference held at Syracuse University's Sagamore Conference Center near Racquette Lake, New York from August 22nd to the 25th, 1961. Syracuse University's Department of Chemical Engineering and Metallurgy made the arrangements for conducting this conference with the assistance of the Adirondack Conference Center staff, under Contract No. DA-30-069-ORD-3298. The conference was sponsored by the Ordnance Materials Research Office, Watertown, Mass. The general planning and operations were transacted through a conference committee composed of representatives of the Army and Syracuse University with N. L. Reed of the Ordnance Materials Research Office as chairman.

This conference, which was the eighth of a series devoted to various aspects of materials research of interest to the U. S. Army Ordnance Corps, was intended to provide Government and associated Non-Government groups with information on the present status of research on the subject of mechanisms operating in metals at elevated temperatures, principally to investigate and evaluate the physical metallurgical factors involved. The scope of this conference included the structural aspects of metals, the role of imperfections in diffusion and mechanical properties, phase transformation, and solid-gas reactions. The lectures and discussions defined, more explicitly, the role played by the factors evaluated and indicated areas where information is lacking or inconclusive. Out of this, it is hoped that future research programs may be developed which will result in more complete knowledge in this extremely important field of metallurgy.

A total of 70 persons associated with research in the area of the conference subject attended and contributed from their knowledge and experiences with talks, comments, and discussions. This group was made up primarily of representatives from government agencies, universities, and industrial research organizations.

The Committee is greatly indebted to those who contributed to the success of this conference, especially to the speakers including the dinner speaker, Dr. Bruce Inverarity, Director of the Adirondack Museum at Blue Mountain Lake, New York, whose talk on Adirondack Lore is not included in these proceedings.

The attendees were welcomed by N. L. Reed, Chairman of the Conference and Assistant Director of the Ordnance Materials Research Office and by Dr. R. A. Galbraith, Dean of Engineering at Syracuse University.

by the Conference Committee

N. L. REED	Chairman Ordnance Materials Research Office
J. J. BURKE	Secretary Ordnance Materials Research Office
J. L. MARTIN	Ordnance Materials Research Office
A. F. JONES	Ordnance Materials Research Office
P. R. KOSTING	Army Research Office - Durham
C. R. CORNTHWAITE	Office, Chief of Ordnance
V. WEISS	Syracuse University Research Institute
J. V. LATORRE	Syracuse University Research Institute

TECHNICAL PROGRAM

Tuesday, August 22, 1961

7:15 P.M.

SESSION I

"THE STRUCTURAL ASPECTS OF METALS"

Moderator:
Mr. John Burke, Ordnance Materials Research Office, Watertown, Mass.

Speaker:
Dr. Volker Weiss, Syracuse University Research Institute, Syracuse, New York

Wednesday, August 23, 1961

9:00 A.M.

SESSION II

"THE ROLE OF IMPERFECTIONS IN DIFFUSION"

Moderator:
Dr. W. B. Robertson, Yale University, New Haven, Connecticut

Speaker:
Dr. C. E. Birchenall, University of Delaware, Newark, Delaware

Prepared Discussion:
"DISLOCATIONS AND DIFFUSION IN SILICON", Dr. H. J. Queisser, Shockley Transistor, Palo Alto, California

Wednesday, August 23, 1961

7:00 P.M.

SESSION III

"RECRYSTALLIZATION AND PHASE TRANSFORMATION"

Moderator:
Dr. E. P. Abrahamson, II, Watertown Arsenal Laboratories, Watertown, Massachusetts

Speaker:
Dr. John Newkirk, Cornell University, Ithica, New York

Prepared Discussion:
"THE ROLE OF ELECTRON CONFIGURATION ON RECRYSTALLIZATION", Dr. E. P. Abrahamson, II

Thursday, August 24, 1961

9:00 A.M.

SESSION IV

"SOLID-GAS REACTIONS"

Moderator:
Dr. James Bechtold, Westinghouse Research Laboratory, Pittsburgh 35, Pennsylvania

Speaker:
Dr. E. A. Gulbransen, Westinghouse Research Laboratories, Monroeville, Pennsylvania

Thursday, August 24, 1961

3:30 P.M.

SESSION V

"GRAIN BOUNDARY BEHAVIOR IN HIGH TEMPERATURE DEFORMATION AND FRACTURE"

Moderator:
Dr. Klaus Zwilsky, New England Materials Laboratory, Medford, Massachusetts

Speaker:
Dr. N. J. Grant, Massachusetts Institute of Technology, Cambridge, Massachusetts

Friday, August 25, 1961

8:30 A.M.

SESSION VI

"PANEL DISCUSSION"

Chairman:
Mr. N. L. Reed, Ordnance Materials Research Office, Watertown Arsenal, Watertown, Massachusetts

THE STRUCTURAL ASPECTS OF METALS

by

Dr. Volker Weiss

and

Mr. G. T. Schaeffer

ABSTRACT

This introductory lecture represents an up-to-date review of the structural aspects of metals with special reference to the behavior of metals at elevated temperatures. The properties of metals at elevated temperature may also, according to Smekal, be classified as structure sensitive and structure insensitive properties. Among the latter are the thermal expansion, the electrical and thermal conductivity, the compressibility and the specific heat. Here relatively simple assumptions concerning the makeup of a solid lead to good agreement between theory and experiment. Examples are the relationships of Wiedemann and Franz, Dulong and Petit, and the Grueneisen Rules. No such simple relationships have not been found for structure sensitive properties such as most mechanical properties of solids. As these properties are often strongly affected by not "visible" growth defects of crystals or not spectroscopically determinable impurities one cannot expect to predict them. Defect theory is therefore primarily concernred with an analysis in retrospect, i.e. with the deduction of the types and arrangements of structural defects from the experimental evidence.

After a brief review of the ideal crystal structure and its consequences with respect to properties the classes of lattice defects with respect to their geometrical order are discussed. These are point defects (zero order) such as vacancies and interstitials, line defects (first order) i.e. dislocations, and area defects (second order) such as grain boundaries. The various interactions between these defects as well as their motion under external and internal forces are discussed. Microscopically observed deformation characteristics are explained in terms of the motion and interaction of these defects. Modern experimental techniques yielding some direct evidence of the existence of the various defects postulated are briefly reviewed.

Finally the modes of failure of metals at elevated temperatures will be discussed. They are evaporation, creep and fracture. No final and generally applicable laws have been found to date which would allow a prediction of these technically so important and scientifically so baffling events, but many facets have become clarified through careful consideration of the defect structures of metals.

1.0 INTRODUCTION

It is the objective of this conference to discuss the various mechanisms known to be operative in metals at elevated temperature and to pinpoint the areas that are in need of clarification through future research efforts. Although this is an "elevated temperature" conference the primary emphasis is on mechanisms rather than on the behavior of metals above a certain temperature. It is therefore quite conceivable that room temperature properties of certain low melting metals will be discussed as characteristic examples of elevated temperature mechanisms. Thus, if we wanted to define an elevated temperature range in terms of operative mechanisms, it would have as the lower limit some fraction of the absolute melting point. This is borne out by such simple a property as the maximum service temperatures for which metals can be used. They are around 45-63% of the absolute melting point (W-45%, Mo-59%, Ti-46%, Steel, δ-63%, Al-60%), see Figure 1.

This introductory lecture is intended to present a review of the structural aspects of metals with emphasis on the elevated temperature mechanisms and properties. It should also provide the background for the more detailed sessions on diffusion, transformation and recrystallization, solid-gas reactions and imperfections and mechanical properties that are to follow. It is therefore nothing more than an up-dated review of the subject presented to fit in the topical frame of the conference. As quite recently several excellent reviews and symposia have been given on this subject (1-10) the effort is mainly one of restatement with a different frame of reference.

When a metallurgist mentions the word structure, one expects him to talk about crystal structure; and when we also know that he is primarily interested in deformation and fracture, we expect to hear a great deal about dislocations. However, before dealing with these aspects a few comments concerning the atomic and electronic structures of metals are in order. Finally the modes of failure will be discussed briefly.

1.1 ELECTRONIC STRUCTURE

Modern theory of solids tells us that we have to treat and "understand" the elementary particles, their motion and interactions by way of their wave functions and the laws of quantum mechanics (11-18). Thus from an atomic point of view the structure of metals is characterized by regular arrangements of positive ions with more or less free electrons between them (19). In certain instances, among them under elevated temperature conditions, these free electrons can to a fairly good approximation be treated as an electron gas (20).

With the help of this classical free electron theory of metals it was possible to explain electrical conductivity and its relationship to thermal conductivity by the Wiedemann-Franz law. Sommerfeld's quantum mechanical treatment (21) of the electron gas was able to account for the electron's contribution to the heat capacity, the electrochemical potential, the Peltier and Thomson effects and the Hall effect.

Bloch (22) and Brillouin (23) also accounted for the motion of an electron in a periodically changing potential and have thereby generated the electron band theory of metals. According to this theory the electrons are energetically separated into energy bands. There are forbidden energy regions for electrons. An electron can only move in a band that is incompletely filled as electrons near the top of a band have infinite inertia. This band model is illustrated in Figure 2 (12). As the interatomic distance decreases bands may overlap which can give increased electrical conductivity since a not completely filled band may overlap a filled band. Because of the tendency to achieve the lowest energy state the band theory also allows for an interpretation of polymorphism of metals and alloys as the band structure is dependent upon

the crystal structure (14). From that point of view it is important to know how the band structure changes with temperature and if at some temperature there is a different crystal structure which will lead to a lower energy state.

With the exception of the transition metals the electrons have little measurable contribution to the heat capacity (14). In the transition metals the contribution is proportional to the absolute temperature T according to:

$$C_v = \frac{1}{2} \pi^2 n_o RT/T_o \qquad \text{Equation 1}$$

where n_o is the number of free electrons per atom, R the gas constant and T_o the degeneracy temperature. (T_o: Ni = 3470 °K, T_o: Pd = 1,750 °K). To go further into detail of the free electron theory would go beyond the scope of the conference.

One aspect worth mentioning here, however, is the question of why the free electrons do not leave the crystal, and together with answering this question to explain the working of the field emission microscope (24). The density and potential in a crystal vary periodically, i.e. the potential at a nucleus becomes negatively infinite. At larger distances the ions attract the electrons with a potential V = -e/4x. The average potential within a crystal is therefore negative, see Figure 3. Here E_m is the maximum kinetic energy, W the work function and *E_f the Fermi energy.* Thus, in order to remove electrons from a crystal we must apply a very high field as illustrated in Figure 4.

The stronger the field the greater is the likelihood of an electron tunneling through the narrow triangular potential barrier. An estimate of the field strength required at room or lower temperatures can be obtained from the work function (W_w = 4.5 eV) and yields 20-30MV/cm. This is achieved by having a very small tip radius of the material (cathode) to be investigated. The electrons will leave perpendicularly to the surface and form an image on a fluorescent screen that represents a replica of the electron density on the tip surface, see Figure 5. The scattering, which is due to thermal motion of the atoms and radial velocity components of the electrons yields a resolution of approximately 10-20 Å.

The ion emission microscope (25) works on a slightly different principle. Here a low pressure gas is introduced ($p \approx 10\,\mu$) which is ionized in the vicinity of the tip (now anodic). As the locus of the ionization is again a function of the atomic arrangement at the surface the positive gas ions are accelerated towards the screen where an image of the tip surface is formed. This method, employing a field of approximately 500 MV/cm, has an even higher resolution because of the *low de'Broglie wave length of the* ions. Professor Newkirk will present some photographs obtained with this technique and demonstrate their interpretation.

So much for the electronic structure of metals. Can we talk about defects in this structure? The answer must be yes, however, these defects are responsible for the particular electrical, magnetic and chemical characteristics of an element but have little effect on the mechanical properties. They can also be predicted a prior; from quantum mechanics and a minimum energy condition. A typical example of such a defect structure is the electron configurations of the transition metals and the rare earth elements. The band structure itself can be considered a defect structure imposed by the periodic potential of a crystal. Similar arguments can be made, e.g., for overlapping bands as a function of the lattice spacing, for impurity bands in semiconductors, for F-centers, etc.

1.2 ATOMIC STRUCTURE

Most metals in the solid state have a close-packed or nearly close-packed structure (fcc, cph), see Figure 6. This means that the atoms can be thought of as spheres touching each other in a close-packed arrangement. An exception is the bcc structure which is not a close-packed structure (Li, Na, W, Fe). While in a close-packed structure the coordination number (number of nearest neighbors) is 12, the coordination number for the bcc lattice is 8. There are also some metals with a coordination number 4 (Ge, Sn) where covalent bonds are present and others (Ga, Hg, Bi) where other influences are active. The Hume-Rothery 8-N rule applies to most elements in the B subgroup. The number of nearest neighbors is 8-N where N is the number of the group to which the element belongs.

Mie suggested (26) to express the mutual potential of two atoms or ions by the binomial expression:

$$\phi(r) = -\frac{a}{r^m} + \frac{b}{r^n} \qquad \text{Equation 2}$$

Such a potential, illustrated in Figure 7, consists of an attractive part $-\frac{a}{r^m}$ and a repulsive part $+\frac{b}{r^n}$. Since for a small but finite n, ϕ depends very little on the distance between atoms, it is evident that second nearest neighbors, etc. may have an effect on the lattice energy. This explains to some degree the stability of the bcc lattice ($m \approx n$).

Mie's equation for the potential allows the derivation of the two Grüneisen Rules. The first rule pertains to the bulk modulus K of a solid which is given by:

$$K.V_o = \frac{m.n}{g} |U_o| \qquad \text{Equation 3}$$

where V_0 is the equilibrium volume and U_o the equilibrium lattice energy. For the change in compressibility as a function of pressure one obtains:

$$\frac{\partial K}{\partial_p} = \frac{m + n + 6}{3} \qquad \text{Equation 4}$$

which yields approximately the right results for the alkali halides (27) with m=1, n=9, i.e. 5.33. Some alkali metals show low values (Li: 2.6, Na: 2.8, K: 2.8, Rb: 5.22, Cs: 5.20) while other metals show much higher values. Bridgman (28) concludes that in these cases the compressibility of the ions themselves may be responsible.

Grüneisen's second rule pertains to the thermal expansion to the melting point. Here the assumption is made that melting occurs as the atomic separation reaches the inflection point of the curve. The volume expansion at the melting point, $3\epsilon_{melt}$, is given by:

$$3\epsilon_{melt} = \frac{1}{8\gamma} \qquad \text{Equation 5}$$

where $\gamma = (m + n + 3)/6$ the Grüneisen number. Some γ values for metals are shown in the table below.

TABLE I

Body-Centered Cubic

Metal	Li	Na	K	Rb	Ca	W	Fe	Mo	Ta
	1.17	1.25	1.34	1.48	1.29	1.62	1.60	1.57	1.75

Face-Centered Cubic

Metal	Al	Co	Ni	Cu	Pd	Ag	Pt	Au	Pb
	2.17	1.87	1.88	1.96	2.23	2.40	2.54	2.40	2.73

Thus for γ = constant we should observe the relationship:

$$\alpha T_m = \text{constant} \qquad \text{Equation 6}$$

where α is the expansion coefficient, as is indeed the case, see Figure 8. For metals and ionic compounds the middle curve with $3\alpha T_m \approx 6\%$ applies.

The specific heat of all solids should be, according to Dulong and Petit, 3R. This is due to the 1/2 kT of kinetic and potential energy per degree of freedom. Each atom with 3 degrees of freedom has therefore an average energy of 3kT, each gram-atom 3Nkt = 3RT and the specific heat, $C_p = (\partial E/\partial T)\big|_{p = const} = 3R = 5.96$ cal. deg.$^{-1}$ mol.$^{-1}$. This, however is not observed at lower temperatures where $C_v \sim (T/\theta_D)^3$ where θ_D is the Debye characteristic temperature, cf Figure 1. At room and elevated temperatures the specific heat is close to the 3R value or higher. The increase can be, according to Born and Brody (29), due to the anharmonic terms in the vibration spectrum or in transition metals due to the electronic contribution (30) as mentioned before. Some values are presented in Table II.

Although the free electrons are responsible for the conductivity of metals the crystal structure and its defects (+ thermal vibration) determine its temperature dependence. *A perfect lattice (0^oK) would have infinite conductivity since the electron waves could pass through it unscattered.* As soon as thermal vibrations and defects are introduced the amount of scattering determines the conductivity. Calculations show it to be proportional to T^{-1} for $T \gg \theta_D$ and to T^{-5} for $T \ll \theta_D$. In general one can express the resistivity (Cu, Au) by the formula:

$$R = A + BT + CT^2 + D.\ \exp\{-Q/kT\} \qquad \text{Equation 7}$$

where the last term may be attributed to scattering due to Schottky defects (see below).

If we accept Smekals classification of the properties of solids into structure sensitive and structure insensitive properties (31) the above discussed properties belong to the latter category. They can be deducted from the electron theory of metals with the assumption of a periodic structure of the atoms and a binomial expression for the potential between two atoms. The agreement with experimental data is surprisingly good. In the following chapters the structure sensitive properties will be discussed in terms of the defects responsible for them. A division into defect-sensitive and defectinsensitive properties would be more appropriate (1, 2) as the properties in question are often affected by minute impurities or defects of

atomic dimensions. It should be pointed out, that the defect structures themselves were obtained in retrospect from an analysis of these structure sensitive properties. However, for the sake of obtaining a logical sequence, the order of discussion will be reversed, i.e. a discussion of the failure modes will follow the discussion of the various lattice defects.

TABLE I

Observed specific Heats, C_v, in cal-deg^{-1} per gm-atom

Temp-°C	Pd	Pt	Cu	Ag	Au
0	5.60				
20		5.95		5.75	5.8
500	6.594	6.38	6.2	6.0	6.0
900	7.072			6.13	
1000	7.146	6.65	6.5		6.12
1300	7.251				
1500	7.232				
1600		6.8			

2.0 LATTICE DEFECTS

2.1 IDEAL CRYSTAL STRUCTURE

An ideal crystal is defined as one whose atoms are uniquely positioned in accordance with the laws of crystallography. Early experimental evidence, especially x-ray diffraction studies were certainly in support of the theory that there is not much difference between real and ideal crystals. However, a careful examination of all the consequences of an ideal crystal structure made it obvious that the real crystal differs from the ideal crystal in that it contains defects which destroy the uniqueness of the postulated arrangement. Although these defects generally elude conventional x-ray or optical examinations because of their small dimensions, they are primarily responsible for a number of physical and mechanical properties with which we are familiar and which are generally referred to as material characteristics.

Some of the consequences that led to the conclusion that real crystals are far from perfect are listed below:

1. X-ray extinction: The diffraction intensity from a perfect crystal would be considerably lower than the observed one due to primary extinction, i.e. double reflection in the direction of the incident beam (32).

2. Electrical conductivity: At 0°K the electrical conductivity of a perfect crystal should be infinite except when the Bragg conditions are fulfilled.

3. Theoretical shear strength: The elastic shear strain should be ≈ 0.25 while observed values are near 10^{-4} to 10^{-5} (10).

4. Theoretical fracture strength: Should be commensurate with theoretical shear strength, e.g. $\sim$0.1E (33).

5. Activation energy for self diffusion: The only mechanism for self diffusion in a perfect crystal would be atomic exchange. The activation energy for such an exchange. The activation energy for such an exchange in Cu is according to Huntington and Seitz (34) $\approx$10.3eV while the experimental determinations lead to an activation energy of 2.09 eV (35).

As it is extremely difficult to obtain direct "photographic" type evidence of the defects within a crystal, defect theory is primarily concerned with an accounting for the experimentally observed phenomena with the help of models. Nevertheless, subsequent critical and very refined experimentation has yielded a significant amount of direct irrefutable evidence of a good share of these defects so that their existence is now generally accepted with confidence.

Several systematic schemes for defects have been given by various authors. Seitz (36) proposes six primary types of imperfections, 1) phonons 2) electrons and holes, 3) excitons, 4) foreign atoms (interstitial of substitutional), 5) vacant lattice sites, 6) dislocations; plus three transient types of imperfections, 1) light quanta 2) charged radiation and 3) uncharged radiation. Pick (37) proposes a system consisting of a.) chemical imperfections (impurity concentration) b.) structural imperfections and c.) electrical imperfections.

The following discussion will be limited to structural defects in "nearly perfect crystals" since they are primarily responsible for the mechanical behavior of metals. According to Seeger (1) they can be classified very logically in terms of their geometrical extent, i.e.:

0 - order defects or atomic defects such as vacancies, interstitials, atoms at wrong positions (in compounds), etc.

I - order defects such as a dislocation line and

II - order defects such as grain or twin boundaries.

2.2 *0-ORDER DEFECTS*

Frenkel (38), Wagner and Schottky (39) and Jost (40) have postulated that at elevated temperature there are always some vacancies and often also atoms in interstitial locations. The two basic possibilities for such defects are known as Frenkel defects and Schottky defects, illustrated schematically in Figure 9. In the former, atoms are removed from their regular lattice sites and placed interstitially. In the latter the removed atoms are removed to the crystal surface. The creation of Schottky defects causes a loss in crystal density. The creation of Frenkel defects can also cause density changes as the expansion due to the interstitials is often overcompensated for by the lattice contraction due to the vacancies. Thermodynamical calculations (1) show that for both cases the number of defects increases exponentially with the temperature according to:

Frenkel: $n = \sqrt{N \cdot N^I} \exp\left\{-1/2 \frac{W_F}{KT}\right\}$ Schottky: $n = N \exp\left\{-\frac{W_S}{KT}\right\}$ Equation 8

where:

n = number of defects

N = number of atoms in crystal

N^1 = number of available interstitial positions

W_F, W_s = energy for the creation of a Frenkel or Shottky defect

Thus the activation energy for the thermal production of Frenkel defects is 1/2 the defect energy while that for the creation of a Schottky defect is equal to the defect energy. Mott and Gurney (41) have shown that the number of defects in thermal equilibrium is larger than the above indicated; for Schottky defects by a factor of 10^3 -10^4, for Frenkel defects by a considerably smaller factor.

In the derivation of the above equation it was also assumed, that the activation energy for the formation of a defect is known. A simple relationship for this activation energy exists, however, only for Schottky defects in monatomic solids.

At absolute zero temperature this energy is equal to the binding energy per atom as:

$$U = -\frac{1}{2}\sum_k V(r_k) \qquad \text{binding energy}$$

$$U_1 = -\sum_k V(r_k) \qquad \text{removal energy}$$

Equation 9

$$U_2 = -\frac{1}{2} U_1 \qquad \text{energy gain by putting atom on surface}$$

i.e. $W_s = U$.

The most exact theoretical procedure for the calculation of activation energies of Schottky defects is due to Fumi (42) who reports for the noble metals

	Cu	Ag	Au
W_s theoretical, eV	0.87	0.72	0.62
W_s experimental, eV	0.90	0.8	0.67

There is no simple way of estimating the activation energy for the formation of Frenkel defects, or interstitial atoms in general, as the energy for the interstitials depends upon the available volume. Since the activation energies for the various processes are of the order of a few electron volts, even small differences cause the dominance of a particular type of defect. Thus it is justified to assume that in a certain lattice structure Frenkel, Schottky or anti-Schottky defects are dominant.

One group of experimental observations for which these point defects can account is in the field of diffusion in metals, which is intimately related to the motion of the point defects. For the motion of interstitials in Cu Huntington and Seitz (34) and Huntington (43) estimated

for the activation energy between 0.25 and 0.5 eV while the experimental value is approximately 0.7 eV. The activation energy for the motion of a vacancy is estimated by Hintington (44) somewhat above 1 eV. Two additional mechanisms for self diffusion have been proposed by Zener (45, 46):

a. direct exchange of atoms and

b. exchange by a ring mechanism

Huntington and Seitz (34) have calculated the activation energy for direct exchange in Cu as 10.3 eV. Zener's ring-mechanism requires an activation energy (in Cu) of 4 eV. The experimental value for the activation energy of self diffusion in Cu is 2.09 eV (25) which is closest to that predicted for the vacancy diffusion mechanism.

For the production of these point defects there are three basic mechanisms:

1. Thermal vibrations
2. Radiation damage
3. Plastic deformation

The equilibrium concentration for thermally created defects was discussed early in this chapter. Measurements of the electrical conductivity on Cu and Au yield a defect concentration of approximately 1/400 and 1/200 respectively at their respective melting points (47).

Neutron bombardment of a metal causes primarily Frenkel defects along the high energy position of the neutron path. As the neutron slows down we obtain a zone of local melting-displacement spike where the defect concentration is that which corresponds to the melting temperature. In addition we may find dislocation rings, microcrystals, etc. This is illustrated in Figure 10.

The creation of point defects as a result of plastic deformation will be discussed in the next chapter on line defects. In this case the motion of dislocation lines containing jogs represents the most likely mechanism for the formation of interstitials and vacancies.

Finally we should discuss some experimental evidence for the existence of point defects as discussed. In addition to measurements of the activation energy for diffusion, changes in the resistivity can be used to estimate the defect concentration. Foreign atoms, interstitials, vacancies and any other irregularity in a crystal lattice cause an increase of the resistivity due to their additional scattering effects of the electrons. This change is generally proportional to the defect concentration. Jongenburger (48) estimated for vacancies in Cu

$$\Delta\rho = 1.25\,\mu\Omega\ \text{cm/\% vacancies} \qquad \text{Equation 10}$$

For the case of vacancy pairs this value increases to about $2\,\mu\Omega$ cm/% vacancy pairs. Interstitials in Cu cause an increase of the resistivity:

$$\Delta\rho \sim 0.5\,\mu\Omega\ \text{cm/\% interstitials} \qquad \text{Equation 11}$$

With these relationships one can check the predictions made for thermal defects and the activation energies associated with them. On quenching to very low temperature the elevated

temperature defect structure can be "frozen in". From the increase of the resistivity as compared to its equilibrium value and subsequent changes with temperature one can obtain both the energy of formation and migration of these defects. Thus Kauffman and Koehler (49) observed for gold an activation energy of 0.4 eV which is most likely due to the migration of vacancy pairs as the activation energy for self diffusion is between 1.9 and 2.0 eV, that for the formation of vacancies 0.6 to 0.8 eV and that for the migration of simple vacancies between 1.4 and 1.7 eV.

Additional data exist for alloys showing long range and short range order. For the former it could be concluded that the ordering process is due to the migration of vacancies. In alloys with short range order the ordering process is too fast to obtain useable diffusion measurements. According to Zener (50) the different size atoms cause a stress system which in turn leads to an ordered state that minimizes the stress state. This is observed from internal friction experiments where increased damping is obtained during this recovery period.

A summary of recovery data on Cu is presented in Figure 11 where the resistivity changes for quenched, irradiated, deformed polycrystals and deformed single crystals are plotted as a function of temperature. We observe five distinct steps of recovery:

I Stage: between 35°K and 45°K
Activation energy 0.1 eV. This stage is only observed as a result of neutron bombardment and probably due to the changes occurring in the microcrystals of the displacement spikes.

II Stage: between 100°K and 200°K
Activation energy 0.2-0.5 eV. Occurs in irradiated as well as deformed specimens and is probably caused by the migration of vacancy pairs, vacancy complexes or interstitials, most likely pairs.

III Stage: between 220°K and 270°K
Activation energy 0.72 eV occurs in irradiated and deformed samples. Most likely due to the migration and annililation of interstitials.

IV Stage: At about 370°K and 570°K
Activation energy 1.2 eV, occurs in quenched, irradiated and deformed specimens. Most likely due to the migration of vacancies and their disappearance at dislocations or grain boundaries.

V Stage: between 500°K and 610°K
Activation energy $\approx$ 2.1 eV. Coincides in Cu with hardness recovery due to recrystalization. The activation energy is close to that for self diffusion.

In summary it can be said that:

1. Point defects are present in metals as a result of the various manufacturing techniques, i.e. solidification and plastic deformation. The equilibrium concentration near the melting point is somewhere below 1%. They are also produced as a result of neutron bombardment.

2. The mechanism for the motion of point defects are, in order of increasing activation energies: migration of vacancy complexes, migration of vacancy pairs, migration of single vacancies and self diffusion. With the exception of self diffusion the annihilation and migration of these defects do not seem to affect the mechanical properties of a material but are responsible for increased damping and resistivity changes. Self diffusion and recrystallization lead also to a recovery in hardness.

3. The preceding remarks pertain primarily to noble and alkali metals. In alloys additional events connected with the interaction of vacancies and phase transformation complicate the scheme of events. Both Ni and Pt (transition metals) show recovery phenomena commensurate with that of Stage IV, i.e. migration of single vacancies.

2.3 LINE DEFECTS

These defects have a linear extent and are called dislocations. They were postulated independently by Taylor (51), Orowan (52) and Polanyi (53) as a mechanism to explain the plastic behavior of metals. Considerable experimental evidence has since been gathered (54), (1,2) which proves their existence beyond any doubt.

2.31 GEOMETRICAL CONFIGURATIONS

The two basic types of dislocations are the edge dislocation and the screw dislocation whose configurations for a simple cubic lattice are shown in Figure 12. The characteristic entity which describes a dislocation is the Burgers vector, $\vec{b}$ defined as indicated in Figure 12 from the Burgers circuit. A dislocation line may be defined as the line separating the slipped from the unslipped region, Figure 13. It can be curved or straight. The portions of the dislocation line that are parallel to b are made up of screw dislocations, the ones normal to $\vec{b}$ are made up of edge dislocations the composite being called a γ dislocation. Dislocations can combine or separate according to the vector equation:

$$\vec{b}_1 + \vec{b}_2 \rightarrow \vec{b}_3 \qquad \text{Equation 12}$$

The stability of such a reaction is determined by the energy dissipation or consumption of the reaction. The latter is proportional to $\vec{b}^2$ although it is also influenced to a minor degree by the elastic anistropy of the crystals. Thus:

$$b_1^2 + b_2^2 = (\vec{b}_1 + \vec{b}_2)^2 + Q$$

$$Q = -2\,\vec{b}_1 \cdot \vec{b}_2 \qquad \text{Equation 13}$$

where Q is the reaction energy of the process which is positive (attractive force) if the Burgers vectors of two parallel dislocation lines include an angle larger than 90°, zero if this angle is 90° and negative (repulsive force) if this angle is less than 90°. The above equation for Q can be utilized as a criterion for stability of a dislocation. If the product $\vec{b}_1.\vec{b}_2$ of the components is positive, the dislocation b_3 is stable, if $\vec{b}_1.\vec{b}_2$ is zero it is undecided and if $\vec{b}_1.\vec{b}_2$ is negative it is unstable. This can be applied to the determination of the possible Burgers vector of the four basic metallic crystal structures.

1. Simple cubic: (CsCl) $b = a\langle 100\rangle$ shortest.
   Stability of $b = a\sqrt{2}\langle 110\rangle$ and $b = a\sqrt{3}\langle 111\rangle$ in two or three $b = a\langle 100\rangle$ undecided.
   All others unstable.

2. Body Centered Cubic: $b = \frac{1}{2} a\sqrt{3}\langle 111\rangle$ shortest, $b = a\langle 100\rangle$ next shortest. Both vectors are stable. This is the only case of its kind where two Burgers vectors having different lengths are stable. All others are unstable.

3. Face Centered Cubic: $b = \frac{1}{2} a\sqrt{2}\langle 110\rangle$ shortest.
   Stability of $b = a\langle 100\rangle$ undecided.

4. Close Packed Hexagonal: $b = 1/3\ a\langle 11\bar{2}0\rangle$ shortest, stable.
   $b = C\langle 0001\rangle$ next shortest, stable. Stability of $b = 1/3\sqrt{a^2 + c^2}\langle 11\bar{2}3\rangle$ with respect to dissociation in $\vec{a}$ or $\vec{c}$ vectors undecided.

The second characteristic of a dislocation is its slip plane. Since the energy of a dislocation depends indirectly on its slip plane by way of anisotrony of the elastic constants it is hard to predict theoretically. In general the slip planes are those with densest packing, i.e. (111) in fcc and (0001) in cph. However, in many materials having the same crystal structure different crystallographic planes are observed as slip planes, i.e. (110), (112) and (123) in bcc. (10).

Dislocations with different Burgers vectors can meet at a single point. Such triple or quadruple points or nodes cannot exist in simple cubic systems as there all $\langle 100\rangle$ vectors are either orthogonal or antiparallel. The same is true for the $\underline{c}$ dislocations in the cph system. However, the $\underline{a}$ dislocations within themselves can form stable triple points. In the fcc lattice we can expect stable triple points and stable quadruple points. Generally these dislocation lines will have different slip planes. If three dislocation lines have three different slip planes their point of intersection is immobile. Such immobile nodes are important as sources of dislocation lines.

As we shall see later, the thermal generation of dislocation lines is a very unlikely event, except at very high temperatures. Similarily we shall find that stresses of the order of the theoretical yield strength ≈ 0.1 G would be required for the generation of a dislocation line in a perfect crystal. However, since yielding and fracture and therefore the motion of a considerable number of dislocation lines takes place at stresses of $\approx 10^{-3}$ to 10^{-4} G, another mechanism for the generation at very much lower stresses and temperatures must be active. This mechanism was first pointed out by Frank and Read (55, 56). It assumes an anchored dislocation line which bulges out under the influence of an applied stress, reaches the crystal surface where it causes a step, continues (backwards) to pass over the remainder of the slip plane, where finally the two short pieces of the dislocation line join up again and the process can be repeated, Figure 13. The anchor points required for this mechanism are provided among others by the above discussed nodes. However, gliding much below the theoretical shear strength is also observed in systems where such immobile intersections do not exist. One may therefore assume that anchor points can also be formed through dislocations in other than the microscopically observed glide planes which have a very low mobility.

This mechanism for a dislocation source has the consequence that all dislocation lines are in one particular slip plane. During their motion, however, it might happen that a particular dislocation line jumps from one slip plane to a parallel slip plane causing a dislocation jog as illustrated in Figure 14. The motion of such a jog may be conservative or nonconservative,

i.e. cause a change in volume (vacancies or interstitials) or not. Even for most general crystal structures such jogs contain always some edge-component and are never pure screw dislocations. Jogs in dislocation lines that have predominantly edge character are able to move along with the dislocation line through the absorption of vacancies or the creation of interstitials. This causes a lifting or climbing of the dislocation line, a process which occurs during recovery and elevated temperature creep. Even if a thermal production of jogs is impossible due to a very high activation energy, a c dislocation ring containing jogs may climb if the resulting Burgers vector has a component normal to the plane of the dislocation ring (57). Figure 15 illustrates the process for dislocation lines having predominantly screw character. As the line bulge out between the jogs lines of predominantly screw character will meet behind the jogs causing either interstitials or vacancies.

Finally we have to concern ourselves with partial dislocations, i.e. dislocations whose Burgers vector is not a vector in the Bravais lattice. The most important cases are the stacking faults in close-packed systems, namely fcc and cph. These are illustrated in Figure 16 for the fcc and the cph lattice. A reaction between partial dislocations is schematically illustrated in Figure 17. This dislocation 1/6 <110> is also called a Cottrell dislocation and the reaction is called the Cottrell-Lomer reaction. This dislocation is completely immobile, can neither climb nor glide, and plays a role in the strain hardening of fcc metals.

2.32 *THEORETICAL CONSIDERATIONS*

From the preceeding geometrical considerations it is evident that the presence of a dislocation line causes a stress field in the crystal. Since the distortions have atomic dimensions it is not feasible to use continuum mechanics, that is, theory of elasticity, for the description of the stress field in the immediate vicinity of the dislocation line, however, such calculations are extremely helpful in understanding the long range stress field of the dislocation. The equations describing this long range stress field of a single dislocation are given below:

$$\sigma_{rr} = -\frac{b}{2\pi}\frac{G}{1-\nu}\frac{\sin\phi}{r}\left(1-\frac{a^2}{r^2}\right)$$

$$\sigma_{yy} = -\frac{b}{2\pi}\frac{G}{1-\nu}\frac{\sin\phi}{r}\left(1+\frac{a^2}{r^2}\right)$$

$$\sigma_{ry} = \frac{b}{2\pi}\frac{G}{1-\nu}\frac{\cos\phi}{r}\left(1-\frac{a^2}{r^2}\right) \qquad \text{Equation 14}$$

$$\sigma_{zz} = -\frac{b}{2\pi}\frac{\nu G}{1-\nu}\frac{\sin\phi}{r}$$

The geometrical orientation to which this equation pertains is illustrated in Figure 18. In general one can see that the stress caused by a dislocation decreases to the inverse power of the distance from the dislocation, i.e. 1/r. The above equations pertain to the stress field of an edge dislocation. A similar dependence of the stress on the distance from the dislocation is obtained for the stress field of a screw dislocation as indicated by the equations below:

$$\sigma_{yz} = \frac{Gb}{2\pi}\frac{1}{r}$$

$$E_{\phi z} = -\frac{b}{4\pi r} \qquad \text{Equation 15}$$

The reaction force between two screw dislocations is repulsive if they are parallel and attractive if they are anti-parallel, Seeger (1) has proven that one can obtain a stable network of screw dislocations if three screw dislocations are arranged such that the direction of one of them disects the angle between the two remaining into two equal parts.

Stable arrangements of edge dislocations on two parallel slip planes are illustrated in Figure 19. Thus edge dislocations of equal sign will line up one above the other while edge dislocations of opposite sign will line up under 45°.

Of special importance is the so called pile up of dislocations in a glide plane. Considering the Frank-Read mechanism for the creation of dislocations in one glide plane a number of dislocations of the same sign will be generated in this glide plane and move in the same direction. As soon as the first dislocation of this group hits an obstacle, e.g. the grain boundary or a dislocation in another slip plane, it will be blocked and exert a repulsive force on the following dislocations. Such a dislocation pile up is illustrated in Figure 20. The equations that determine the equilibrium position of such a dislocation pile-up have been derived by Eshelby, Frank and Nabarro* and are in agreement with experimental observations**.

Continuum mechanics also allows us to discuss the energy of a dislocation. It is defined by the work which is necessary to create the dislocation in question in an otherwise perfect crystal. It is obvious that this energy depends upon the length of the dislocation line and therefore energy values for dislocations are given in terms of their energy per unit length. The energy of a single dislocation line in a crystal of infinite extent is therefore infinity if we assume the dislocation line to be straight. Thus we also have a dependence of the energy of the dislocation on the size of the crystal. If we consider a statistical arrangement of an equal number of positive and negative parallel dislocations, the energy of the dislocations remains finite. An order-of-magnitude estimate of such an arrangement gives an energy of 3.9 eV for aluminum and 4.5 eV for copper. These energies are in the order of magnitude of the energies required for the creation of interstitial atoms but considerably higher than those required for the formation of vacancies.

The discussion of the energy of a dislocation gets further complicated by the fact that dislocation lines need not be straight, but can curve, bow out around an obstacle, etc. and have various geometrical shapes. Straight dislocation lines made up of edge dislocations have an energy per unit length approximately equal to $b^2.G$ and screw dislocations approximately 2/3 of this value. Thus these energies must be furnished in order to increase the length of the dislocation line by the unit length. As a dislocation line assumes a curved shape, part of the dislocations will be screw type and part will be edge type so that the line tension of a dislocation is not constant along the dislocation line. According to Stroh (58) one can give a line tension of a dislocation ring of radius R in the form:

$$E_e \approx \frac{Gb^2}{8\pi} C \log \frac{R}{r_o} \qquad \text{Equation 16}$$

*Phil Mag. v 42 (1951) p 351.

**Gould, J.R., M.S. Thesis 1959, Syracuse University

where r_0 is the unelastic region that had to be eliminated from continuum mechanical consideration, R, the radius of curvature of the dislocation and C a constant of the order of unity. With the help of this equation the activation energy of a Frank-Read source can be estimated as:

$$U \approx \frac{8\sqrt{2}}{3b} \frac{E_\ell^2 (\tau_k - \tau)^{3/2}}{\tau_k}$$

Equation 17

$$\tau_k = \frac{E_e}{b\,R}$$

With the help of continuum mechanics it is also possible to make some thermodynamic studies concerning the stability of the dislocation. For plausible values of r. one obtains a shear stress of 0.02 G to be required to produce such a dislocation source. Stresses of that magnitude cannot be applied to a single crystal of macroscopic dimensions and since the plastic deformation of a single crystal occurs at stresses which are lower by a factor of about 10^3 it must be assumed, that dislocations are present in the as-received crystal which have been generated by some other mechanism, probably occurring during the growth of these crystals. Once a crystal contains a dislocation it is possible that the local stress concentration in the immediate vicinity of the dislocation is sufficient to cause the thermodynamic or spontaneous generation of new dislocations. This mode of generation of new dislocations from an existing dislocation has, however, to date not been established experimentally.

Another interesting aspect of the continuum mechanics treatment of the stress field of dislocations concerns the interaction between dislocations and point defects. In general the energy of the formation of a point defect at an edge dislocation is considerably below that for the generation of the same point defect in a perfect part of the crystal. The interaction between dislocations and impurities will also cause a migration of the impurities in the neighborhood of the dislocation in order to relieve the stress field of the dislocation. Further motion of dislocations which are surrounded by an impurity atmosphere is determined by the diffusion rate of the impurities.

In order to get some better insight into the motion of dislocations it is necessary to consider the stress field in the immediate vicinity of the dislocation. Two basic models have been proposed: 1) the Frenkel model which is an arrangement of mass points coupled through springs (59) and 2) the Peierls model which is an extension of the continuum elasticity approach where the nonlinearity of the elastic distortions is considered only in the slip plane (60). In both cases the dislocations move in a field of a periodically changing potential. The most important result of the calculations with the help of the Peierls model is the determination of the Peierls stress t_p which is defined as the stress required to move a dislocation at a temperature T with a given mean velocity. These Peierls stresses are given for aluminum in the table below:

TABLE III

Peierls Stresses in Aluminum

Slip Plane	Dislocation Type	Dislocation Width	Peierls Stress
(010)	90° dislocation	0.50 a	$0.1.10^{-5}$ G
(010)	0° dislocation	0.76 a	$5.\ 10^{-3}$ G
(111)	0° half dislocation	0.92 c	$1.2\ 10^{-4}$ G
(111)	120° half dislocation	0.68 c	$3.3\ 10^{-4}$ G
(111)	90° dislocation	0.68 c	$1.3\ 10^{-3}$ G
(111)	30° dislocation	0.85 c	$0.9\ 10^{-3}$ G

Comparison with the critical shear stresses indicates that the results listed in the above table are in disagreement with the experimental results by a factor of approximately 50. This disagreement is probably due to the fact that in the calculation for Peierls stress there are two parameters which are not clearly defined. These parameters both enter in the equation as negative exponentials and one might expect that both parameters were chosen too low. As the temperature increases the Peierls stress is reduced. This reduction is caused by two events: 1. With increasing temperature an increasing number of dislocations of higher order are formed. (These dislocations are caused by the fact that the dislocation line becomes wavy as it progresses across a crystal. The waves may move sideways and thereby reduce the Peierls stress) and 2. The thermal motion of the lattice. The latter causes an increase in the width of the dislocation line which again causes a decrease in the Peierls stress.

The split-up of complete dislocations into partial dislocations can also be treated with the help of a Peierls model. The elastic interaction between the partial dislocations tend to increase the separation while the surface energy of a stacking fault tends to hold them together. One finds, according to Seeger (1) with the help of a Peierls model that the close-packed metals can be classified in two groups with respect to the strength of the separation of the partial dislocations. Namely one group with high stacking fault energy where $\gamma > 10^{-2}$ G b^2/c in which case the separation is only dependent on the length of the Burgers vector and not on the value of γ. The metals aluminum and probably magnesium, zinc and cadmium belong to this group. If $\gamma < 10^{-2}$G b^2/c the partial dislocations are clearly separated. This separation is relatively sensitive to the stacking fault energy and varies as γ^{-1}. The metals cobalt, copper and probably nickel, silver and gold belong to this group.

It was already indicated in the discussion of the geometrical aspects of dislocations that plastic deformation will be associated with climbing of the dislocation line that is the formation of jogs. If many of the dislocations are present in the form of extended dislocations, i.e. dislocations split up into partial dislocations, the jog formation will only be possible if the partial dislocations show a constriction. With the help of Peierls' model it is again possible to determine the energy required for the constriction of a dislocation and bring it in relation to the activation energy for the formation of the jog. The results of this calculation are shown below:

ACTIVATION ENERGIES FOR JOG FORMATION

Metal	Jog Type	Activation Energy
Al		eV
Al	(100)	0.4
	(110)	0.34
Cu	(100)	4.2
	(110)	4.1
Zn	Intersection jog	~ 1
	Diffusion jog	~ 4
Cd	Intersection jog	~ 0.8
	Diffision jog	~ 4.

This explains the difference in mechanical behavior of otherwise similar materials such as aluminum and copper. As aluminum has a high stacking fault energy, the energy for the constriction of an extended dislocation is very much lower compared to copper which has a much lower stacking fault energy.

2.33 EVIDENCE OF THE EXISTENCE OF DISLOCATIONS

Because of their smallness one must not expect to see dislocations except those in crystals with large lattice constants compared to atomic dimensions. The majority of the evidence in support of the existence of dislocations is indirect evidence. In this group fall the examination of etch pits which are caused by preferential chemical attack of a metal in the region disturbed by the stress field of a dislocation. Other methods are the coloring of dislocations or the study of dislocations in photo sensitive crystals. One very elegant and convincing piece of evidence is the observation of the motion of a low angle boundry which is shown in Figure 21 (61). One of the most striking experimental pieces of evidence that has been obtained is the observation of the motion of the dislocations in very thin films under the electron microscope.

The following film was made by P. Hirsch and associates. It shows the motion of dislocation lines in a very thin stainless steel foil as photographed through the electron microscope. The effect that allows us to see the dislocation lines and the location over which they have passed (which will show up as either a dark or a lighter region) is the so-called Moire effect, i.e. the interference phenomena obtained when one looks through two slightly misaligned screens. This picture is chosen here because it not only allows us to observe the presence, motion and generation of dislocation lines, but also gives a very good insight into the complexity of the processes occurring as the result of the motion of these dislocations such as the annihilation of a grain boundary, the interaction between partial dislocations, the formation of extended dislocations, and the creation of dislocations near the edge of the foil.

After seing this picture you will probably agree with me that any mathematical attempt for an accounting of the phenomena occurring in a real crystal will lead to tremendous difficulties. Nevertheless it is also obvious that these phenomena do occur and that we have to find some sort of a scheme to account for them if we want to be able to understand and predict the phenomena occuring in solids.

3.0 AREA DEFECTS

The last type of defects that we have to discuss, are the defects of second order, that is the defects having a two dimensional extent. These defects are the stacking faults which we have already discussed, the low angle boundaries, high angle boundaries and twin boundaries. We shall see that the good majority of them can be generated in terms of a more or less systematic arrangement of the defects of 0 and 1st order. We shall limit the following discussion to low angle boundaries, which can be generated by a vertical array of evenly spaced edge dislocations, high angle boundaries, which cannot be described crystallographically, and phase boundaries, especially those that can be generated through dislocation lines.

3.1 LOW ANGLE BOUNDARIES

A low angle boundary is schematically illustrated in Figure 22. The specific energy of a grain boundary can be defined as the additional energy that the boundary has per unit area as compared to the single crystal. Read and Shockley (62) have shown that the difference between free energy and internal energy of a grain boundary is small and is primarily affected by the angular dependence of the elastic constants. The energy of a grain boundary made up of such dislocations is given below:

$$E(\phi) = E_o \cdot \phi \left(1 - \log \frac{\phi}{\phi_{max}}\right) \qquad \text{Equation 18}$$

and illustrated in Figure 22 as a function of the angle ϕ. The constants E. and ϕ_{max} depend on the crystallographic orientation of the grain boundaries and details of dislocation model. The parameter ϕ_{max} cannot be obtained theoretically from elasticity and it is therefore not possible to obtain the absolute value of the grain boundary energy, and therefore of the constant E_o. However, in a plot of E/ϕ vs. ϕ we should, in accordance with equation 18, obtain a straight line. This is illustrated in Figure 23. The fact that the geometrical build-up of such a low angle boundary is completely feasible and indeed often occurs is illustrated by the fact that the motion of low angle boundaries under an applied shear stress proceeds exactly as predicted by dislocation theory (61).

3.2 HIGH ANGLE BOUNDARIES

It is surprising that the above equation for the free energy for low angle boundaries also applies to grain boundaries having much higher angle. This is especially true for silicon iron as illustrated in Figure 23. However, in zinc and lead no decrease with increasing angular difference is observed. No dependence of the grain boundary energy on the orientation difference was also observed for high orientation differences in silver. This was analyzed by Read (63) who showed that in a high angle boundary the dislocation packing would be extremely dense. Cavities will therefore be present in the region of the grain boundary. In order to generate such a grain boundary a pressure p must be applied to create these cavities. The specific energy of the grain boundary can be estimated from $p\Delta V = \frac{1}{2}(b.p)$. In other words, the energy of a high angle grain boundary becomes independent of the orientation difference.

Studies of internal friction, the relaxation of the shear modulus, and stress relaxation in polycrystals have shown that the mobility of high angle boundaries can be expressed (64) in terms of its apparent viscosity where the activation energy is at least approximately equal to the activation energy for self diffusion. From this Ke (65) concluded that the grain boundaries

are made up of small regions of misaligned atoms which are more or less equivalent to a diffused vacancy. A comparison of the activation energy values for volume diffusion and those for grain boundary relaxation shows that this is not always the case (see table below) especially not for copper.

TABLE IV

Comparison of Activation Energies for
Self Diffusion and Grainboundary Relaxation

Metal-Alloy	Self Diffusion k cal	Grainboundary Relaxation k cal
α - Brass (29% Zn)	41.7	41.0
α - Iron	78.0	85.0
Aluminum	33.0	34.5
Copper	48.0	32.0

However, as the impurity concentration increases the degree of agreement is also improved. Mott (66) has suggested a so called island model of the grain boundaries which assumes that a grain boundary is made up of islands of n atoms which have a good fit with the neighboring grains. The velocity v of the motion of such a grain boundary under a shear stress is given by the equation:

$$v = C.\frac{1}{kT} \exp\left(-\frac{nL}{kT}\right).\tau \qquad \text{Equation 19}$$

L = Heat of fusion per atom

For n = 14 good agreement is reached with experimental results on aluminum. Recent Russian work* on the background intensity of polycrystalline Cu and Ag led these authors to the conclusion, that grain boundaries in these metals have an apparent thickness of several hundred Å. This value decreases with increasing purity. The motion of a high angle boundary is illustrated in comparison to that of a low angle boundary in Figure 22. This type of grain boundary sliding was indeed observed and will be discussed later during this conference in greater detail.

It may also be possible to have high angle boundaries made up of a number of parallel dislocation walls.** Although the energy increases, they might be stable due to the absorption of impurities.

3.3 PHASE BOUNDARIES

Little is known about the make-up of a phase boundary and the growth of a new crystalline phase at the expense of a second phase. This problem, however, is of extreme importance to the practical metallurgist. The driving force for a transformation to occur is always a lower free energy of the new growing phase. We can distinguish between transformations that require

*Arkharoo, V.I., Borisov, B.S. and Vangengeim, Phys. Metals and Metallography v 10/3, (1960) p. 53.

**Orlov, A.N. and Shvarte, I.A., Phys. Metals and Metallography v 10/3 (1960) p. 175.

diffusion and those that occur without the diffusion. The Martensite transformation belongs to the latter group. Here we can generally speak of two stages namely: a) microscopically homogenous shearing which might also cause a slight change in volume and b) subsequent arranging of the atoms to their final lattice location. Both phases occur in the austenite-martensite transformation, however, only the first phase in cobalt. The shear angle in cobalt is approximately 20^{o} and one might assume (1) that a dislocation mechanism is co-operative. Figure 24 shows a mechanism whereby the required shear stage of the transformation is accomplished by means of a spiral source, that is a third dislocation climbs around a polar dislocation made up of two dislocations. In order for this mechanism to work it is necessary to have three dislocations with Burgers vectors b_1, b_2 and b_3 which are energetically feasible and indeed present. This topic of phase transformations will be discussed in very much greater detail by Professor Newkirk later during this conference.

4.0 FAILURE MECHANISMS

In this chapter an attempt will be made to survey the mechanisms of failure in metal parts with special consideration of their behavior at elevated temperatures. The discussion will be limited to four modes of failure and their explanation in terms of the defect reactions discussed previously. They are: 1) Deformation under increasing loads, in other words the phenomena occuring during a tensile test. 2) The deformation under constant load or stress, i.e. the various creep phenomena. 3) The occurrence of fracture and 4) Evaporation.

4.1 DEFORMATION UNDER INCREASING LOAD

The discussion centers on the shape of the stress strain curve and the mechanisms which can account for the stress strain curve. Although materials showing complete brittleness, that is no plastic deformation prior to fracture, are of considerable theoretical interest, the technical usage of such materials is rather rare. In general the materials employed for technical applications show some degree of plasticity or ductility. For this reason the discussion will primarily deal with the phenomena occurring above the yield strength, that is crystal plasticity.

The plastic deformations of crystals has been shown to take place in the form of sliding of crystallographic planes on top of each other. This slip mechanism can be described in terms of the slip direction and the slip plane, Figure 25. Evidence was also presented that this slip is accomplished by the motion of dislocations through a crystal. The slip direction is that direction having the shortest Burger's vector and therefore it is given by the direction of the shortest lattice vector in the Bravais lattice. This is indeed the case.* The only exceptions are the intermetallic compounds PbTe, AgMg and the ordered phase of β^1 - CuZn. This may be explained in terms of the ordering process occurring in these crystals. A complete dislocation in the unordered phase having a smaller Bravais lattice than the ordered phase, may split up into two partial dislocations in the ordered phase between which we have a stacking fault. These stacking faults constitute the boundaries between the ordered and the anti-phase regions. This applies to the slip direction of PbTe, AgMg, and the ordered phase of β^1 - CuZn. It should also be noted that during the motion of these partial dislocations the order of the intermetallic compounds is destroyed. Cottrell (67) and Rachinger (68) have explained this in terms of a very low energy of ordering. Seeger (2) has pointed out that in all alloys where the ordering takes place below the melting point one might expect the presence of partial dislocations in the ordered structure. It will also be extremely unlikely, even if

*See (2) p. 26.

the energies of ordering are high, that these dislocations will combine to complete dislocations so that one can always expect the slip direction to be determined by the incomplete dislocations.

As already indicated, it is much more difficult to define the slip plane in terms of dislocations mechanics. The energy and the Peierls stress of a dislocation determines whether a lattice plane can function as slip plane or not. However, the density of packing has a considerable effect as is illustrated by the low temperature results on hexagonal metals. There it can be shown that slip plane is the basal plane if $c/a > \sqrt{3}$ and it is one of the prism planes if $c/a < \sqrt{3}$. This pertains to metals having a high stacking fault energy. In metals having a low stacking fault energy one must consider the action of partial dislocations and thus it may be possible that even in metals having a strongly subnormal c/a ratio such as osmium and rhenium the basal plane might be the preferred slip plane.

The deformation of single crystals under increasing load is best discussed on the basis of the shear stress shear strain diagram illustrated in Figure 26. The definition of the critical shear stress is also indicated in Figure 26. As the shear stress is increased above the critical shear stress we have a strain hardening portion of the stress-strain diagram which again, at least in fcc metals, can be subdivided into three stages.

The critical shear stress for metal single crystal at room temperature is in the neighborhood of 20-50 gm/mm^2. Schmid (69) has shown that the critical shear stress for a given slip system is independent of the crystal orientation. This statement has become known under the name "Schmid's Shear Stress Law". In terms of dislocation mechanics it can be stated that "the force acting on the dislocations is responsible for the initiation of slip". It should be noted, however, that there are deviations from this law and that an orientation dependence becomes marked if the crystallographic orientation lies somewhere near the edge of the stereographic orientation triangle. At low temperatures the critical shear stress generally decreases with increasing temperature while at higher temperatures this quantity becomes nearly temperature independent. An increase in the deformation rate is equivalent to a decrease in the test temperature. Here, too, the velocity dependence of the critical shear stress is very small. Examples of the critical shear stress as a function of the absolute temperature are given in Figure 27.

In alloys having low concentrations of second elements we generally find an increase of the critical shear stress with increasing alloy concentration. The critical shear stress at low temperatures becomes now quite temperature dependent. In the high temperature region where the critical shear stress again becomes almost independent of the testing temperature a serrated stress strain diagram is observed (cf. Figure 27) indicating that the deformation occurs in form of jumps.

The existence and temperature dependence of the critical shear stress may be interpreted as follows. Assuming (70) that the mean distance between dislocations in annealed single crystals is between 10^{-4} and 10^{-3} cm, there is in a crystal a very large number of long dislocation sources and the generation of dislocations can occur under very low stresses. This dislocation network causes an internal stress field in the crystal whose periodicity ℓ_b is given by the spacing of the immobile dislocations.

Figure 28 shows such an arrangement schematically. The shear stress necessary to move the dislocations in the glide plane is given by:

$$\tau_G = \frac{G}{2\pi(1 - \nu)} \frac{b}{\ell_0} \qquad \text{Equation 20}$$

for edge dislocations and:

$$\tau_G = \frac{G}{2\pi} \frac{b}{\ell_0} \qquad \text{Equation 21}$$

for screw dislocations. This mechanism is independent of the temperature with the exception of the temperature dependence of the shear modulus G. Another contribution to the critical shear stress comes from the process where dislocations have to intersect each other. This process is associated with the formation of dislocation jogs and the creation of atomic defects. Cottrell (71) and Mott (72) have shown that the activation energy for such a process is decreased under the presence of a shear stress. The shear stress required for such a climbing is given by:

$$\tau = \tau_G = \frac{U_o - kT \log \left(N.F.b. \frac{v_o}{\dot{a}}\right)}{v}$$

N = number of dislocations per unit volume
F = area per dislocation per activation
v_o = Debye frequency ($\sim 8.4.10^{12}$ cps)
$\dot{a}$ = strain rate
v = activation volume
T = temperature
U_o = activation energy

Equation 22

The first part of this equation is the previously discussed component illustrated in Figure 28. The above equation is only valid as long as $t > t_G$. The temperature T_o ($t = t_G$) which may be interpreted as the temperature above which the critical shear stress is temperature independent is given by:

$$T_o = \frac{U_o}{k \log \left(N.F.b. \frac{v_o}{\dot{a}}\right)} \qquad \text{Equation 23}$$

Thus at absolute zero the critical shear stress is independent of the deformation velocity a and is given by:

$$\tau_T = 0^{\circ}K = \tau_G + \frac{U_o}{v} \qquad \text{Equation 24}$$

The above comments pertain primarily to metals having a high stacking fault energy. In metals having a low stacking fault energy we need the additional mechanism of constriction before a climbing process can take place. This is a contribution to the energy of the climbing process

which is considerably higher than that required for the formation of the jog. While in metals having a high stacking fault energy one may conclude that edge dislocations move faster than the screw dislocations which causes an elliptical shape of the dislocation lines. The same statement cannot be made for metals having a low stacking fault energy. Here several processes may be active which could be characterized by their activation stress, their temperature and their activation energy. Thus the critical shear stress versus test temperature curve is obtained from the sum of these individual contributions as illustrated in Figure 29. This schematic illustration represents the actual case present in deformed copper single crystals.

The remainder of the stress strain diagram is characterized by the fact that the shear stress increases with increasing shear strain. The oldest proposal for an explanation for this phenomenon is due to Taylor (51) who explains strain hardening in terms of a reduction of the movement of dislocations which is due to the stress fields created by the increasing number of dislocations. A second model for the explanation of strain hardening is called the strain exhaustion hypothesis. This model states that the flow stress is determined by the number of dislocation sources which have the lowest activation stress. These sources are generally the longest sources. Strain hardening is caused by a blocking of a number of these sources so that with increasing strain more and more sources having a higher critical flow stress must be activated. These two hypotheses can be combined by making the assumption that the strain hardening is due to a number of dislocations becoming blocked inside the crystal during the deformation process.

Latent strain hardening is the type of strain hardening which takes place in a non-active slip system, if it is suddenly called upon through a change of the loading on the crystal. The Bauschinger effect is a special case of such latent strain hardening. Here it is observed that after a certain degree of strain hardening has been reached in one direction the start of plastic flow in the opposite direction occurs under a much lower stress. This is illustrated in Figure 30 which is taken from Sachs and Shoji (73). The reduction in the shear stress at which plastic flow is initiated in the opposite direction is due to an unstressing of piled-up dislocations. The general case of latent strain hardening is illustrated in Figure 30 (74) which shows the stress-strain curves for Zn single crystals first loaded in one direction in the basal plane and then in the directions inclined at angles of 60° and 120° to the first, again in the basal plane.

Often the primary slip system is relieved by its conugate slip system or double slip. This causes a gradual change of the orientation of the slip plane with respect to the specimen axis. If the latent strain hardening of the conjugate slip system is larger than that of the primary slip system, the specimen axis rotates beyond the symmetry axis of the two slip systems. If the latent strain hardening is smaller in the conujugate slip system, the specimen axis never reaches the symmetry axis but bends towards the (211) pole lying on that axis.

The flow curves of the hexagonal metals which deform primarily in basal glide can be postulated from the above equations. One finds, that the slope of the stress strain curve in the strain hardening region must be given by:

$$\frac{d\tau}{da} = \phi = \frac{d\tau_G(a)}{da} \qquad \text{Equation 25}$$

and does not depend upon the test temperature. This is due to the fact that the temperature dependent term becomes zero after differentiation, since the activation volume v(a) does not

change with the strain, see equation 24. (As long as the slip system is limited to the basal plane, the density of the dislocation forest does not change). The theory thus predicts a temperature independent slope of the stress strain curve at low temperatures. The results on Cd and Mg confirm these predictions, see Figure 27. At higher temperatures the strain hardening coefficient decreases markedly. It also becomes rate sensitive. Polanyi and Schmid (75) have connected this softening with the start of the static recovery in Cd. Similar evidence was obtained for Zn (76).

Some data are also available on the effect of alloying. Figure 31 shows the effect of Al and Zn additions to Mg. In the former case the slope ϕ first increases, but for concentrations in excess of 6.8%, decreases. Small additions of Zn to Mg seem to have little effect on the slope of the curve, see Figure 31. In Zn-Cd crystals the strain hardening coefficient at room temperature decreases with increasing Cd concentration (10) a phenomenon generally observed in fcc alloy crystals. The critical shear stress increases in all cases, as discussed above.

By far the largest amount of data is available for fcc single crystals. The flow curves of these crystals fall all in the general pattern illustrated in Figure 32 which shows the presence of three distinct regions (identified as I, II, III). These regions are characterized by three distinctly different strain hardening coefficients.

Region I, also called easy glide region, is characterized by a very low strain hardening coefficient, ($\phi/G = 1.4.10^{-4}$) which, however, depends on the crystal orientation with respect to the direction of stress and the thickness of the specimen. It can increase to about 10 times that of region II. Suzuki, Ikeda und Takeuchi (77) have shown that this orientation dependence disappears as the specimen diameter is below 0.4 mm. Seeger (2) concludes that two basic mechanisms must be active to account for the observed behavior. One of them is identical to that operative in hexagonal metals, discussed above, equation 20. No barriers are created during this process. The second mechanism which is needed to explain the thickness and orientation effect is believed (2) to be the formation of dislocation barriers in the form of Cottrell-Lomer dislocations. Such a model leads to a strain hardening coefficient of approximately ($\phi/G = 6.10^{-4}$ which is in general agreement with the experimental results. The conditions necessary for the creation of Cottrell-Lomer dislocations and their effect on moving dislocation lines explain the observed orientation and thickness dependence.

In the transition from region I to region II a second group of Cottrell-Lomer dislocations is added which limits the motion of the dislocations in the primary slip plane in all directions.

Region II is characterized by a very high strain hardening coefficient. The motion of dislocations in the (111) plane is now limited in all directions by the Cottrell-Lomer barriers (as shown in Figure 33). The strain hardening coefficient is nearly temperature independent. The length of the dislocation line decreases linearly with increasing strain (78). Temperature cycling experiments (79) have shown that the high strain hardening coefficient is not due to an increase in the density of dislocation forest, but rather that the slip in the secondary system has a catalytic action on the formation of additional Cottrell-Lomer dislocations. The fact that alloying additions have little influence on the strain hardening coefficient in this region is not in conflict with the above model as the strain hardening exponent depends on nb/l where l is a model constant related to the length of the dislocation line. The metal surface in region II may, according to Mader (78) be termed structured microslip. Recent measurements have shown that the dislocation density in Cu and Al single crystals increases from $\approx 10^8/cm^2$ in the annealed state to $\approx 10^{10} - 10^{11}/cm^2$ if stressed beyond the easy glide region, a > 10^{-3}.

In region III of the flow curve an irreversible temperature dependence is observed, see Figure 32. Here then, the mechanism responsible for the high strain hardening coefficient of region II is partially eliminated by thermally activated processes (2). This recovery, a typical example of dynamical recovery, is strongly stress dependent. The process responsible for this recovery is thermally activated cross slip of screw dislocations (80, 81, 79). Such cross slip again depends on the stacking fault energy and occurs easily in Al and Pb at room temperature, while not in Cu and other fcc metals. On the surface glide bands and fragmented glide bands are observed.

The energy of stacking faults is a dominant factor governing the deformation modes of alloy crystals. In Cu-Ge and Cu-Ga alloy crystals it decreases rapidly with increasing concentrations of Ge or Ga from $\approx$ 105-165erg/cm^2 to $\approx$ 10erg/cm^2 as a function of the electron-concentration. (1.15 to 1.2, phase boundary 1.40) This causes an increase in t_{III} (cross slip) and the formation of deformation twins, independent of temperature but dependent on the concentration.**

4.2 DEFORMATION UNDER A CONSTANT LOAD OR STRESS

Since the last lecture of this conference by Professor Grant is primarily concerned with the phenomena occuring under a steady applied stress or load, they will not be covered here. It might only be mentioned that the beta-creep portion of transient creep in fcc metals appears to be related to the region III of the flow curve (82).

4.3 FRACTURE

A description of the occurrence of fracture in terms of the crystal defects has been presented by Petch (83) and Cottrett (84). Here we are mainly concerned with the creation of cracks within a grain. From there on the engineering fracture concepts for polycrystalline materials such as fracture mechanics developed by Irwin and associates or the Neuber concept developed at Syracuse University (85) can be applied with more or less success. From a defect structure point of view the question arises as to what mechanisms are responsible for the formation of a crack across a single grain.

The problem is how the conversion from glide dislocations to cavity dislocations takes place. Four possible models are shown in Figure 34 taken from Cottrell (86). The mechanisms illustrated are: 1) pile-up of edge dislocations, 2) pile-up in a slip band of edge dislocations against a grain boundary, 3) shear on two intersecting slip bands and 4) slip band crossing a tilt boundary. In order for any of these systems to work it is necessary that the elastic energy which the dislocations bring with them is not rapidly dispersed through plastic flow in the nearby material. In materials having only one or two easy slip systems the mechanisms are feasible-the brittleness of hexagonal metals can be explained on this basis, cf. Figure 4. For cubic crystals with good slip systems in several directions, Mott (87) and Stroh (88) pointed out that a yield drop is required for the mechanism to work. Such a phenomenon gives rise to dislocation avalanches which run together and form a crack before nearby dislocation sources can start working. With the help of these micromechanisms for crack formation, and the Griffith concept, Cottrell (83) and Petch (84) were able to define fracture in terms of the yield strength, the dislocation pinning strength and the surface tension by the well known equation,

*Hordon, M.J. and Averbach, B.L. Acta Met. v 9 (1961) No. 3, p. 237.

**Haasen, P. and King, A. Zeit. Metallkunde v 51/12 (1960) p. 722.

$$\sigma_y \, k_y \, d^{1/2} = \beta G \gamma$$

σ_y = yield strength

d = grain size

γ = surface tension

$k_y = \sigma_D \cdot \ell^{1/2}$ Equation 26

σ_D = unpinning stress for dislocation

ℓ = spacing of sources

This equation gives information on both brittle and ductile fracture. When the left hand side exceeds the right hand side, the yield stress is more than sufficient to propagate the microcracks. On the other hand, when the right hand side is larger than the left hand side, the yield stress does not suffice to propagate the microcracks. The equality sign defines the condition for fracture transition. It is interesting to note, that the surface energy finds its way into the above equation via the Griffith concept. Thus far, there was no direct information available concerning the effect of surface tension. Recent experiments on the effect of liquid metals on the fracture of solid metals (89) illustrate the predicted role of surface tension rather drastically.

4.4 EVAPORATION

The final failure mechanism mentioned before is that of evaporation. Quantum mechanics gives the following formula for the vapor pressure (90).

$$P_{(T)} = \left(\frac{2\pi M}{h^2}\right)^{3/2} (kT)^{5/2} \exp. \{(F_k - E_b)/kT\}$$

F_k = force energy of lattice vibration

M = molar mass Equation 27

E_b = binding energy

For high temperature this reduces to:

$$P_{(T)} = \frac{(18\pi M \omega_D^2)^{3/2}}{\sqrt{kT}} \, e^{-E_b/kT} \qquad \text{Equation 28}$$

The evaporation rate itself* is governed by the composition of the surrounding atmosphere. If we assume that none of the evaporated atoms return we obtain the curves shown in Figure 35 (91). An indication concerning the relative evaporation rate of two elements constituting a dilute solid solution of one of them can be obtained with the help of Raoult's law which states

*With the help of the Clausius-Clapeyron equation one can calculate the heat of evaporation per atom $q(T) = E_b - \frac{1}{2} k T$ as a function of the temperature. Equation 29

that the vapor pressure of a component A of a dilute solution is reduced approximately by the mole fraction of A present. However, it has been repeatedly pointed out that this is only a very rough approximation and may not apply at all. If the law applied strictly, no disturbance of a chemical makeup of the solid in question would occur. It is well known that the evaporation rate also depends on the crystallographic orientation. This is the underlying effect made use of in thermal etching.

5.0 SUMMARY

The properties of solids that can be derived from the electron theory of metals or similar assumptions fall in the group of structure insensitive properties. Here the agreement between theoretical prediction and experimental evidence is satisfactory. An application of the same principles to mechanical properties of materials, most of which are structure sensitive, leads to disagreement between theory and experiment to the order of 10^{-3} or more. This is due to the fact that the mechanical properties are extremely sensitive to structural defects. Such defects are introduced both in the manufacture as well as during the service life of metal parts.

These defects can be classified according to their geometrical order into point defects (vacancies and interstitials) line defects (dislocations) and area defects (low and high angle boundaries). By far the most experimental evidence exists for fcc metals. Generally the mechanism of interaction between like and unlike defects and the motion of these defects contain temperature dependent and temperature independent terms. The temperature dependence is usually exponential and mechanisms have been deduced whose activation energies are in agreement with the experimentally observed activation energies. Most of the defect reactions were arrived at in retrospect, however, there exists now considerable quasi-direct experimental evidence for the existence of these defects and some of their reactions. The stress-strain curve for face centered cubic single crystals can be almost completely defined in terms of the various dislocation reactions. An application of these mechanisms to materials in the polycrystal state cannot be expected at the present time in any quantitative sense, however, some qualitative considerations are possible.

For an accounting of the various modes of failure namely deformation under increasing load, creep, fracture, and evaporation, the defect concepts developed can also be applied. This is especially true for the three mechanical failure modes which are extremely structure sensitive. To a first approximation, evaporation may be considered a structure insensitive property of material and thermodynamical treatments of the phenomena are usually adequate.

REFERENCES

1. A Seeger, Encyclopedia of Physics, Vol. VII/1, Springer-Verlag (1955) p. 383.
2. A. Seeger, Encyclopedia of Physics, Vol. VII/II, Springer-Verlag (1958) p. 1.
3. Creep and Fracture of Metals at High Temperatures, Proc. Sympl Natl. Phys. Lab., Her Maj. Stat. Office, London (1956).
4. Conference on Creep of Metals, Nat. Phys. Lab., Teddington, England (1946).
5. I. E. Campbell, High Temperature Technology, John Wiley, New York (1956).
6. Symposium on "High-Temperature Materials, Methods, and Measurements," The Electro-Chemical Society (1951).
7. C. L. Clark, High Temperature Alloys, Pitman Publishing Co., New York (1953).
8. G. V. Smith, Properties of Metals at Elevated Temperatures, McGraw-Hill, New York (1950).
9. High Temperature Properties of Metals, Am. Soc. Metals (1952).
10. E. Schmid and W. Boas, Plasticity of Crystals, F. A. Hughes and Co., London (1950).
11. F. Seitz, The Modern Theory of Solids, McGraw-Hill Book Company, Inc., New York (1940).
12. C. Kittell, Introduction to Solid State Physics, John Wiley and Sons, Inc., New York (1956).
13. C. Zwikker, Physical Properties of Solid Materials, Permagon Press, New York (1954).
14. N. F. Mott and H. Jones, The Theory of the Properties of Metals and Alloys, Clarendon Press, Oxford (1936).
15. W. Hume-Rothery, Atomic Theory for Students of Metallurgy, The Institute of Metals, London (1960).
16. U. Dehlinger, Theoretical Metallurgy, Springer-Verlag, Berlin (1955).
17. F. Kohlrausch, Selected Topics of Physics, Vol. 5, Structure of Matter, Springer-Verlag, Berlin (1949).
18. A. H. Cottrell, Theoretical Structural Metallurgy, St. Martin's Press, Inc., New York (1957).
19. C. S. Barrett, Structure of Metals, McGraw-Hill (1952) p. 297.
20. P. Drude, Ann. der Physik, Vol. 7 (1902) p. 687.
21. A. Summerfeld, Zeit. Phys., Vol. 47 (1928) p. 1.
22. F. Block, Elecktronentheorie der Metalle, Handbuck der Radiologie (1933) p. 226.

23. L. Brillouin, Die Quantenstatistik, Springer, Berlin (1936).

24. E. W. Muller, Modern Research Techniques in Physical Metallurgy, Am. Soc. Metals (1953) p. 33.

25. R. H. Good, Jr., and E. W. Muller, Encyclopedia of Physics, Vol. 21, Springer-Verlag, Berlin (1956) p. 174.

26. G. Mie (1905).

27. H. Ebert, Phys. Zeit, Vol. 36 (1935) p. 388.

28. P. W. Bridgman, Rev. Mod. Phys., Vol. 7 (1935) p. 1.

29. M. Born and E. Brody, Zeit. Phys., Vol. 6 (1921) p. 132.

30. P. S. Epstein, Phys. Rev., Vol. 41 (1932) p. 91.

31. A. Smekal, Encyclopedia of Physics, 2nd Edition, Vol. 24/II Springer, Berlin (1933).

32. R. W. James, The Optical Principles of the Diffraction of X-Rays, G. Bell, London (1948).

33. A. A. Griffith, Phil. Trans. Roy. Soc., Series A., Vol. 221 (1921) p. 163.

34. H. B. Huntington and F. Seitz, Phys. Rev., Vol. 76 (1949) p. 1728.

35. J. E. Dorn, Symposium on Creep and Fracture of Metals at High Temperatures, Teddington (1954).

36. F. Seitz, Imperfections in Nearly Perfect Crystals, John Wiley, New York (1952) p. 3.

37. H. Pick, Naturwiss, Vol. 14 (1954) p. 346.

38. J. Frenkel, Zeit. Phys., Vol. 35 (1926) p. 652.

39. C. Wagner and W. Schottky, Zeit. Phys. Chem. Section B, Vol. 11 (1930) p. 163.

40. W. Jost, J. Chem. Phys., Vol. 1 (1933) p. 466.

41. N. F. Mott and R. W. Gurney, Electronic Processes in Ionic Crystals, Oxford (1948).

42. F. G. Fumi, Phil. Mag., Vol. 46 (1955) p. 1007.

43. H. B. Huntington, Phys. Rev., Vol. 91 (1953) p. 1092.

44. H. B. Huntington, Phys. Rev., Vol. 61 (1942) p. 325.

45. See reference (36) p. 289.

46. C. Zener, Acta Cryst., Vol. 3 (1950) p. 346.

47. A. D. Le Claire, Acta Met., Vol. 1 (1953) p. 438.

48. P. Jongenburger, Appl. Sci. Res. B., Vol. 3 (1953) p. 237.

49. J. W. Kauffman and J. S. Koehler, Phy. Rev., Vol. 88 (1952) p. 149.

50. C. Zener, Elasticity and Anelasticity of Metals, University of Chicago Press, Chicago (1948) p. 111ff.

51. G. I. Taylor, Proc. Roy. Soc. A., Vol. 145 (1934) p. 362.

52. E. Orowan, Zeit. Phys., Vol. 89 (1934) p. 634.

53. M. Polanyi, Zeit. Phys., Vol. 89 (1934) p. 660.

54. A. H. Cottrell, Dislocations and Plastic Flow in Crystals, Oxford (1953).

55. F. C. Frank and W. T. Read, Phys. Rev., Vol. 79 (1950) p. 722.

56. W. T. Read, Dislocations in Crystals, McGraw-Hill (1953) p. 70.

57. A. Seeger, Report of the Bristol Conference on Defects in Crystalline Solids, The Physical Society, London (1955) p. 391.

58. A. N. Stroh, Proc. Phys. Soc. Lond., Ser. B, Vol. 67 (1954) p. 427.

59. J. Frenkel and T. Kontorova, J. Phys. U. S. S. R., Vol. 1 (1939) p. 137.

60. R. Peierls, Proc. Phys. Soc. Lond., Vol. 52 (1940) p. 34.

61. J. Washburn and E. R. Parker, J. Metals, Vol. 4 (1952) p. 1076.

62. See reference (36) p. 352.

63. W. T. Read, Conference on Mechanical Effects of Dislocations in Crystals, Birmingham (1954) - see also reference (56) p. 172.

64. K. Lucke, Zeit. Metallkunde, Vol. 44 (1953) p. 370, 418.

65. T'ing Sui Kê, J. Appl. Phys., Vol. 19 (1948) p. 285.

66. N. F. Mott, Proc. Phys. Soc. Lond., Vol. 60 (1948) p. 391.

67. A. H. Cottrell, Deformation and Flow of Solids, Madrid Colloquim, Springer-Verlag (1956).

68. W. A. Rachinger and A. H. Cottrell, Acta Met., Vol. 4 (1956) p. 109.

69. E. Schmid, Proc. Int. Cong. Appl. Mech. Delft. (1924) p. 342.

70. A. Seeger, Zeit. Naturforsch, Vol. 9a (1954) p. 758.

71. A. H. Cottrell, L'Etat Solide (Bericht Vom 9. Solvay-Kongress fur Physik) Brussel: R. Stoops, (1952) p. 421.

72. N. F. Mott, Phil. Mag., Vol. 44 (1953) p. 742.

73. G. Sachs and H. Shoji, Ziet. Physik, Vol. 45 (1927) p. 776.

74. E. H. Edwards and J. Washburn, Trans. A. I. M. E., Vol. 200 (1954) p. 1239.

75. M. Polanji and E. Schmid, Naturwiss, Vol. 17 (1929) p. 301 - see also reference (10).

76. R. Drouard, J. Washburn and E. R. Parker, Trans., A. I. M. E., Vol. 197 (1953) p. 1226.

77. H. Suzuki, S. Ikeda and S. Takenchi, J. Phys. Soc. Japan, Vol. 11 (1956) p. 382.

78. S. Mader, Zeit. Physik, Vol. 149 (1957) p. 73.

79. A. Seeger, J. Diehl, S. Mader and H. Rebstock, Phil. Mag., Vol. 2 (1957) p. 323.

80. J. Diehl, S. Mader and A. Seeger, Zeit. Metallkunde, Vol. 46 (1955) p. 650.

81. See reference (67) p. 90.

82. A. Seeger, Zeit. Naturforsch, Vol 11a (1956) p. 958.

83. N. J. Petch, Phil. Mag., Vol. 3 (1958) p. 1089 - see also J. Heslop and N. J. Petch, Phil. Mag. Vol. 3 (1958) p. 1128.

84. A. H. Cottrell, Trans. Met. Soc. A. I. M. E., Vol. 212 (1958) p. 192.

85. V. Weiss, Proc. Seventh Sagamore Ord. Mat. Res. Conf. (1960).

86. A. H. Cottrell, Fracture, Technology Press and John Wiley (1960) p. 20.

87. N. F. Mott, J. Iron Steel Inst., Vol. 183 (1956) p. 233.

88. A. N. Stroh, Advances in Physics, Vol. 6 (1957) p. 418.

89. W. Rostoker, J. M. McCaughey and H. Markus, Embrittlement by Liquid Metals, Reinhold Publ. Corp. New York (1960).

90. G. Leibfried, Encyclopedia of Physics, Vol. VII/I Springer-Verlag, (1955) p. 316.

91. G. F. Vanderschmidt, Proc. Fifth Sagamore Ord. Mat. Res. Conf. (1958) p. 78.

ACKNOWLEDGEMENT

The authors would like to express their gratitude to the personnel of the Metallurgical Research Laboratory for their help in the preparation of this manuscript. Special thanks are due to the following members of the staff:

Mr. K. S. Grewal
Mr. J. J. McKeon
Mr. J. F. Schell
Mrs. D. A. Anderson
Miss C. L. Swanson

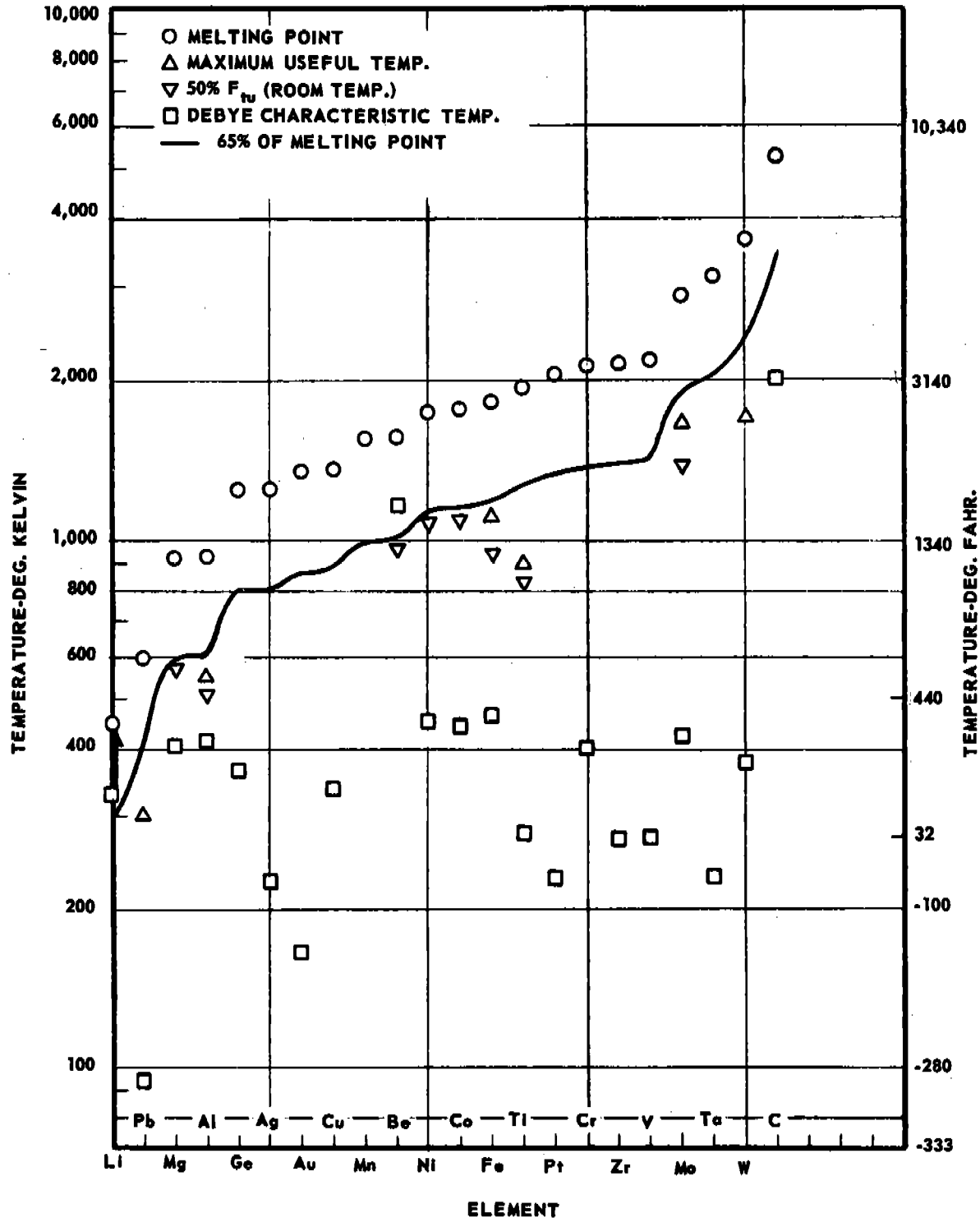

ARRANGEMENT OF METALS IN ORDER OF INCREASING MELTING POINT

FIGURE 1

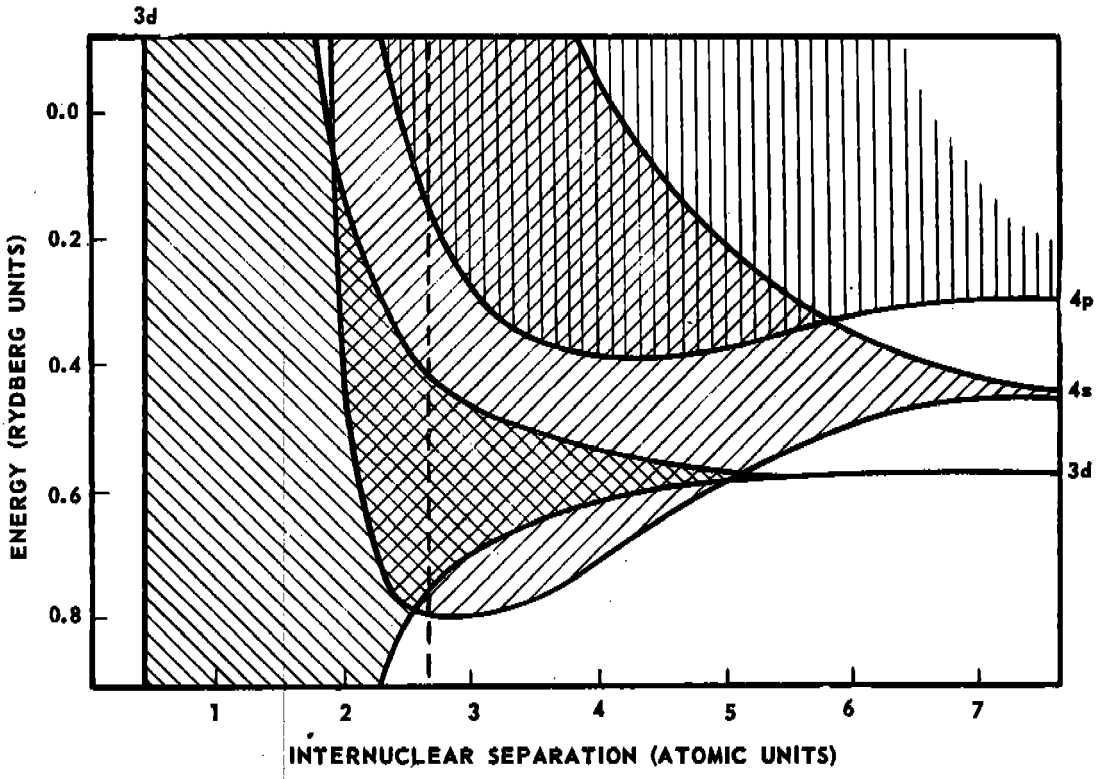

FIGURE 2

ENERGY BANDS IN COPPER AS A FUNCTION OF INTERNUCLEAR SEPARATION. [AFTER H. M. KRUTTER, PHYS. REV. 48, 664 (1935)]

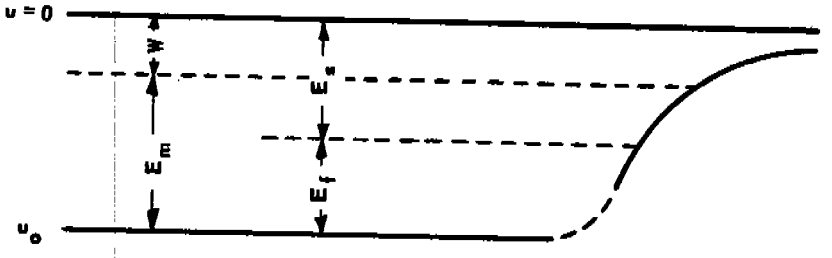

FIGURE 3

MEAN POTENTIAL INSIDE AND OUTSIDE THE CRYSTAL

FIGURES 2 & 3

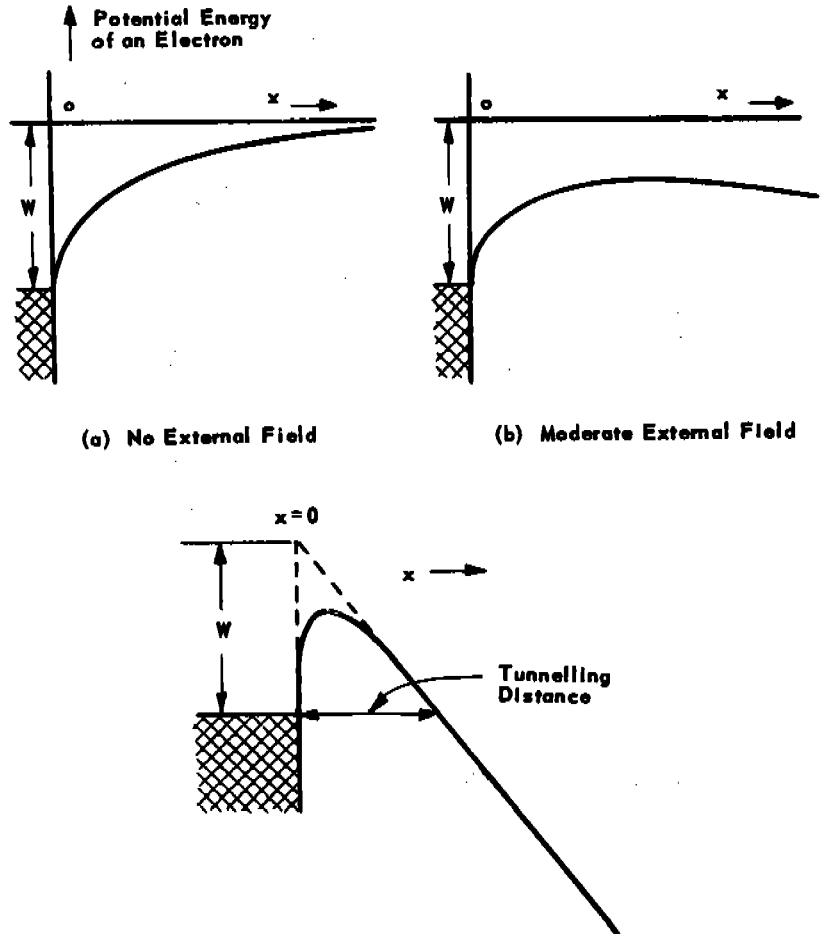

POTENTIAL ENERGY OF AN ELECTRON AS A FUNCTION OF ITS DISTANCE X FROM THE SURFACE OF A METAL

FIGURE 4

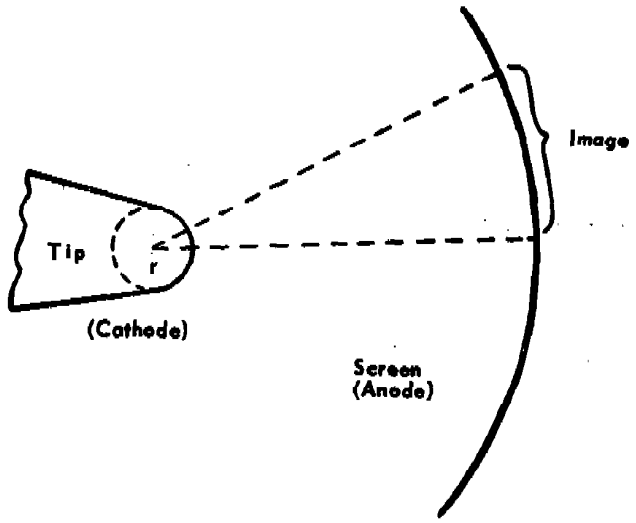

SCHEMATIC DIAGRAM ILLUSTRATING MECHANISM OF IMAGE FORMATION

FIGURE 5

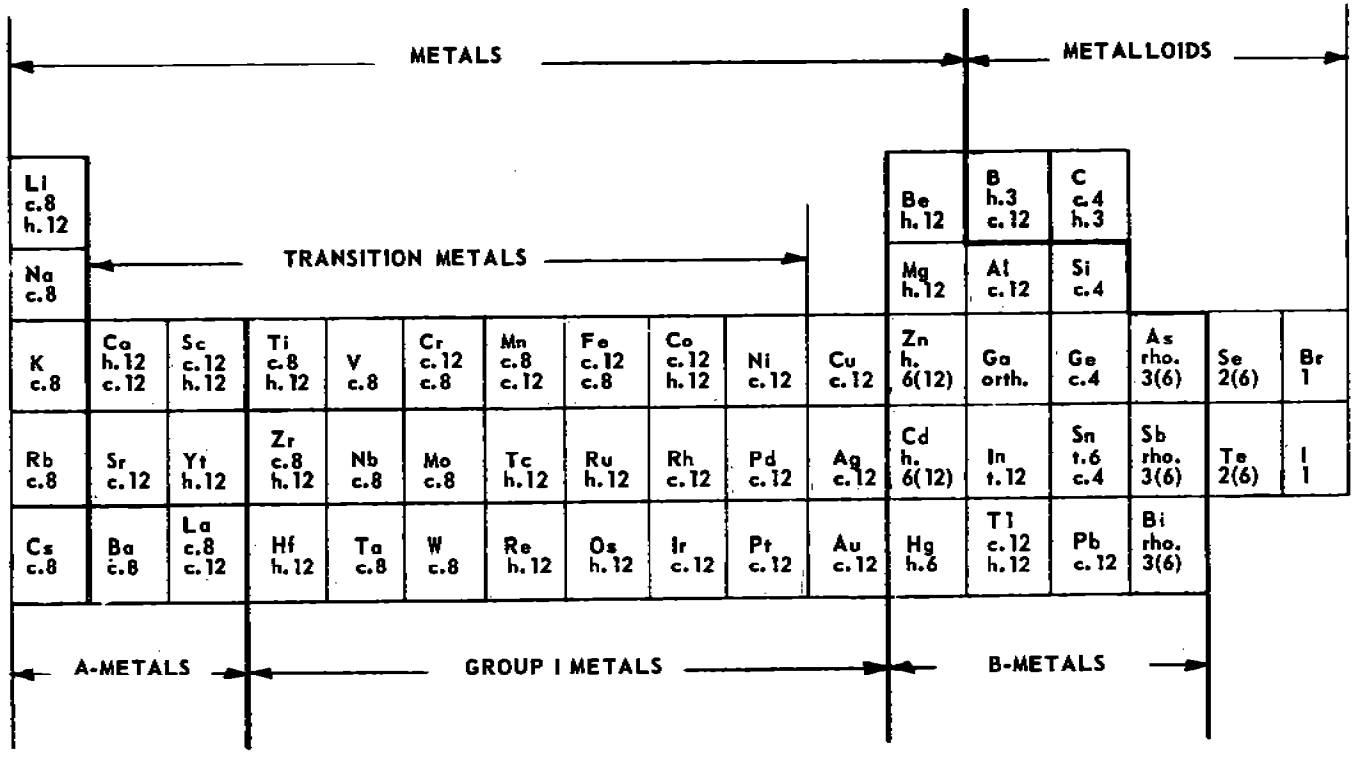

CRYSTAL STRUCTURES OF THE ELEMENTS

c. - CUBIC
h. - HEXAGONAL
t. - TETRAGONAL
rho. - RHOMBOHEDRAL
orth. - ORTHORHOMBIC

FIGURE 6

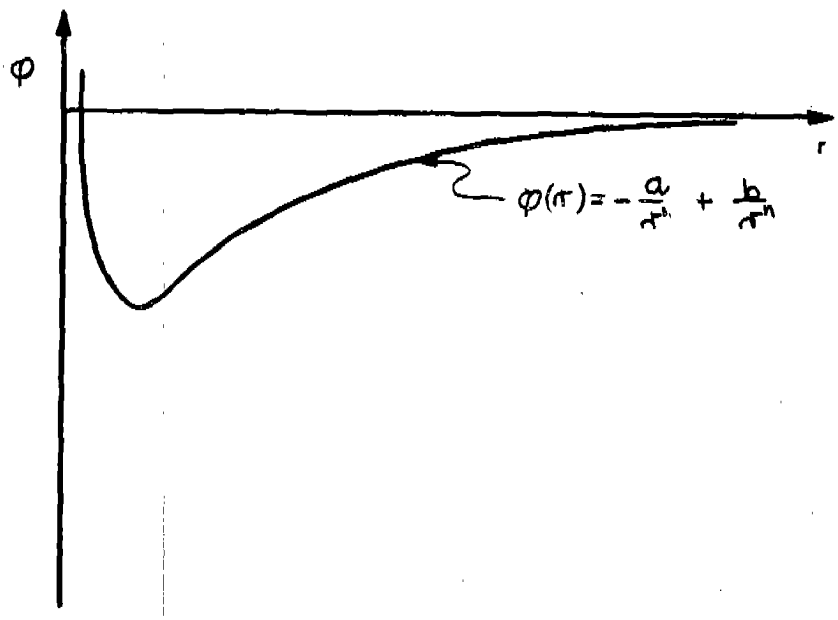

FIGURE 7

MIE'S POTENTIAL FOR TWO ATOMS

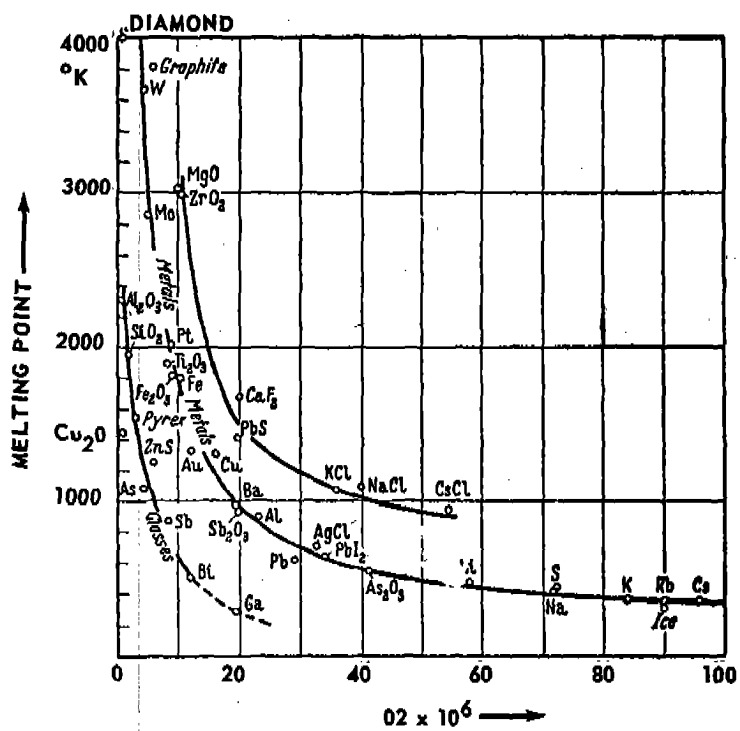

FIGURE 8

RELATION BETWEEN EXPANSION COEFFICIENT AND MELTING POINT. (ZWIKKER)

FIGURES 7 & 8

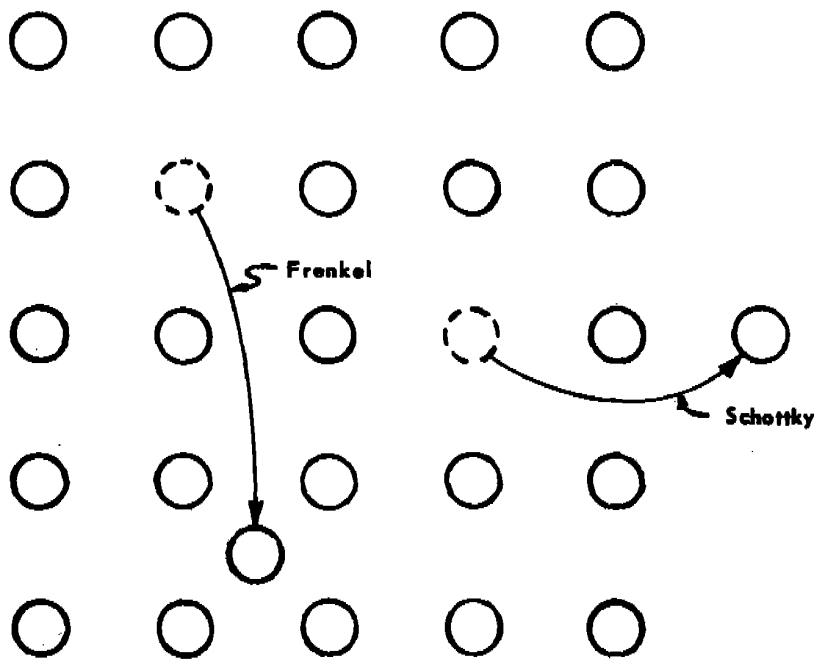

SCHOTTKY AND FRENKEL DEFECTS IN A CRYSTAL. THE ARROWS INDICATE THE DIRECTION OF DISPLACEMENT OF THE ATOMS.

FIGURE 9

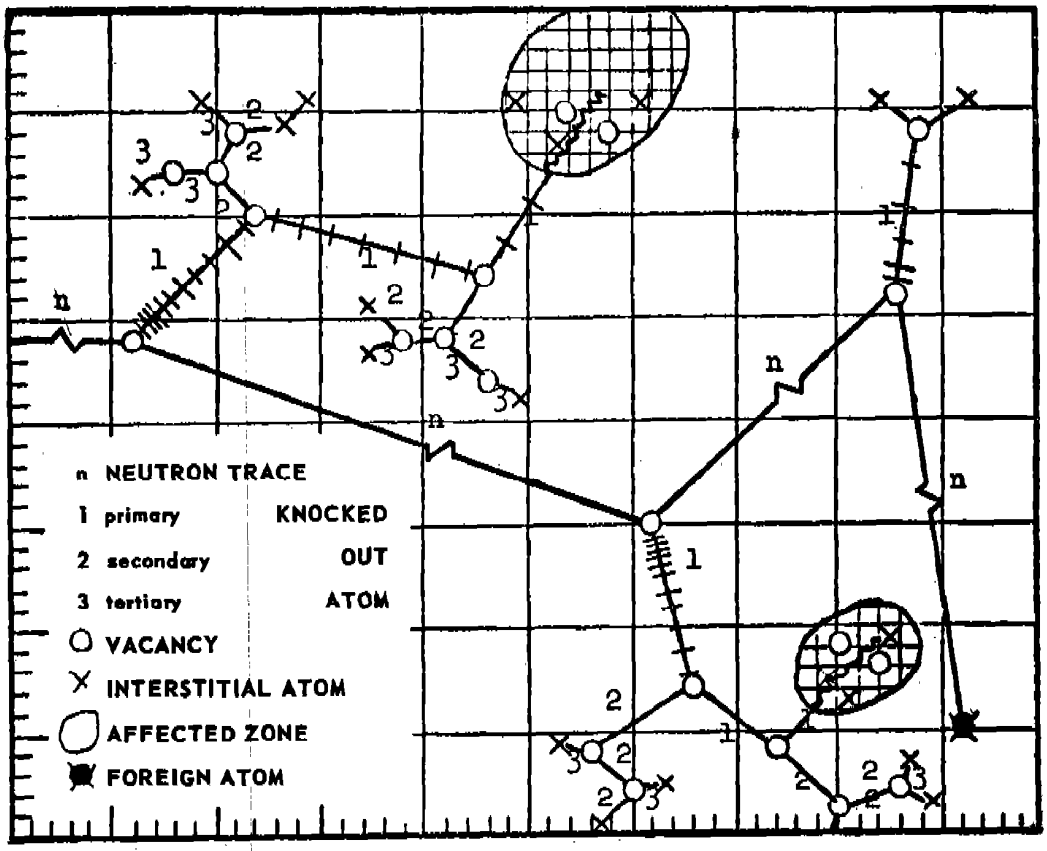

FIGURE 10

MECHANISM OF THE EFFECT OF IRRADIATION ON CRYSTALS. [E. SCHMID, PROC., FIFTH SAGAMORE ORD. MATS. RES. CONFERENCE (1958), p. 206].

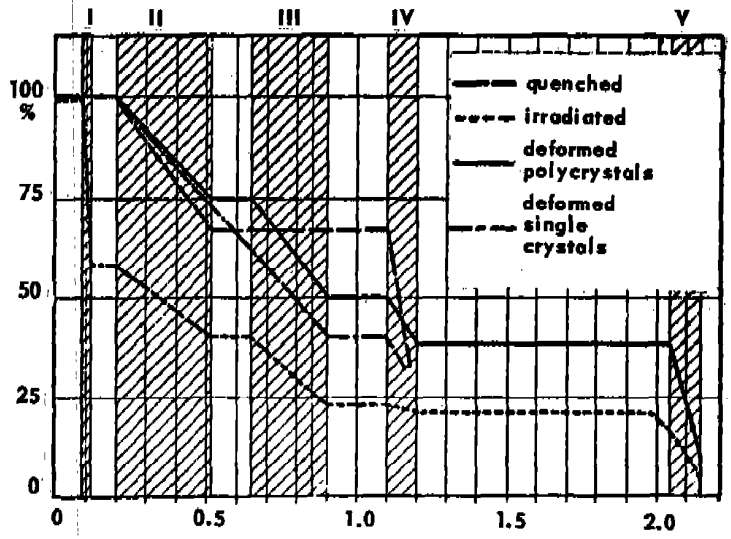

FIGURE 11

SCHEMATIC REPRESENTATION OF THE RECOVERY OF THE RESISTIVITY OF COPPER, (SEEGER).

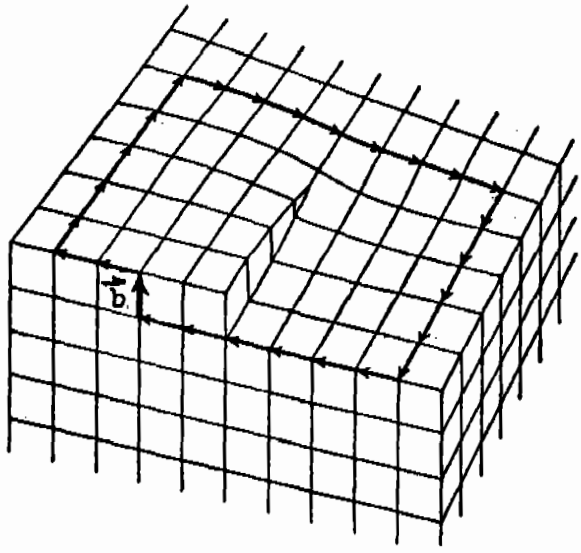

(a) SCREW DISLOCATION

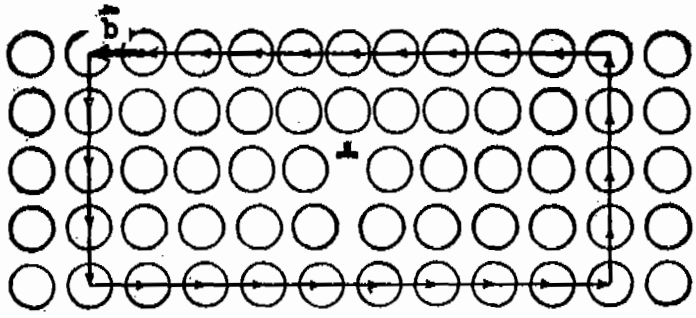

(b) EDGE DISLOCATION

SCREW AND EDGE DISLOCATIONS WITH THEIR RESPECTIVE BURGERS CIRCUITS

FIGURE 12

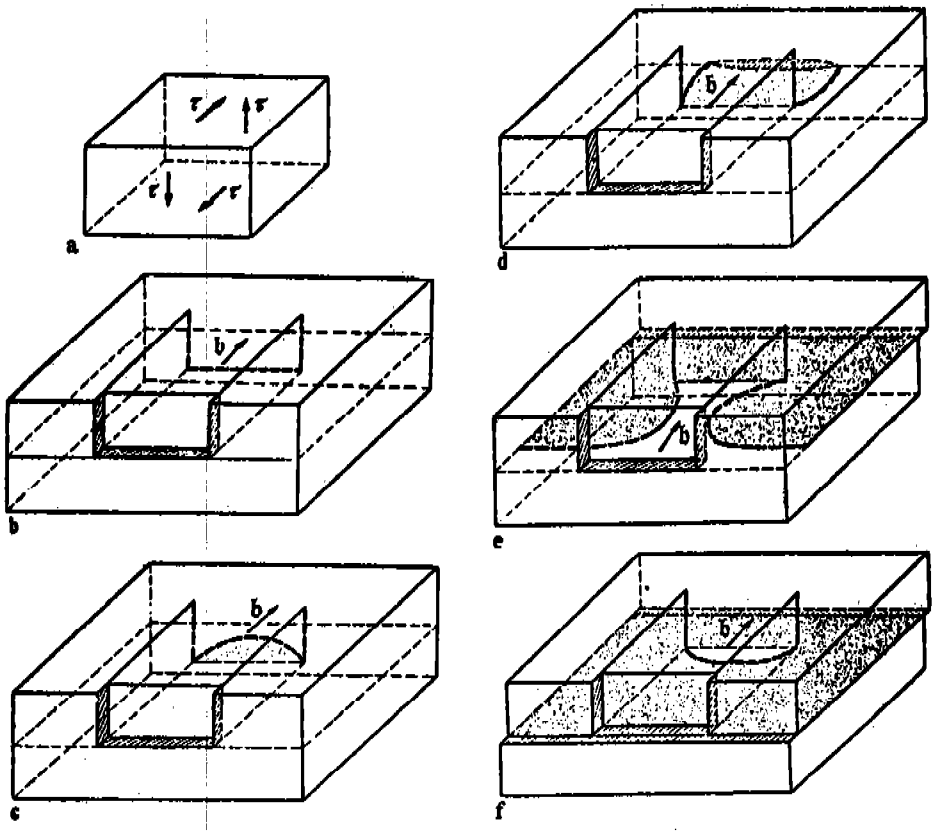

THE OPERATION OF A FRANK-READ SOURCE

FIGURE 13

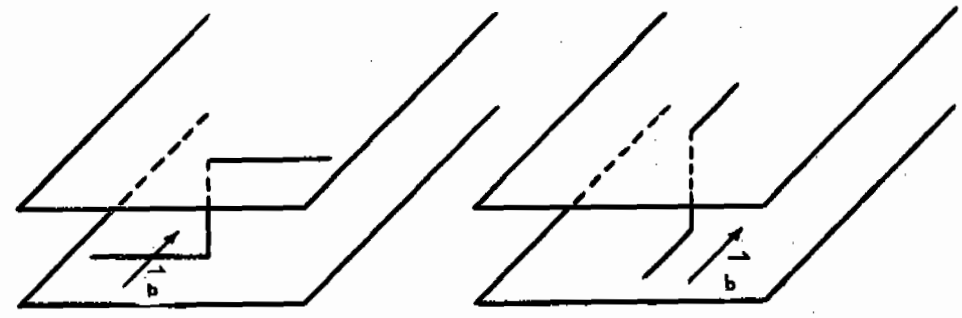

SCHEMATIC ILLUSTRATION OF A JOG

FIGURE 14

SCHEMATIC ILLUSTRATION OF A JOB

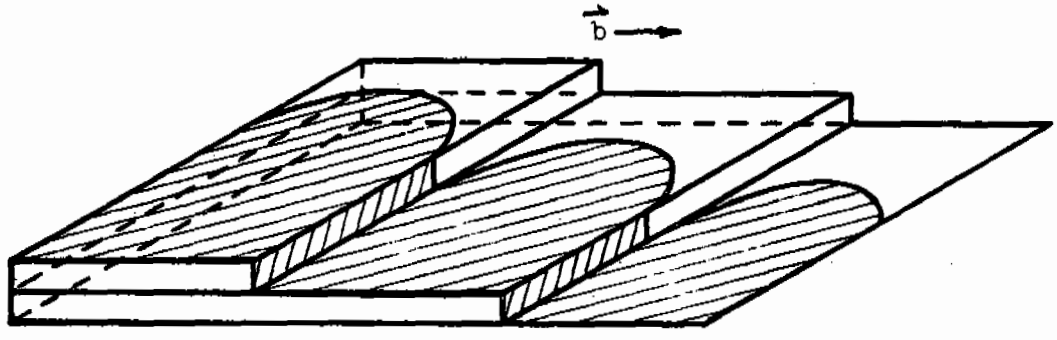

FIGURE 15

FORMATION OF VACANCIES AT JOGS OF DISLOCATION LINES HAVING PREDOMINANTLY SCREW CHARACTER

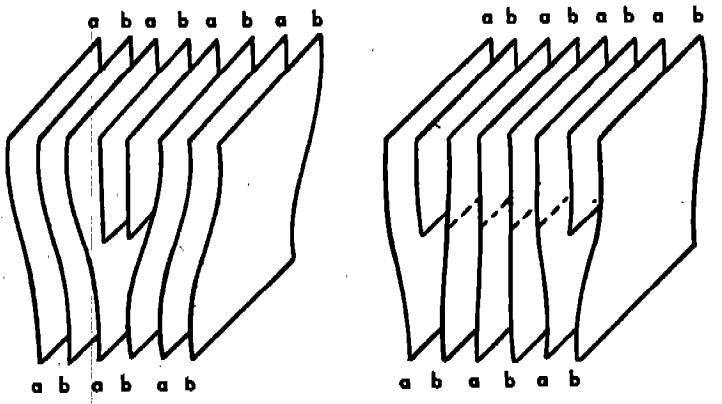

FIGURE 16

COMPLETE DISLOCATION EXTENDED TO FORM A STACKING FAULT IN FCC AND CPH CRYSTALS (100) AND (2110) PLANES RESPECTIVELY

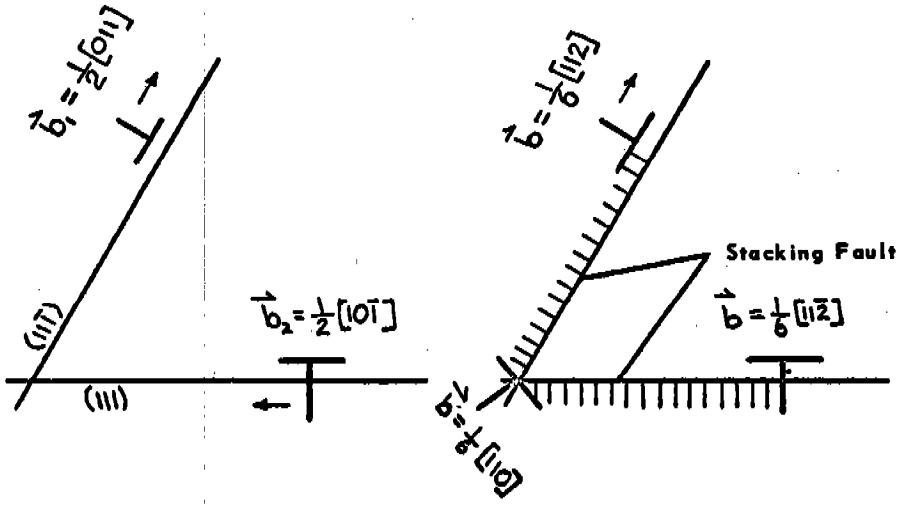

FIGURE 17

LOMER-COTTRELL REACTION

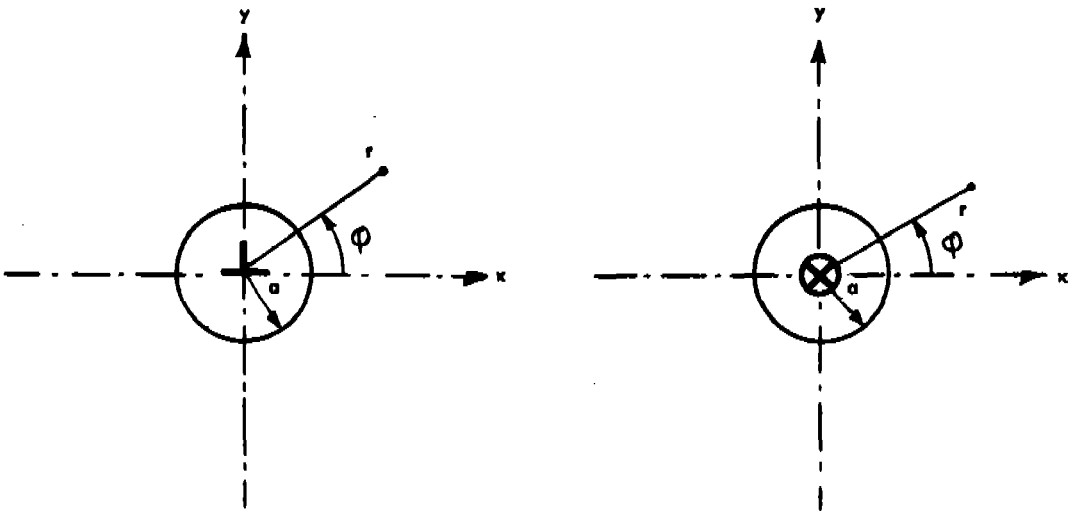

Edge Dislocation

$$\sigma_{rr} = -\frac{b}{2\pi}\cdot\frac{G}{1-\nu}\cdot\frac{\sin\varphi}{r}\left(1-\frac{a^2}{r^2}\right)$$

$$\sigma_{\varphi\varphi} = -\frac{b}{2\pi}\cdot\frac{G}{1-\nu}\cdot\frac{\sin\varphi}{r}\left(1-\frac{a^2}{r^2}\right)$$

$$\sigma_{r\varphi} = \frac{b}{2\pi}\cdot\frac{G}{1-\nu}\cdot\frac{\cos\varphi}{r}\left(1-\frac{a^2}{r^2}\right)$$

$$\sigma_{zz} = -\frac{b}{2\pi}\cdot\frac{\nu G}{1-\nu}\cdot\frac{\sin\varphi}{r}$$

Screw Dislocation

$$\sigma_{\varphi z} = \frac{Gb}{2\pi}\cdot\frac{1}{r}$$

$$\epsilon_{\varphi z} = -\frac{b}{4\pi r}$$

FIGURE 18

THE LONG RANGE STRESS FIELD OF DISLOCATIONS

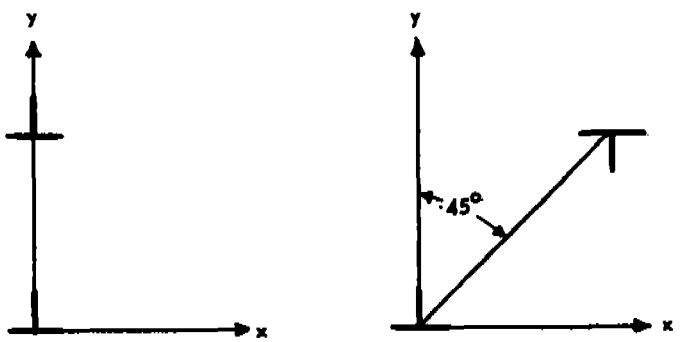

FIGURE 19

STABLE ARRANGEMENTS OF EDGE DISLOCATIONS
OF EQUAL AND OPPOSITE SIGNS

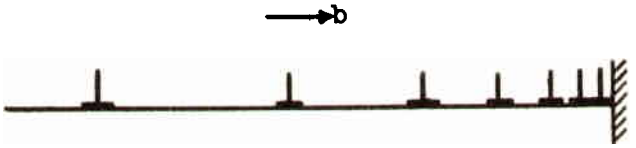

FIGURE 20

PILE-UP OF EDGE DISLOCATIONS AGAINST A BARRIER (SCHEMATIC)

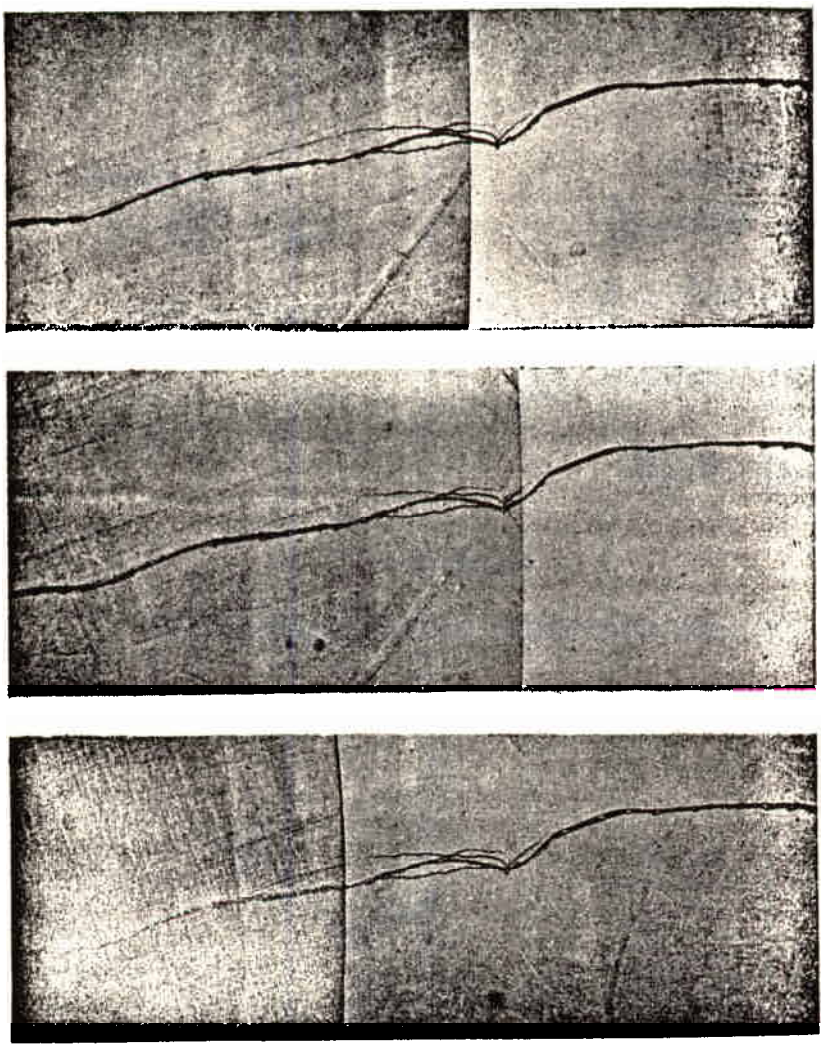

FIGURE 21

MOTION OF A LOW ANGLE BOUNDARY UNDER STRESS

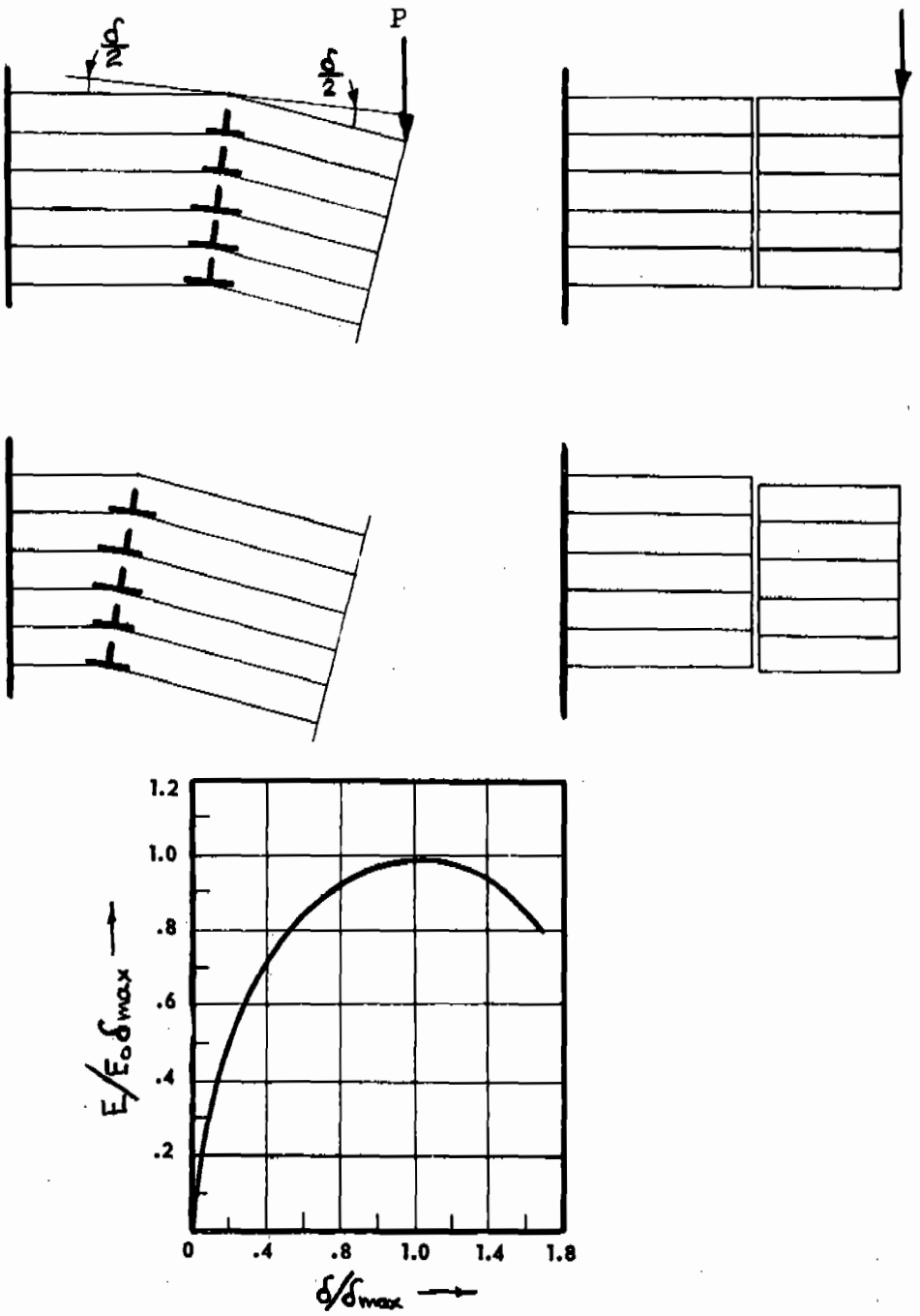

MOTION AND ENERGY OF A LOW ANGLE BOUNDARY IN COMPARISON WITH THAT OF A NONCRYSTALLOGRAPHIC BOUNDARY

FIGURE 22

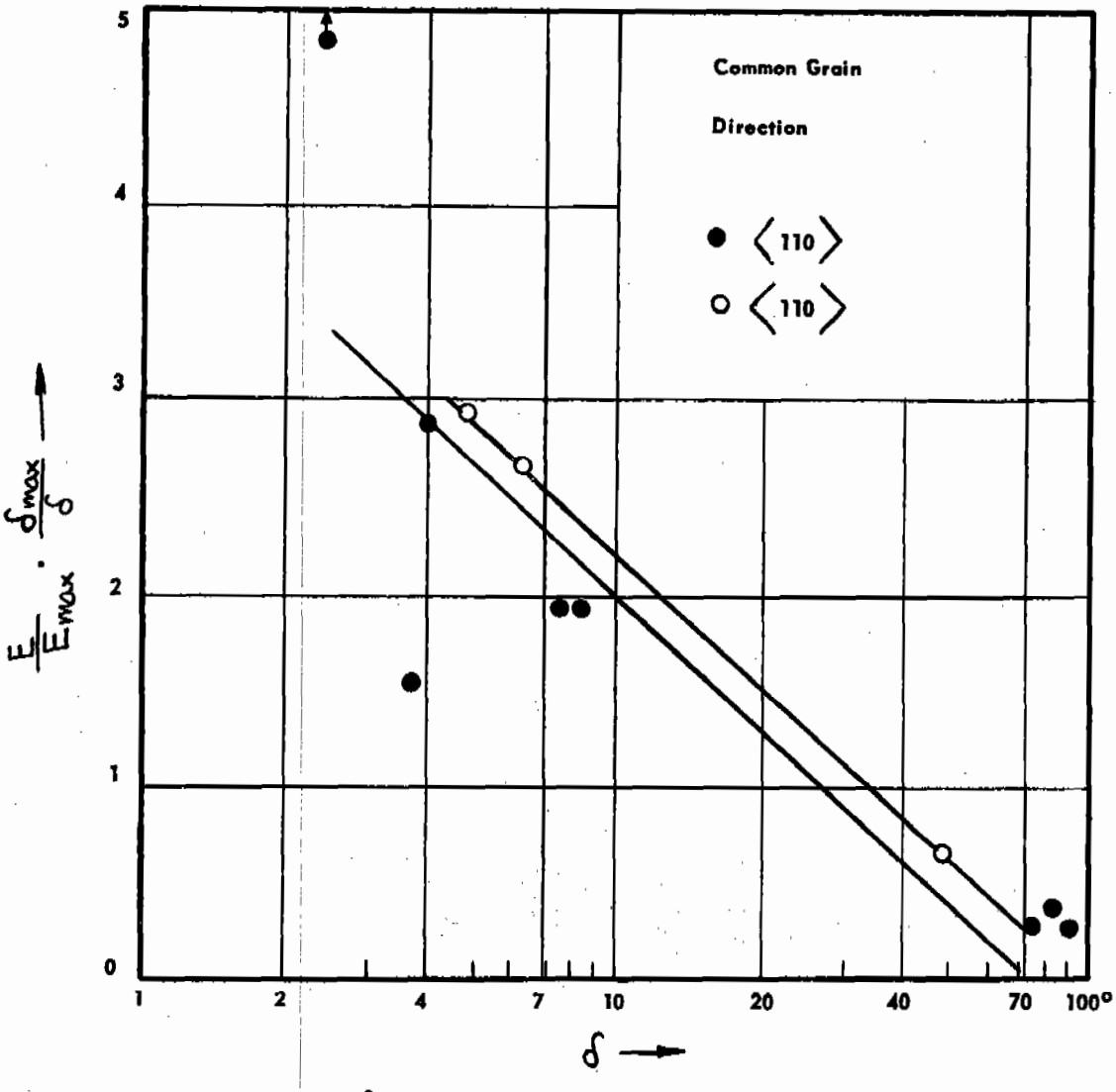

THE EFFECT OF δ ON THE RELATIVE GRAIN BOUNDARY ENERGY IN SILICON-IRON

FIGURE 23

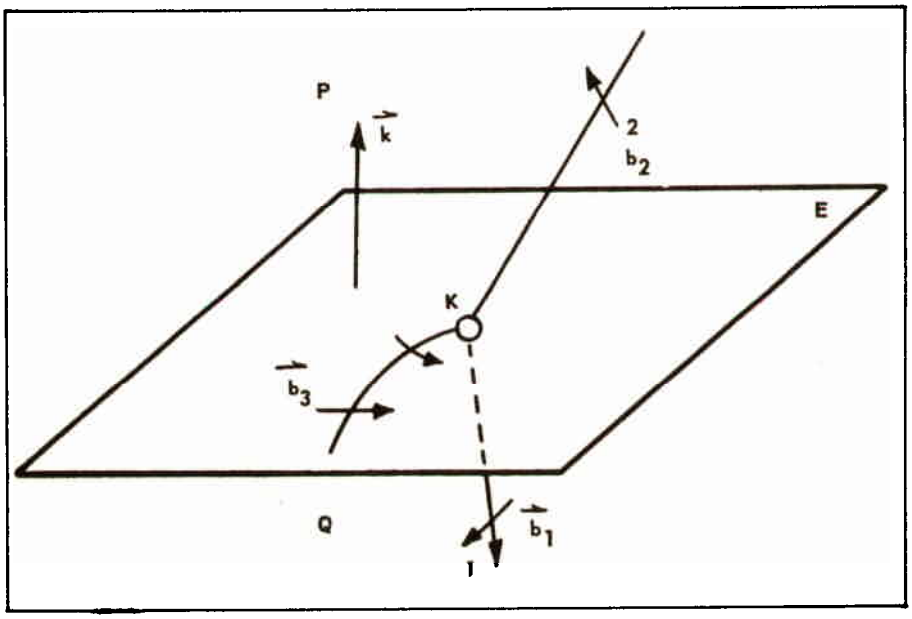

FIGURE 24

NODE IN PHASE BOUNDARY E BETWEEN PHASES P AND Q.
BOUNDARY MOVES IN DIRECTION $\vec{k}$.

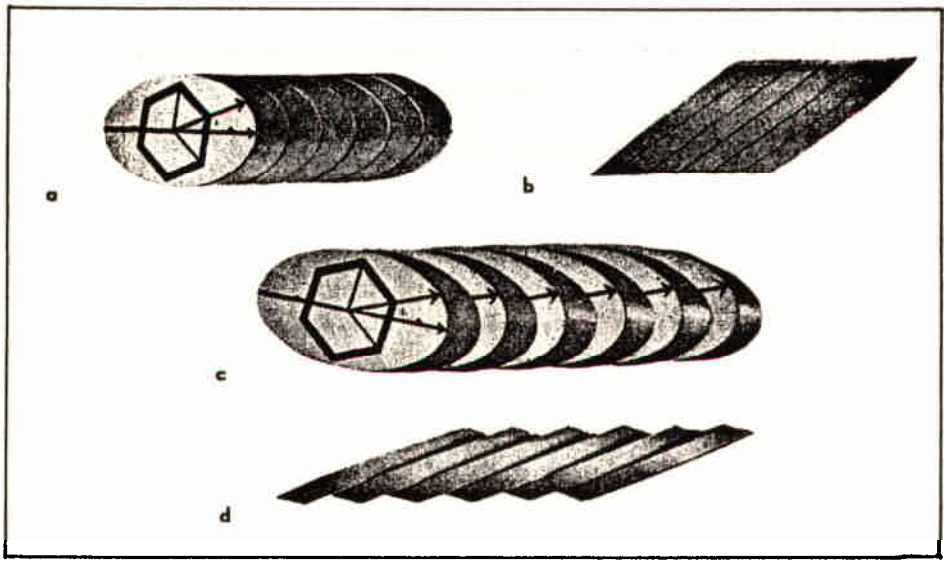

FIGURE 25

SLIP MODEL

FIGURES 24 & 25

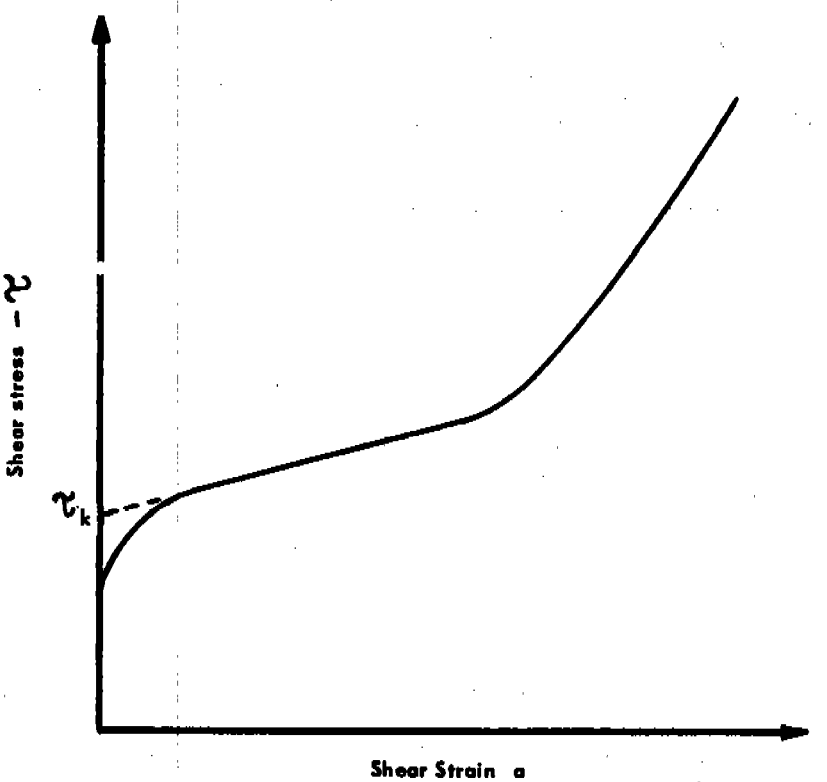

SHEAR STRESS-STRAIN DIAGRAM, SCHEMATIC

FIGURE 26

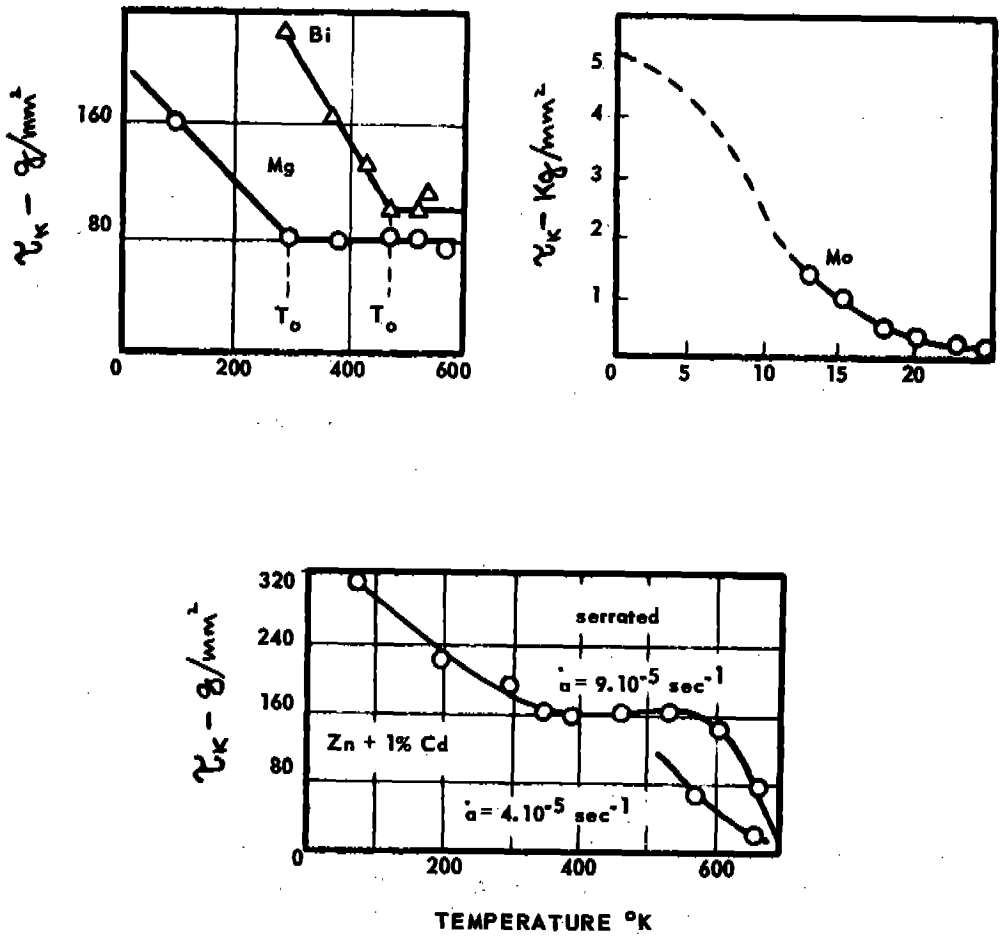

CRITICAL SHEAR STRESS OF Mg, Bi, Mo and Zn PLUS 1% Cd AS A FUNCTION OF TEMPERATURE

FIGURE 27

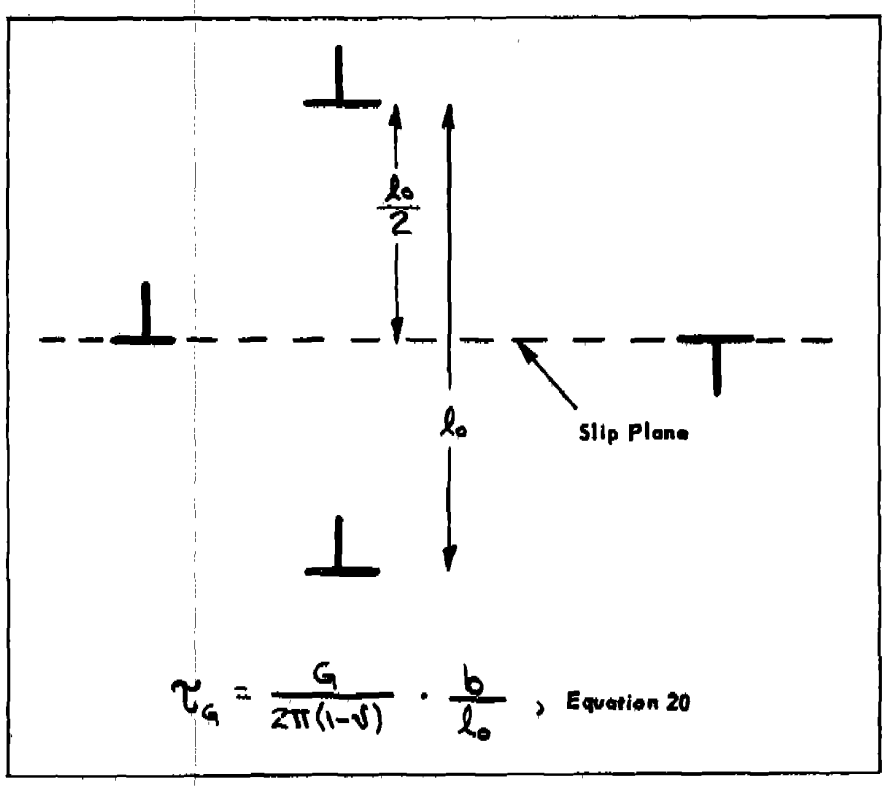

DISLOCATIONS IN A SLIP PLANE PASSING BETWEEN TWO SESSILE DISLOCATIONS. MODEL FOR THE DERIVATION OF EQUATION 20

FIGURE 28

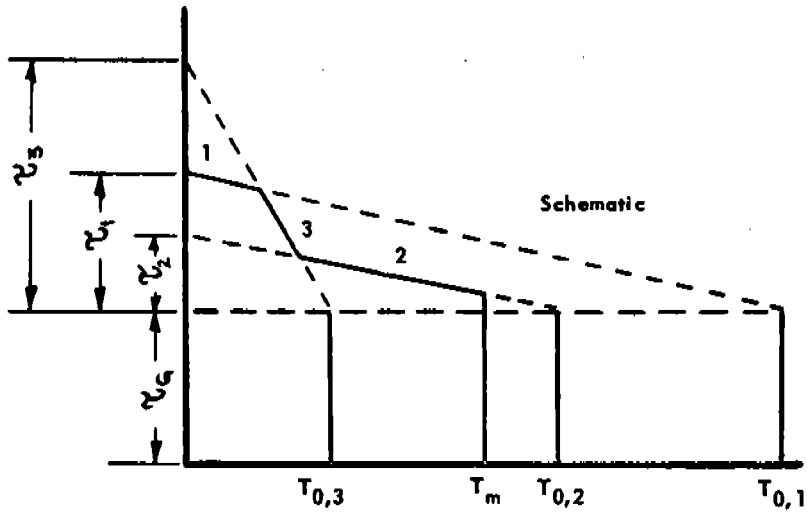

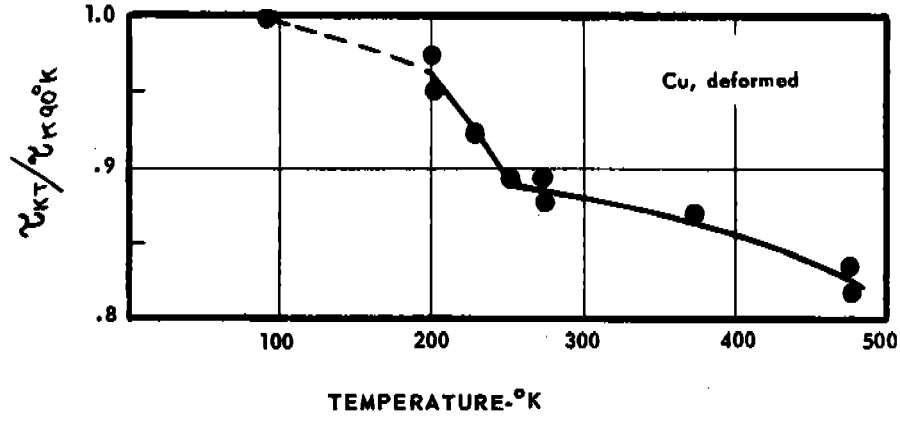

CRITICAL SHEAR STRESS OF METALS HAVING A LOW STACKING FAULT ENERGY AS A FUNCTION OF TEMPERATURE

FIGURE 29

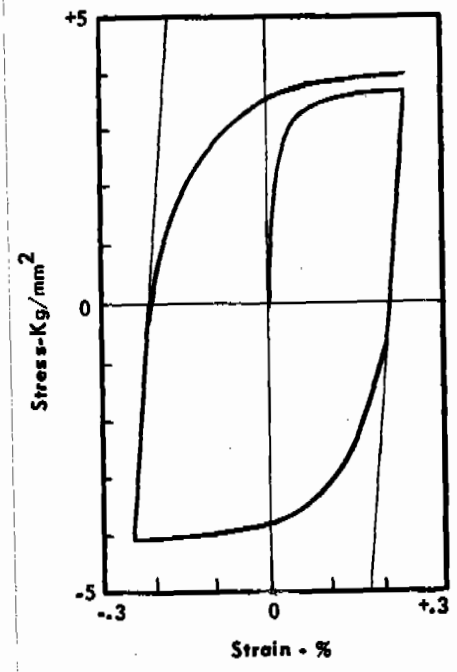

a)

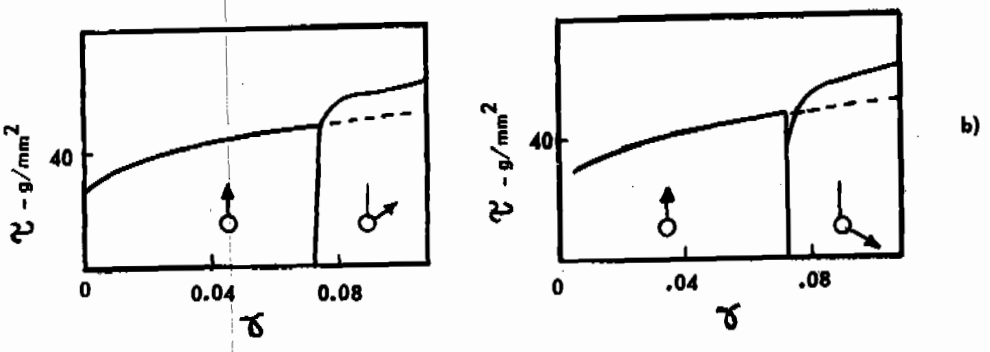

b)

BAUSCHINGER EFFECT IN BRASS AND LATENT STRAIN HARDENING IN ZN SINGLE CRYSTALS.

FIGURE 30

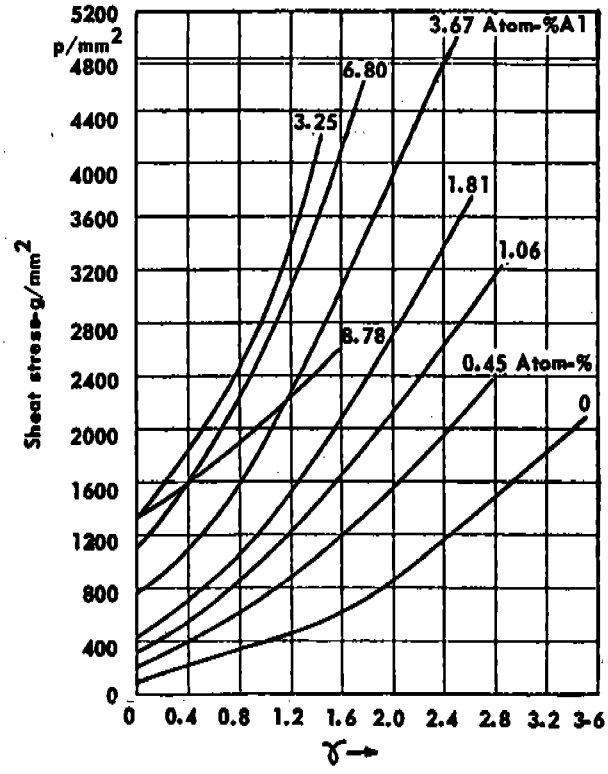

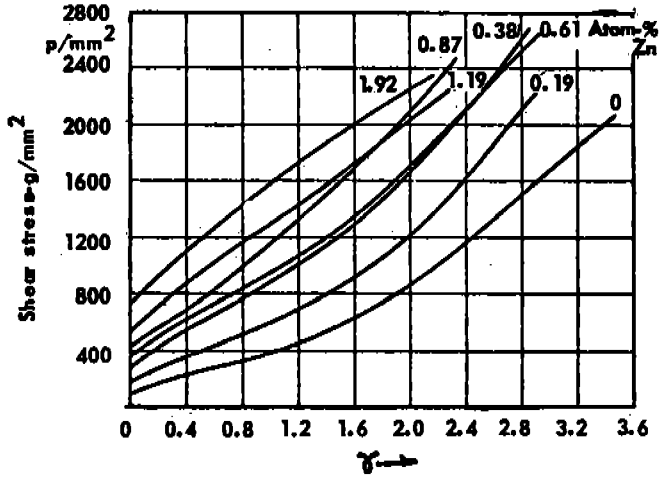

THE EFFECT OF ALLOYING ADDITIONS ON THE SHEAR STRESS-STRAIN CURVE OF MG CRYSTALS WITH Al AND ZN ADDITIONS

FIGURE 31

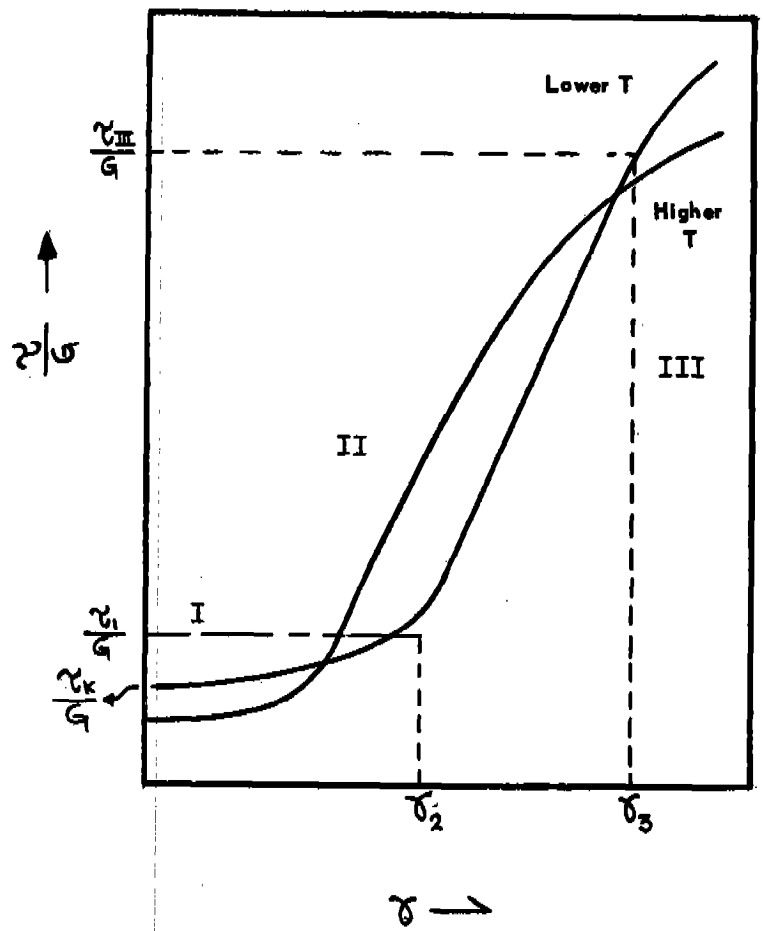

SCHEMATIC ILLUSTRATION OF THE SHEAR STRESS-STRAIN CURVE AND ITS TEMPERATURE DEPENDENCE FOR FCC METAL CRYSTALS.

FIGURE 32

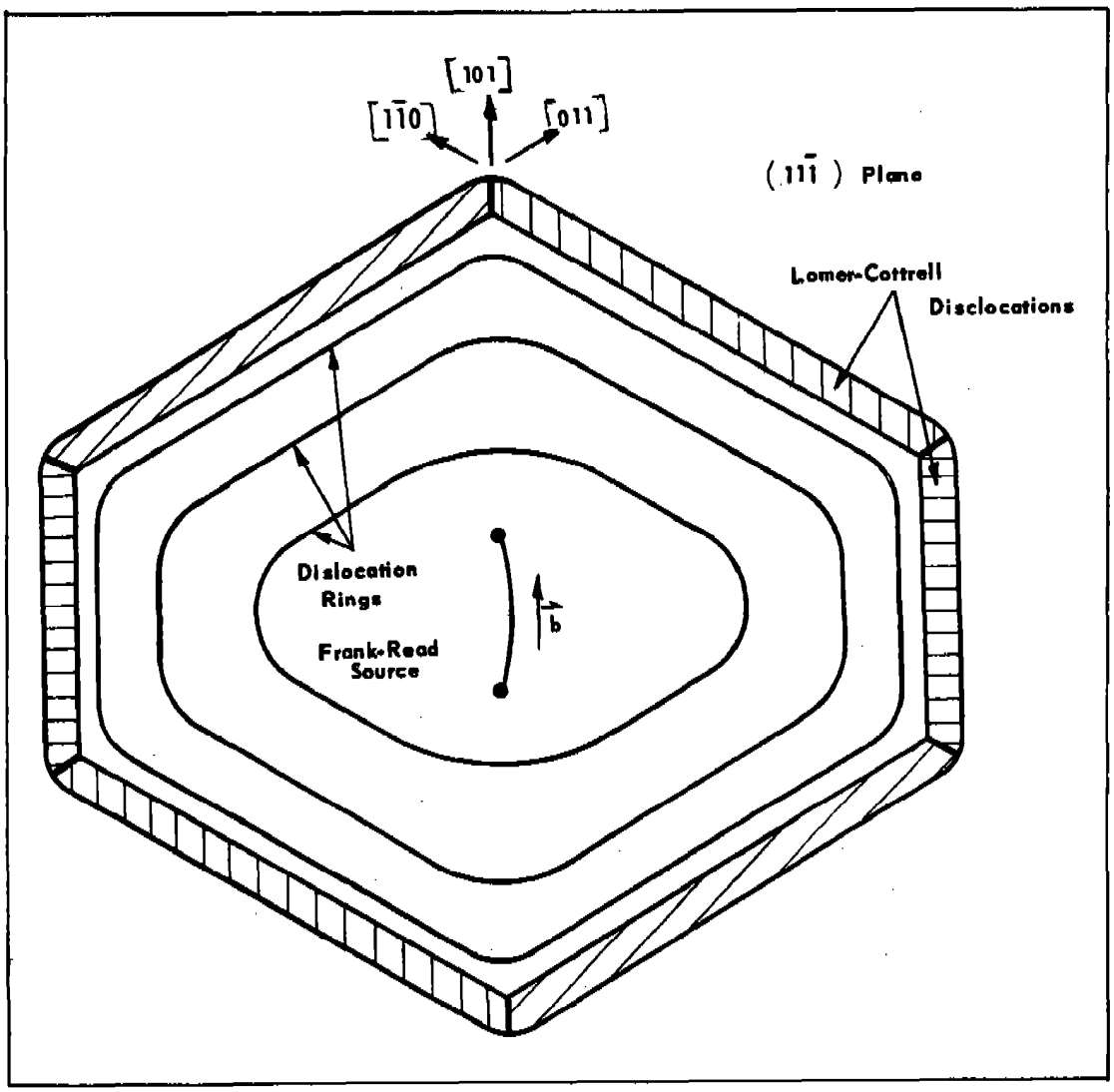

COTTRELL-LOMER BARRIERS LIMITING THE DISLOCATION PATH, SCHEMATIC

FIGURE 33

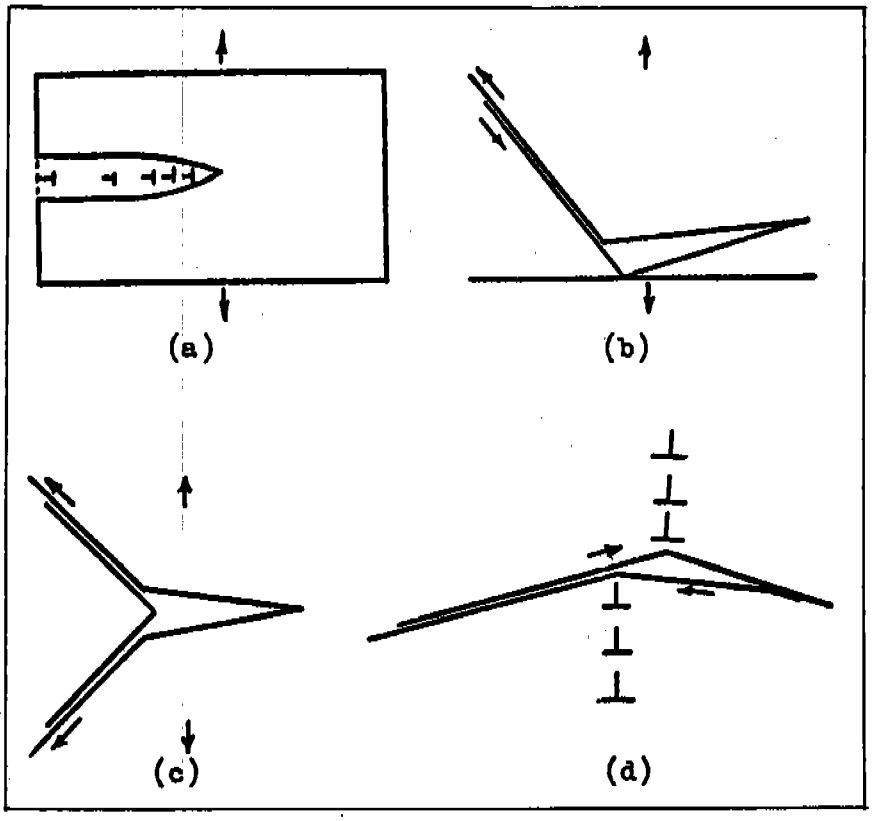

DISLOCATIONS AND CRACKS (a) ELASTIC CRACK REGARED AS PILE-UP OF EDGE DISLOCATIONS (b) CRACK FORMED FROM PILE-UP AGAINST A BOUNDARY (c) CRACK RESULTING FROM SHEAR ON TWO BANDS (d) CRACK FORMED AT A TILT BOUNDARY

FIGURE 34

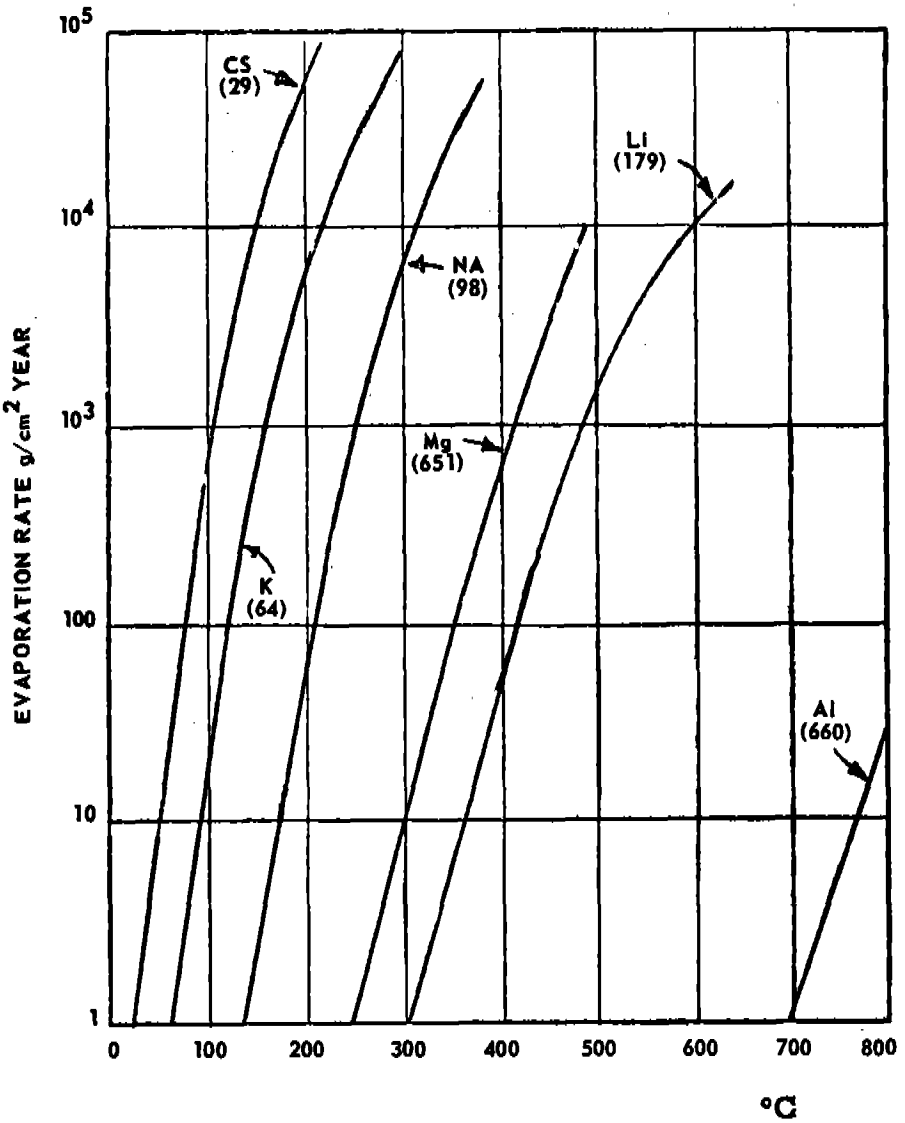

RATE OF LOSS OF VARIOUS METALS AS A FUNCTION OF TEMPERATURE. (THE MELTING POINT (°C) IS SHOWN BELOW EACH METAL)

FIGURE 35

ACKNOWLEDGMENT

The authors would like to express their gratitude to the personnel of the Metallurgical Research Laboratory for their help in the preparation of this manuscript. Special thanks are due to the following members of the staff:

Mr. K. S. Grewal
Mr. J. J. McKeon
Mr. J. F. Schell
Mrs. D. A. Anderson
Miss C. L. Swanson

THE ROLE OF IMPERFECTIONS IN DIFFUSION

by

Dr. C. E. Birchenall

ABSTRACT

The identification, description and determination of the concentrations of point defects in crystals lie at the core of the problem of diffusion in solids. The identification of the important defects has been accomplished and their concentration has been measured in certain cases, but the theoretical description of the defects has been only approximate. Nevertheless, kinetic and phenomenological theories have been developed which seem to describe many aspects of solid state diffusion adequately, but the underlying assumptions of these theories continue to be explored. Experimental techniques have improved greatly in recent years, allowing improved precision of measurement. Parallel improvements in the electron theory of solids and computational methods may lead to comparable improvements in the theory of diffusion eventually.

Some of the current active aspects of the study of volume diffusion which seem likely to continue in a fruitful way are: (1) the drift effect imposed on the random motions of atoms as a result of the variation of the thermodynamic activity coefficients of the elements with change in composition in a solution, (2) correlation effects in the motion of isotopic tracers, (3) the effects of small concentrations of solute atoms on the diffusivities of both solute and solvent atoms, (4) the interactions of point defects with dislocations and the influence of strain rate on diffusivity, (5) the Curie point anomaly. In view of the existence of many recent reviews several important and active aspects of volume diffusion are not discussed.

Boundary and surface diffusion seem likely to be the subjects of more frequent and more careful investigation than they have in the past. The very narrow boundary region assumed to apply to very pure metals has been shown not to be applicable to at least some solid solutions. In alloys it is necessary to establish how the boundary structure depends upon composition and variations in composition as well as on relative orientations of neighboring grains. In the study of surface diffusion careful correlations of the detailed structure of the exposed surface, the symmetries of the planes lying in the real surface and the presence and concentration of adsorbed impurities are required. Only the first hesitant steps have been taken in these directions and much more remains to be done.

Paper for the Eighth Sagamore Ordnance Materials Research Conference, "Mechanisms Operating in Metals at Elevated Temperatures", August 22-25, 1961.

INTRODUCTION

A major purpose of this conference is to attempt to distinguish the important problems of the immediate future within the subject area under discussion. In the case of diffusion in metals it is necessary to note that at least one review has been undertaken recently for just this purpose[1]. There are other review articles[2-5] prepared recently that serve to identify some of the problems that might otherwise be given greater prominence here. Thus the relative emphasis on topics in this report should not be taken as the only evidence of their relative importance.

The frequency of the special review articles and the number of references accruing between annual reviews[6] should be an accurate indicator of the general importance of diffusion in materials problems. It seems likely that research activity on diffusion in solids will intensify rather than abate, and that its value as a tool for studying the structure and binding of solids will increase at the same time that its relevance to the understanding and control of technological processes also increases.

VOLUME DIFFUSION

THE EQUILIBRIUM DEFECTS

Diffusion in crystals is the result of the motion of point imperfections. It is necessary and desirable to have evidence which is as direct and unambiguous as possible about the nature and concentrations of the point imperfections. Until a few years ago evidence about the nature of the dominant imperfections was exclusively theoretical for metals, derived from the calculations of Huntington and Seitz[7] and Zener[8], later followed by Brooks[9], Fumi[10] and others. These calculations involve finding the small residue, the energy of defect formation, from a number of large positive and negative contributions, some of which have uncertainties of the same order as the magnitude of the remainder, as pointed out by Lomer[11] and Amar[12]. Amar calls attention particularly to the uncertainties arising from the use of the mass of the free electron in calculating the Fermi energy and correlation energy and the assumption of a uniform distribution of electron density within the Wigner-Seitz cell in calculating the electronic self-energy instead of the experimentally observed effective electron mass and a more realistic radial electron distribution function.

Experimental studies like the Kirkendall shift of markers and quenching-in of high temperature defect demonstrate the need for a defect-type explanation for diffusion rather then a description in terms of rotating rings of atoms. The quenching experiments give reasonable values for the defect concentrations, but, apart from the theoretical basis cited, the explanations of these effects are virtually symmetrical with respect to vacancy or interstitial-type defects.

Therefore, it is reassuring that high precision direct measurements of x-ray and gravimetric densities by Simmons and Balluffi[13] have shown that vacancies are really present and that they are present in the expected concentrations. The fact that similar measurements have been done much earlier on nonstoichiometric ionic crystals[14] should not detract from the recognition of the importance and difficulty of demonstrating these effects in metals.

It is desirable to extend these comparative density measurements to the highest possible precision and to apply them to a wide range of systems. With these expectations concerning the nature and concentrations confirmed, the quenching methods may be pursued with a new degree of confidence, as long as it is recognized that the technique requires great care in

performance and interpretation. For example, note the wire size effect studied by Takamura[15]. Also the association of vacancies into pairs or larger aggregates complicates the low temperature behavior.

The comparison of x-ray and gravimetric densities does not give direct evidence about the effective volume of a vacancy, or the configuration of atoms about a vacancy. This problem can be approached through theoretical calculations of the type mentioned above or by fitting more empirical interaction potentials and minimizing the energy of the system with respect to variation of the positions of a group of atoms around a vacant site. Both types of calculation benefit greatly from the growth of large capacity and high speed computers. One activity of this sort is mentioned below.

Information about defect volume can also be obtained from the effects of pressure in diffusion. However, this measurement mixes the defect volume and the volume increase required for the defect to make a diffusion jump. A more desirable measurement is the effect of pressure on defect concentration at constant temperature, a measurement which may only be possible in the near future by one of the indirect methods.

EXPERIMENTAL METHODS

Zener and Wert [16a] proposed an adaptation of reaction rate theory to diffusion which gave the equation

$$D = \alpha f \nu a^2 \exp\left(\frac{\Delta S}{R}\right) \exp\left(-\frac{\Delta H}{RT}\right) \qquad (1)$$

where α is a geometrical factor determined by the crystal structure and diffusion mechanism, f is the Bardeen-Herring correlation coefficient which was omitted from the original theory, ν is the vibration frequency of the diffusing atom, a is the lattice parameter, R is the gas constant, T is the absolute temperature, ΔS is the sum of the entropy of formation and activation entropy for motion per mole of defect and ΔH is the sum of the enthalpy of formation and activation energy for motion per mole of defect. The equation has the empirically observed Arrhenius form.

Assuming that the activation energy for motion is used to strain the lattice and that the macroscopically observed temperature coefficient applies, Zener[16b] has been very successful in explaining the magnitude of ΔS and consequently of the frequency factor as a whole. This success has prompted too much concern about the significance of frequency factors which do not conform readily to the Zener model. It seems appropriate to reiterate Zener's initial suggestion - if the experiment does not fit, repeat the experiment. On at least two recent occasions[17a, 17b] the causes of the theoretical excitement have evaporated when the experimental measurements were repeated belatedly. And in at least one of these instances the more interesting problem that remains, the probable need for several types of jump in β tin, seems to have made no strong impression on the theorists. Evaluation of the correlation factor f for competing jumps in anisotropic crystals has not been carried through.

Although a great deal of the real progress that has been made in diffusion studies in the past decade is the result of improvements in experimental precision of measurement, it is unwise to take it for granted that optimum precision is obtained in every experiment and on every conceivable system. Discrepancies still remain, some large, some small, some of unknown magnitude. However, it would be profitable for new groups entering the field to check out their

techniques on some material other than pure silver, which might be described justly as done to death.

Improvements in precision have been confined mainly to the measurements of self-diffusion in metals and alloys using radioactive tracers. With reasonable care in the counting procedures most of the errors arise from temperature measurements and sectioning of the specimens. Precision grinding techniques[3, 18] have lead to the greatest share of improvement recently.

It appears that the development of the electron microprobe x-ray analyzer[19] has greatly improved the precision of chemical interdiffusion measurements. In addition, and as important, it reduces the time of making such measurements which previously depended on multitudes of precise quantitative analyses by conventional methods on very small samples. The extension of chemical interdiffusion measurements to a wide variety of cases, accompanied by the study of marker shifts and self-diffusion measurements, is an obvious, challenging, but tedious field for study.

INTERSTITIAL DEFECTS

The fact that interstitials probably do not contribute significantly to self-diffusion in pure metals does not eliminate them from interest. Interstitials are produced as a part of radiation damage and must diffuse during annealing-out of the damage. The elaborate calculation by Vineyard et al[20] offers an example of the application of modern computer techniques to the investigation of the theories of physical processes in solids which may make it easier to improve those aspects of the theories which bear on diffusion. In this particular case, the stability of the interstitial pair in the form of a dumbbell with its axis normal to a cube face and bisected by the face is shown to be stable relative to a single interstitial in the body-center of a face-centered cubic crystal within the limitations imposed by the model.

In the study of interstitial alloys investigators should continued to remain alert for those instances in which solute atoms are distributed over both substitutional and interstitial positions. Because the size factor should lie in the range where it is favorable for neither type of solubility, the total solubility in a metallic solvent should be small and preference for boundary and dislocation diffusion should be high.

THEORY OF VOLUME DIFFUSION

There are four main directions in which the theory of volume diffusion has advanced recently.

(1) LeClaire[21] has examined the classical theory of diffusion in the presence of a concentration gradient. He predicts that the change in barrier height for a diffusion jump which varies along the concentration gradient imposes a general drift on the otherwise random motion of the diffusing atoms. These drift effects have been observed in αAgCd alloys by Manning[22] and in αCuZn alloys by Camagmi, Pavallini and Shuttleworth[23]. The part of the drift that arises from the variation in the self-diffusion coefficient or mobility with concentration may be more important than the drift that arises from the nonideality of the solution. The latter is responsible for the Kirkendall effect. The phenomenological theory of Darken is not complete because it omits the former effect.

(2) Although isolated defects in solids may diffuse by random jumps the resulting displacements of the atoms may not be random. In particular, the displacements of tracer atoms,

which are observed in self-diffusion, may be highly correlated because of the high probability that an atom which has just exchanged places with a vacancy will jump back. Once Bardeen and Herring recognized the need for a correlation correction, the theory for self-diffusion in lattices of high symmetry was advanced rapidly by Compaan and Haven[25] and by Lidiard and LeClaire[26]. An excellent account of the theory is given by Lidiard, so there is no need to repeat it here.

(3) LeClaire and Lidiard also examined the correlation problem for solute diffusion by a vacancy mechanism in a face-centered cubic lattice. Manning[27] pointed out that the various jump probabilities that contribute to the diffusion coefficient (see Equation 5 below) may not have the same temperature dependence, so that the correlation factor as a whole is expected to have a temperature coefficient in general which may not be exactly exponential.

Also in the case of alloy diffusion the trend is away from attempts to explain the concentration dependence of diffusivities in concentrated alloys toward high precision studies in very dilute alloys. The theory of self-diffusion of solvent atoms in dilute solution was developed by Reiss[28]. The difficulty in expanding this type of treatment to even modestly concentrated solutions has been discussed in detail by Lazarus[4].

In the case of a solute atom that diffuses by a vacancy mechanism in a face-centered cubic solvent lattice the correlation coefficient f can be calculated approximately, according to Lidiard and LeClaire[26], when only jumps involving the nearest neighbor sites of the solute atom are considered. They find

$$f \approx \frac{2w_1 + 7k_1}{2w_1 + 2w_2 + 7k_1} \tag{2}$$

where w_1, w_2 and k_1 are respectively the probabilities per second that a vacancy in a site nearest the solute atom exchanges with one of the four solvent atoms that are simultaneously nearest neighbors of solute and vacancy, with the solute atom itself, or with one of the other solvent atoms which are nearest neighbors of the vacancy. The last type of jump is said to dissociate the vacancy and solute pair and further correlation in their motion is neglected in this approximation.

On the other hand for self-diffusion by the vacancy mechanism in a pure substance, if the jump direction has two-fold symmetry or higher the correlation factor is given exactly by

$$f = \frac{1 + \overline{\cos \theta}}{1 - \overline{\cos \theta}} \tag{3}$$

where θ is the angle between the directions of two consecutive jumps of the tracer atom and the bar over $\cos \theta$ indicates that the average value is taken.

For two different isotopes of the same element with masses $m_1 > m_2$, diffusing in the same material with diffusivities D_1 and D_2, Schoen[29] defines the strength of the isotope effect, S, by the equation

$$S = \frac{(D_2/D_1) - 1}{(m_1/m_2)^{1/2} - 1} \tag{4}$$

If the diffusivity were inversely proportional to the square root of the isotope mass S would have a value of unity. This behavior is consistent with the observations in a number of systems, but Schoen observed that Cd isotopes diffusing in Ag and Cu gave diffusivities substantially independent of their mass corresponding to $S \approx 0$. The diffusivity of a solute atom is proportional to the correlation factor times w_2, the probability of exchange per unit time with a vacancy, or

$$D \propto \frac{w_2 (2w_1 + 7k_1)}{2w_2 + 2w_1 + 7k_1} \tag{5}$$

If $w_2 >> w_1 + \frac{7}{2}k_1$ the diffusivity is independent of w_2. That is, the rate controlling jump of the vacancy is with the solvent atoms. In this case the mass of the solute atom should be immaterial and the strength of the isotope effect should be small. However, if $w_2 << w_1 + \frac{7}{2}k_1$ the diffusivity is proportional to w_2. In this case, and in the case of self-diffusion in a pure metal, it is desirable to establish as precisely as possible the strength of the isotope effect.

This technique appears to be very useful for exploring the association between solute atoms and defects and as a test for detailed theories of vacancy jump mechanisms. It is doubtful that the full range of possibilities is clear at the present time. This field may be one of the most popular aspects of diffusion in the near future.

(4) One of the most noteworthy of recent trends is the probing of the underlying assumptions of reaction rate theory as it relates to diffusion by Rice and his coworkers[30]. This endeavor tends to sharpen the understanding of dynamical contributions to the diffusion jump which are treated very superficially in earlier models. The necessity for correlated displacements of atoms around the saddle point is shown to restrict the configurations leading to a diffusion jump to only a fraction of the configurations having energy in excess of the activation energy. These considerations lend general support to Zener's proposal that the activation energy is the energy necessary to strain the lattice to produce the saddle point configuration and remain consistent with the form of the relations employed in the simpler theories. The jump frequency is found to be relatively insensitive to changes in the normal modes of vibration resulting from the introduction of a vacancy as a neighbor. Appreciable relaxation about a vacancy is predicted, and the activation volume ΔV is given approximately by

$$\Delta V \approx \frac{V_a}{(\gamma - 1/3)} \tag{6}$$

where V_a is the atomic volume and γ is the Gruneisen constant. Since γ is often about 2 to 3, the activation volume should be roughly half the atomic volume, as is sometimes reported.

EFFECTS OF STRAIN

There is general agreement that prior strain has relatively little effect on diffusion coefficients measured in conventional experiments which invariably required enough time at the diffusion temperature to anneal out the effects of strain. However, Cohen and his coworkers[31] have reported that the continuous deformation of iron in compression during diffusion increased the measured self-diffusion coefficients in direct proportion to the rate of straining. Similar results have been obtained for silver in torsion by Lee and Maddin[32]. They attribute the decrease in activation energy associated with diffusion during deformation to the formation of excess vacancies through dislocation interactions, thus eliminating the contribution of the heat of formation of vacancies from the activation energy for diffusion. It has been suggested

also that maintaining a higher than normal dislocation concentration may account for the enhanced diffusivity, with a heat of motion equivalent to that expected in low angle grain boundaries (see below). Forestieri and Girifalco[32] found similar strain rate effects in silver, noting that the magnitude of the effects diminishes with rising temperature.

Using conditions that overlap those of the other groups working with silver, Darby, Tomizuka and Balluffi[33] fail to find significant strain rate effects which clearly exceed the experimental uncertainties. Here lies the most important, unresolved, flat contradiction in experimental results in the current diffusion literature. The results on both sides are plentiful. Only a more careful set of investigations under varied conditions seems likely to resolve this contradiction.

EFFECT OF PRESSURE

High hydrostatic pressure decreases the rate of diffusion in crystals. According to Zener's model the activation volume is given by

$$\Delta V = -RT\left[\frac{\partial \ln (D/a\, f\, a^2\, \nu}{\partial P}\right]_T \qquad (7)$$

Many of the high pressure studies on diffusion in metals have been done by Nachtrieb and his coworkers[34]. Although there is less optimism about predicting mechanisms from measurements of activation volume than formerly, it is probably too early to give up the attempt. In any case, if vacancies are present there must be appreciable relaxation of the neighboring atoms to be consistent with the observed activation volumes which, as stated above, are on the order of one-half the atomic volume for self-diffusion in pure crystals of the elements.

Measurements of self-diffusion in lead by Hudson and Hoffman[35] up to 4×10^4 kg/cm^2 pressure suggest that the activation volume is about two thirds of the atomic volume up to half the maximum pressure and then decreases as the pressure increases.

For nitrogen diffusing interstitially in iron, where the activation volume is almost entirely the volume change produced by the atom jump, the activation volume was found by Bosman, Brommer and Rathenau[36] to be only about 4 pct. of the volume of a nitrogen atom.

As the techniques improve for producing and measuring high temperatures and pressures simultaneously it is probable that work in this field will become increasingly valuable.

THE CURIE POINT ANOMALY

Birchenall and Mehl[37] observed that their self-diffusion measurements in alpha iron did not obey the Arrhenius equation, but the precision of measurement was too low to associate definitely the deviations from the usual behavior with the presence of the Curie temperature within the range of measurement. After better sectioning techniques were developed Borg and Birchenall[38] showed that an abnormal decrease in diffusivity occurred while cooling through the Curie point range. Cohen and coworkers[39] confirmed this result and found similar behavior for Ni^{63} diffusing in very dilute solution in alpha iron. Stanley and Wert[40] find a similar effect in αFe-18% V alloys. On the other hand, Borg and Lai[41] have been unable to find any deviation from the Arrhenius equation for Co^{60} diffusing in dilute solution in alpha iron, and there appears to be no large anomaly near the Curie temperature in pure cobalt[42].

in delta iron consist of a single point by Cohen's[43] group, and new experiments have been made covering a range of temperature by Staffansson and Birchenall[44] and by Borg and Lai[40]. The measurements do not agree very well in absolute value, but the activation energy in delta iron appears to be much lower than it is above the Curie point in the alpha range. Although Cohen's[39] line in the alpha range extrapolates into the region covered by the experimental points in the delta range, the line is based on points with rather large scatter. The Borg and Birchenall[38] line requires a continuous curvature of the Arrhenius plot above the Curie temperature in order to extrapolate to the delta range values smoothly.

Because of the extra energy required to remove a vacancy from a system with well-ordered spins, it seems that a thermodynamic effect leading to an abnormal decrease in equilibrium vacancy concentration is necessary when cooling through the Curie point range. If the energy of motion were unaffected, the diffusivity should reflect directly the decrease in vacancy concentration. However, the decrease in diffusivity in alpha iron seems to be too large to be accounted for by this source alone, while in cobalt a much larger effect should be observed than even the present scatter of data allow. Some other effect must be present, probably connected with the activation energy for motion. Two experiments are in progress which may help to elucidate this effect. Borg and Lai are diffusing gold, which has no magnetic moment, into alpha iron. Staffansson and Birchenall are measuring self-diffusion in alpha iron parallel and perpendicular to the axis of a magnetic field saturating the sample. Additional experimental and theoretical studies are likely to be required before this phenomenon is understood.

GRAIN BOUNDARY AND DISLOCATION DIFFUSION[45]

Burgers model of a low angle grain boundary as a parallel array of edge dislocations leads to the expectations that, if atom mobilities are greater along dislocations than in the undisturbed volume of the crystal, (1) the self-diffusion coefficient averaged over all directions in a low angle grain boundary should increase as the misorientation of neighboring grains increases, (2) diffusivity should be anisotropic within the boundary plane, preferring the direction parallel to the dislocation lines, and (3) the region about the boundary participating in enhanced boundary diffusion should be very narrow for self-diffusion in a pure metal. Furthermore, for high angle grain boundaries variation of diffusivity with misorientation angle should be relatively small and anisotropy should be small.

These expectations have been confirmed by experiment. Using first the simple boundary conditions for grain boundary diffusion* of Fisher[46] and later more exact solutions by Whipple[47] and Vorisov, Kzolikov and Lynbov[48], all for constant surface concentration, grain boundary diffusivities have been obtained for polycrystalline pure metals[49]. Numerous measurements have also been made in alloys[50].

Hoffman and Turnbull[51] showed that the diffusivity in low angle boundaries is proportional to the dislocation density, or that the mobility of atoms along the pipes is independent of boundary angle for a Burgers-type boundary. The mobility along dislocations in silver boundaries was found to agree well with the value measured in isolated dislocations by Hendrickson and Machlin[52]. Hoffman[53] showed that diffusion within low angle boundaries is anisotropic and that the anisotropy extended to higher angles than was anticipated.

*These calculations assume isotropic diffusion within the boundary. Therefore, they are most suitable for use with high angle boundaries which predominate in polycrystalline samples.

Usually the activation energies for grain boundary diffusion are found to be about half those for volume diffusion in the same material. Hart[54] proposed that apparently low activation energies for volume diffusion obtained from relatively low temperature measurements are the results of contributions from rapid diffusion along dislocation networks. Rather extreme examples of this type of behavior are probably contained in the work of Jaumot and Smith[55] on zinc single crystals.

In the study of diffusion of sulfur in alpha iron Ainslie et al[56] found that sulfur diffuses at a rate characteristic of substitutional diffusion, that there was a large grain boundary preference and that sulfur in the grain boundaries could exceed the normal solubility of sulfur in iron single crystals. It was shown that the sulfur was highly concentrated in the grain boundary region. The volume for some microns on either side of the boundary was dense with dislocations induced by the diffusion of sulfur. In a sense the diffusing atoms plough their own furrow. The structure is probably a transient one if the temperature is high enough, but for a considerable time the amount of solute held may greatly exceed the true solubility. Inman and Tipler[57] may have observed similar behavior earlier for phosphorus in alpha iron, but their observations were obscured by precipitation effects.

It is obvious from these studies that grain boundary diffusion in alloys can be very complex. The need for studies on systems in which grain boundary adsorption can be controlled is evident. It is important to determine whether such phenomena remain sensitive to the history of treatment or whether stationary boundary structures can be made in which diffusivities may be measured without changing the structure. The numerous Russian studies[58] on diffusion in ternary and higher systems may be a step in this direction, although there is no indication that they are combining structure observations with their diffusion measurements.

SURFACE DIFFUSION[45]

With the great improvements recently made in the techniques for observing the configurations and changes in configurations of atoms on crystal surfaces it would seem that the study of surface diffusion might advance rapidly in the immediate future. There seem to be basically three kinds of techniques available at this time.

Field emission and field-ion microscopy permit high resolution observation of the surfaces of a limited range of metals. The technique has been applied recently to the surface self-diffusion of tungsten by Barbour et al[59]. Gomer and Hulm[60] had studied oxygen diffusion on tungsten surfaces earlier. Similar results may be obtained, although with lower direct resolution, from the study by means of electron microscopy of particles nucleating and growing on surfaces[61]. Low energy electron diffraction as applied by Farnsworth[62] and by Germer[63] yields information about groupings of small concentrations of atoms on surfaces and should be adaptable to mobility studies.

Grooves form at the intersection of a grain boundary with a free surface when a metal is heated to reasonably high temperature. The thermal grooving may take place by volume diffusion, surface diffusion or evaporation or some combination of these processes. Mullins[64] has deduced the kinetics of grooving for the contributing processes, and Mullins and Shewmon[65] and Gjostein and Rhines[66] have measured surface diffusion coefficients under conditions for which the kinetics favor this type of control, assuming that the diffusivity is constant of the range of orientations on the surface defining the groove. These investigators obtain values for surface self-diffusion of copper in agreement with each other but not with the tracer measurements of Hackerman and Simpson[67].

The third type of measurement based on the spreading of radioactive tracers differs in an essential way from the other two methods. Surface diffusion is observed only for those tracer atoms which remain on the surface. The tracer is no longer contributing to the measurement when it has taken a volume diffusion jump although the counting procedure may still record its presence. In the methods that depend on surface contour, all atoms on the surface are observed in principle and their average motion investigated. On the other hand the tracer method offers a selectivity which permits its extension beyond the self-diffusion case more fruitfully.

The average number of jumps an atom can take before being trapped into the specimen is given approximately by the ratio of the surface diffusivity D_S to the volume diffusivity D_v. The best methods of resolution, probably autoradiography, under the most favorable conditions (weak beta radiation) cannot resolve less that 10^5 jumps in the same direction. It is substantially impossible by this method to measure surface diffusion unless D_S/D_v is greater than 10^6. Consequently, the diffusion coefficients for surface migration are likely to be more significant the lower the temperature of measurement.

All sorts of surface studies show the great care that is needed to produce clean, or even reproducibly dirty, surfaces, to characterize those surfaces, and to ascertain that they remain unchanged topographically during the measurement. Surface diffusion measurements at 750°C. on various copper planes [67] show an unexpected anisotropy on the {100} faces. Since isotropic diffusion is to be expected if the face is normal to an axis of three-fold or higher symmetry some effect of faceting or adsorption might be suspected. It was mentioned above that the average of these measurements does not agree with growing measurements.

Similarly surface self-diffusion coefficients by the tracer method on polycrystalline silver by Nickerson and Parker[68] disagree with grooving kinetics measurements of Winegard and Chalmers[69]. Unpublished experiments with refined methods by Drew and Pye[69] on {321} faces of silver single crystals yield values which lie between, but not especially close to, the earlier measurements. The tentative results up to 500°C. obey the equation

$$D_{Ag(s)} = 10^{-4} \exp(-8700/RT) \text{ cm}^2 \text{ per second}$$

but deviations become pronounced for $D_S = 10^6 D_v$. No anisotropy has been observed on this surface. Its detailed topography has not yet been studied. Diffusion under oxygen pressure is appreciably faster than it is under vacuum, but it is uncertain whether the surface rearranges. It should be recalled that the surface energy of silver is markedly affected by adsorbed oxygen.

SUMMARY

The understanding of almost every aspect of solid state diffusion is incomplete in spite of the fact that many advances have been made in recent years. It appears that the opportunity to apply improved techniques to more carefully controlled materials has never been better. Theoretical advances, especially those related to correlation effects, have opened up new approaches to the study of mechanism, that all-too-often ambiguous pursuit that lies at the core of the problem. However, the obvious theoretical problems are also very formidable and progress on some of them may depend on the development of new experimental data.

Of all the aspects of diffusion none seems to offer greater challenge and promise of reward than the study of surface diffusion which plays an important role in many phenomena - catalysis, nucleation of surface reactions, condensation, thermal etching - to list a few. It appears that the tools are at hand. All that is needed is the skill, the determination and the infinite patience required to use them properly.

REFERENCES

1. "Diffusion and Mass Transport", a report dated Nov. 15, 1959, prepared for the NAS-NRC Committee on Perspectives in Materials Research by a panel under the chairmanship of D. Lazarus, to be published.
2. C. E. Birchenall, Met. Rev. 3, 225 (1958).
3. C. T. Tomizuka, in "Methods in Experimental Physics," Vol. 5, Academic Press, New York, 1959.
4. D. Lazarus, in "Advances in Solid State Physics," Vol. 10, Academic Press, New York, 1960.
5. C. E. Birchenall in the Proceedings of the Fourth International Conference on Reaction of Solids, Amsterdam, 1960, to be published.
6. a. P. G. Shewmon, Ind. Eng. Chem. *51*, 402 (1959).
   b. P. G. Shewmon and F. R. Winslow, Ind. Eng. Chem. *52*, 343 (1960).
   c. P. G. Shewmon and G. R. Love, Ind. Eng. Chem. *53*, 325 (1961).
7. H. B. Huntington and F. Seitz, Phys. Rev. *61*, 315 (1942), *76*, 1728 (1949); H. B. Huntington, Phys. Rev. *61*, 325 (1942). H. B. Huntington, Phys. Rev. *91*, 1092 (1953).
8. C. Zener, Acta Cryst. 3, 346 (1950).
9. H. Brooks in "Impurities and Imperfections," pp. 1ff, Am. Soc. for Metals, Cleveland, 1955.
10. F. G. Fumi, Phil. Mag. *46*, 1007 (1955).
11. W. M. Lomer, in Prog. in Metal Physics, 8, 255 (1959).
12. H. Amar, AEC Report NYO-2565, November, 1960.
13. R. O. Simmons and R. W. Balluffi, Phys. Rev. 117, 52 (1960), *119*, 980 (1960).
14. E. R. Jette and F. Foote, J. Chem. Phys. *1*, 29 (1933), but see also W. L. Roth, J. Appl. Phys. Suppl. *30*, 3038 (1959); H. Pick and H. Weber, Z. Physik. 128, 409 (1950).
15. J. Takamura, Acta. Met. 9, 547 (1961).
16. a. C. Wert and C. Zener, Phys. Rev. *76*, 1169 (1949).
    b. C. Zener, Chap. 11 in "Imperfections in Nearly Perfect Crystals, Wiley, N.Y. 1952.
17. a. P. J. Fensham, Australian J. Sci. Res. *3A*, 91 (1950); *4*, 229 (1951). J. D. Meakin and E. Klokholm, Trans. A.I.M.E. *218*, 463 (1950).
    b. H. W. Paxton and E. G. Gondolf, Arch. Eisenhuttenw, *30*, 55 (1959). W. C. Hagel, submitted to A.I.M.E. 1961.
18. F. H. Eisen and C. E. Birchenall, Acta. Met. *5*, 265, (1957).
19. R. Castaing, Publ. O.N.E.R.A. No. 55 (1951); Y. Adda, J. Philibert, C. Mairy and P. Bouchert, Rept. C.E.A. No. 880 (1958); Y. Adda and A. Kirianenko, J. Nucl. Met. *2*, 120 (1959).
20. J. B. Gibson, A. N. Goland, M. Milgram and G. H. Vineyard, Phys. Rev. *120*, 1229 (1960). See also A. Seeger and E. Mann, J. Phys. Chem. Solids, *12*, 326 (1960).
21. A. D. LeClaire, in Colloque sur La Diffusion a l'Etat Solids, p. 1, Antre d'Etude, Nucleaires de Saclay, France, 1959.
22. J. R. Manning, Phys. Rev. *116*, 69 (1959).
23. P. Camagni, Pavallini and R. Shuttleworth, quoted in Ref. 21.
24. J. R. Bardeen and C. Herring, Chapter 10 in "Imperfections in Nearly Perfect Crystals," Wiley, N.Y., 1952.
25. K. Compaan and Y. Haven, Trans. Farad. Soc. *52*, 786 (1956); *54*, 1498 (1958).
26. A. B. Lidiard, Phil. Mag. *46*, 1218 (1955); A.D. LeClaire and A. B. Lidiard, Phil. Mag. *1*, 518 (1956); A. B. Lidiard, Chapter in Encyclopedia of Physics, Vol. 20, Springer-Verlag, Berlin, 1957.
27. J. R. Manning, Phys. Rev. Lett. *1*, 365 (1958)
28. H. Reiss, Phys. Rev. *113*, 1445 (1959).
29. A. H. Schoen, Phys. Rev. Lett. *1*, 140 (1958). See also Univ. Microfolms, L.C. Card No. Mic 58-5492.

30. S. A. Rice, Phys. Rev. *112*, 804 (1958); S. A. Rice and N. H. Nachtrieb, J. Chem. Phys. *31*, 135 (1959); A. W. Lawson, S. A. Rice, R. D. Corneliussen and N. H. Nachtrieb, J. Chem. Phys. *32*, 447 (1960); O. P. Manley and S. A. Rice, Phys. Rev. *117*, 632 (1960); S. A. Rice and H. L. Frisch, J. Chem. Phys. *32*, 1026 (1960); O.P. Manley, J. Phys. Chem. Solids, *13*, 244 (1960). See also, D. Lazarus, Solid State Physics, *10*, 71 (1960).

31. F. S. Buffington and M. Cohen, Trans. A.I.M.E. *194*, 859 (1952). U. Ujiiye, B. L. Averbach, M. Cohen and V. Griffiths, Acta Met. *6*, 68 (1958). See also I. Ya. Dektyar and V. S. Mikhalenkov, Ukrain. F. Z. *3*, (1958).

32. C. H. Lee and R. Maddin, Trans. A.I.M.E. *215*, 397 (1959), A. F. Forestieri and L. A. Girifalco, J. Phys. Chem. Solids *10*, 99 (1959).

33. J. B. Darby, Jr., C. T. Tomizuka and R. W. Balluffi, J. Appl. Phys. *30*, 104 (1959), *32*, 840 (1961). See also A. V. Savitzkii, Fiz. Metall. i Metalloved, Akad Nauk, SSSR, Ural. Filial *10*, 564 (1960), and P. Chollet, I. Grosse and J. Philibert, Compt. rend. *252*, 728 (1961).

34. N. H. Nachtrieb, H. A. Resing and S. A. Rice, J. Chem. Phys. *31*, 135 (1959).

35. J. B. Hudson and R. E. Hoffman, Phila. Meeting of A.I.M.E., Oct., 1960.

36. A. J. Bosman, P. E. Brommer and G. W. Rathenau, Physica, *23*, 1001 (1957).

37. C. E. Birchenall and R. F. Mehl, Trans. A.I.M.E. *188*, 144 (1950).

38. R. J. Borg and C. E. Birchenall, Trans. A.I.M.E. *218*, 980 (1960).

39. F. S. Buffington, K. Hirano and M. Cohen, Acta Met. *9*, 434 (1961), K. Hirano, M. Cohen and B. L. Averbach, Acta Met 9, 440 (1961).

40. J. Stanley and C. Wert, J. Appl. Phys. *32*, 267 (1961).

41. R. J. Borg and D. Lai, unpublished research, Lawrence Radiation Laboratory, Livermore, Calif.

42. H. W. Mead and C. E. Birchenall, Trans. A.I.M.E. *203*, 994 (1955).

43. F. S. Buffington, I.D. Bakalar and M. Cohen, Trans. A.I.M.E. *188*, 1374 (1950).

44. L. I. Staffansson and C. E. Birchenall, Report from the University of Delaware, AFOSR-733, 1961.

45. For a review of this field see C. Leymonie, "Les Traceurs Radioctifs en Metallurgie Physique, Dunod, Paris, 1960, pp. 86-115.

46. J. C. Fisher, J. Appl. Phys. *22*, 74 (1951).

47. R. T. P. Whipple, Phil. Mag. *45*, 1225 (1954).

48. V. T. Vorisov, V. M. Kzolikov and B. Ya Lyubov, Izvest. Akad. Nauk. S.S.S.R., Otdel. Tekh. Nauk, *10*, 37 (1956). See also H. S. Levine and C. J. MacCallum, J. Appl. Phys. *31*, 833 (1960) for a criticism of Refs. 46,47,48.

49. For example, see R. E. Hoffman and D. Turnbull, J. Appl. Phys. *22*, 634, 984 (1951) and B. Ikkerse, Acta Met. *2*, 551 (1954).

50. For example, see S.R.L. Couling and R. Smoluchowski, J. Appl. Phys. *25*, 1538 (1954) and S. Yukawa and M. J. Sinnott, Trans. A.I.M.E. *203*, 996 (1955).

51. D. Turnbull and R. E. Hoffman, Acta Met. *2*, 419 (1953). See also B. Okkerse, T. Tiedema and W. Burgers, Acta Met. *3*, 300 (1955).

52. A. A. Hendrickson and E. S. Machlin, Trans. A.I.M.E. *200*, 1035 (1954).

53. R. E. Hoffman, Acta Met. *4*, 97 (1956).

54. E. W. Hart, Acta Met. *5*, 597 (1957).

55. F. E. Jaumot, Jr. and R. L. Smith, Trans. A.I.M.E. *206*, 164 (1956).

56. N. G. Ainslie and A. U. Seybolt, J. Iron and Steel Inst. (London) *194*, 341 (1960), N. G. Ainslie, R. E. Hoffman and A. U. Seybolt, Acta Met. *8*, 523 (1960), N.G. Ainslie, V. A. Phillips and D. Turnbull, Acta Met. *8*, 528 (1960).

57. M. C. Inman and H. R. Tipler, Acta Met. *6*, 73 (1958).

58. For example, see V. I. Arkharov, S. M. Klotsman, and A. N. Timofeev, Phys. Metals Metallog. *5*, No. 2, 152 (1957), *6*, 255 (1958), and A. A. Pentina, Phys. Metals Metallog. *4*, No. 3, 122 (1957).

59. J. P. Barbour, et. al. Phys. Rev. *117*, 1452 (1960).

60. R. Gomer and J. K. Hulm, J.Chem. Phys. 27, 1363 (1957).

61. For example, see R. B. Kehoe; R. C. Newman and D. W. Pashley, Phil. Mag. *1*, 783 (1956), Brit. J. Appl. Phys. 7, 29 (1956).

62. R. E. Schlier and H. E. Farnsworth in Advances in Catalysis, 9, 434 (1957). H. E. Farnsworth and H. H. Madden, in "Structure and Properties of Thin Films," Wiley, 1959, pp. 517ff.

63. L. H. Germer and C. D. Hartman, J. Appl. Phys. *31*, 2085 (1960).

64. W. W. Mullins, J. Apply. Phys. *28*, 333 (1957).

65. W. W. Mullins and P. G. Shewmon, Acta Met. 7, 163 (1959).

66. N. A. Gjostein and F. N. Rhines, Acta Met. 7, 224 (1959).

67. N. Hackerman and N. Simpson, Trans. Farad. Soc. *52*, 638 (1956).

68. R. A. Nickerson and E. R. Parker, Trans. ASM *42*, 376 (1950).

69. W. C. Winegard and B. Chalmers, Canadian J. Phys. *30*, 422 (1952); W. C. Winegard, Acta Met. *1*, 230 (1953).

70. J. B. Drew and J. Pye, unpublished research, Franklin Institute Laboratories for Research and Development, Philadelphia, Pa.

Prepared Discussion

DISLOCATIONS AND DIFFUSION IN SILICON

by

Dr. H. J. Queisser

INTRODUCTION

In this note two comments are made about interrelations of impurity diffusion and dislocations in silicon. There will first be a discussion of impurity diffusion along the dislocations of a small angle grain boundary in silicon. Theoretical descriptions and physical interpretations for the observed diffusion enhancement are reviewed. Secondly, the generation of dislocations by diffusion of large concentrations of undersized impurities will be discussed. Regular patterns are observed on boron-doped silicon surfaces. These patterns are attributed to slip caused by the stress in the diffused layer.

A. *DIFFUSION ALONG DISLOCATIONS IN SILICON*

Diffusion experiments were carried out with silicon bicrystals having grain boundaries with a misfit of 10° or smaller. These experiments are described in detail elsewhere[1] and shall only be summarized here.

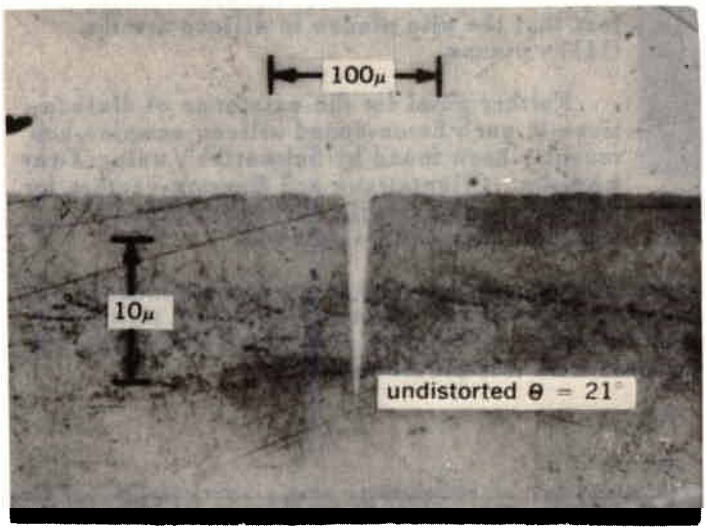

Figure 1. BEVELED AND STAINED SECTION OF A PHOSPHORUS DIFFUSED SILICON BICRYSTAL. PHOSPHORUS-DOPED (N-TYPE) MATERIAL APPEARS WHITE, P-TYPE DARK. DIFFUSION "SPIKE" AT GRAIN BOUNDARY.

Figure 1 shows a beveled and stained section of a p-type silicon bicrystal into which phosphorus was diffused. The p-n junction, as revealed by the staining, is an isoconcentration line. It is seen that the enhanced diffusion at the boundary gives a spike-shaped diffusion front.

Three reasons may be given for the higher grain boundary diffusivity: the concentration enhancement due to the Cottrell attraction[2], a possible similar vacancy enhancement, and a decrease in jump energy at the dislocations.

The first contribution may be estimated theoretically[1]. It follows that the higher the misfit of an impurity, the more enhanced should be the

[1] K. Hubner and W. Shockley in "Structure and Properties of Thin Films", ed. by Neugebauer et al. p. 302 (John Wiley and Sons, New York, 1959); H. J. Queisser, K. Hubner, and W. Shockley, Phys. Rev. 123, 1245 (1961). This work was supported by U.S. Air Force Cambridge Research Laboratory.

[2] A.H. Cottrell, "Dislocations and Plastic Flow in Crystals" p. 56 Clarendon Press, Oxford 1953.

the diffusion at the grain boundary versus bulk diffusion. Recent, unpublished measurements with different donors and acceptors verify this prediction.

A new mathematical treatment of grain boundary diffusion[1] describes the diffusion behavior in terms of the individual dislocations of the small angle boundary. A relation between the tip angle of the spike, the velocity of spike advance and two parameters is theoretically predicted by the so-called "spike-velocity" method. This prediction is fulfilled by the experiments. One dislocation carries about 400,000 times as much phosphorus diffusion flux at 1050°C as does an area of one Burgers vector square of good silicon.

Studies of three layer structures[2] showed interesting interactions between the two impurities that were diffused subsequently into the silicon. It was possible to obtain two diffusion spikes within each other. However, boron diffusions revealed unexpected anomalies. There appeared to be no preferential grain boundary diffusion into previously phosphorus-doped material. On the other hand, phosphorus diffusions caused wide short-circuits through boron-diffused layers at the grain boundary. This indicates some strong interactions with "third atoms" at grain boundaries, as pointed out in Prof. Birchenall's[3] talk.

B. DIFFUSION - INDUCED DISLOCATIONS IN Si

Diffusion of sufficiently high concentrations of undersized substitutional atoms, such as boron in silicon, causes stress which is relieved by the formation of dislocations[4]. The presence of these dislocations has been made apparent by etching of highly boron-doped silicon surfaces[4] or by etching cleavage planes perpendicular to the exposed surface[5].

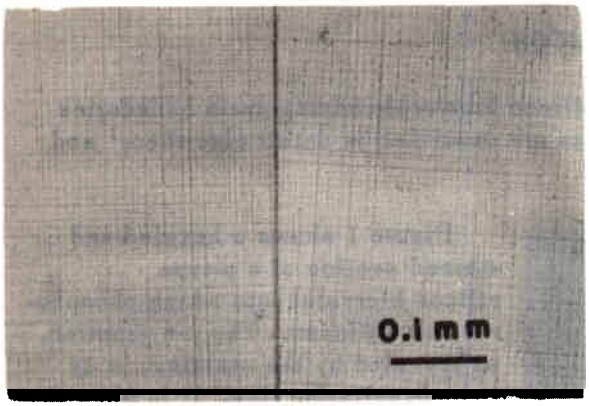

Figure 2. SLIP PATTERNS ON HIGHLY BORON-DOPED (100) SURFACE OF A SILICON BICRYSTAL WITH GRAIN BOUNDARY IN A (110) PLANE

Figure 2 shows a typical example of a surface slip pattern. A bicrystal slice was used in this experiment, which is of course not necessary. The dark center line is the boundary, as revealed by etching. Both grains show sets of lines along (110) - directions. All observed patterns on different crystallographic surfaces can be interpreted *as intersections* of (111) - type planes with the surface. This is consistent with the fact that the slip planes in silicon are the (111) - planes.

Further proof for the existence of dislocations in such boron-doped silicon samples has recently been found by Schwuttke[6], using X-ray methods. Orientations and Burgers-vectors for the dislocations on the different diffused surfaces have been obtained.

Theoretical estimates of strain and dislocation energy are used to predict a minimum amount of boron impurities necessary to favor the formation of dislocations over a strained lattice[3,7]. This minimum amount is estimated to be 3×10^{-15} boron atoms/cm^2 Si surface. Experiments with different amounts of doping agree with this prediction.

---

[1] K. Hubner and W. Shockley in "Structure and Properties of Thin Films", ed. by Neugebauer et al. p. 302 (John Wiley and Sons New York, 1959); H.J. Queisser, K. Hubner and W. Shockley, Phys. Rev. 123, 1245 (1961. This work was supported by U.S. Air Force Cambridge Research Laboratory.

[2] H.J. Queisser, "Diffused Three Layer Structures Along Small Angle Grain Boundaries in Silicon" IRE Conf. on Solid State Device Research, Stanford 1961.

[3] E. Birchenall, Proc. Eighth Sagamore Conf.

[4] H.J. Queisser Bull. Am. Phys. Soc. 6, 106 (1961) and J. Appl. Phys. (September 1961); work sponsored by Air Force Cambridge Research Laboratories

[5] S. Prussin J. Appl. Phys. (Sept. 1961)

[6] G.H. Schwuttke, (private communication)

[7] W. Shockley, manuscript in preparation

RECRYSTALLIZATION AND PHASE TRANSFORMATION

by

Dr. John Newkirk

INTRODUCTION

Most commercially practical materials, high temperature alloys in particular, do not lend themselves well to study by the fundamental approach which most solid state scientists prefer. There are too many components and too many concurrent, overlapping and often competing processes in action at once to allow theories and experiments to be devised which are satisfyingly unambiguous and complete. One school, consisting mostly of the practical alloy developers, has boldly met nature head-on and largely by the "next element in the periodic table" approach have in less than ten years improved oxidation resistance of service alloys by more than two orders of magnitude and increased their strength at 2000°F. by about one order and yet at a production cost of less than half an order higher. This is very respectable progress.

Nevertheless, the weight of evidence indicates that returns, by the empirical approach, must decline seriously before long. Empiricism must therefore be replaced by basic understanding of the effects of common variables on processes related to the manufacture and service of refractory materials. Alloy research and development by the fundamental approach has consequently become the objective of increasing numbers of basic physical scientists. Mostly their work is highly specialized, through the intense study of some single phenomena or process (such as grain boundary mobility) which contributes to the over-all behavior of an alloy in service. After all of the sub-processes are well-understood, there will remain the problem of how one process will influence the others as all act together.

At present we are still at the stage where scientists are hard at work trying to identify and solve problems connected with the unit processes making up recrystallization, grain growth, phase transformations and other long range reactions in crystalline materials. Usually they work with simple systems and study phenomena, hoping that their results can be applied, in principle at least, to more complex metal mixtures. Consequently the literature is full of new information about phenomena, which are more or less related to problems of high temperature metallurgy. Much of this information is illustrated by experiments with materials like lead, silver, lithium fluoride, etc., not particularly inspiring to practicing refractory metals men. As basic understanding develops, we can expect to reap the due rewards in more sophisticated and more effective alloy design. The work of Beattie and Hagle, described later in this paper, proves that some of the practical rewards of basic understanding have already arrived.

With the foregoing paragraphs as my defense I shall now describe what appears to be the highlights of the current status in the fields of recrystallization and phase transformations in metals, accenting phenomena, and de-emphasizing materials. I have picked out those areas in which there has recently been especially significant activity, and in which there appears to be above normal promise of further gain through further effort. The significance of the cited work is pointed out and where possible I have suggested what further steps might be taken to extend our knowledge of recrystallization and phase transition phenomena.

RECRYSTALLIZATION

The most recent survey of the status of the field of recrystallization appeared as a series of papers by Lücke, Beck, Burgers, Detert, Stuwe and Dehlinger (1) earlier this year. W. C. Leslie is now preparing an extensive survey on recrystallization, to be presented at the 1961 Metals Congress and published soon thereafter. Also, there is in preparation, and due for publication early in 1962, a survey on a closely related subject, viz., grain boundary migration by K. Lücke (2). Surveys on phase transformations are mentioned in a later section of this paper.

Within the scope of this conference, recrystallization is understood to be an irreversible process of atom rearrangement which occurs by grain boundary motion during annealing, in which no true phase change is involved and in which diffusion distances for matrix solvent atoms are of the order of only a few lattice dimensions. New crystals grow at the expense of the original ones. There is no long range composition change and the driving energy derives from some source other than the difference in the *chemical* free energies of the recrystallized and the unrecrystallized materials.

Prior to and during total recrystallization, the process of recovery occurs wherein lattice strains which may be present in the matrix, are relieved with only slight changes in the gross microstructure. Recovery is a relatively brief process and is usually accompanied by changes in certain physical and other properties. Atoms are especially mobile during recovery due to the presence of many lattice imperfections. Therefore, they can easily move, generating a relatively unstrained lattice through an unorganized crystallographic relaxation. This local rearrangement sometimes results in the migration of dislocations, vacancies and impurity atoms to positions of alignment, thereby forming subgrain boundaries. The rearrangement polygonizes and relaxes the original strained structure.

Concurrently, this atom rearrangement may lead to the generation of small misoriented regions having little or no mechanical strain and low energy. These relatively stable regions act as the nuclei of a subsequent recrystallization stage. They continue to grow at the expense of their unstable neighbors until the recrystallization process is completed or the necessary free energy for driving the reaction has been dissipated. It follows that whatever tends to promote strain recovery by polygonization will diminish the generation and growth of true recrystallization nuclei. One might in that case expect a larger final recrystallized grain size because of the few initial nuclei.

Usually the more an unrecrystallized material is plastically strained, the smaller is the recrystallized grain size. Heavy cold working therefore can be said to increase the amount of recovery by nucleus formation relative to the rate of subsequent growth of the nuclei.

It is clearly appreciated by now that the enlargement of recrystallization nuclei is a highly complex process. Consequently several workers have recently been concentrating on studies of the nature of recrystallization boundaries and their migration characteristics. Their work is discussed in more detail in a following section. It is enough to say at this point that the contact interface between the recrystallized and unrecrystallized material is the focus of nearly all of the factors which affect the kinetics of the recrystallization reaction. Anything which alters that interface affects the kinetics of recrystallization.

As yet the mechanisms causing many of the recrystallization kinetic effects are quite imperfectly understood. Further studies of the nature and behavior of grain boundaries in

single phase materials are therefore badly needed. However, new techniques and special materials (for example, ultra high purity metals) for such studies are becoming increasingly available so that the probability of success in work of this type appears to be high. Therefore most of what follows in this section concerns grain boundaries, their structure, their properties, how they move, and how they can be observed.

I. *GRAIN BOUNDARY STRUCTURE AND RECRYSTALLIZATION*

A point on a grain boundary can in general be described by specifying angular degrees of tilt and degrees of twist of the adjoining crystals at that point. The structure and placement of atoms at small angle boundaries (ca. 10^{-4} radians) is now fairly well understood in these terms, as is exemplified by well known experimental work of Vogel in 1955 and more recently of Hirsch and co-workers.

For large angle boundaries however, the picture is not nearly so clear. Several models have been proposed which will be briefly outlined here.

1. The "island" of group-process model, suggested by Mott (3), describes zones or islands of more or less close crystallogrphic registry between the adjoining crystallites, with corresponding regions of poor fit, which are sometimes described as disordered or melted. It is proposed that the cohesion of two adjoining crystals arises mainly through their interaction at the islands of good fit. The movement of the boundary would require groups of atoms on one side of the regions of misfit to "melt," i.e., to leave their positions of crystalline regularity as the disordered interface passes through. The theory has recently been tested using the "group melting" criterion. This is described later.

2. The "undercooled liquid" model described by Ke (4) assumes that a crystallographically disordered region of 2 to 3 atom distances in thickness exists between adjoining grains. This region is supposed to have a quasicrystalline structure similar to that usually associated with the glassy state. Boundary motion in this model would involve individual and unorganized atom removal from original lattice positions to other crystallographic positions on the new grain across the boundary.

3. Kronberg and Wilson (5) have shown geometrically that there may be "special" orientations of high angle boundaries for which the lattice sites of the undistorted crystals on both sides of the boundary are coincident at the boundary. They proposed that these special positions of adjoining crystals should be associated with a lower boundary energy and higher boundary mobility than that of positions a few degrees away in any direction. Considerable support has been found for their ideas. This also will be discussed in more detail later.

4. Read and Shockley (6) proposed that a grain boundary can be described in terms of arrays of screw and edge dislocations. Boundary movement could then be explained by allowing the dislocations to move according to standard rules for their glide in the slip plane and for climb normal to the slip plane.

Considerable work has been done to clarify the true nature of recrystallization boundaries, mostly in terms of the preceding four concepts. Unfortunately the experimental work has not resolved completely the role of impurity atoms which reside at or near the boundary itself. Recently, with the increased application of zone refining methods, more definite results have been reached, notably by Aust and Rutter (7). These authors reduced the impurity level in several metals, probably to a few parts per million, and then added very small amounts of

known impurities to specimens of controlled crystalline orientation. They could then study rates of boundary motion under more closely controlled conditions then have ever before been possible.

The recent results of several investigators on the rates of grain boundary motion will now be discussed relative to the various models of grain boundaries which have been outlined above.

THE "ISLAND" THEORY

According to Mott's model a boundary must move by the disordering or melting of a group of atoms on one side of the boundary and reordering them as a part of the newly forming lattice on the other side. Aust and Rutter (8) have tested the group aspect of the theory by comparing the entropies of activation predicted by Mott with their observed activation entropy for boundary motion in pure lead. Figure 1 shows that a consistent disagreement of about 15 cal. per degree per gram atom exists between Mott's theory and their experiments. The theory also predicts the rate of boundary migration in terms of controllable variables and reasonable assumptions. However, the experimentally determined rates, even with the purest zone refined lead are from 100 to 1000 times less than those predicted.

The apparent failures of the Mott theory do not necessarily deny his physical picture of the grain boundary. They only indicate that boundary motion does not proceed by the process of disordering (melting) groups of "n" atoms each, which are presumed to occur at intervals along the boundary.

UNDERCOOLED LIQUID

Recent evidence has been found which indicates that boundary motion occurs by single atom jumps. Assuming that the elementary process in moving a boundary consists of activating not a group of atoms as in the Mott theory, but rather a single atom, one can neglect the entropy term in the boundary velocity expression:

$$V = k \frac{\Delta F}{T} e^{-\frac{Q}{RT}}$$

where K includes the atom vibration frequency and Planck's constant. This allows a calculation which can be compared with measured boundary mobility rates. A comparison of this type was made for refined lead by Aust and Rutter and good agreement was found for special Kronberg-Wilson boundaries, but not for those of crystals in random large-angle orientation relationship. These results may be qualitatively explained in terms of residual impurities, the effects of which are not taken into account by the theory but which effects are least in the case of the special boundaries. It seems to be justified to take this work as further evidence that boundary mobility occurs not by group processes but by unorganized activation of single atoms. For the case of lead the activation energy for grain boundary migration was measured by Aust and Rutter to be approximately 6 Kcal per gram atom, which, as Turnbull (9) points out, might be expected to be the same as for grain boundary self-diffusion. An approach to this comparison can be made using the data summarized in Table I. The close agreement among the activation energies implies that grain boundary diffusion and grain boundary migration occur by similar basic processes. Even more to the point would be a comparison of boundary motion with selfdiffusion at grain boundaries. Unfortunately such data are not available for highly pure lead.

TABLE I

FREE ENERGIES OF ACTIVATION FOR LEAD, 300°C

	F_A Kcal per G Atom	Source
Grain boundary migration	Δ 5.2 ± 0.5	Aust and Rutter (1958)
Grain growth	6.2 ± 0.7	Bolling and Winegard (1958)
Grain boundary diffusion	9 5-6	Okkerse (1954) Turnbull and Treaftis (1958)

About 12 years ago Kronberg and Wilson suggested that special grain boundaries may exist which should have high mobility. These boundaries are characterized by a high density of atomic sites which are common to the unstrained lattices on both sides of the interface. An example of this arrangement is given in Figure 2. This diagram shows a (111) plane of two face-centered cubic crystals which have been rotated 22 or 38 degrees about their common <111) crystallographic axes. One in seven of the atomic sites in one crystal coincide with those in the other. The coincident atoms are shown as white areas. As the boundary moves, these special atoms need not move at all. Also, since these special boundaries have relatively good lattice matching between the adjoining crystals, one might expect that foreign atoms will have less tendency to segregate there than at the higher energy random boundaries. It follows that the properties of special boundaries should be less influenced by the presence of impurities than are random boundaries where the degree of misfit is higher and the tendency for solute segregation is therefore greater. Again, supporting evidence for this concept is found in the fact that the activation energy for boundary motion of lead is highly dependent upon impurity (Sn) concentration when the boundaries are of the random type but is very small for Kronberg-Wilson boundaries and practically independent of concentration in the dilute range studied by Aust and Rutter (see Figure 3). Energy cusps of the Kronberg-Wilson type were observed by Aust and Rutter in lead. In copper however they have not been detected though they were specifically sought by Gjostein and Rhines (10). The reason for this is not clear.

A basic feature of the Kronberg-Wilson model is its insensitivity to the curvature of the boundary. One can see from Figure 2 that the pattern of the set of coincident atoms is unchanged whether or not the boundary is curved. This geometrical circumstance is favorable for the development of the curvature which is often necessary for boundary migration and sharply distinguishes the K-W special boundaries from twin boundaries. In twinning the atomic matching is even better but no curvature is possible. Since twin boundaries move relatively slowly it is clear that boundary coherency alone does not govern the migration rate.

THE LUCKE-DETERT THEORY (13)

The retarding effect of substitutional impurity atoms on recrystallation kinetics has been known by empirical experience for a long time. In the refractory metals the varying potency of different solute elements for retarding recrystallization is especially striking though there appear to be some curious and little understood exceptions. For example in molybdenum a few elements actually depress the one hour recrystallization temperature, though most elements have the normal elevating influence. (See Figure 4).

In tungsten interstitial impurities appear to have little effect on the recrystallization temperature, while minute increases of trace substitutional metallic elements can increase the recrystallization temperature by amounts up to 900°F (12).

The Lücke-Detert (L-D) theory is an attempt to account for the effects of impurities on the migration behavior of random grain boundaries. In this theory it is assumed that interaction forces exist between foreign atoms in solid solution and the boundary, acting to increase the concentrations (or low temperatures) of impurities at the boundary (see Figure 5). At high concentrations the moving boundaries are held back by the foreign atoms, and the speed of the boundary is controlled by the rate of transfer of the foreign atoms diffusing behind it. At low concentrations (or high temperatures) the boundary is not held up by the foreign atoms and breakaway occurs, allowing the boundary to move faster. It is predicted that below the critical concentration for breakaway, the recrystallization temperature would drop much faster with decreasing concentration than it does above this concentration. Besides this effect, the total amount of solute accumulating at the boundary at steady state should be temperature dependent, thereby causing a more potent inhibiting effect on migration rate at lower temperatures. Therefore the migration rate in an impure material would be influenced by at least two temperature-dependent processes, viz. a) solvent atom transfer across the boundary and b) solute segregation to the boundary. The presence of impurities would thus be expected to increase the temperature dependence of migration rate and to give a measured activation energy for migration which is larger than that corresponding to the simple transfer of solvent atoms across the interface. Many qualitative observations support these ideas.

To explain quantitative measurements, Lücke and Detert propose that the speed of a boundary is controlled by the rate of bulk diffusion of the foreign atoms in the newly formed lattice behind the boundary. If this proposition were true, the activation energy for grain boundary migration should equal that for bulk diffusion of the solute in the matrix lattice. In fact, however, recent quantitive measurements of the effect of tin in lead (see Figure 6) do not support the idea that bulk diffusion controls the boundary migration rate. However, Turnbull (9) has pointed out that experimentally determined activation energies may be abnormally high due to the influence of inclusions in retarding grain boundary motion. For the case of silver and gold in lead, Aust and Rutter found that the apparent activation energies for grain boundary motion were lower than those predicted by several orders of magnitude. Leslie and co-workers (15) have recently shown that the effect of manganese on boundary motion in iron is about 1000 times larger than predicted by the Lücke-Dietert theory. The latter work (Fe) covered a relatively broad concentration range and so constitutes a better test of the theory than does the cited work on lead.

An evident weakness of the L-D theory is that it takes no account of the now recognized orientation dependence of the kinetics of grain boundary migration. Also, only elastic interactions are considered; possible chemical and electronic effects are ignored. Furthermore, in molybdenum (16) the presence of Ni, Co and Fe actually increases the recrystallization rate, an effect which is not easily explained in terms of the L-D model. See Figure 4.

Incoherent boundaries are believed by some (42) to be governed by a diffusion coefficient which may be identified with the grain boundary diffusion coefficient, presuming that such a single valued quantity exists. Turnbull points out (9) that there is no theoretical justification for this assumption and that other controlling factors must be identified before complete understanding of incoherent grain boundary motion is reached. It is clear that much more will have to be learned about the interaction of different solute atoms with various types of grain boundaries before a satisfying picture of grain boundary migration can be had.

DRIVING ENERGY

The three most probable sources of driving energy for recrystallation are: 1) The difference in bulk free energy of the recrystallized and unrecrystallized material, 2) the difference in sub-grain boundary free energies and 3) the difference in free surface energies. Creep, polygonization and other local thermally activated local atomic adjustments reduce the difference in bulk free energy during the early stages of annealing, thereby lessening the probability of total recrystallization. Semmel and Machlin (17) feel that at least in silver the energy of dislocations in the unrecrystallized material play only a small part in driving the reaction and that excess point defects, especially vacancies produced by the applied plastic deformation provide the major source of driving energy. They propose that internal vacancy sinks are not infinite and that the long vacancy degradation time which they observed is a measure of the time required for the excess vacancies to diffuse to the specimen surface. Their views could be checked more directly if some technique could be applied for observing the number and distribution of point imperfections.

Walter and Dunn (18) showed by an ingenious but simple experiment that under suitable conditions surface impurity atoms can effect an actual reversal of the growth of suitably oriented adjoining silicon-iron crystals. They show that surface impurities can be an important factor in and sometimes control, the competitive growth of crystals in an aggregate. Essentially their method consisted in observing the position of the boundary between two crystals which presented respectively their (100) and (110) planes to the free surface of the specimen. When held at 1200°C in a good vacuum the boundary advanced into the (100) grain, i.e., the grain which had a low density plane at the surface. However, when impure argon was admitted to the atmosphere the boundary retreated into the (110) grain. These authors conclude that one effect of surface impurities is to reduce the free energy of the (100) surface below that of the higher density (110) surface and that this difference is enough to control the direction of grain growth. Walter and Dunn's work is wholly qualitative but is a strong indicator that surface effects must not be neglected in considering the mechanism and kinetics of recrystallization and grain growth, especially in sheet materials. This is further evidence that more study of the surface structure and energy of crystals is needed to complete our understanding of their bulk behavior. Real and formerly unexpected benefit might be gained through the application of surface energy sources in driving metal reactions.

In another series of experiments (19) Aust and Rutter showed that the driving energy for grain boundary motion could derive from the sub-grain boundaries which existed in as-solidified crystals of high purity lead. They found that migration of a recrystallized grain boundary into a striated grain removes the striations as it sweeps ahead, suggesting that the energy of the relatively disordered striation structure provides the driving energy for the boundary migration. One may also offer the suggestion, on the basis of Semmel and Machlin's ideas, that point defects, instead of striation boundaries, provide the energy for the boundary movement. However the likelihood of this is slight since, in the experiments with lead, new grains would not grow in a direction normal to the direction of the striations and grew most rapidly when the interface was so oriented that it intersected a maximum number of the striation boundaries.

EFFECTS OF THERMAL GROOVING

Another influence on boundary migration kinetics is the groove which constantly tends to form along the line where the boundary intersects the specimen surface. Mullins (20) and others have advanced a theory to express this effect quantitatively. Evidence to support the Mullins concept is given in Figure 7 in which successive positions of a boundary are seen as

an organized pattern of grooves. This effect is said to result from spasmodic movement of the intersection of the boundary with the surface. The spasmodic motion is explained as follows: A migrating boundary becomes stuck at the surface due to the lower energy at a groove in the surface. Meanwhile the boundary below the surface can continue to migrate so far that the portion close to the surface becomes nearly parallel with the surface. This constitutes a very unstable situation so that the edge at the surface pops out of its old thermal groove and moves along the surface very rapidly until it catches up with the interior boundary. There it moves so slowly that surface forces and thermal atomic motion can again cause the formation of a groove which pins the boundary edge and the cycle is repeated. Whether surface boundaries will always move in a spasmodic manner or follow a steady state behavior probably depends upon many factors which are not yet evaluated. Very recent unpublished studies of G. V. Smith show that spasmodic recrystallization boundary movement can occur without the influence of a thermal surface groove.

EFFECTS OF INCLUSIONS

It is well established that foreign particles can retard the motion of grain boundaries. For example the relatively small amount of recrystallization and consequent sustained high elevated temperature strength in the refractory alloy F48 (Mo 5, W 15, Zr 1, C.03, N .01, Ox .03) is probably due to the presence of stable compound inclusions. See Figure 8. Also the power of finely dispersed thoria to inhibit grain growth in tungsten is well known. Most of the recent basic work in this area has been done on silicon-iron sheet because of the commercial importance of this soft magnetic material. The presence of certain sulfides in Si-Fe is known to be necessary for the successful development of the desired secondary recrystallization texture. Apparently the function of the sulfide inclusions is to retard primary recrystallization so that secondary recrystallization can proceed. This retarding effect of minor impurities is not thoroughly understood, nor is it always recognized when experimental observations of boundary migration rates are interpreted. It was mentioned earlier that activation energies measured in recrystallization experiments may sometimes appear to be abnormally high as a result of the unrecognized retarding influence of inclusions. This effect is especially marked when there are many different degrees of dispersions of the inclusions. The measured activation energy then would be the result of the operation of at least two thermally activated processes, one of which would be the interaction of the moving boundary with the array of inclusions. Any work which is done on the kinetics of boundary movement should not neglect the inclusion effects.

The foregoing paragraphs illustrate that with different materials and under different experimental conditions it is apparently possible for the main driving energy for recrystallization to come from one of several sources. No one has attempted to generalize on the subject, though a complete theory would be useful. More experimental work following the methods of Aust and Rutter and of Leslie and co-workers, where experimental conditions are carefully controlled, should pave the way to a more thorough description of the process of grain boundary migration.

EFFECT OF ELECTRONIC STRUCTURE

Some empirical observations by Abrahamson and co-workers (21) have indicated that there may be a direct and fundamental relationship between the rate of change of the recrystallization temperature of a metal and the electronic structure of added solute elements. On the hypothesis that recrystallization is an atomic bonding phenomenon they reasoned that the outer shell electrons might be directly involved in the recrystallization or boundary motion process.

Their first experiments consisted of adding small amounts of solute metals to 99.95+ Pct iron and observing the temperature at which a cold rolled specimen softened (i.e. recrystallized) during a one hour anneal. As expected, all of the transition elements raised the recrystallization temperature, with the greatest effect occurring at or less than 0.10 at .% solute. Of more interest is their finding that a linear correlation exists, when the number of outer s shell electrons in the solute is constant, such that the logarithm of the rate of change of recrystallization temperature with atomic per cent solute is a linear function of the number of outer d shell electrons of the solute atom. Figure 9 illustrates their results and shows that the curves for solutes having 0, 1 and 2 outer s shell electrons are parallel and that 1 and 2 have a definite minimum effect at seven d electrons. Also, in iron, for solute atoms having a like number of outer d shell electrons, the fewer outer s shell electrons there are the greater is the magnitude of rate of change of recrystallization temperature. These experimental results are as yet not supported by any detailed theory. More recent work which I hope Dr. Abrahamson will describe to us during the discussion period, has provided qualitative confirmation of his earlier findings. These observations are most interesting, and a satisfying interpretation in fundamental terms would be very welcome. To my knowledge no one except Abrahamson and his immediate co-workers are studying recrystallization from this point of view.

INFLUENCE OF GRAIN BOUNDARY MOBILITY ON PREFERRED ORIENTATION

The origin of recrystallization textures in cold worked, then heat treated metals is still not clearly identified. In an attempt to explain the origin of textures in recrystallized polycrystalline sheet copper and silicon-iron, Hibbard and Tully (22) performed a very ingenious experiment. They coldrolled single crystals of copper and Si-Fe in orientations specifically chosen to produce individually the major known components of the polycrystalline deformation texture. The orientation dependence of the recrystallization kinetics was then observed with respect to the primary recrystallization textures of these specimens. Surprisingly, they found that in both copper and Si-Fe the orientation components which recrystallized the fastest in the rolled single crystal specimens are not those which are present in the normal recrystallized textures of initially polycrystalline material. Therefore they could not rationalize or synthesize polycrystalline behavior on the basis of their single crystal experiment. Their results suggest that the interaction of adjoining grains during the deformation of polycrystalline aggregates plays an important role in determining not only the rolling texture but the final recrystallized texture as well.

Aust and Rutter have had some very recent results (unpublished) which in part support the oriented nucleation-growth theory of Burgers (23). In this theory the growth selectivity could be due to differences in large angle boundary mobility by virtue of randomly occurring Kronberg-Wilson boundaries. Also, Burgers suggested that these special orientation relationships might be associated with the low energy cusps in the curve of interfacial energy vs. angular misorientation derived by Read and Shockley (6). In their studies of grain boundary mobility in pure lead Aust and Rutter found that the temperature dependence of the grain boundary migration rate is smaller for large angle coincidence-type boundaries than for large angle *random* boundaries. In Figure 10 the upper curve refers to a coincidence-type boundary of the sort discussed by Kronberg and Wilson. The mobilities of these two types of boundaries are similar at 300°C, but at 175°C the coincidence-type has a greater mobility by a factor of four. This observation suggested an experiment by which the authors could show that competitive growth of randomly oriented recrystallized grains into a striated mono-crystal of zone-refined lead produced a multi-crystalline aggregate with preferred orientations of the

coincidence type during annealing at 175°C but not at 300°C. This preferred orientation clearly resulted from the higher mobility and lower energy of large-angle coincidence boundaries compared to large angle non-coincidence boundaries.

These results are in outright disagreement with any theory of annealing textures which presumes that textures are determined by oriented nucleation alone. The oriented growth theory of Beck (24) states that the orientation dependence of grain boundary mobility alone is sufficient to account for observed annealing textures and that grains in preferred relative orientations can grow most successfully in competition with their randomly oriented neighbors. Aust and Rutter's results do demonstrate the importance of grain boundary mobility in determining whether preferred orientation relationships are introduced by a twinning process in which relative grain boundary energy is the decisive factor. However, in Beck's oriented growth theory it is assumed that the highest mobility boundaries are only those of maximum misfit and consequently of maximum relative energy without regard to the coincidence site boundaries of lower relative energy. This assumption is not in accord with the experimental findings on lead.

It is possible that the experimental work of Aust and Rutter, supporting the oriented nucleation-growth selectivity theory of Burgers (23) for the origin of recrystallization texture, may initiate a break-through in our understanding of the subject. Continued experiments of the Aust-Rutter type in other systems including refractory alloys would be most useful.

PHASE TRANSFORMATIONS

Excellent and recent reviews of the fundamental aspects of this subject are included in "Perspectives in Materials Research" (25). Also, still useful are the proceedings of the Institute of Metals Symposium on the Mechanism of Phase Transformations in Metals (26). A review of the theory of diffusional growth in solid-solid transformations has been made by J. S. Kirkaldy and will soon be published as part of an AIME monograph (27). H. T. Aaronson also has in preparation a review of phase transformation processes in which he gives special attention to the morphology of the product phase. This review is due late this year. Therefore only those parts of the subject wherein critical problems are well recognized, especially those concerned with refractory metals and alloys, are discussed here. I shall attempt to define the problems and to indicate, where possible, the most promising approach to their solution.

A large amount of effort has been spent trying to apply the quantum mechanical theory of cohesion to the calculation of the differences in thermodynamic properties of phases (62). In spite of these attempts it is not yet possible to calculate the stability of one phase relative to another from fundamental principles. What success there has been in this area has come mainly from the use of empirical crystal chemical correlations, and at this point it appears that the empirical approach will probably continue to be the most fruitful.

A solid state system may undergo a phase change by a discontinuous (sometimes called first order) or a continuous (second order) transition. In the former case the process is by nucleation and growth of small domains of the new phase and all reaction occurs at the interface between it and the surrounding matrix. In the case of the continuous transition there is a continuum of intermediate states between the initial and final states without a sharp phase interface, i.e., the process occurs homogeneously throughout the system.

Continuous phase changes are not uncommon in metal systems. For example order-disorder transitions are sometimes but not always of the second order type. There exist at present a

few phenomenological theories about the order of phase transitions.[28,29] Some of these are in part consistent with observation. For example in systems having a close-packed structure there is apparently a strong tendency for an order-disorder reaction to be first order. But as yet no theory exists by which the transition type can be predicted from 1st principles.

A defect in theories of continuous transitions is that they treat those transitions as homogeneous first order processes which are governed from start to finish by a single relaxation time. This cannot be an accurate assumption because the many small coherent antiphase domains which form initially must be structurally isolated from one another and will presumably grow according to one relaxation time constant. Later in the process competitive intersection sets in and the more stable domains (largest, least strained, etc.) grow at the expense of the others. The latter process is distinctly different from the first and as far as I know no theory takes this two stage mechanism into account.

Discontinuous phase changes in general occur by nucleation and growth, as do the primary and secondary recrystallization processes. The overall rate of the reaction is specified by the frequency of nucleation and the rate of motion of the new phase boundaries. Both of these parameters are now fairly well understood in simple systems and it only remains to apply them to the useful interpretation of phase transitions in practical materials. Recent analytical results of Ham (30) on diffusion-limited precipitation processes show that unfortunately no conclusion about the morphology of the precipitate can be drawn from the time exponent of the transformation law. More will be said about the problem of precipitate morphology in a later section.

An appreciation of the effects of high specific surface energy of very small particles in discontinuous phase transitions has resulted from a rigorous theoretical treatment of Lifshits et al (31). These authors recognized that, because of the small size of precipitate particles during early stages of nucleation, the solute concentration still greatly exceeds that corresponding to equilibrium in the presence of large crystals of precipitate. They arrived at the conclusion that in general a characteristic size distribution should be approached asymptotically with time.

A very serious problem in the field of solid state transformation kinetics is our poor understanding of the structure of solid-solid interfaces, their interaction with impurities and their influence on the growth of a new and different phase. The interface may separate domains which differ in crystalline orientation, structure, composition or all three. A limiting case is that of the coherent interface which separates domains which are nearly continuous crystallographically but which differ in composition. Recent theoretical work of Cahn and Hilliard (32) has indicated that across a coherent boundary the free energy associated with the boundary will be least if the composition change occurs over several layers, i.e. if the composition boundary is somewhat diffuse. Experimental confirmation of their results remains to be done. This is technically difficult since observations must be made on an atomic scale.

Boundaries separating domains which differ only in crystallographic orientation (single phase aggregate) can in many cases be represented as dislocation arrays. Those separating two different crystalline phases can sometimes be represented as a single phase grain boundary with an equivalent array of dislocations, though their energy appears to be slightly less than that of the equivalent grain boundary. This similarity has been applied in a few cases (33) but the risk of oversimplification is great and caution is needed.

It was pointed out in an earlier section that no satisfactory model exists for large angle incoherent grain boundaries or between phases which differ greatly in structure. That such boundaries need not be completely isotropic has been shown by Hoffman (34) who found that in silver at non-special tilt boundaries as large as 45° the rate of diffusion is clearly anisotropic. This is apparently the result of second order crystallographic influences which are quite imperfectly understood. Broadly speaking, it is expected that structural differences will contribute much more to the boundary energy than composition differences. Thus the energy of a semi- or incoherent boundary is likely to be much greater than that of a coherent one, regardless of composition effects.

New techniques may very well be successfully applied to the observation and characterization of grain boundaries. Individual dislocations can now be rendered visible by a variety of methods including electron microscopy, X-ray diffraction microscopy, etch pitting techniques, ion emission microscopy and Borrmann micro-radiography (35). It seems that the solution of some of the grain boundary problems may soon be reached by the application of these new techniques.

INTERFACE MOTION AND MORPHOLOGY

The motion of boundaries in phase changes is related to that occurring during recrystallization, with the important additional requirement that where composition changes are involved a continued supply of solute atoms by diffusion to and across the interface is essential. Measurements of growth rates in precipitation systems have indicated that the kinetics is determined by the volume diffusion of solute to the interface (also sometimes by diffusion along a grain boundary) rather than the process of crossing the boundary. The morphology of the precipitated particles however is often different from that expected on the basis of diffusion alone. In these cases the interfacial characteristics, diffusion rates or some other kinetic or thermodynamic property may control the shape of the product.

The morphology of transformation products has been considered recently by several authors. Dubé, Aaronson and Mehl (36) propose that in the case of decomposition of austenite in hypoeutectoid steel, the proeutectoid ferrite morphology can be classified according to the following terms:

1. Grain boundary allotriomorphs
2. Grain boundary idiomorphs
3. Widmanstatten sideplates, sometimes called Widmanstatten sawteeth
4. Intra-granular idiomorphs
5. Intra-granular Widmanstatten plates

These morphological forms are sketched in Figure 11.

Aaronson in particular, has been looking at a number of transformations with special attention given to the morphology of transformation products. He has found that the Dubé system of morphological classifications often applies. Good examples of the various shapes, as seen by section polishing, are given in his recent study of a hypoeutectoid Ti-Cr alloy (37). Many other examples can be found (for example, Figure 12 in the present paper) of structures which seem to fit the Dubé system. The general applicability of the system and, more important,

the understanding of the factors which determine what morphology will be taken by a transformation product, are important areas for future study. Evidently such properties as grain boundary energy and structure are important as well as bulk and boundary diffusion rates, dislocation climb and other motion behavior, lattice strain energy and bulk free energy relationships between the matrix and transformation product. A few generalities about reaction product morphologies appear to be emerging from the work of Aaronson and others. For example when the crystal structure of a cubic lattice precipitate is very close, both in lattice type and parameter, to the parent matrix, the precipitate usually takes the form of intragranular equiaxed idiomorphs, which are cubic in shape and are sometimes orthogonically sliced through the cube center (38,39).

Kirkaldy has concluded that most of the unsolved morphology problems in solid-solid transformations are those of complexity rather than principle. He recognizes that the problems of morphological growth may not be soluble through a theory which is limited to macroscopic situations and in which therefore classical thermo-dynamics can be freely applied. Actual situations, involving the kinetic nucleation of very small units of a new crystalline species and their diffusional growth may require sequences of structural and thermodynamic metastability analogous to some chemical and bio-chemical processes. The nucleation processes, requiring the cooperative action of small numbers of atoms, may not lend themselves to the standard thermodynamic treatment. To meet this possibility he advances "variational principles" on which he bases theories to explain observed morphological growth for steady and non-steady state processes. These theories are too involved for discussion here but have evoked considerable interest and remain to be thoroughly tested experimentally.

The drastic effects which high energy boundaries may have on transformation kinetics has not been much exploited, though some of them are at least qualitatively recognized. For example it has been shown that tin can precipitate from a lead-tin solid solution at an appreciable rate at temperatures as low as -70°C. It is now fairly well established that the abnormal rate of this reaction occurs by virtue of very rapid diffusion along the moving incoherent boundary between both the precipitate lamellae and the reoriented lattice of the solute (40). Another mechanism of abnormally rapid diffusion reactions, for example in Al-Ag, Al-Cu, Al-Zn alloys, at temperatures as low as -60°C involves the influence of a high concentration of vacancies at the reaction temperature which were retained by rapid quenching (41). The scientific and technological impact of these high diffusion rate phenomena are probably not yet fully appreciated.

MARTENSITIC REACTIONS

All the transformations discussed above involve the movement of a so-called non-glissile interface, i.e., one which requires thermal activation for the interface to move. The other main class of transformations, including most twinning and martensitic transitions, involve the rapid organized movement of atoms without thermal activation. Such interface motion is called glissile. The dislocation motions by which glissile interfaces move has been theoretically proposed in a recent high quality review (25). The verification of the theoretical details, however, is yet to be done.

Another problem concerning the martensite reaction is the anomalous combination of effects of some elements. Chromium for example, is know to favor the formation of the α-phase of iron (Cr forms a closed -loop in the Fe-Cr system); on the other hand Cr is found to lower the Ms temperature. Alternative explanations for these apparently inconsistent effects are offered by Zener (magnetic specific heat effect) (43) and by Kaufman (regular solution thermodynamic effects) (44). The question is apparently still not settled.

NUCLEATION

Although cases are occasionally reported (45) in which homogeneous nucleation is thought to have occurred, nearly all actual metal crystals contain ubiquitous nucleation sites such as impurity particle surfaces, grain boundaries and dislocations where nucleation catalysis occurs before true homogeneous nucleation can be achieved. Furthermore, the most reliable nucleation theory predicts that the frequency of homogeneous nucleation should be a strongly decreasing function of the degree of lattice misfit between the two structures. Consequently the conditions necessary for developing a very high motivating free energy, i.e. high supersaturation (low temperature), are usually such that atomic mobility in the bulk crystal is too low to allow the reaction to proceed at a sensible rate. Quantitative observation of nucleation frequency in solids is experimentally quite difficult and more definitive experiments on the subject are badly needed to clarify the theory. What little qualitative information is available seems to support the theoretical description by Brooks (46). In cases where very high particle densities (from 10^{15} to 10^{18} per cm^3) are observed, either the structural misfit has been very small, e.g. Co from Cu-Co, Zn from Al-Zn, Fe from Cu-Fe, or the supersaturation (driving energy) has been very large, e.g., Cu from Al-Cu, Cu from Si-Cu and Sn from Pb-Sn.

The inoculation treatment used by Saulnier (47) in studies of precipitation in Al-Si alloys has provided a stimulus to the understanding of nucleation. He found that by rapidly quenching dilute alloy of Si in Al from the homogenizing temperature and holding it for a suitable time at room temperature or below, the number of silicon precipitate particles formed during aging at 200°C was of the order of 10^{16} per cm^3 instead of about 10^6 which form during ordinary aging at 200°. Saulnier believes that this inoculation treatment leads to the formation of vacancy clusters (dislocation loops) which might serve as nucleation catalysts or that, because of the high supersaturation and the high silicon mobility due to the excess vacancies present after the rapid quench, actual homogeneous nucleation occurred at room temperature. The latter interpretation is apparently favored since the number of silicon particles seen during aging after inoculation is much larger than the number of dislocation loops which formed, as observed by electron microscopy. No doubt commercial application has often, perhaps unknowingly, been made of the inoculation principle. A sound understanding of the phenomenon and its influence upon transformation kinetics however, is much to be desired so that the phenomenon can intelligently be put to more effective use.

The interaction of various types of precipitates in complex high temperature alloys often leads to their physical behavior which is quite difficult to understand. For example in iron or nickel base alloys (1200°F to 1800°F service) which are hardened by precipitation of Ti-and Al-containing phases, the hardening has been attributed mostly to the η phase (hcp Ni_3Ti) by Craver et al (48), the γ' phase (fcc Ni_3Al) by Beattie and Hagel (49) and to both by Lena (50). The picture is made unclear by the reported absence of γ' in the phase diagram of Taylor and Floyd (51) at low aluminum contents and by the characteristically coarse dispersion of η which would not be expected to contribute much to hardening. A further complication in Fe-Ni base alloys has been the appearance of a grain boundary transformation, notably after cold working, which significantly reduces the notched stress-rupture properties. Attempting to resolve these problems Mihalisin and Decker (52) studied the transformations in Ni-base alloys containing Ti and Al, with special emphasis given to mutual solubilities of phases and to non-equilibrium transition structures. They concluded that under non-equilibrium conditions during aging the γ' structure which forms by continuous precipitation can have any composition between fcc Ni_3Al and Ni_3Ti and that the non-equilibrium Ti-rich γ' phase decomposes on overaging to the equilibrium η phase by an intragranular as well as a grain boundary reaction. They conclude that hardening is due mainly to the γ' phase, thereby confirming Beatty and Hagel. Boron

additions retard the grain boundary conversion to η but have no effect on the intragranular reaction. Replacing Ti by Al retards the $\gamma' \rightarrow \eta$ conversion, both at and away from grain boundaries. The micro-structures of the γ, γ' and η phases which they found at various stages of precipitation are reproduced in Figure 12.

This type of study illustrates the empirical approach by which useful information can be obtained about complex phenomena and systems commonly found in high temperature alloys. Continued study of fundamental processes are much needed; but in most practical materials the compositions and treatments which have been found empirically to give the best properties are anything but simple. The most effective approach to their understanding has been through intelligent though still empirical methods.

Pursuing this problem in a systematic way, Beattie and Hagel (53) have recently had success in characterizing multicomponent austenitic alloys by certain features of their transformation processes. They found that certain groups of elements act as one, and that the relationships among some precipitation processes are relatively simple. Reporting on extensive aging studies of seven complex cobalt or nickel-base austenitic alloys, they propose that the precipitation reactions in all seven alloys could be grouped into one of two classes, depending on the base composition. They point out that their findings are largely consistent with earlier little known work of Laves and Wallbaum (54) and constitute a recognition of important generalizations about the transformation behavior of many austenitic refractory alloys.

According to Laves and Wallbaum (confirmed by Beattie and Hagel) elements in the central portion of the periodic table can be divided into groups A and B, as shown in Figure 13, with respect to their precipitation behavior in binary A-B alloys. They found a consistent change in crystal chemistry for the B-rich intermetallic phases as the B-member passes to the right from cobalt and its homologues to nickel and its homologues. The vertical line dividing the chart separates element groups of clearly different crystal chemistry B-elements to the left of the line combine with A-elements to form the complicated structures of Laves (AB_2) or σ (unstoichiometric) phase; adding molybdenum and tungsten to the A-group introduces μ phase (A_6B_7) as well as more examples of Laves and 6 phases. B-elements form ordered close packed structures of the formula AB_3. This general behavior has been confirmed several times, (55) although as Beatty and Hagel point out, there are indications that the dividing line should be moved to the left to bisect the cobalt group, since several examples of ordered AB_3 cobalt compounds are known, as well as Laves, σ and μ phases of cobalt. The Laves-Wallbaum dividing line apparently also separates B members that seek minimum interstitial space (Kasper polyhedra) (56) from those that seek crystal structures of high symmetry.

The Laves-Wallbaum correlation is a useful aid in interpreting structures in precipitation alloys. Using, for example, a study of the Ni-base alloy known as René 41 by Hagel and Beattie, it is seen that at first the nickel-rich matrix favors the precipitation of γ' over the μ phase. After enough γ' has been precipitated, the matrix is depleted in nickel and is left relatively rich in cobalt. Therefore, by the Laves-Wallbaum criteria, the precipitation of a structure with Kasper polyhedra is favored. This is the Co_7Mo_6 phase which was in fact found to occur in René 41. Here is a case in which the change in matrix which is necessary to promote the precipitation of a different phase automatically and conveniently provides the proper delay for further strengthening after the effects of the first strengthening reactions have been fully exploited. This sequence illustrates a promising possibility for introducing true and sophisticated metallurgical design into the development of high temperature alloys. Further examination of these ideas is certainly justified.

Important parts of the field of transformation which I shall only mention are a) the effects of high static pressure on phase stability and transformation kinetics, and b) the effects of high energy mechanical shock on the structure of solids. High pressure phenomena have been treated in a recent volume (63) which contains the proceedings of an international conference on the subject. Dynamic shock treatment has also been the subject of a major conference, the proceedings of which are available in book form (64). These areas are still unexploited and undoubtedly still contain undiscovered branches having scientific as well as technological importance.

NEW TECHNIQUES FOR OBSERVING STRUCTURES DURING RECRYSTALLIZATION AND PHASE TRANSFORMATIONS

During the last annual meeting of the American Institute of Mining, Metallurgical and Petroleum Engineers a conference was held on the subject "Direct Observation of Imperfections in Crystals." The proceedings of the conference are to be published as a hard cover volume by Interscience Publications, Inc., recently acquired by John Wiley and Sons, Inc. The volume is due for public release in November, 1961

Among the items presented at the conference were several new techniques by which transformations and recrystallization can be observed. Some techniques are outlined here since they will probably find useful application in future experimental studies. For detailed description and application examples, I refer you to the Proceedings of the cited conference.

X-RAY DETECTION OF THE ONSET OF RECRYSTALLIZATION

C. S. Barrett has found that the progress of recrystallization in a cold worked or fine grained metal can be conveniently and accurately followed by the growth of sharp spots in Debye-Sherrer diffraction patterns observed by means of a counter diffractometer instead of the usual photographic film. The counter, with large detector aperture, is set in a stationary position on one of the strong Debye rings and the specimen is then rotated or oscillated a few degrees. The diffracted intensity is recorded on a chart in the usual way. The first presence of recrystallized grains is recognized by the sudden appearance of definite intensity peaks from the recrystallized grains in place of the relatively smooth record from the cold worked matrix. Recrystallization is also indicated by a drop in the intensity of the background between the peaks. Barrett found that the temperature at which recrystallization started in similar cold worked specimens was remarkably independent of heating rate. The method is apparently rapid, relatively convenient and gives quite reproducible results.

THERMIONIC EMISSION MICROSCOPY

When a conducting surface is heated to a high enough temperature, electrons are emitted from the surface at a rate which is characterized by the electron emission work function of the surface. The emitted electrons may be electrically drawn from the surface in straight lines which are normal to the macroscopic surface. By a suitable electron optical system, the electrons can be focused and projected as an enlarged image of the emitting surface upon a fluorescent screen (57). Since different surfaces (material, topography and crystallographic orientation) emit at different rates, the projected image represents the surface features of the emitting specimen. Any change of the specimen surface is seen as a region of contrast on the image. Thus, recrystallization and phase transformations can be directly observed at magnifications roughly equivalent to those attainable by optical microscopy. Without special treatment a surface must be heated to about 600°C so that enough thermal electrons will be emitted to

provide a useful image. For lower temperature emission a very thin layer of thorium or barium is vapor deposited onto the specimen surface, thereby lowering the electronic work function. The practical upper temperature limit is about 1300°C, above which serious instrumental deterioration sets in.

Although the motion of grain boundaries at high temperature is dramatically shown by this technique, the limitation remains that only the specimen surface is visible. Therefore the interpretation of the observed transformation kinetics is not simple with respect to the three dimensional process which is actually occurring.

FIELD ION MICROSCOPY

This technique, developed and exploited most actively in this country by E. W. Müller (58), depends upon abnormal electron tunneling at minute surface projections of a fine tip. The tip is maintained at a positive electro-potential with respect to a surrounding atmosphere of gas (helium) at low pressure. According to a simplified picture of the process, the gas atoms are ionized in a region close to the specimen surface and then are repelled in a direction at right angles to that part of the surface where ionization occurred. The ions are accelerated as they move radially from the specimen tip to a concentric fluorescent screen. In practice the screen consists of the walls of the glass container on which has been deposited a suitable fluorescent material. Since the number of ions emitted at a given point on the tip depends upon the structure of the tip material, the pattern formed on the fluorescent screen represents the actual surface topography of the point. Under best conditions, individual atom sites can be observed and crystallographic planes can be identified.

Pound and Moazed have used field electron emission microscopy for observing the fundamental kinetics of nucleation of metal vapor on tungsten tips (59). The method of field ion microscopy has potential applications of more direct interest to high temperature materials, in that the strain recovery process at the tip can be viewed directly on an atomic scale. Preliminary observations of this type have been made very recently by Müller (35).

X-RAY DIFFRACTION MICROSCOPY

Several variations of X-ray diffraction microscopy have recently been developed (60). All depend upon forming a topographical image from a single crystal specimen by the Bragg diffraction of white or characteristic X-rays. Image contrast may be due to differences in primary extinction from point to point on the specimen, surface topography, regions of strain, or other internal defects of various sorts. Most of the methods are very sensitive to deviations in crystallographic orientation so the position of a phase or intercrystalline boundary can be clearly seen. The Lang and the Berg-Barrett methods are especially sensitive to strain gradients. They are therefore appropriate for studying strains around precipitates or other foreign particles in a matrix crystal. The linear resolution however is only about three microns. The method of Bonse uses a highly collimated beam of monochromatic X-rays and therefore features great sensitivity to small orientation differences.

These diffraction methods are capable of producing topographical pictures of line defects including individual dislocations and should therefore be useful for studying the structures of grain boundaries. Figure 14 shows a light micrograph and three X-ray diffraction micrographs of the same surface of a lithium fluoride crystal which had been slightly distorted by horizontal compression. The slip lines and all sub-grain boundaries have been made visible by etching as seen in (a). The slip lines are visible in some diffraction photomicrographs and not others,

depending on the relative orientation of the Burgers vector of slip and the diffracting planes (details described in reference 61). The grain boundaries appear in different contrast in b, c and d, depending on factors which are not yet resolved. Very little application has so far been made of these new and powerful techniques, although they are instrumentally much simpler than electron microscopy.

ELECTRON MICROSCOPY

This method is now well recognized as a powerful tool for watching recrystallization and other processes in thin film specimens on a nearly atomic scale. The increased application of high accelerating voltage makes it possible to examine relatively thick specimens. However, the application of thin film behavior to the bulk behavior of the material can still be misleading. Most of the effort in electron microscopy of crystalline solids is directed at an understanding of the behavior of point and line defects and therefore has been more useful in the study of such processes as recrystallization and slip than the transformation behavior of high temperature alloys.

RECAPITULATION

In this brief review of current knowledge in the field of recrystallization and phase transformations a few points stand out as being especially attractive for future work. There is no question that other important and appropriate research areas now exist or will be developed in these fields. Nevertheless, for what value they may be, I submit these suggestions for future research consideration.

Subject	Discussed on page
1) Study the effects of impurity atom (substitutional and interstitial) in high-purity base metals to clarify and generalize recent experimental observations on boundary mobility.	85, 87, 88
2) Gather reliable thermodynamic data on grain boundary self-diffusion to help develop a model of structure of grain boundaries, their mobilities and other properties.	81
3) Apply new diffraction and other techniques to study the nature of grain boundaries and of intra-grain imperfections and of their effects in crystallographic transitions.	79, 87, 88, 92
4) Develop a method for topographic observations of point defects	82, 83
5) Rationalize and evaluate quantitatively the various sources of the controlling driving energies of recrystallization.	82, 84
6) Explain and extend the empirical observations of the effects of electronic structure on recrystallization.	84, 85
7) Define the controlling processes in recrystallization to a point where recrystallization texture can be predicted and synthesized.	85

Subject	Discussed on page
8) Develop a theory by which one can predict from first principles whether a transformation will be one of first or second order.	86
9) Exploit the known ultra-high rate diffusion which is known to occur under some circumstances.	89
10) Investigate experimentally the proposed mechanisms for the motion of a martensite boundary.	89
11) Rationalize the now anomalous effects of some elements on the behavior of martensite.	89
12) Explore the phenomenon of inoculation in phase transformations and apply it to practical use.	90
13) Develop an understanding of the factors which control the morphology of transformation products.	88
14) Look for further validity of the Laves-Wallbaum rule and apply the principle in the design of complex alloy transformations.	91
15) Apply modern techniques to the direct observation of atom positions, grain boundary motion, lattice strains, appearance of new crystals, etc.	92

AKNOWLEDGMENTS

This brief review was prepared while the author was partially supported by the Cornell Materials Science Center, under contract to the Advanced Research Projects Agency of the Department of Defense. Discussions with other members of the Center and stenographic assistance is gratefully acknowledged.

REFERENCES

1. K. Lucke, et al, Z. F. Metalkunde, *52* (1961) 1-46
2. K. Lucke, to be published
3. N. F. Mott, Proc. Roy. Soc., *60* (1948) 391
4. T. S. Ke, Phys, Rev., *72* (1947) 41
5. M. L. Kronberg and F. H. Wilson, Tr. AIME, *185* (1949) 501
6. W. T. Read and W. Shockley, Phys. Rev., *78* (1950) 275
7. See for examples K. T. Aust and J. W. Rutter, Tr. AIME, 1961 and earlier
8. K. T. Aust and J. W. Rutter, Tr. AIME, *215* (1959) 820
9. D. Turnbull, Tr. AIME, *191* (1951) 3
10. N. A. Gjostoin and F. N. Rhines, Acta Met., *7* (1959) 319
12. R. H. Atkinson et al, Westinghouse Lamp Div., WADD Tr. 60-37 on contract AF 33 (610)-5632, May 1960
13. K. Lucke and K. Detert, Acta Met. *5* (1957) 628
14. J. W. Rutter and K. T. Aust, Tr. AIME, *218* (1960) 682
15. W. C. Leslie, F. Plecity and J. T. Michalek, to be published
16. L. P. Jahnke, AIME conference on High Temperature Materials, 1961. Proceedings, Interscience Publications, Inc.
17. J. W. Semmel and E. S. Machlin, Acta Met., *5* (1957) 582
18. J. L. Walter and C. G. Dunn, Acta Met., *8* (1960) 497
19. K. T. Aust and J. W. Rutter, Tr. AIME, *215* (1959) 119
20. W. W. Mullins, Acta Met., *6* (1958) 414
21. E. P. Abrahamson, II and B. S. Blakeney, Jr., Tr. AIME, *218* (1960) 1101
22. W. R. Hibbard and W. R. Tully, Tr. AIME, *221* (1961) 337
23. W. G. Burgers, L'Etat Solide, Brussels, (1952) 73
24. P. A. Beck, Acta Met., *1* (1953) 230
25. Reports of Panels sponsored and distributed by ONR, Washington, D. C. Editor, L. Himmel
26. *Mechanism of Phase Transformations in Solids*, Inst. of Metals Monograph and Report Series *18*, 1955
27. J. S. Kirkaldy, Symposium on "Decomposition of Austenite by Nucleation and Diffusional Growth," AIME, Monograph, 1961

28. T. Muto and Y. Takagi, solid state physics, *1* (1955) 193, Academic Press

29. L. Guttman, ibid, *3* (1956) 145

30. F. S. Ham, J. Phys. and chemistry of solids, *6* (1958) 335

31. I. M. Lifshitz and V. V. Slezov, Soc. Phys., JETP. *8* (1959) 331

32. J. W. Cahn and J. E. Hilliard, J. Chem. Phys., *31* (1959) 688

33. L. H. van Vlack, Tr. AIME, *191* (1951) 251

34. R. E. Hoffman, Acta Met. *4* (1956) 97

35. AIME symposium on "Direct Observation of Imperfertions in Crystals," edited by J. B. Newkirk and J. H. Wernick, Interscience Publications, Inc., New York, 1961

36. A. Dube, H. I. Aaronson and R. F. Mehl, Rev. de Met., *55* (1958) 201

37. H. I. Aaronson, Tr. AIME, 218 (1960) 331

38. J. H. Westbrook, Z. Krist, *110* (1958) 21

39. J. B. Newkirk, Tr. AIME, *209* (1957) 1214

40. D. Turnbull, Acta Met., *3* (1955) 55

41. D. Turnbull, Acta Met., *8* (1960) 277

42. P. A. Beck et al, J. Appl. Phys., *21* (1950) 420

43. U. Roesler, H. Sato, C. Zener, "Theory of Alloy Phases" ASM (1956) 255

44. L. Kaufman, Tr. AIME, *215* (1959) 218

45. R. C. Williams, Tr. AIME, *215* (1959) 1026

46. H. Brooks, unpublished. See D. Turnbull, Solid State Physics, *3* (1956) 225, Academic Press

47. A. Saulnier, Comptes rendus, *251* (1960) 2160

48. C. B. Craver et al, unpublished. See Reference 52

49. H. J. Beattie and W. C. Hagel, Tr. AIME, *209* (1957) 911

50. A. J. Lena, "Precipitation from Solid Solutions," ASM (1959) 244

51. A. Taylor and R. W. Floyd, JL Inst. Metals, *81* (1952) 25

52. J. R. Mihalisin and R. F. Decker, Tr. AIME, *218* (1960) 507

53. H. J. Beattie and W. C. Hagel, Tr. AIME, *221* (1961) 28

54. F. Laves and H. J. Wallbaum, Naturwiss, *27* (1939) 674

55. A. E. Dwight and P. A. Beck, *215* (1959) 976

56. F. C. Frank and J. S. Kasper, Acta Cryst., *12* (1959) 483

57. W. L. Grube, to be published

58. E. W. Muller, JL. Appl. Phys., *28* (1957) 1

59. G. M. Pound and K. L. Moazed, to be published

60. W. W. Webb, in Reference 35

61. J. B. Newkirk, Tr. AIME, *215* (1959) 483

62. D. Turnbull, unpublished report to the NATO Committee on Solid State Sciences, Paris, 1961

63. "Progress in Very High Pressure Research," F. P. Bundy, W. R. Hibbard, Jr., H. M. Strong, Eds., J. Wiley and Sons, 1961

64. "Response of Metals to High Velocity Deformation," P. G. Shewman and V. F. Zackay, Interscience Publ., 1961

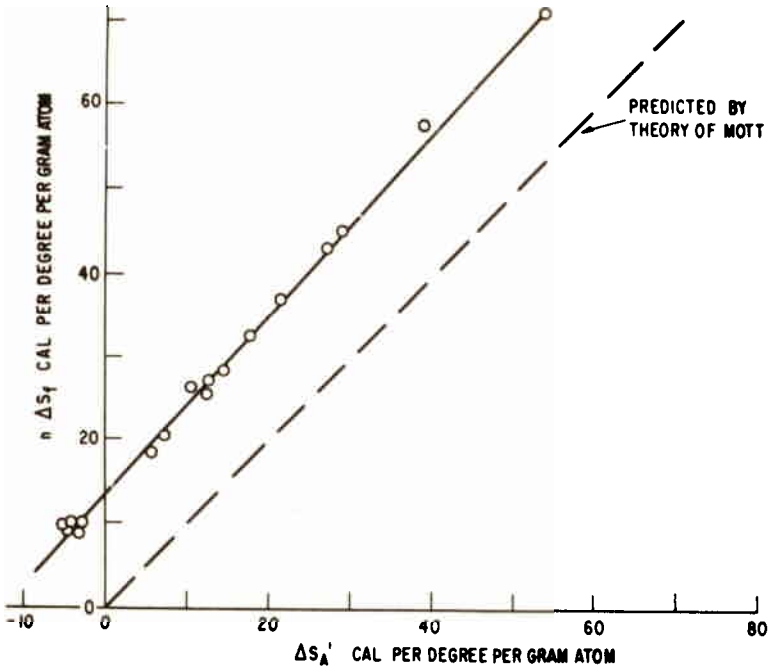

FIGURE 1

COMPARISON OF ENTROPIES OF ACTIVATION FOR GRAIN BOUNDARY MIGRATION PREDICTED BY MOTT WITH THOSE DERIVED EXPERIMENTALLY BY AUST AND RUTTER SHOWS A CONSTANT DIFFERENCE OF ABOUT 15 CAL PER DEGREE

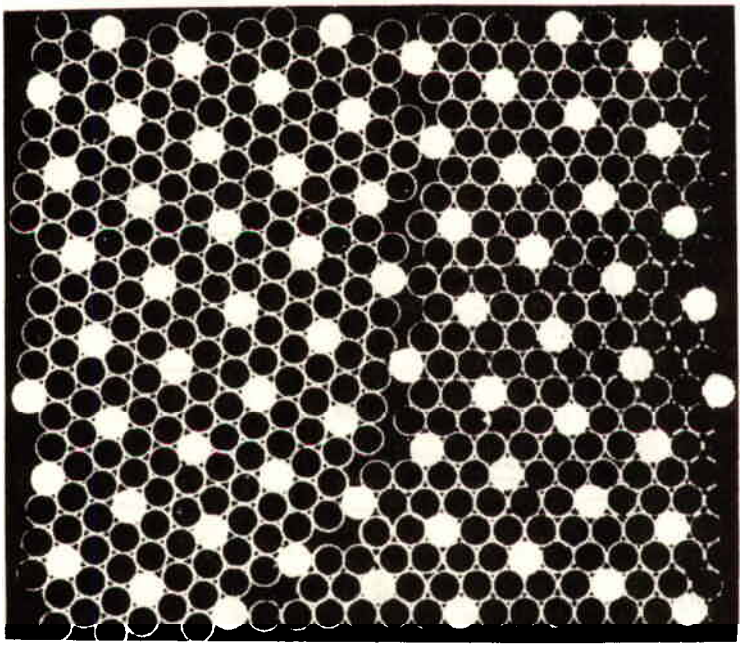

FIGURE 2

KRONBERG-WILSON BOUNDARY SEPARATING TWO GRAINS HAVING AN ORIENTATION DIFFERENCE OF 38 OR 22° ABOUT <111>. NOTICE THE UNDISTORTED HEXAGONAL ARRAY OF WHITE CIRCLES. (AFTER FRANK)

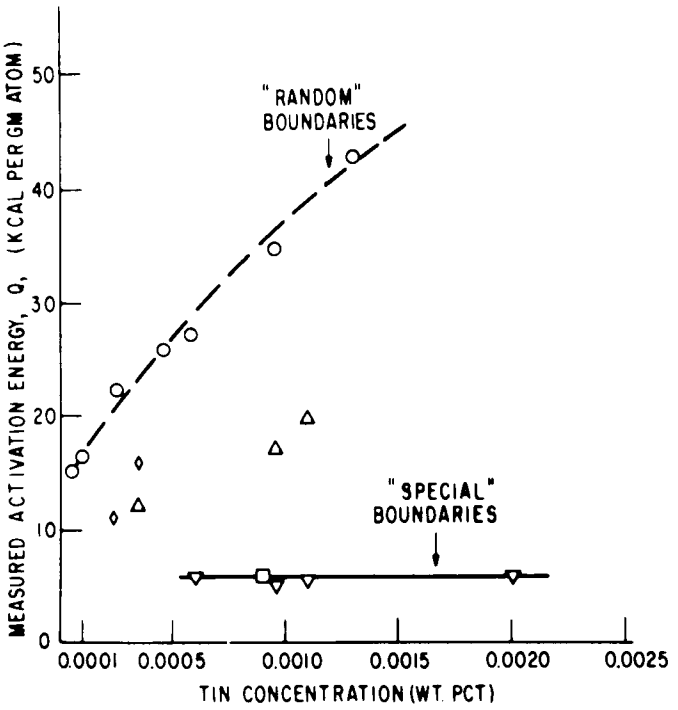

FIGURE 3

EXPERIMENTALLY DETERMINED ACTUATION ENERGIES OF "SPECIAL" OR COINCIDENCE BOUNDARIES ARE SMALL WITH RESPECT TO THOSE OF "RANDOM" HIGH ANGLE BOUNDARIES AND ARE PRACTICALLY INDEPENDENT OF IMPURITY CONCENTRATION. (AUST-RUTTER)

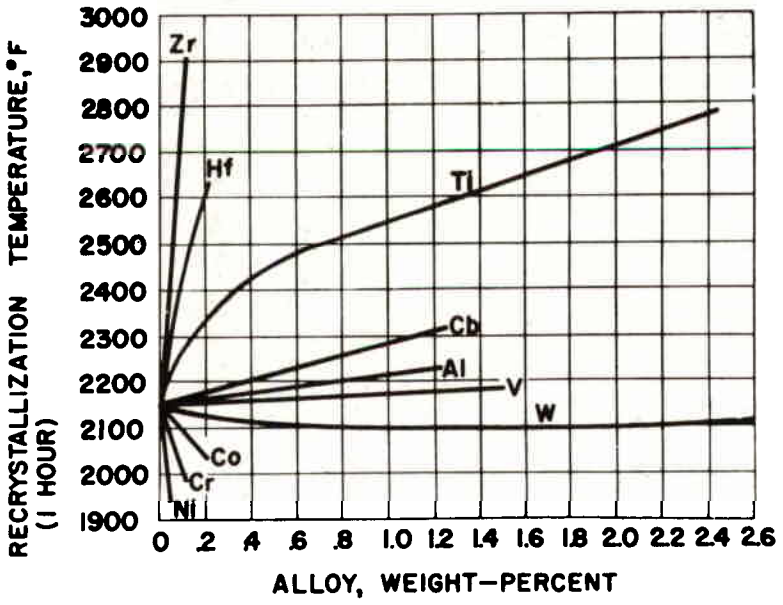

FIGURE 4

DIFFERENT ALLOYING ELEMENTS HAVE WIDELY DIFFERENT EFFECTS ON THE RECRYSTALLIZATION TEMPERATURE OF MOLYBDENUM. (JAHNKE)

FIGURES 3 & 4

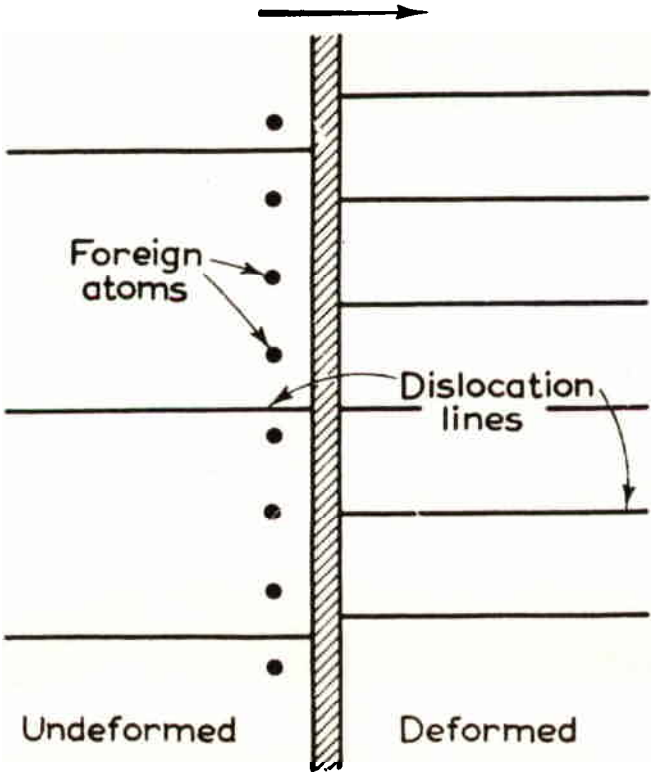

FIGURE 5

LUCKE'S PICTURE OF THE BOUNDARY BETWEEN DISTORTED AND RECRYSTALLIZED MATERIAL. IMPURITY ATOMS ARE DRAGGED ALONG WITH THE BOUNDARY AND MUST DIFFUSE THROUGH THE RECRYSTALLIZED LATTICE BEHIND THE INTERFACE.

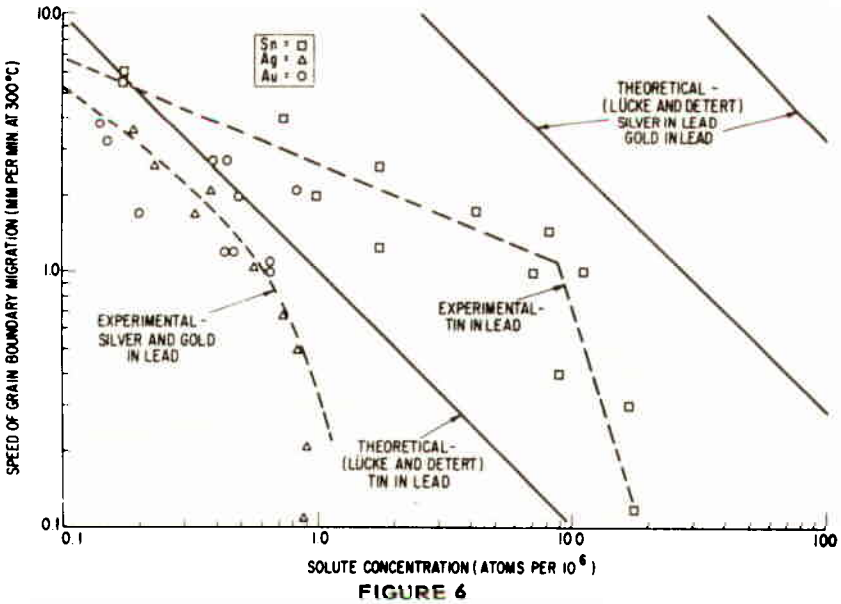

FIGURE 6

GRAIN BOUNDARY MIGRATION RATES OBSERVED BY AUST-RUTTER DO NOT AGREE WELL WITH THOSE CALCULATED ON THE BASIS OF THE LUCKE-DETERT THEORY.

FIGURE 7

THE POSITIONS WHERE THE GRAIN BOUNDARY BECAME STUCK ARE RECORDED IN THE GROOVES WHICH FORMED ON THIS COPPER SHEET ANNEALED 81 HRS. AT 940°C. 73X (MULLINS)

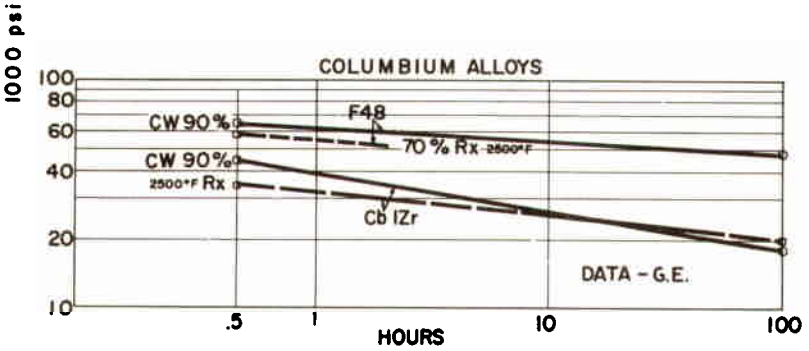

FIGURE 8

THE NIOBIUM BASE ALLOY F48 IS HIGHLY RESISTENT TO RE-CRYSTALLIZATION EVEN AT 2500° F. TEN-HOUR RUPTURE STRENGTH IS GIVEN AS ABSCISSA. (JAHNKE)

FIGURES 7 & 8

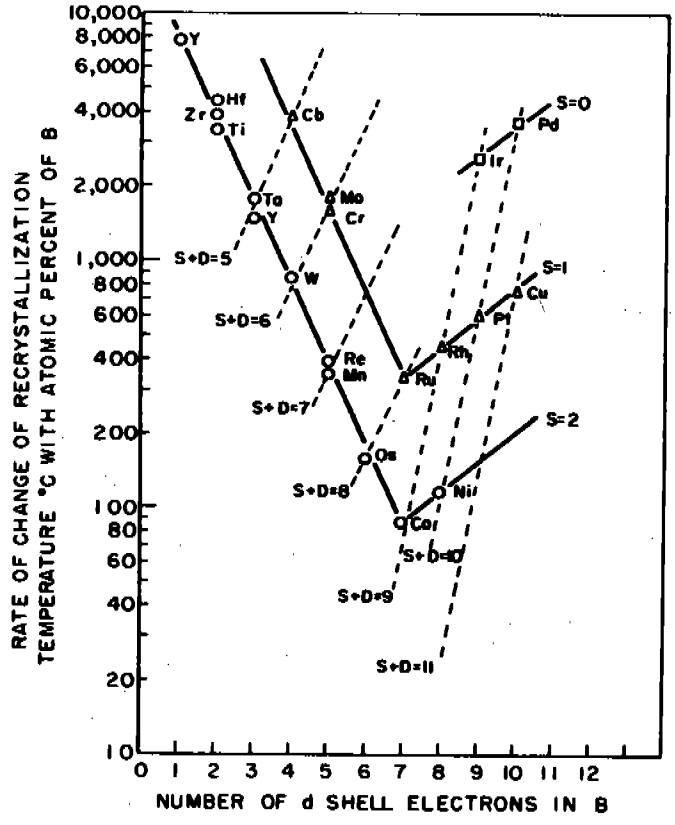

FIGURE 9

THE LOG OF THE RATE OF CHANGE OF RECRYSTALLIZATION TEMPERATURE OF IRON IS A LINEAR FUNCTION OF THE NUMBER OF D-SHELL ELECTRONS OF THE SOLUTE ATOM. THE MINIMUM IN EACH CURVE OCCURS WHERE THERE ARE SEVEN "d" ELECTRONS. (ABRAHAMSON)

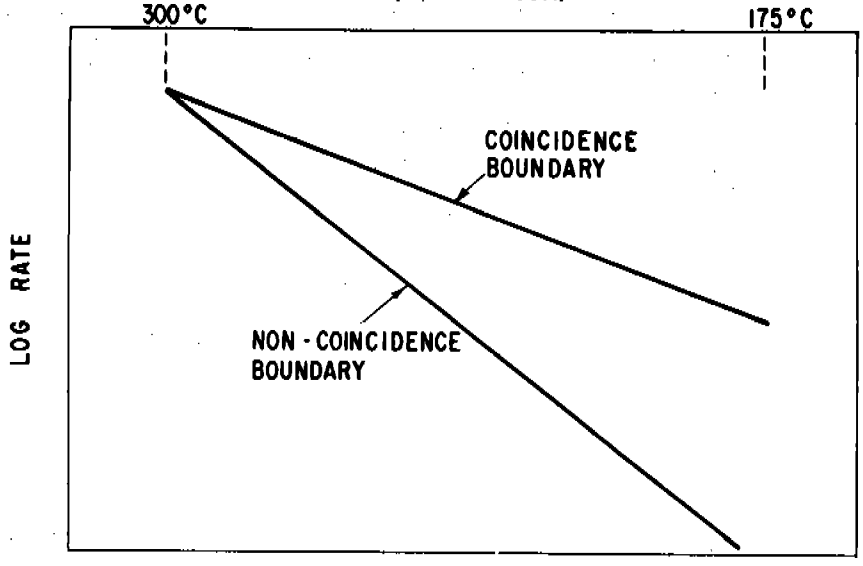

FIGURE 10

TEMPERATURE DEPENDENCE OF THE MIGRATION RATE OF COINCIDENCE AND RANDOM GRAIN BOUNDARIES IN ZONE-REFINED LEAD. (AUST-RUTTER)

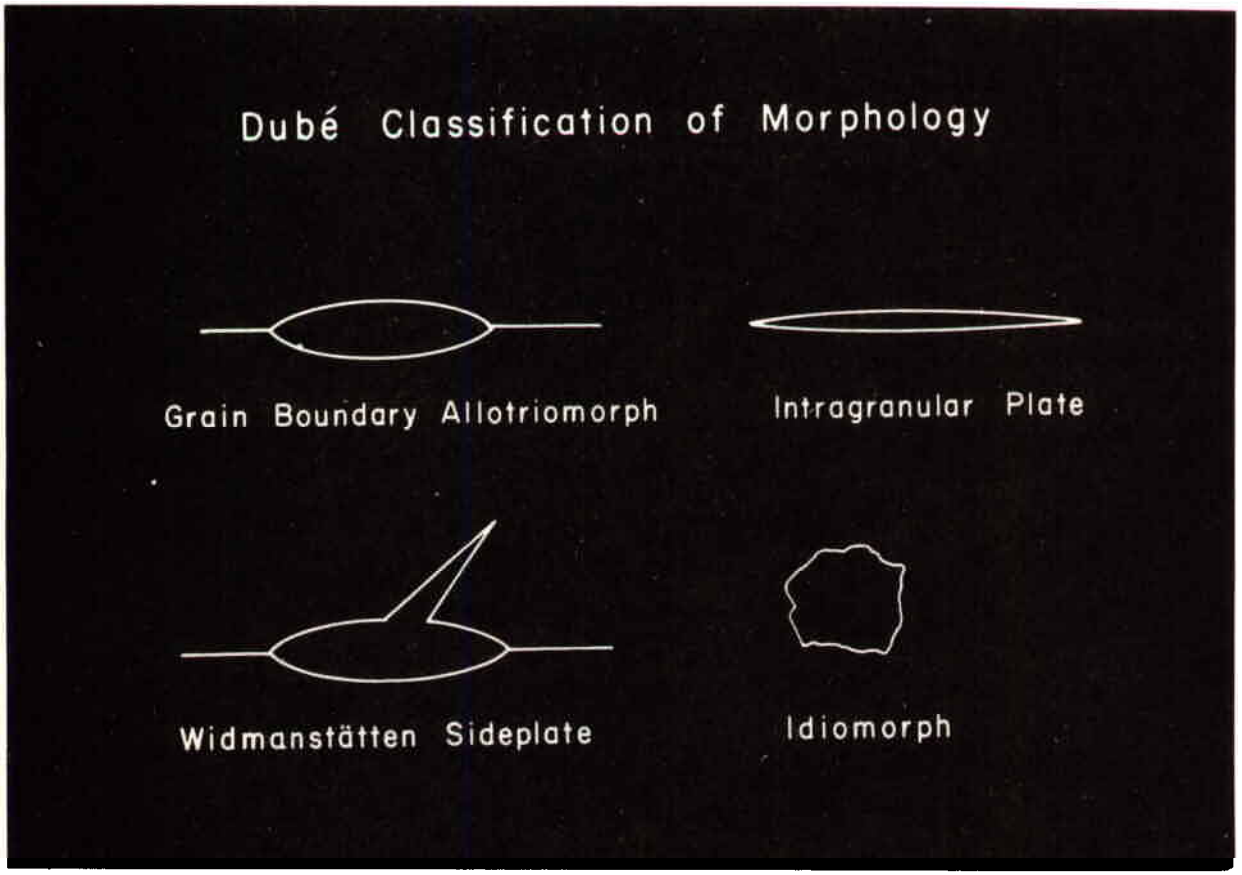

MORPHOLOGIES OF PHASE TRANSFORMATION PRODUCTS ACCORDING TO THE CLASSIFICATION PROPOSED BY DUBE.

FIGURE 11

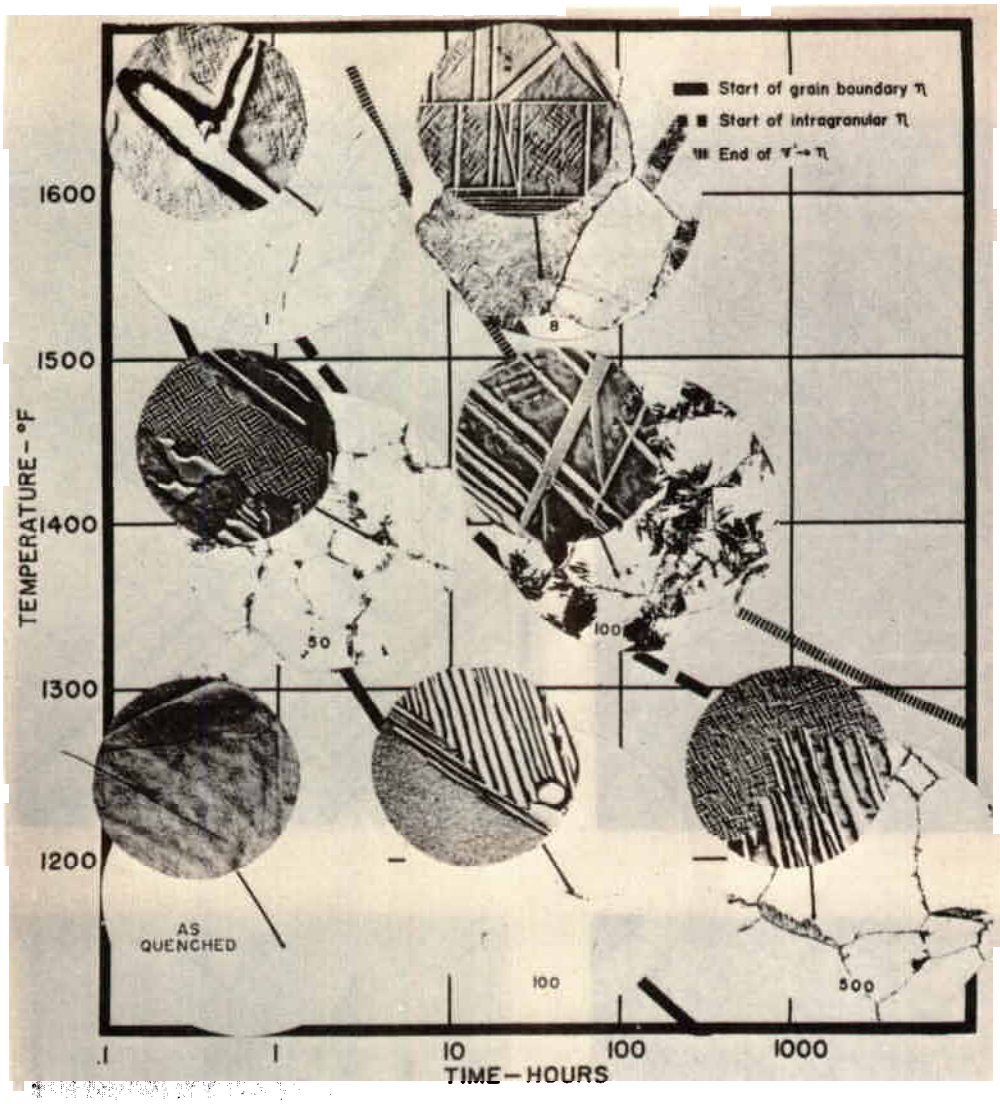

FIGURE 12

TYPICAL MICROSTRUCTURES FOUND IN NI-12. TI_2 ALLOY ILLUSTRATE MANY OF THE DUBE MORPHOLOGICAL CLASSES. (MIHALISIN)

	IV_B	V_B	VI_B	VII_B		$VIII$		I_B	II_B	III_A	
A-group →	Ti	V	Cr	Mn	Fe	Co	Ni	Cu	Zn	Ga	← *B*-group
	Zr	Cb	Mo	Tc	Ru	Rh	Pd	Ag	Cd	In	
	Hf	Ta	W	Re	Os	Ir	Pt	Au	Hg	Tl	

FIGURE 13

ACCORDING TO LAVES AND WALLBAUM ELEMENTS IN THIS PART OF THE PERIODIC TABLE CAN BE DIVIDED BY THE VERTICAL LINE INTO TWO DISTINCTLY DIFFERENT CLASSES WITH RESPECT TO THEIR PRECIPITATION BEHAVIOR.

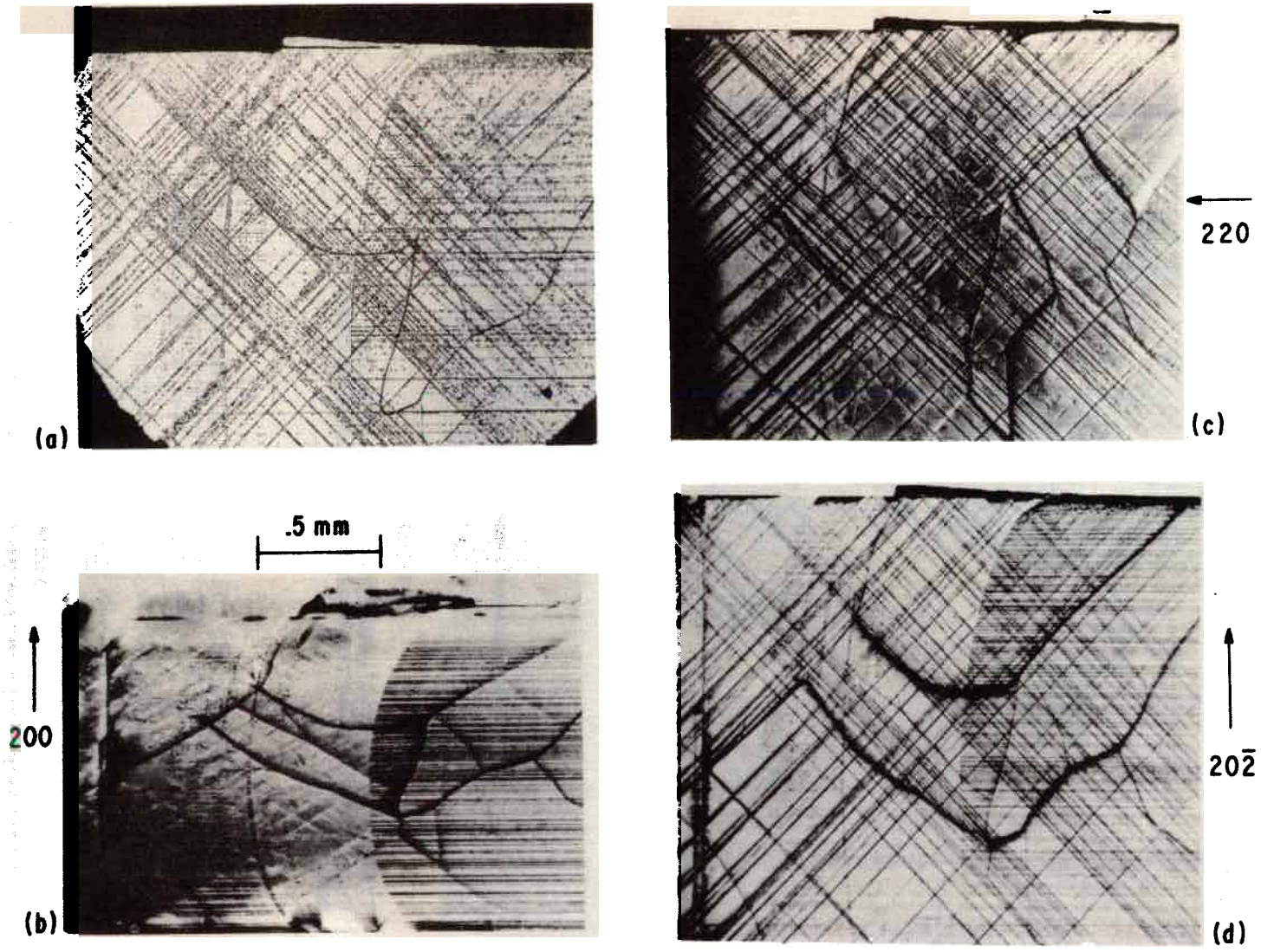

FIGURE 14

SUB-GRAIN BOUNDARIES IN LITHIUM FLUORIDE APPEAR WITH DIFFERENT CONTRAST IN DIFFERENT BERG-BARRETT DIFFRACTION MICROGRAPHS, DEPENDING ON THE HKL REFLECTION USED. SEE TEXT FOR DETAILS.

Prepared Discussion

THE ROLE OF ELECTRON CONFIGURATION ON RECRYSTALLIZATION

by

Dr. E. P. Abrahamson, II

As Dr. Newkirk pointed out in the molybdenum recrystallization versus solute curve, there are both positive and negative changes in recrystallization temperature with solute additions. We have examined titanium[1], zirconium[2], vanadium[3], columbium[4], iron[5,6] and nickel[7] base systems alloyed with dilute binary additions of the transition elements. Figure 1 indicates some typical recrystallization curves. It will be noted that there is an initial positive or negative line or change followed by a break, or limit of linearity, and another linear portion.

In studies of the effect of time on recrystallization, c.f. Figure 2, it was noted that a variation in time from 20 to 4000 minutes did not change the initial slope. The only variation noted was beyond the limit of linearity where the curve changed from a negative to a slightly positive slope.

As seen in Figure 9 of Dr. Newkirk's paper, there is a definite correlation between the number of ground state outer d and s electrons in the solute and the initial rate of recrystallization temperature change by the solute. In a similar manner, studies on iron have also shown that the limit of linearity is also a function of electron configuration, c.f. Figure 3.

Figure 4 indicates, in a periodic manner, the slope correlations to date. It will be noted that the curves are in the form of V's - inverse for titanium, zirconium and vanadium, normal for columbium, iron and nickel. The curves are similar in that the apex of the s = 2 electron curve always occurs at one d electron more than the solvent's configuration. The brittle-to-ductile transition temperature correlation for chromium base alloys[8] is presented to indicate that the correlation holds for other properties. It should be further noted that the role of the solvent's configuration can be seen in the change in the apex, the displacement of apexes in the case of solvents having one d electron, and in the similarity between correlation curves of solvents with the same outer electron configuration.

Prior to the determination of recrystallization in nickel base alloys, an empirical relationship was established between the other curves. This allowed the prediction of the nickel correlation curve well within experimental error.

At the moment it is difficult to present a model to explain these correlations. It is known that similar correlations can be shown for other physical and mechanical properties. Therefore, it will be necessary to construct a model which applies to more than one case.

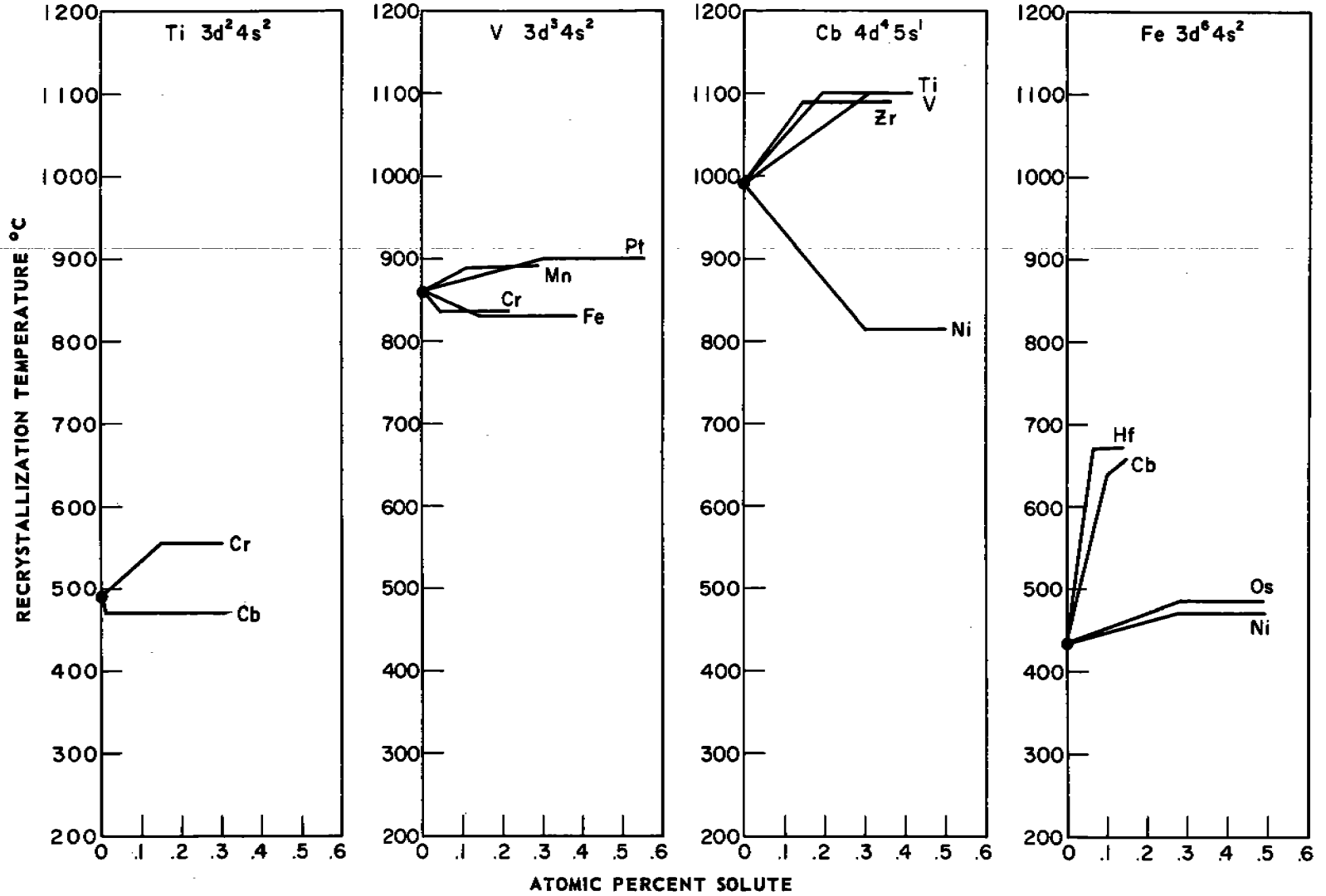

FIGURE 1

CHANGE IN RECRYSTALLIZATION TEMPERATURE WITH BINARY TRANSITION ELEMENT ADDITIONS TO SELECTED TRANSITION ELEMENTS

19-066-87/ORD-61

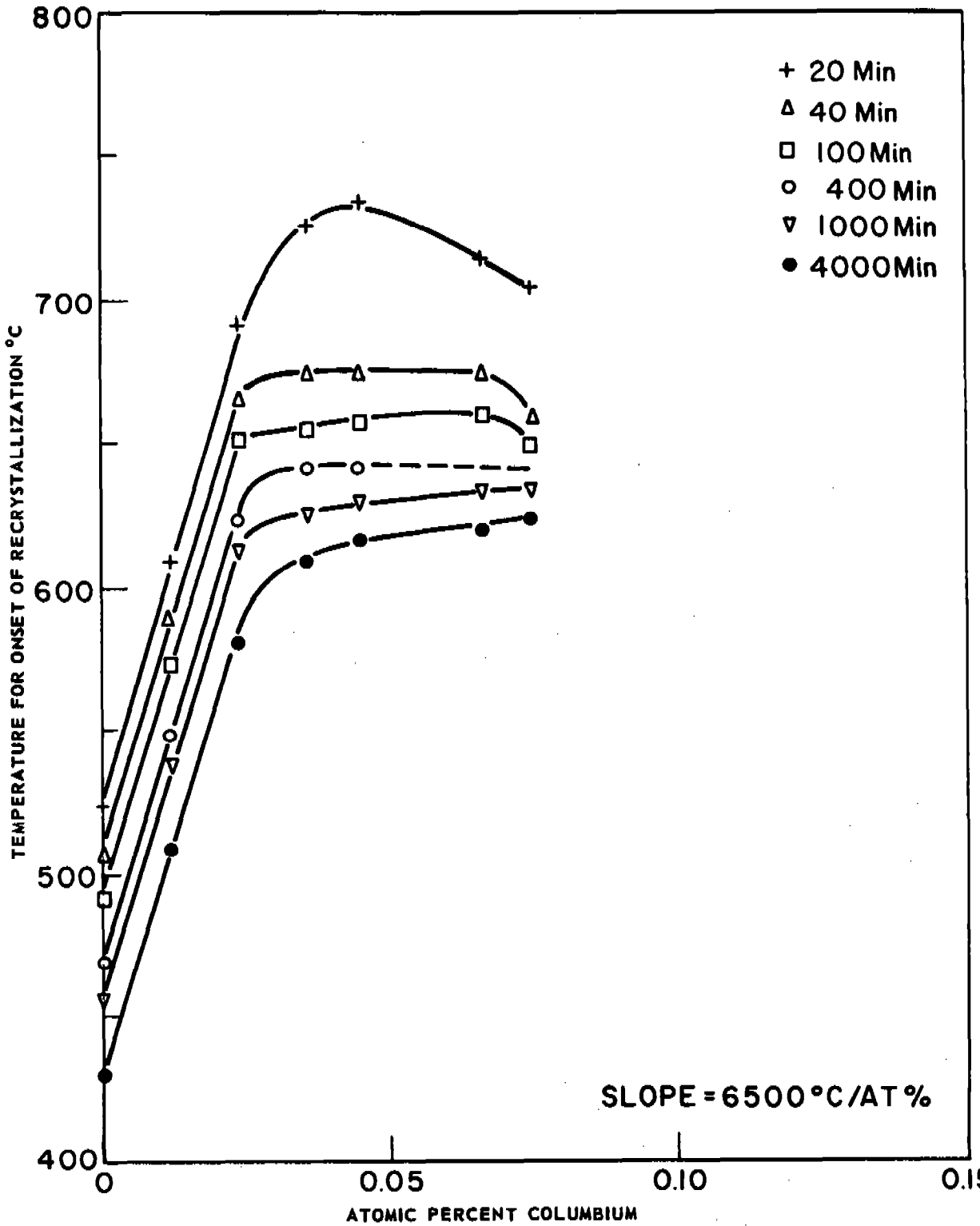

IRON RECRYSTALLIZATION TEMPERATURE AS AFFECTED BY COLUMBIUM FOR A VARIETY OF TIMES, COLD WORK CONSTANT AT 75%

19-066-1621/ORD-60

FIGURE 2

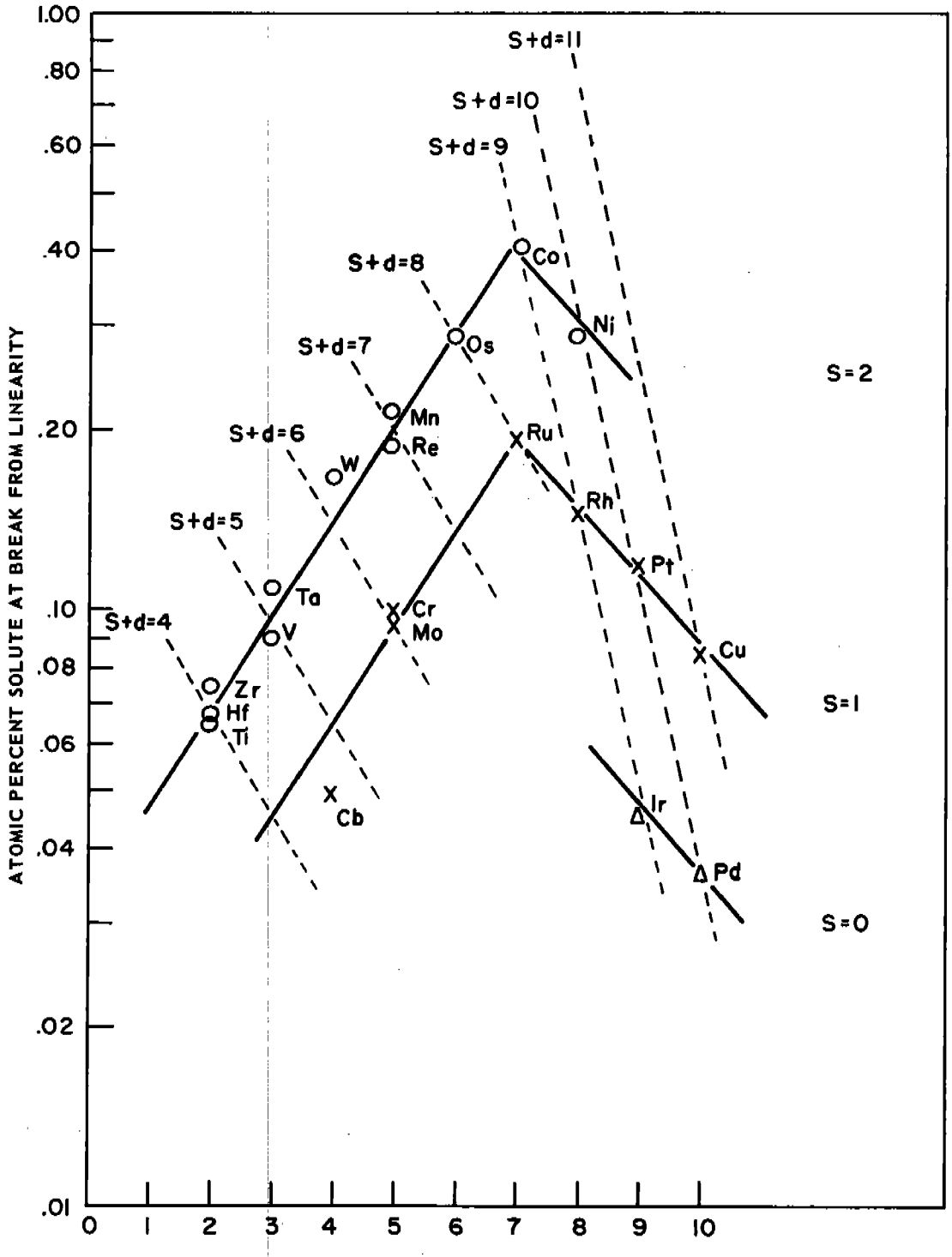

ATOMIC PERCENT SOLUTE AT BREAK FROM LINEARITY
VS GROUND STATE OUTER ELECTRON CONFIGURATION OF SOLUTE

19-066-90/ORD-61

FIGURE 3

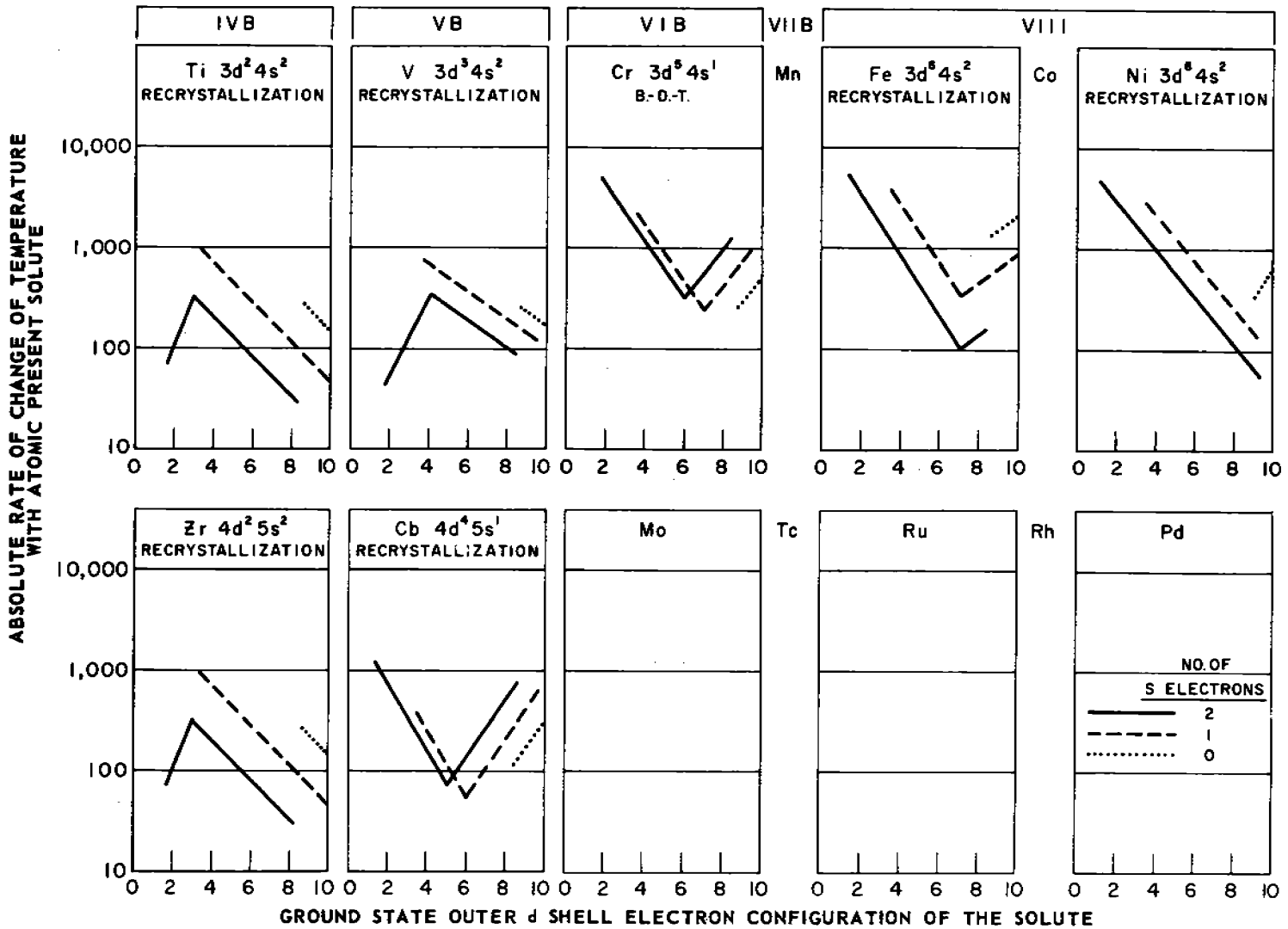

FIGURE 4

THE ROLE OF OUTER ELECTRON CINFIGURATION ON SEVERAL PROPERTIES OF DILUTE BINARY TRANSITION ALLOYS

19-066-1439/ORD-61

SOLID-GAS REACTIONS

by

Dr. E. A. Gulbransen

MICROTOPOLOGY OF THE SURFACE REACTIONS OF OXYGEN AND WATER VAPOR WITH METALS

ABSTRACT

Current theories of metal oxidation assume the formation of a uniform oxide film separating the reacting gas from the metal. According to the Wagner theory of oxidation reaction occurs by the diffusion of metal or oxygen ions through interstitial sites or through cation and anion defects in the oxide film. Much work has been directed toward checking the predictions of the theory and to extending the theory to complex systems.

The microtopological point of view is an attempt to observe changes in surface structure as a result of oxidation. It is assumed that metal structure, dislocation, inclusions, stress and other factors play an important part in the oxidation process. Two particular problems are considered in this paper. First what is the nature of the first stages in oxidation? Second, what is the nature of the localized growths which occur during oxidation?

In the early 1950's, Bardolle and Benard, and Gulbransen, McMillan, and Andrew used low pressure oxidation methods to study the initial step in the oxidation of iron. At temperatures of 650°C to 850°C and low oxygen pressures, small oxide nuclei were formed on iron during the first stages of reaction.

The results suggest that the initial stage of oxidation involves the formation of a thin uniform layer of small oxide crystallites. This was rapidly followed by the formation of much larger oxide crystals along certain parallel and regularly spaced lines on the metal grain. As oxidation continues, the oxide crystals grow, and new crystals form filling the remaining area of the metal. This results in the formation of a uniform mosaic of large oxide crystals.

Recent electron optical studies are presented on the effects of environment, stress and metal structure on the formation of localized oxide growths on iron. Three types of localized growths were found when pure iron was reacted with oxygen and water vapor atmospheres at 450°C. Thin oxide whiskers 100-150 Å in diameter form when pure annealed iron was reacted in dry oxygen. These whiskers grow to lengths up to 500,000 Å long. Thin blade shaped platelets 100 Å thick, 300 to 13,000 Å wide and 80,000 Å long formed when iron was reacted with water vapor containing traces of oxygen. Thin, rounded platelets of oxide 100 Å thick, 75,000 Å high and wide formed when cold worked iron was reacted with dry oxygen.

The environmental conditions for forming these localized growths has revealed many new ideas on the corrosion of iron and the oxidation of metals. The relation of these growths to the metal structure and to the oxide is now being studied as is the problem of whether these growths lead to pitting and trenching of the metal itself. Although it is too early to draw any definite conclusions it appears that electron optical studies of the microtopology of the localized oxide growths offer a new method for observing the effect of crystal imperfections on the chemical reactivity of metals and also for study of metal structure.

Another area of interest is the mechanical properties of these new oxide growths. Calculations show that these crystals have very high elastic strain limits. If these oxide whiskers and platelets have high strengths we may have new structural materials which not only have high melting points, low vapor pressure, high elastic yield limits and high strengths but also are non-reactive in oxygen environments.

I. INTRODUCTION

In recent years the science and technology of surface reactions has become a field of critical importance in modern technology. As a result a great deal of work is being directed at understanding the mechanisms of surface reactions. Real progress has been made due to two developments. Sensitive methods have been devised for the study of the kinetics and crystal structure factors in surface reactions. Theoretical developments have been made to correlate and interpret the mechanisms of gas-metal reactions.

As recently as 10 years ago much work in the field of metal oxidation was directed at testing the Wagner[1] theory of oxidation. During the past decade work has been directed along more practical lines. The development of nuclear reactors has focussed attention on the reactive metals, zirconium and uranium and their alloys while the development of missiles and space vehicles has directed work to the refractory metals such as tungsten, niobium, tantalum and molybdenum. Interest in molecular electronics has led to oxidation studies of metals and semiconductors where the material is in the form of an evaporated or sputtered film.

This paper will discuss another new direction in metal oxidation; namely, the role of metal structure in the initiation and growth of oxide films on metals. The approach is that of the observer school and emphasizes the microtopological structure of the oxide. The paper consists of two parts. The first part is concerned with the initial stages of the oxidation process, while the second part is concerned with the nature of oxide growths occurring during oxidation.

Due to space and time limitations we will limit our discussions to the oxidation and corrosion of iron and stainless steel.

In contrast to other papers no attempt will be made to cover the complete field of oxidation.

II. PRESENT PICTURE OF OXIDATION

The Wagner[1] theory of the oxidation of metals is accepted by most scientists. The theory is based on the diffusion of metal ions or atoms or oxygen ions or atoms through an oxide film. Diffusion occurs through interstitial sites or through cation and anion defects in the oxide. A uniform oxide film is assumed and the metal is assumed to be structureless over a given metal grain. Wagner's theory can only be applied under conditions where a coherent oxide film is formed and where the oxides are not soluble in the metal.

Figure 1 shows a schematic picture of two alternative mechanisms for oxidation. The first involves the diffusion of metal ions through vacancies in the oxide while the second involves the diffusion of oxygen ions or atoms through the oxide. Equations A and B Figure 1 show details of the two mechanisms.

One of the difficulties in the Wagner theory is that complex oxidation and corrosion problems cannot be handled. Thus, how can one apply the theory to the complex localized reactions

involved in stress corrosion cracking of 304 stainless steel or to the complex influence of water on the corrosion of iron? These problems inevitably go back to the selective oxidation or corrosion of localized structures in the metal. Recent developments in metal physics have shown that crystal orientation, dislocations, precipitates, impurities and other defects determine the mechanical properties of the metal. We feel these factors may determine also the chemical reactions of metal surfaces.

III. THERMOCHEMICAL EVALUATION OF THE OXIDATION REACTIONS

Before presenting experiments on the nucleation of oxide films or the formation of localized oxide growths it is essential to consider the thermochemical equilibrium involved. Thermochemical equilibrium does not exist for a system undergoing reaction; for example, iron reacting with oxygen. However, thermochemical calculations may be useful in choosing one of several possible reaction mechanisms. The reactions which do occur are those that are feasible both thermochemically and kinetically.

In a more limited sense, an approximation to equilibrium may exist at certain planes in a metal system undergoing reaction after the initial period. Thus, the concentration of iron in ferrous oxide at the FeO-Fe interface and at the FeO-Fe_3O_4 interface may be estimated from the iron-oxygen diagram[2], although the concentrations within the several phases may be far from equilibrium.

From a chemical point of view five types of reactions may occur during the reaction of iron with oxygen:

Formation or decomposition of the several oxides by direct oxidation.

Reaction with H_2O.

Solid phase reactions with iron or oxygen occurring at the several internal interfaces.

Phase transformation of Fe_3O_4 to FeO at 570°C.

Formation of the spinel Fe_3O_4 from FeO and Fe_2O_3.

Thermochemical calculations are made for the five equilibria involved in the reaction of iron with oxygen, using the data given by Chipman and Murphy[3] on the free energy of formation of ferrous oxide, ferriferrous oxide, and ferric oxide. The equilibrium data are expressed in terms of $\log_{10}K$, where K is the equilibrium constant, or $\log_{10}P$, where P is the pressure of oxygen gas in atmospheres.

Table 1 shows a listing of the reactions of interest together with the results of the calculations. Each of the oxides is stable to direct decompositions over the temperature range considered and in vacua of 10^{-5} mm of Hg. The reactions of iron with water vapor are possible at 400°C but not above 600°C. The reaction to form Fe_2O_3 is the least favorable of the water vapor reactions. Fe_2O_3 can form only if hydrogen is removed.

The reduction of Fe_2O_3 with Fe to form Fe_3O_4 is favorable as is the oxidation of Fe_3O_4 to form Fe_2O_3. The oxidation of Fe_3O_4 with water vapor is not favorable except at low temperatures.

TABLE I

EQUILIBRIA CALCULATIONS ON IRON-OXYGEN REACTIONS

A. Direct Reactions with $O_2(g)$

1. $Fe(s) + 1/2\ O_2(g) \rightleftarrows FeO(s)$
2. $3Fe(s) + 2O_2(g) \rightleftarrows Fe_3O_4(s)$
3. $2Fe(s) + 3/2\ O_2(g)$ j $Fe_2O_3(s)$

B. Direct Reactions with $H_2O(g)$

1. $Fe(s) + H_2O(g) \rightleftarrows FeO(s) + H_2(g)$
2. $3Fe(s) + 4H_2O(g) \rightleftarrows Fe_3O_4(s) + 4\ H_2(g)$
3. $2Fe(s) + 3H_2O(g) \rightleftarrows Fe_2O_3(s) + 3H_2(g)$

C. Fe_2O_3 - Fe_3O_4 Equilibria

1. $4Fe_2O_3(s) + Fe(s) \rightleftarrows 3Fe_3O_4(s)$
2. $2Fe_3O_4(s) + 1/2\ O_2(g) \rightleftarrows 3Fe_2O_3(s)$
3. $2Fe_3O_4(s) + H_2O(g) \rightleftarrows 3Fe_2O_3(s) + H_2(g)$

D. Fe_3O_4 - FeO Equilibria

1. $Fe_3O_4(s) + Fe(s) \rightleftarrows 4FeO(s)$
2. $3FeO(s) + 1/2\ O_2(g) \rightleftarrows Fe_3O_4(s)$
3. $3FeO(s) + H_2O(g) \rightleftarrows Fe_3O_4(s) + H_2(g)$

E. FeO - Fe_2O_3 - Fe_3O_4 Equilibria

1. $FeO(s) + Fe_2O_3(s) \rightleftarrows Fe_3O_4(s)$

TABLE I *(Continued)*

Results on Above Equations

t	A_1	A_2	A_3	B_1	B_2	B_3	C_1
°C	$-\log P_{O_2}$	$-\log P_{O_2}$	$-\log P_{O_2}$	log K	log K	log K	log K
25	86.1	88.7	86.1	*	17.0	8.9	15.4
200	50.4	52.5	50.8		7.58	3.2	10.0
400	34.0	34.3	33.0		3.30	0.45	8.1
600	24.0	24.6	23.3	0.60	1.31	-0.94	7.7
800	18.7	18.6	17.2	0.19	0.33	-1.75	8.0
1000	14.7	14.5	13.0	0.20	-0.15	-2.29	8.70

t	C_2	C_3	D_1	D_2	D_3	E_1
°C	log K	log K	log K	$-\log P_{O_2}$	log K	log K
25	65.5	-7.32	-5.1	96.3	*	5.12
200	37.6	-5.57	-2.2	55.8		3.04
400	22.2	-5.24	-0.63	35.3		2.18
600	13.0	-5.44	+0.09	24.4	0.17	1.90
800	6.5	-5.91	+0.43	17.9	-0.24	1.89
1000	1.4	-6.56	+0.49	13.7	-0.44	2.05

* FeO not stable with respect to Fe_3O_4 and Fe below 570°C.

Fe_3O_4 can be reduced by Fe to form FeO only below 570°C while FeO can be oxidized to form Fe_3O_4 at all temperatures. The reaction of FeO with water vapor is favorable at low temperature but not at the highest temperatures in Table I. Care must be used in interpreting the reactions of iron between 400° and 600°C. This is the temperature range of interest in this work.

The formation of the spinel Fe_3O_4 from FeO and Fe_2O_3 is possible at all temperatures in the absence of iron and oxygen.

IV. STUDIES ON OXIDE NUCLEATION

A. Thin Film Range

The fact that metals react with oxygen to form a non-uniform oxide film is not new. Phelps, Gulbransen and Hickman[4] reviewed the evidence in 1946 for a granular structure in oxide films. These authors, in addition studied the crystalline nature of thin oxide films formed on a wide variety of metals including iron and iron based alloys. Samples of metals were carefully oxidized and the oxide film removed electrochemically.

Figures 2 and 3 show the results of an electron microscope study of the oxide films formed on "Puron"* and pure nickel. Electron diffraction shows the iron oxide film to be Fe_3O_4 and Fe_2O_3 while the nickel oxide film was NiO. The iron specimen was oxidized for 30 minutes at 250°C while the nickel specimen was oxidized 20 minutes at 500°C. The oxide film on iron shows irregular oxide crystals 500 to 1800 Å in size partly oriented to the metal. For the nickel specimen, the oxide film consists of irregular particles 300 to 1500 Å in size. The oxide crystals were randomly oriented to the metal.

It was concluded in 1946 that most metals formed non-uniform granular oxide films for thicknesses which could be studied by electron optical methods (about 500 Å.) The films consists of thicker and thinner sections which may indicate a multilayer structure. Nucleation of oxide occurred not only on the metal surface having only the initial oxide present but also on top of the first layer of oxide crystals. Calculations showed the oxide crystals to be 10^{-3} to 10^{-5} of the linear dimension of the metal grain and 10^{-6} to 10^{-10} of the area. Although some evidence was found for orientation in the films consisting of the larger oxide crystals, in general, very little orientation was found. The crystal size of the oxide crystals was a function of both time and temperature.

B. Work of the French School

In the early 1950's Bardolle and Benard [5] studied the initial stage of oxide formation on carefully annealed and electropolished Armco** Iron between 650° and 850°C in vacuum atmospheres of 10^{-1} to 10^{-3} mm of Hg. At pressures between 10^{-1} and 10^{-2} mm of Hg at 850°C many oriented nuclei were formed on an individual metal grain. Under no condition was a single crystal of oxide formed on the surface of a metal crystal. At pressures of 10^{-2} to 10^{-3} mm of Hg a few well oriented nuclei of oxide were formed. The shapes of the nuclei on different grains were dependent on the orientation. Originally it was thought that the space on the metal surface between oxide crystals was not covered by oxide; however, Bénard[6] has stated recently that the space is occupied by a thin film of randomly oriented oxide crystals. This leads one to conclude that the large oriented nuclei are nucleated or grow from certain oxide crystals in the thin oxide film.

C. Work at Westinghouse

Gulbransen, McMillan and Andrew[7] extended the studies of Bardolle and Bénard[5]. Electron optical methods were used and the oxide crystals formed during oxidation were covered with a thin plastic film and removed electrochemically from the metal. A high purity iron was used and the oxidation conditions were carefully defined. A vacuum microbalance was used to determine the extent of reaction.

*This is a proprietary trade name for a grade of iron produced by Westinghouse Electric Corporation.

**This is a proprietary trade name for a grade of iron produced by Armco Steel Corporation.

Figure 4 shows electron micrographs of stripped oxide films formed on hydrogen annealed electropolished "Puron" grade of iron. Part *a* shows an electron micrograph of an iron specimen oxidized at 850°C to an average thickness of 752 Å. The reaction time was 25 minutes and the initial pressure was 2×10^{-3} mm of Hg of oxygen. On exposing the sample to oxygen the pressure dropped to 10^{-4} mm of Hg indicating the reaction was nearly instantaneous and that carbon monoxide was not formed. Part *b* shows a micrograph of an oxide film removed from an iron sample oxidized at 750°C for 30 minutes to an average thickness of 322 Å. The crystal size of the oxide crystals in the film formed at 850°C was 1 micron or less while the crystallite size in the film formed at 750°C was 0.5 microns or less.

We concluded from Figure 4 that the initial stage of oxidation is a nucleation and growth mechanism with the crystal arrangement depending upon the orientation of the metal grain. The oxide crystals form along certain directions and form broken lines on a particular grain. The spacing of the lines of growth depends upon the crystal orientation and varies from 0.5 to 1.0 microns.

Circular growth patterns occur on some of the metal grains. This is illustrated in Figure 5. Here the oxidation conditions were the same as for Figure *4a*. We relate the circular growth patterns to stress patterns around inclusions in the metal grain. The oxidized specimens were light blue in color and had an average oxide thickness of 752 Å.

The existence of lines of growth for the oxide nuclei was studied by comparing the oxidation of vacuum annealed iron with hydrogen annealed iron and with iron annealed in very pure hydrogen. Figure 6 shows an electron micrograph from a study by Gulbransen and Andrew.[8] Here the iron specimen was annealed in high vacuum after carefully preparing the surface. The specimen was oxidized at 850°C using an initial oxygen pressure of 5×10^{-3} mm of Hg to an average oxide thickness of 453 Å. The micrograph shows a nearly random arrangement of oxide nuclei although each nuclei is oriented to the lattice of the metal. A thin randomly oriented oxide is formed between the larger oxide nuclei.

D. Orientation

The orientation of FeO on α-Fe was studied by Mehl and McCandless[10] and by Bardolle and Bénard[5] using x-ray diffraction. Gulbransen and Ruka[11] studied the same problem using reflection electron diffraction and in addition studied the orientation of Fe_3O_4 and α-Fe. All of the results suggest that the cube plane of FeO or Fe_3O_4 grows on the cube plane of α-Fe, while the [100] direction of the oxide lies parallel to the [110] direction in the metal.

E. Picture of Initial Oxide Formation

Our conception of the initial stages of the oxygen reaction is shown in Figure 7. It may be postulated that the first step involves a chemi-sorbed layer of oxygen atoms. This would be a very transitory stage at 850°C with the quantity of oxygen available. As the reaction continues to a thickness of 100 Å, the formation of a film consisting of small oxide crystallites of the order of the thickness of the oxide film was postulated. The next stage of oxidation appears to be nucleation and growth of larger crystals along certain lines of the metal grain. Along these growth sites a lower free-energy barrier appears to exist for the formation and growth of new oxide crystals.

The properties of these linear growth sites suggest that they represent a substructure in the metal which is influenced by the annealing environment. Hydrogen and impurities in the

hydrogen gas appear to order the sites for oxide nucleation on pure iron. The mechanism of this process is not clear.

These larger oxide crystals are well oriented to the structure of the metal grain. As oxidation continues, the crystals grow and new ones are formed completing the mosaic structure. This is shown in step *d* of Figure 7. Finally, a granular oriented oxide film is formed. Although the oxide crystals were oriented, in no case was a single crystal of oxide observed on a metal grain.

The effect of the annealing environments on the arrangement of the oxide nuclei may aid the understanding of the effect of annealing treatments on the mechanical properties "Puron" and other pure irons. Stanley[9] has made a thorough study of the embrittling of "Puron" when heated in high vacuum and in dry and moist hydrogen atmospheres at temperatures of 700-1100°C. "Puron" is embrittled in dry hydrogen atmospheres at a dew point of -65°C in 10 hr. for the temperature range of 700°C - 1150°C. In moist hydrogen, "Puron" was embrittled in about an hour. Vacuum annealing did not lead to embrittlement. Light micrographic studies showed only minor changes in metal structure.

Stanley's observations on the embrittlement of iron at 700°C and our studies on the effect of hydrogen and its impurities on the oxide nucleation pattern at 700°C appear to be related. Atmospheres which embrittle iron give random nucleation patterns for oxide growth.

V. *STUDIES ON LOCALIZED CRYSTAL GROWTHS*

A. *Early Work*

We distinguish phenomenologically between oxide nuclei observed on iron during the early stages of oxidation at 650°C to 850°C and the formation of long filaments of oxide observed by Pfefferkorn[12,13] in Germany and by Takagi[14] in Japan in the early 1950's. In contrast to the nucleation studies of Phelps, Gulbransen and Hickman,[4] Bardolle and Bénard[5] and Gulbransen, McMillan and Andrew,[7] Pfefferkorn and Takagi studied the edge of wires and fine holes in metal sheets after oxidation using electron transmission microscopy. Unfortunately, the metals used in the experiments were impure and the reaction conditions poorly defined.

On first consideration, one might suggest that oxide nuclei and oxide whiskers could grow from the same nucleating sites on the metal as the initial oxide nuclei observed in low pressure oxidation. However, it is impossible to judge from the shapes and growth characteristics whether the same sites are involved since the conditions of growth of nuclei on a nearly bare surface are very different from the conditions of growth found in thick oxide films.

In this paper we have attempted to extend the work of Pfefferkorn and Takagi by using pure metals and controlled oxidation environments.

B. *General Discussion of Method*

In discussing our work on the growth of localized crystals during oxidation of metals it is essential to make clear the basic philosophy. We assume that dislocations, precipitates, impurities and stress give rise to active sites where localized oxide growths can occur. We also assume that the type and extent of the active sites and the activity of the sites varies with the metal, the metal structure, the oxide film, the environment, the stress level and the

volatility of the metal. If the active site is a property of the metal or oxide film then gas metal reactions offers a good way to observe the effects of the site since the reaction products must accumulate at the site.

Four factors are important in discussing the growth of oxide nuclei and the growth of oxide whiskers and platelets. These are as follows: (a) crystal structure or atomic geometry of the unit cell, (b) crystal size and shape, (c) particle size and shape, (d) orientation of the oxide particles with respect to the underlying metal and (e) the nature of the site in the metal or oxide responsible for the growth of the oxide crystal.

The crystal structure is studied by electron diffraction while crystal size and shape are studied in the electron microscope.

C. *Experimental*

Direct transmission electron microscopy and electron diffraction methods were used. Disc, wire and tensile test specimens were used. The edge of a 5 mil hole in the 5 mil thick disc or tensile test specimens and the edge of a 9 mil wire were studied in the electron microscope. The wire and tensile test specimens could be stressed or reacted under stress if desired.

Five mil thick Armco iron, Puron iron and a zone refined vacuum melted pure iron were used for making the specimens. 9 mil wire was prepared from the high purity iron.

Some of the iron specimens were reacted in the laboratory vacuum microbalance system[15] at 0.1 atm of pure oxygen. A liquid nitrogen trap was used to lower the water vapor concentration to a dew point of -196°C. A second reaction system was used to react the wire or tensile test specimens under stress or without stress, in steam + argon, steam + oxygen mixtures and in steam + oxygen plus HCl vapors. Steam atmospheres were prepared by bubbling welding grade of argon through deoxygenated water at various temperatures.

Both an EMB4 and an EMU-3D RCA electron microscope were used. The latter instrument was used at 100 kv and had vacilities for taking micrographs at 280,000 direct magnification. The crystal structures were determined in the diffraction adapters of the electron microscopes using TlCl as a standard.

D. *Types of Oxide Growths Observed on Pure Iron*

Three types of localized oxide crystal growths are found when iron is oxidized in oxygen or water vapor. These are: (a) thin whiskers, (b) blade-shaped platelets, and (c) fan-shaped platelets.

1. *Oxide Whiskers*

Thin oxide whiskers are the most common localized crystal growths to form on iron. Whiskers are found alone or in combination with platelets of oxide. We have observed that whiskers are formed when annealed pure iron is reacted with dry oxygen. A few small fan-shaped oxide platelets also form in the early stages of oxidation.

Figure 8 shows an electron micrograph of an oxidized disc sample of Puron iron. The specimen was reacted for 48 hr. at 500°C in an atmosphere of dry oxygen at 0.1 atm. having a dewpoint of -196°C.

Figure 8 shows the whiskers to be 300-600 Å in diameter and 15,000 Å in average length. Some of the whiskers grew to lengths up to 75,000 Å. A surface density of 5×10^7 to 10^8 whiskers per cm^2 was estimated. Studies on specimens oxidized for 220 hr. at 500°C in wet oxygen atmospheres showed whiskers having lengths up to 500,000 Å.

Studies on oxide whiskers at high magnification show that great care must be used in using the electron microscope if contamination is to be avoided. Figure 9 shows an electron micrograph of a small iron oxide whisker at high magnification. The micrograph shows a heavy sheath of contamination around the oxide core. The central core was 100 to 150 Å in diameter. This value is in agreement with the minimum whisker thickness observed by Takagi[14].

The identificiation of the outer sheath as contaminant was proved by two experiments. First, continued electron bombardment of the whisker caused the outer sheath to grow in diameter at a rate of 1 to 7 Å per sec. Secondly, photographs of whiskers taken quickly at low beam-intensities show very little contamination. The oxide whiskers formed at 400°C were 100 to 150 Å in diameter.

Electron diffraction analyses showed the whiskers to be hexagonal α-Fe_2O_3 with the d_{hkl} values agreeing to 0.1% of the x-ray diffraction values. No evidence was noted for exotic crystal habits observed by other workers.[12,13,14] Some of these exotic crystal habits may be introduced by electron bombardment and by contamination.

Intense electron bombardment of the whiskers melts the oxide at the tip or at other points along the whisker. These whiskers when re-oxidized do not grow at the tip although some growth may occur in their thickness. Growth may stop due to destruction of the growth step at the tip. Heating the oxide whiskers in pure hydrogen at 500°C reduced the oxide whiskers to metal.

The existence of oxide whiskers having lengths to diameter ratios of 5000 suggests a calculation of the maximum stress at the root of the whisker. Using the flexure formula $S = MC/I$, we have calculated the maximum stress S for a whisker 500,000 Å long and 100 Å in diameter. Here M is the maximum bending moment and I/C is the section modulus. A stress of 510 g/cm^2 was calculated. This is a very low stress considering the length to diameter ratio.

2. *Thin Blade-Shaped Platelets*

If annealed or cold-worked iron wire is reacted with water vapor, thin blade-shaped platelets of oxide are formed in addition to oxide whiskers. The genesis of the blade-shaped oxide platelet is shown in Figure 10 for a reaction temperature of 400°C and a 10% water vapor + 90% argon atmosphere. The results are also shown in Table 2. During the first 2 hr. of reaction, both whiskers and platelets were formed on the wire. The whiskers were 100 to 150 Å in diameter and average 10,000 Å in length. The platelets were very thin, 1000 to 1500 Å wide and grew to lengths up to 10,000 Å long. We estimated the thickness of the oxide platelets to be 100 Å or less. After 6 hr. of reaction, most of the whiskers have disappeared and platelets were observed. As the time of reaction increases, the size of the platelets increases. After 23 hrs. of reaction the platelets were 2500 to 6000 Å wide and up to 70,000 Å long. The surface density was of the order of 10^8 per cm^2. The platelets grew in a parallel arrangement along the axis of the wire. About 0.6% of the surface area was involved in the reaction to form platelets.

Table 2 shows the results of an electron diffraction analysis of the thin blade-shaped platelets. The d_{hkl} values could be correlated exactly with the x-ray diffraction values for α-Fe_2O_3. The shape of the platelets suggest that the reaction of water vapor with annealed pure iron starts at a point. As reaction proceeds, certain nucleating centers broaden to form an array of blade-shaped platelets. Figure 10c shows a whisker growing at the tip of a platelet. It appears that platelet growth has taken over after the whisker was formed. Such being the case, one might then postulate that the transition from whisker to platelet occurs very rapidly once the transition conditions prevail. One explanation for the transition of whiskers to platelets is that hydrogen dissolves in the lattice of the oxide or metal and enlarges the reaction area along certain crystallographic directions.

TABLE II

Crystal Structure and Habit of Localized Growths Formed On Iron Wire at 400° At 0.1 atm H_2O + 0.9 atm Argon

Time	Crystal Structure	Effect of Time Crystal Habit	
		Whiskers	Platelets
2	α-Fe_2O_3	many, 100-150 Å diam., 10,000 Å long on average up to 30,000 Å long; density $\approx 3.0 \times 10^7/cm^2$	many, 100 Å thick, 1000 to 1500 Å wide; up to 10,000 Å long; density $\approx 2.0 \times 10^7/cm^2$
6	α-Fe_2O_3	few whiskers, 100-150 Å diam., 30,000 Å long	many, 100 Å thick; 2000 to 3000 Å wide; up to 30,000 Å long; density $\approx 10^8/cm^2$
12	α-Fe_2O_3	none	many, 100 Å thick; 2000 to 4000 Å wide; up to 60,000 Å long, density $\approx 10^8/cm^2$
23	α-Fe_2O_3	none	many, 100 Å thick, 2500 to 6000 Å wide; up to 70,000 Å long; density $\approx 10^8/cm^2$

3. *Rounded Platelets*

Thin rounded platelets of oxide are formed when cold-worked iron is reacted with dry oxygen. Figure 11 shows an electron micrograph of the crystal habit of the oxide film formed during the oxidation of cold drawn iron wire at 400°C for 48 hr. in 1.0 atm. pressure of dry oxygen.

Thin oxide platelets grow perpendicularly along the axis of the wire to a height of 40,000 Å and to lengths up to 70,000 Å. The thickness of the platelets was estimated to be of the order of 100 Å or the same as that found for the blade-shaped platelets. Internal and external stress was probably important in the growth of oxide platelets. The thickness of the platelets appears to be uniform over the platelet and appears to be the same for a large number of platelets examined irrespective of oxidation time. Electron diffraction analyses show the oxide platelets to be hexagonal α - Fe_2O_3. Stress calculations at the root of the platelets show values similar to those calculated for the oxide whiskers.

E. Discussion of Localized Growths

Two interpretations may be given for the origin of localized oxide growths. They may arise from nucleation sites within the oxide layer or they may arise from nucleation sites in the metal. Let us consider the two interpretations.

α-Fe_2O_3 and Fe_3O_4 are formed on iron when oxidized below 570°C.[16] Electron diffraction studies have shown that Fe_3O_4 is formed adjacent to the metal and α-Fe_2O_3 in the outer layer in contact with oxygen. Since the localized growths are α-Fe_2O_3, it is probable that the α-Fe_2O_3 crystals are nucleated on the Fe_3O_4 interface at certain defects in the oxide structure. These sites could be areas of local stress in the oxide film, crystal boundaries, etc.

On the other hand, Bardolle and Bénard,[5] and Gulbransen, McMillan and Andrew,[7] have shown that oxidation is a discontinuous process. Oxide nuclei are observed at a very early stage of the oxidation process. These experiments suggest that oxide whisker growth may be a continuation of chemical reactivity at the same nucleation sites brought out by low-pressure oxidation. Gulbransen and Andrew[8] have shown that the pattern of the nucleation sites can be changed by annealing in hydrogen. Annealing in hydrogen leads to a linear type of nucleation pattern.

These observations together with the experimental work of this paper lead us to suggest a reaction mechanism in which the metal structure itself determines the localized crystal growths. The mechanism is supported by experimental observations that chemical composition of the metal, chemical environment and stress have major influence on the chemical reactivity of metals.

Figure 12 shows our interpretation of the formation of localized oxide growths in oxygen and in water vapor. Figure 12a shows a nearly random pattern of nucleation sites. We postulate that a metal having this pattern of nucleation sites reacts with oxygen to form fine long whiskers of oxide in addition to the normal oxide film.

Figure 12b shows our interpretation of the nucleation pattern of a cold-worked specimen of iron. An ordered arrangement of nucleation sites is formed in the metal by the metallurgical treatment. Platelets of oxide are formed when a metal having this metallurgical structure is reacted with oxygen. Line growth of oxide is formed. The minimum distance between sites has not been determined but probably is of the order of a few 100 Å to a micron.

Figure 12c shows the nucleation pattern after water vapor has reacted with iron. After reaction, pointed and blade-shaped oxide platelets are formed. This fact suggests that water vapor during reaction acts to enlarge the reaction site possibly along certain crystallographic directions. We postulate that hydrogen ions from the water vapor reaction diffuse into the metal at 400°C and modify the impurity distribution or the nucleation sites. The water vapor generates new reaction sites as reaction occurs. However, the growth of the reaction site appears limited to a width of about 8000 Å.

Earlier work has suggested that reaction occurs by surface diffusion of metal ions to the growth step at the tip of the whisker or platelet where reaction with oxygen occurs. This mechanism is supported by the fact that localized melting of the whisker tip stops growth of the whisker. We have confirmed this observation of Takagi.[14] We have also noted that vacuum annealing does not affect the length of the oxide whiskers. In the absence of oxygen no growth occurs.

VI. EFFECT OF MOISTURE ON THE CORROSION OF IRON

The effect of humidity on the corrosion of iron is well known. Hudson[17] and more recently Copson[18] have compared the rate of corrosion of ingot iron specimens in dry and moist climates and in industrial and marine atmospheres. Ingot iron in the dry atmosphere of Khartoum corroded at a rate of 28 millionths of an inch per year while a specimen in the wet country atmosphere of Llanwrtyd Wells corroded at a rate of 1888 millionths of an inch per year. Observations of this kind led Vernon[19] to make critical laboratory studies on the effect of humidity on iron. From these studies he developed a generalization known as the "Principal of Critical Humidity." For iron at 25°C, the rate of corrosion increased rapidly for humidities above 65 percent. Dry oxidation changed to a rapid electrochemical reaction. Local electrochemical action was assumed to take place between local anode and cathode areas through an invisible adsorbed film of water.

This model of localized electrochemical action is the basis of present-day interpretation of wet corrosion. For pure single phase metals the sites for local cathodes and anodes have not been identified. Part of the difficulty is that liquid phase corrosion reactions on iron are complex since hydrated oxides are often formed and the corroding metal is often removed from the reaction site.

To show the effect of water vapor on the corrosion of iron we will compare the reaction of pure zone refined iron wires with oxygen, water vapor and several mixtures of water vapor and oxygen. For these gas phase conditions, electrochemical action and solution of the corrosion product in the liquid phase are eliminated. The complex hydrated oxides also are not stable.

Figure 13 shows four transmission electron micrographs of the crystal habit of the localized corrosion products. The specimens were reacted at 450°C for 48 hrs. in the following atmospheres:

1. dry oxygen having a dewpoint of -78.5°C,
2. 10 percent water vapor + 90 percent argon,
3. 10 percent water vapor + 90 percent oxygen, and
4. 3.13 percent water vapor + 96.87 percent oxygen.

The latter gas mixtures have O_2/H_2O mole ratios corresponding to 70 percent and 21 percent humidity in air at 25°C.

Figure 13a shows oxide whiskers formed when iron was reacted with dry oxygen. These whiskers were 100-150 Å in diameter and grew to an average height of about 5000 Å. Electron diffraction analyses showed the whiskers to be only α-Fe_2O_3. These whiskers were formed in addition to the normal oxide film. Figure 13a suggests that the nucleation sites on the metal or on the oxide were 100-150 Å in diameter. Since the diameter was constant along the length of the whisker, we conclude that the area of the nucleation sites were not elongated as the whisker grew. The area of the nucleation site appeared to be independent of time or the extent of oxidation.

Figure 13b shows the crystal habits formed when iron reacts with a 10 percent water vapor + 90 percent argon mixture. Many thin pointed blade-shaped platelets were formed. These were 100-150 Å thick, about 7,000 Å long, and about 70,000 Å high. Electron diffraction analyses showed these platelets to be only α-Fe_2O_3. The surface density of the platelets was estimated to be about $10^8/cm^2$.

The shape of the oxide platelets suggests that the site for reaction enlarges as the reaction proceeds, whereas in the iron-oxygen reaction the area of the site remains constant. The uniform thickness of the platelets suggests that the width of the nucleating area remains constant. One explanation for the effect of water vapor is that hydrogen atoms or ions from the water vapor act to enlarge the area for reaction.

Figures 13c and d show the crystal habits of the corrosion product when iron was reacted with mixtures of oxygen and water vapor corresponding to mole ratios of O_2/H_2O of 30/1 and 9/1. Oxide platelets were the predominant crystal habit for both environments. To prevent the growth of oxide platelets the O_2/H_2O ratio must be increased to a high value. At 450°C the influence of water vapor on the localized corrosion process is much greater than its influence on the corrosion of iron at room temperature. We conclude that Vernon's "Principle of Critical Humidity" can be extended to the gas phase corrosion reactions of iron.

Let us consider in more detail the localized growths observed after reacting iron in oxygen and in water vapor plus argon atmospheres. Assuming the same surface density for the whiskers and platelets, the electron micrographs suggest that the reaction sites in the metal for the water vapor reaction are over 50 times the area of those observed for the dry oxygen reaction. The total amount of oxide in the oxide platelets is about 250 times the amount of oxide in the oxide whiskers.

These experiments may help to explain the unique effect of water vapor on the corrosion of iron at ambient temperatures. Certain differences of course exist. The corrosion rate will be slower, hydrated oxides may form instead of α-Fe_2O_3, the corrosion product may dissolve in the liquid phase, and electrochemical action may be present. The factor which has not been foreseen in earlier studies is the effect of water vapor itself on the reaction site without electrochemical action.

To control the corrosion of ingot iron in humid atmospheres, two factors must be considered in addition to any electrochemical effects. Hydrogen from the water vapor reaction with iron must be prevented from entering the metal, and growth of the localized reaction sites must be inhibited by the addition of suitable alloying elements.

VII. EFFECT OF STRESS ON THE CORROSION OF IRON AND STAINLESS STEEL

We have classified stress effects into three types: (1) internal stress due to cold work, (2) internal stress due to precipitation of a second phase, and (3) externally applied stress.

A. Effect of Cold Work

The effect of stress introduced by drilling a 5 mil hole in Armco Iron was studied. One specimen was drilled and then annealed in high vacuum of less than 10^{-6} mm of Hg at 850°C for 16 hours. A second specimen was vacuum annealed before drilling the hole. Both specimens were reacted at 500°C in oxygen at 0.1 atm for 66 hours without external load. Figure 14 shows electron micrographs of the two specimens after oxidation in dry oxygen. Small whiskers of α-Fe_2O_3 are found on the specimen drilled before annealing. For the specimen drilled after annealing, both whiskers and platelets of oxide are found. Stress introduced by cold working has a large influence on the extent of whisker growth. In addition, a large number of platelets of oxide form as a result of cold work.

B. Effect of External Stress

Two samples of 9 mil 304 stainless steel wire in the "as received" and cleaned condition are reacted at 500° C for 24 hrs. in 0.1 atm of dry oxygen. A stress of 44,000 psi is applied externally during reaction to one specimen, while a second specimen is reacted without stress.

Figure 15 shows electron micrographs of the two 304 stainless steel surfaces. The specimen reacted under no stress conditions shows no unusual crystal habits in the oxidation products. However, the specimen reacted under a stress of 44,000 psi shows a few well- defined platelet growths on certain areas of the surface.

The platelets grow along straight lines parallel to the axis of the wire. In addition, certain areas, 2μ on an edge, show a concentration of oxide platelets. This is shown in Figure 16. The platelets are of the order of 100 Å thick, 30,000 Å high, and grow to lengths of 60,000 Å. No whisker growths are observed. We conclude that stress is a major influence on the crystal habits of the reaction products formed when 304 stainless steel is reacted with dry oxygen.

VIII. INITIAL STEP IN STRESS CORROSION CRACKING

Stress corrosion cracking of stainless steels in high pressure water-water vapor atmospheres at 300°C is the cracking of the metal under combined influence of stress and corrosion. The usual method for study is to expose U bend specimens in autoclaves. However, only empirical information can be obtained from such tests.

Two steps are usually associated with stress corrosion cracking. These are the initiation of the crack and the propagation of the crack. The initiation step is probably one of localized corrosion under the influence of stress. It is usually assumed that crack initiation is tied up with a special driving force which acts to give a highly localized corrosion reaction.

Gulbransen, Copan and van Rooyen[18] have proposed that a study of localized growths in gas phase reactions can lead to an understanding of the initiation stage of the stress corrosion cracking phenomenon.

A. Experimental

We can simulate a stress corrosion system by using a reaction atmosphere of oxygen, water vapor and a trace of chloride ion in the form of a trace of hydrochloric acid. Stress can be introduced by an initial strain or by reacting under stress.

Table 3 shows the results of applying different loads to the stainless steel wires. Increasing the stress level in the material favors the growth of platelets. At the highest stress level large platelets alone were formed. Figure 17 shows an electron micrograph of these platelets formed at 600°C in wet oxygen + a trace of HCl in 138 hours under an initial stress level of 59,000 psi. Electron diffraction studies showed the growths to be the hexagonal oxide X_2O_3 where X was either iron or chromium.

B. Discussion

Figure 18 shows a schematic diagram of how localized chemical reaction can lead to the formation of sub-microscopic trenches or cracks in the metal. Figure 18a shows an oxide platelet formed as a result of gas phase reaction of an ordered arrangement of nucleation sites. A deep trench may form at the root of the platelet. Although we have not demonstrated the existence of a narrow trench, the length to thickness ratio of 1000 to 1 for the platelet suggests that the source metal for the oxide platelet must be very localized. The formation of trenches a few hundred angstroms in thickness can lead to a high stress concentration and to a condition for propagation of the crack nuclei.

TABLE III

Effect of Strain on Crystal Habit, Corrosion of 304 Stainless Steel, Wet O_2 + Trace of HCl Vapor, 600°C, 138 Hrs. of Reaction

Strain	Crystal Habit
41,000 psi	Platelets 100 Å thick, up to 30,000 Å high and long. Whiskers 300-500 Å diameter up to 40,000 Å long.
52,000 psi	Platelets 100 Å thick, up to 60,000 Å high and long. Whiskers - a few
59,000 psi	Platelets 100 Å thick, up to 100,000 Å high, 200,000 Å long. Whiskers - none

Figure 18b shows a schematic drawing of how localized chemical or electrochemical reaction can occur for liquid phase reactions. We assume the metal has a set of aligned nucleation sites as was demonstrated in Figure 15 and shown shcematically in Figure 18a. The thickness of the active area for reaction was about 100 Å in Figure 15. In liquid phase reaction the corrosion product may dissolve and as a result may not accumulate to form a coherent oxide structure. Again, we postulate the formation of a narrow trench which leads to a high stress concentration and conditions for propagation of the crack nuclei.

The chemical and electrochemical conditions of liquid phase reaction suggest that more rapid localized corrosion may occur than in gas phase reactions. Some of these conditions are: (1) diffusion of the metal ion through or on the surface of the oxide platelet is not necessary, (2) local electrochemical cells may accelerate the rate of localized corrosion, (3) pH shifts may occur at the site of reaction which could accelerate the rate of reaction, and (4) a sharper radius of curvature and larger stress concentration may exist at the root of the trench if a coherent metal oxide structure is absent.

Although much experimental work remains to demonstrate the role of this new structure element, we feel that some evidence supports our point of view. Studies on 20 chromium-80 nickel alloys and pure nickel shows no evidence for platelet types of oxide growths. These materials are reported to be less sensitive to stress corrosion cracking.

IX. NEW MATERIALS

Three crystal habits have been demonstrated in this paper: (1) oxide whiskers, (2) oxide blade-shaped platelets, and (3) oxide rounded platelets. Selected area electron diffraction studies suggest that these crystals are probably single crystals.

Calculations show that these crystals have very high elastic strain limits. Thus, a 150 Å diameter whisker bent to a 1500 Å radius gives an estimated elastic strain limit of at least 5 percent. Due to the difficulties of handling 150 Å diameter whiskers direct measurements of the strength has not been carried out.

If these whiskers and platelets have high strengths which are characteristic of metal whiskers we may have new structural materials which have high melting points, low vapor pressures, high elastic yield limits, non-corrosive and perhaps high strengths. The big problem is to find a practical way of growing and processing these crystals into usable shapes and sizes.

X. CONCLUSIONS

A. Oxide Nucleation

Useful information can be obtained on the growth of oxide films at high temperature from a study of the crystal habit and structure of the oxide film. These films are formed by reaction with limited quantities of oxygen at low pressures.

Electrochemical-stripping techniques were used to remove the oxide layer from the oxidized samples of highly annealed and electropolished iron. These samples were then studied in the electron-diffraction camera and electron microscope.

Several stages in the oxide-growth process were studied over the temperature range of 650° to 850°C using different amounts of oxygen at low pressures.

The results suggest that the initial stage of oxidation involves the formation of a thin uniform layer of small oxide crystallites. This was rapidly followed by the formation of much larger oxide crystals along certain parallel and regularly spaced lines on the metal grain. As oxidation continues, the oxide crystals grow, and new crystals form filling the remaining area of the metal surface. This results in the formation of a uniform mosaic of large oxide crystals.

The origin of the lines of growth of the oxide crystals on the metal may be related to the hydrogen annealing process.

It is also concluded that the concept of a uniform growth of an oxide film must be discarded.

B. Localized Crystal Growths

Electron microscope and electron diffraction studies show several unusual crystal habits of the oxide film to occur when iron is oxidized in oxygen or water vapor atmospheres. These are (1) fine oxide whiskers 100-150 Å in diameter, (2) rounded platelets of oxide about 100 Å in thickness, and (3) blade-shaped platelets about 100 Å in thickness.

In dry oxygen atmospheres whiskers grow on annealed pure iron specimens. Blade-shaped platelets grow in water vapor or in mixed water vapor and oxygen atmospheres. Rounded platelets grow on iron containing impurities when stress is present in oxygen atmospheres.

Impurities, stress and environment appear as critical factors in determining the type of growths of localized oxide crystals on iron.

Water vapor has a unique action in the corrosion of iron. Water vapor acts during reaction to increase the area of the site for localized reaction from a point site to a line site. This leads to a large increase in the extent of localized action.

The surface density of the whiskers and blade-shaped platelets is of the order of $10^8/cm^2$. The fraction of the surface area involved in oxide whisker formation is less than 0.1 percent.

If the origin of the nucleation sites and the mechanism of growth can be determined, we will then have a better understanding of corrosion and the substructure of metals.

ACKNOWLEDGMENT

The author is greatly indebted to his present associates, Mr. K. F. Andrew and Mr. T. P. Copan and to his earlier associates, Dr. R. T. Phelps, Dr. J. W. Hickman and Mr. W. McMillan for carrying out most of the experimental work upon which this paper is based.

Recommended Research Activities

I. Techniques

A. Develop furnaces, reaction systems and methods for determining the kinetics of reactions at temperatures above 1200°C. Progress in the field of high temperature studies are seriously limited by the present state of technology in ceramic ware, furnace systems, temperature measurement and methods for measuring reaction kinetics.

B. Develop methods for the determination of crystal structure and composition of thin and thick films on metals "in situ" above 1200°C. Both x-ray diffraction and electron diffraction methods must be considered. Again, progress in the field of high temperature studies is limited by lack of structural facilities.

II. Problems

A. Study of the role of metal structure including dislocations, impurities, inclusions and stress on the mechanism of oxidation of metals and the formation of localized growth at the oxide-gas interface.

This problem was discussed in my lecture to the 8th Sagamore Conference. I personally feel that a great deal of useful knowledge can be gained in these studies.

B. Oxidation of Alloys Having High Temperature Possibilities

1. Phase diagram studies of the oxides,
2. Crystal structure studies,
3. Adhesion studies,
4. Kinetics of oxidation,
5. Composition studies,
6. Study of role of various alloying elements.

The object of these studies would be to understand the basic processes occurring in the oxidation of alloys. Few people have tried to study the complete problem.

C. Mechanism of Oxidation of Refractory Metals and Alloys

1. Role of solution of oxide in metal,
2. Mechanism of breakdown of oxide film,
3. Nucleation and growth of higher oxides,
4. Effects of impurities and alloying elements on the oxidation processes,
5. Crystal structure studies.

The mechanisms of oxidation of the refractory metals molybdenum, tantalum, niobium and tungsten are not understood. To attack these problems requires a large effort coordinating many techniques. A number of groups have made a start on this problem but a new imaginative approach is needed.

D. Reactions of Pure Metals and Alloys In H_2O, $H_2O + H_2$, $CO + CO_2$, Cl_2, SO_2 and Other Gas Atmospheres.

A few studies of gas reactions in these atmospheres have been made but much more work could be done.

E. Studies on Oxide Whiskers and Platelets

1. Crystal structure and orientation on the metal,
2. Methods for study of mechanical properties and electrical properties,
3. Methods for harvesting, aligning and consolidating crystals into fibers or sheets,
4. Application of new materials.

These studies are aimed at finding whether these unique crystals can be used to make new materials. These crystals appear to be elastic, non-corrosive and strong. This project must be carried out by scientists of proven imagination.

REFERENCES

1. Wagner, C., "Diffusion and High Temperature Oxidation of Metals," in Atom Movements, A.S.M., Cleveland, 1951, p. 153.

2. Benard, J., Bull. Soc. Chim., France, 1949, pp. 73-87.

3. Chipman, J. and Murphy, J. W., Industrial and Engineering Chemistry, 25, 319, (1933).

4. Phelps, R. T., Gulbransen, E. A., and Hickman, J. W., Industrial and Engineering Chem. 18, 391, 1946.

5. Bardolle, J. and Bénard J., Rev. Met., 49, 613, (1952).

6. Bénard, J., Private Communication.

7. Gulbransen, E. A., McMillan, W., and Andrew, K. F., Trans. Am. Inst. Mining Met. Engrs., 200, 1027 (1954).

8. Gulbransen, E. A., and Andrew, K. F., Jnl. of the Electrochem. Soc., 106, 551, (1959).

9. Stanley, J. K., Trans. Am. Soc. Metals, 44, 1097 (1952).

10. Mehl, R. F., and McCandless, E. L., Trans. AIME 125, 531, (1937).

11. Gulbransen, E. A. and Ruka, R. J., Industrial and Engineering Chemistry, 43, 697 (1951).

12. Pfefferkorn, G., Naturwiss. 40, 551 (1953).

13. Pfefferkorn, G., Z. Metallkunde, 46, 204 (1955).

14. Takagi, R., J. Phys. Soc., Japan, 12, 1212 (1957).

15. Gulbransen, E. A., Advances in Catalysis, Vol. V., Academic Press, New York, pp. 119-175 (1953).

16. Hickman, J. W., and Gulbransen, E. A., Trans. AIME, 171, 306 (1947).

17. Hudson, J. C., "Corrosion of Iron and Steel," Chapman and Hall, 1940, p. 93.

18. Copson, H. R., Corrosion, p. 533 (1959).

19. Vernon, W.H.J., Trans. Faraday Soc., 23, 162, 1927 - Trans. Faraday Soc. 27, 264, 1931.

20. Gulbransen, E. A., Copan, T. P., and van Rooyen, D., Westinghouse Research Laboratories, Scientific Paper 6-94602-1-R5, September 18, 1957.

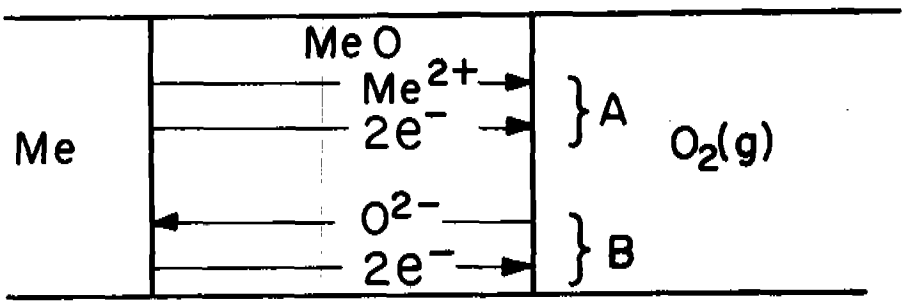

$$Me \rightarrow Me^{2+} + 2e^- \qquad \tfrac{1}{2} O_2(g) \rightleftharpoons O^{=} + \square_C + 2\oplus \qquad (A)$$

$$Me + O^{2-} \rightarrow MeO + 2e^- \qquad \tfrac{1}{2} O_2(g) + 2e^- \rightleftharpoons O^{2-} \qquad (B)$$

$\oplus$ ELECTRON HOLE Me^{3+}

$\square_C$ Me^{2+} VACANCY

OXIDATION SCHEME

19-066-1721/ORD-61

RM 9531

FIGURE 1

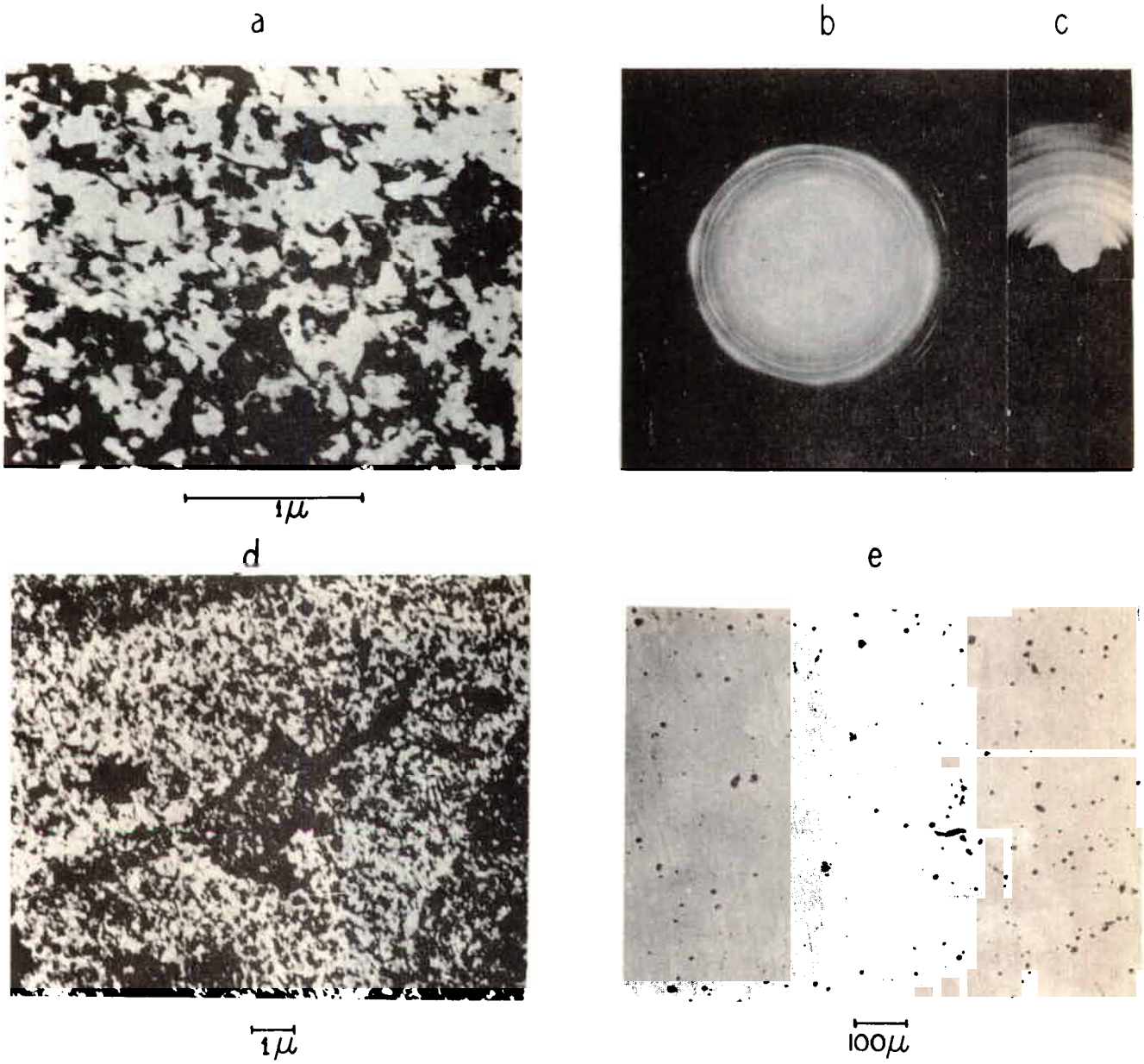

OXIDE FILM OF IRON

Fe 30-250

a. E.M. STRIPPED FILM
b. E.D.T. STRIPPED FILM
c. E.D.R. FILM ON METAL
d. E.M. STRIPPED FILM
e. L.M. FILM ON METAL

19-066-1722/ORD-61

302955

FIGURE 2

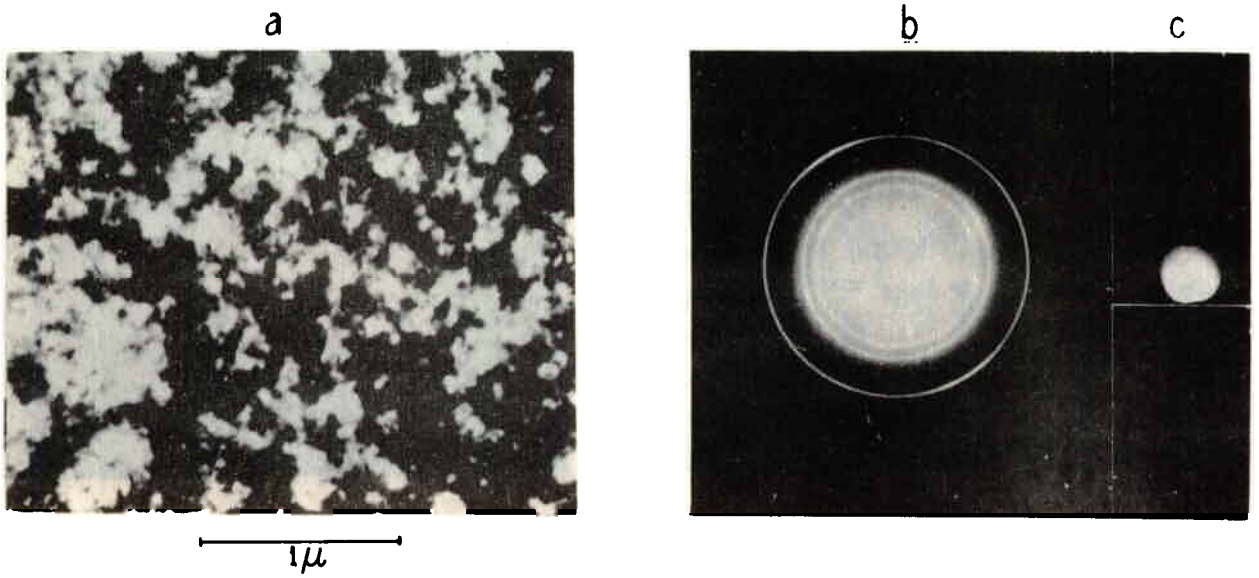

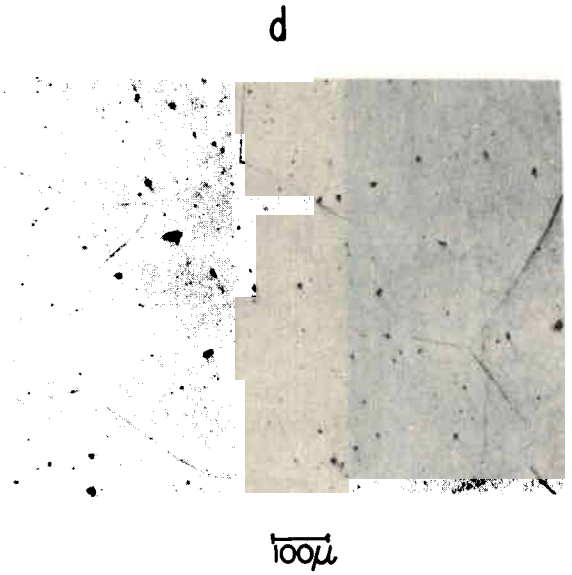

OXIDE FILM OF NICKEL

Ni 5-500

a. E.M. STRIPPED FILM
b. E.D.T. STRIPPED FILM
c. E.D.R. FILM ON METAL
d. L.M. FILM ON METAL

19-066-1723/ORD-61

302960

FIGURE 3

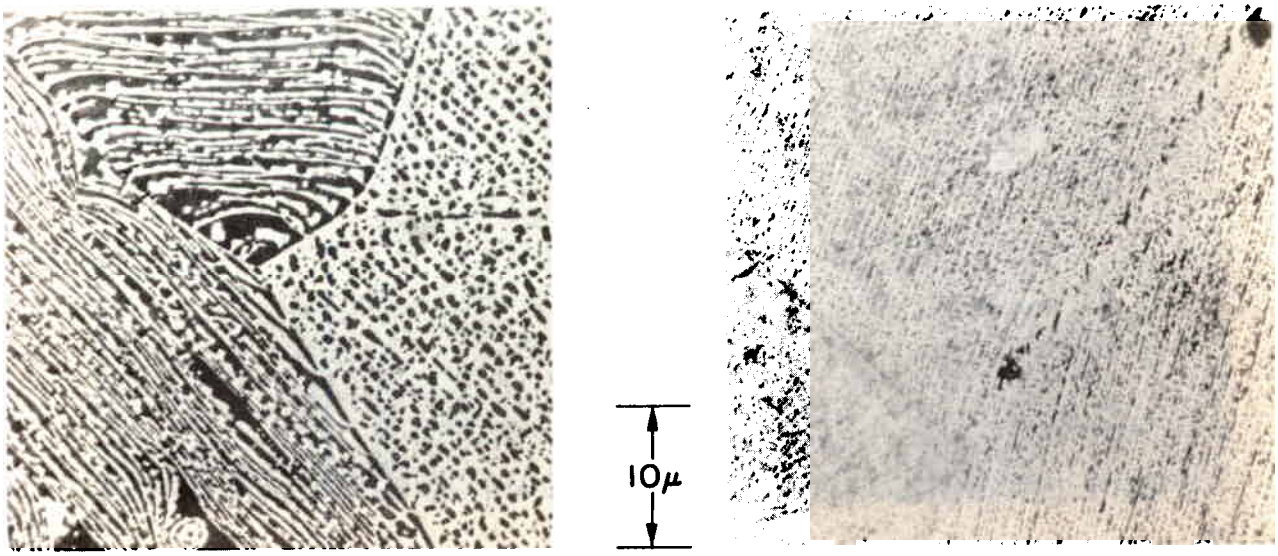

A. B.

FIGURE 4

OXIDE FILM STRIPPED FROM PURON ANNEALED IN HYDROGEN PASSED OVER HOT COPPER.

H_2 - 850°C - 20 HRS. - COOL IN H_2

A. 752Å THICK OXIDE - 850°C

B. 322Å THICK OXIDE - 750°C

19-066-1728/ORD-61 1653-a, 1637-c (60-12), (60-14) RM 14250

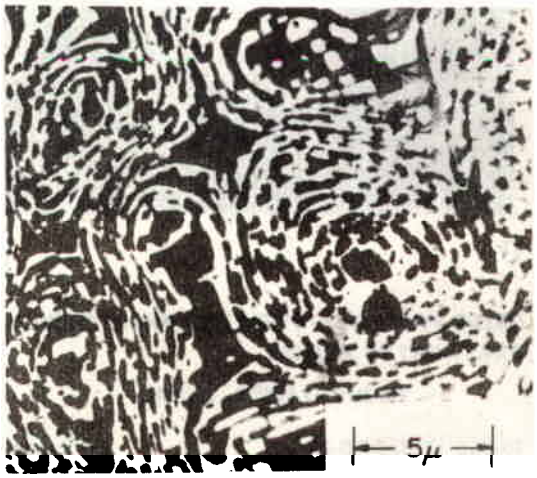

FIGURE 5

CIRCULAR GROWTH PATTERN IN OXIDE FILM (752Å) FORMED ON PURON ANNEALED IN HYDROGEN PASSED OVER HOT COPPER.

H_2 - 850°C - 20 HRS. - COOL IN H_2

19-066-1729/ORD-61 RM 14252

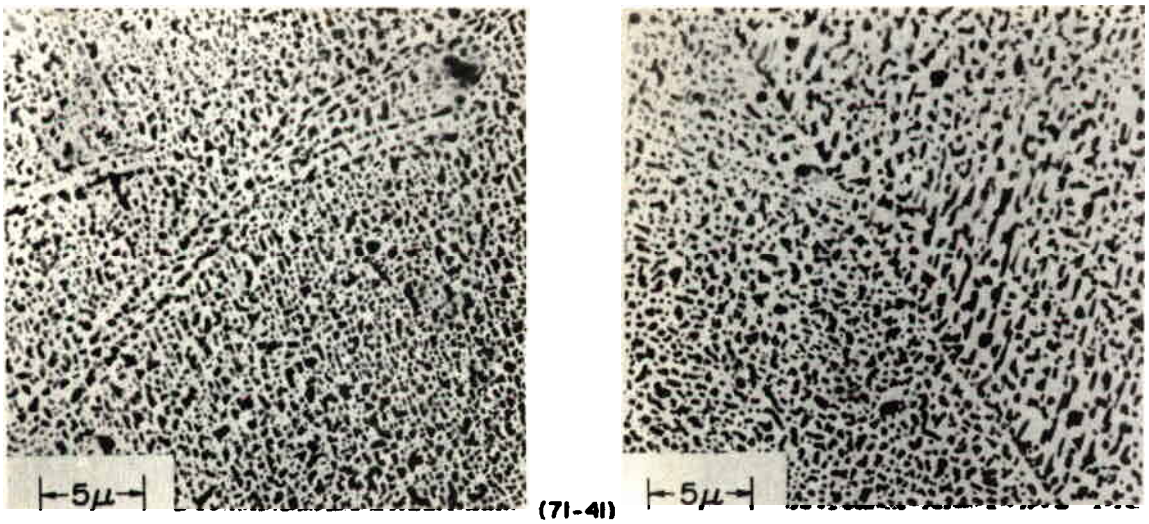

A B

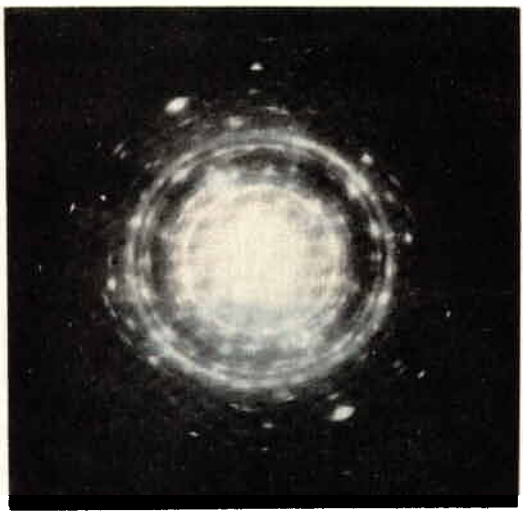

C

OXIDE FILM (453A) STRIPPED FROM VACUUM PRETREATED PURON

VACUUM - 875°C - 20 HRS.

19-066-1727/ORD-61 **RM 14248**

FIGURE 6

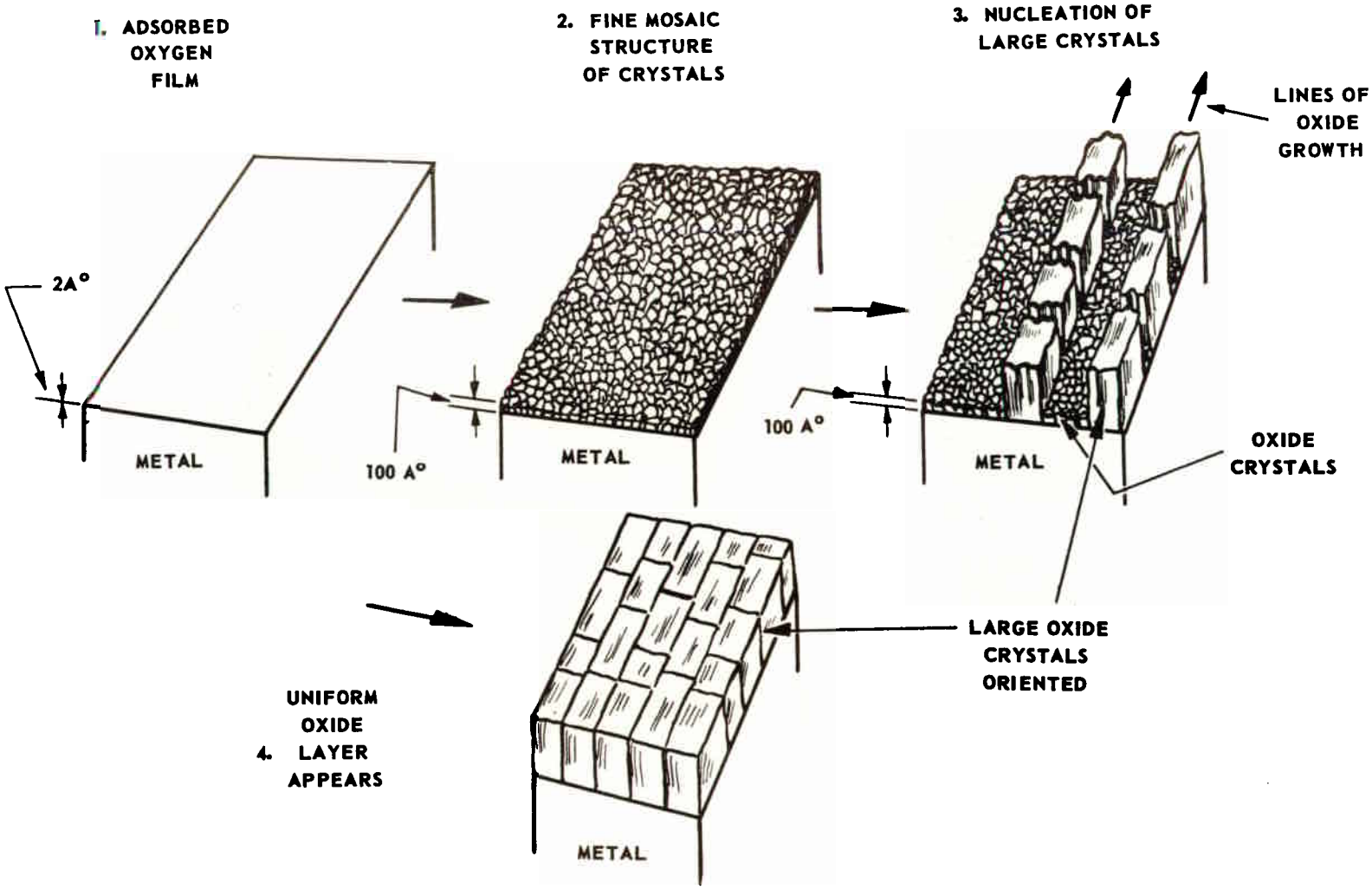

OXIDATION MECHANISM

19-066-1720/ORD-61

RM 9480

FIGURE 7

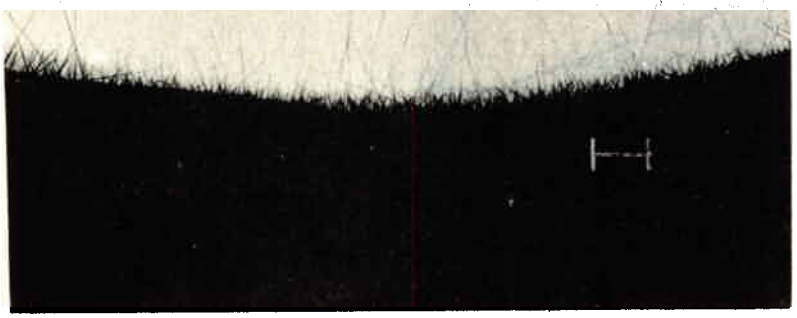

FIGURE 8

FINE OXIDE WHISKERS FORMED ON "PURON" AT 500°C IN DRY OXYGEN FOR 48 HOURS. NO APPLIED STRESS. MAG. 8000X

19-066-1726/ORD-61

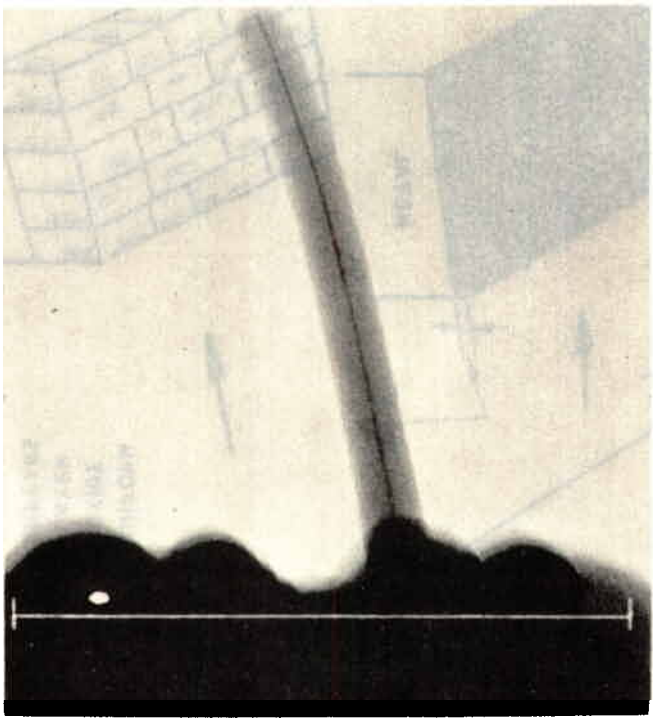

FIGURE 9

CONTAMINATION ON OXIDE WHISKERS FORMED ON "ARMCO" IRON. MAG. 90,000X

19-066-1725/ORD-61

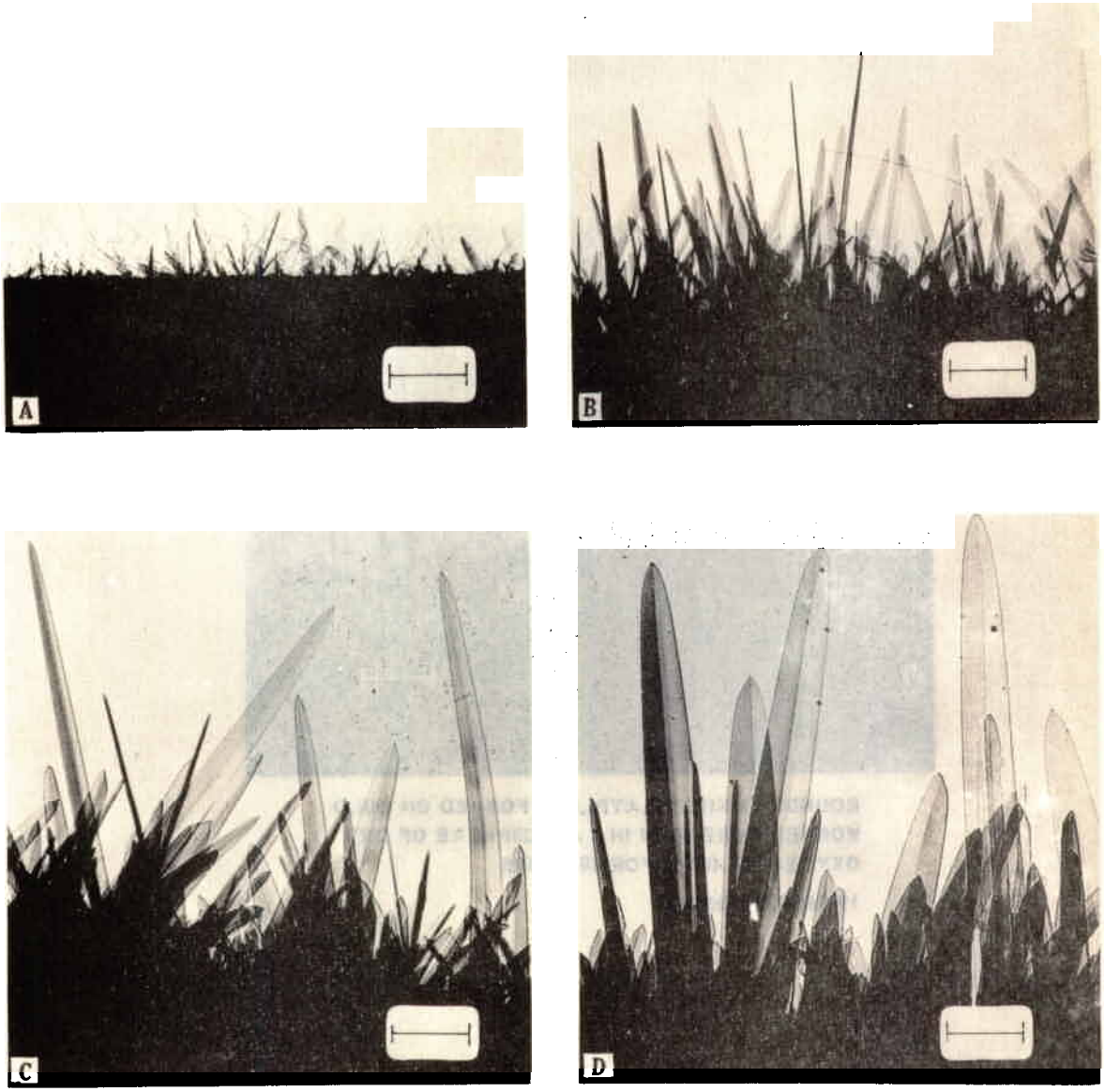

BLADE-SHAPED OXIDE PLATELETS FORMED ON ANNEALED PURE IRON IN 10% H_2O AND 90% ARGON AT 400°C.

(A) 2 HOURS, (B) 6 HOURS, (C) 12 HOURS, (F) 23 HOURS.

19-066-1730/ORD-61

FIGURE 10

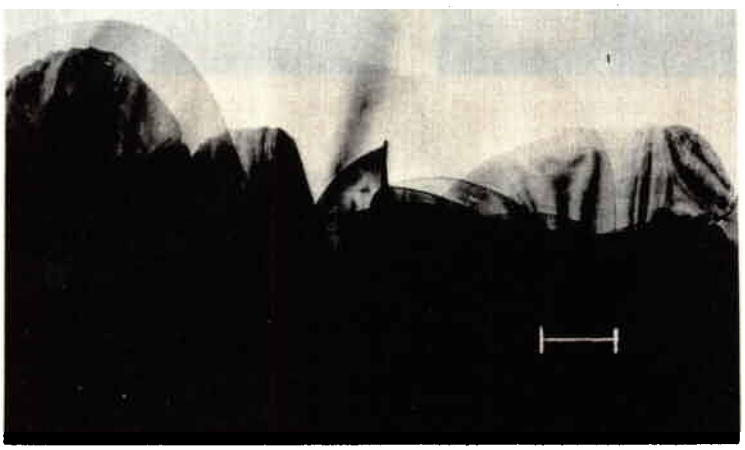

ROUNDED OXIDE PLATELETS FORMED ON COLD WORKED PURE IRON IN 1 ATMOSPHERE OF DRY OXYGEN AT 400°C FOR 48 HOURS

19-066-1731/ORD-61

FIGURE 11

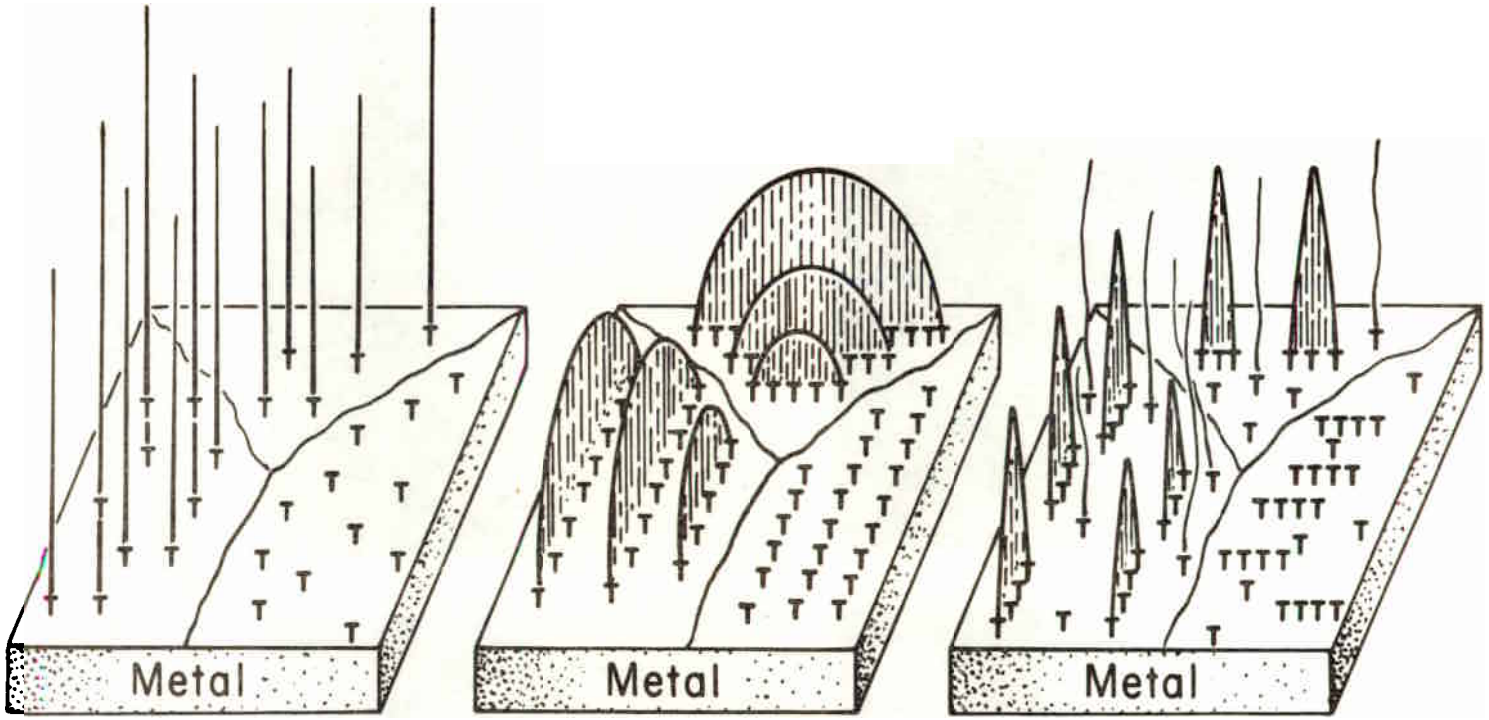

(a)
ANNEALED PURE IRON
DRY OXYGEN, 400°C

(b)
COLD WORKED PURE IRON
DRY OXYGEN, 400°C

(c)
ANNEALED OR COLD WORKED PURE IRON
H_2O VAPOR, 400°C

LOCALIZED OXIDE GROWTH HABITS IN THE OXIDATION OF IRON
(a,b) OXYGEN REACTION, (c) WATER VAPOR REACTION

11-066-1719/ORD-61

FIGURE 12

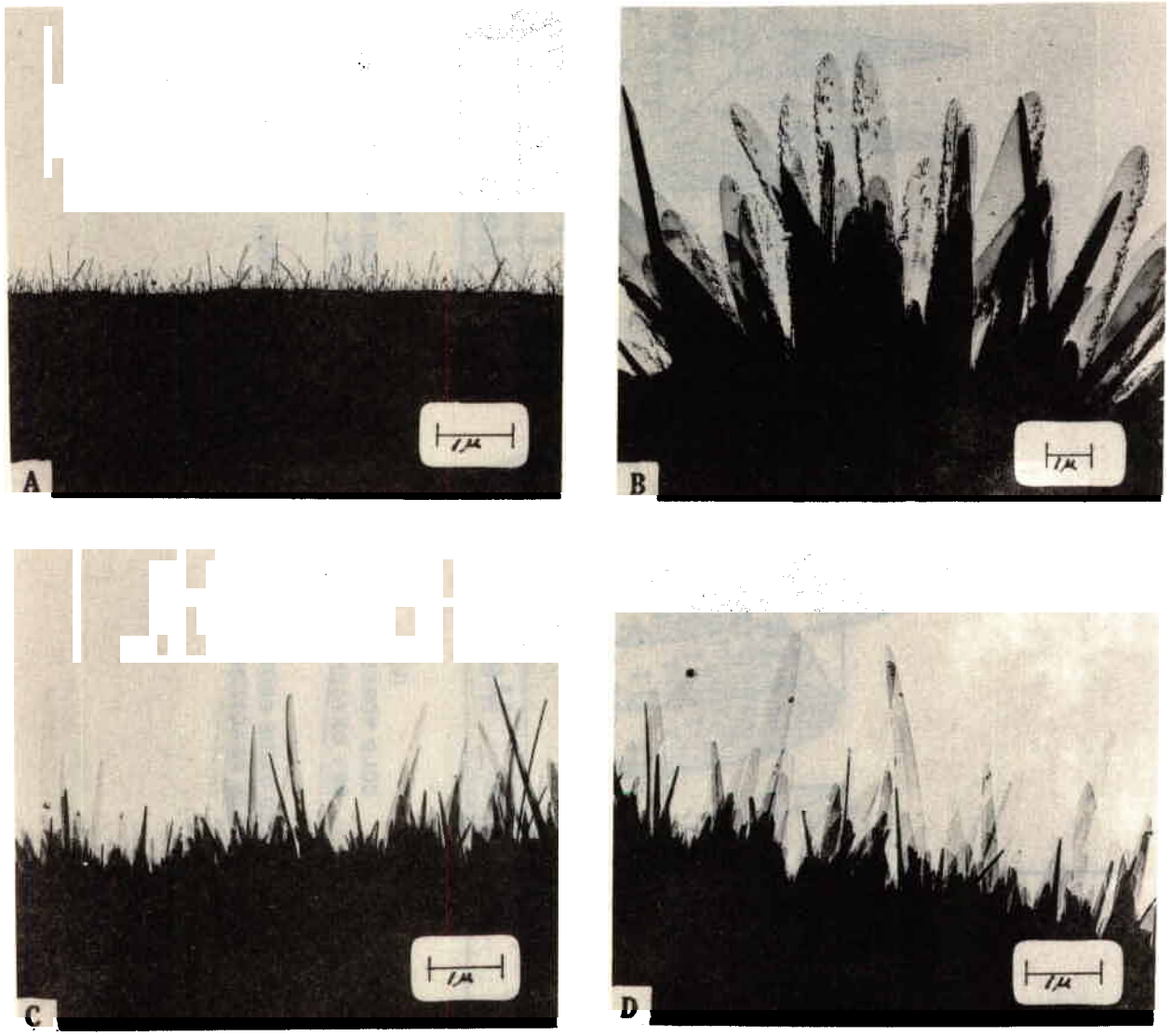

EFFECT OF MOISTURE ON CRYSTAL HABITS OF THE CORROSION PRODUCTS FORMED ON IRON AFTER REACTING AT 450°C FOR 48 HOURS IN (A) DRY O_2; (B) 10% H_2O + 90% Argon, (C) 10% H_2O + 90% O_2; and (D) 3.13% H_2O + 96.87% O_2.

19-066-1732/ORD-61

FIGURE 13

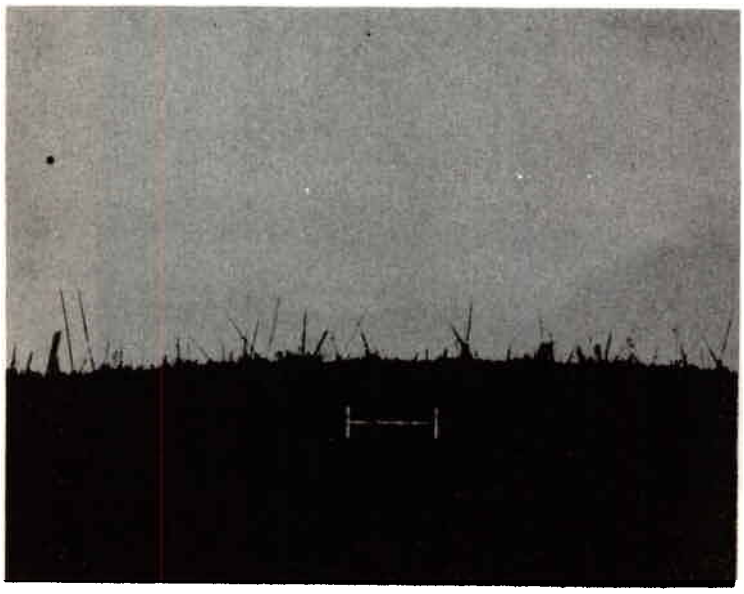

a

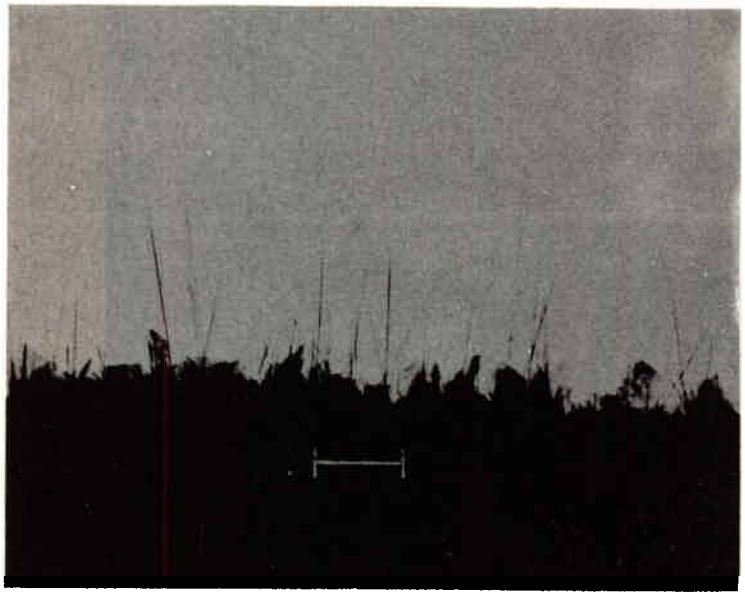

b

EFFECT OF COLD WORK AND ANNEALING TREATMENT OF OXIDES FORMED ON "ARMCO" IRON. (a) HOLE DRILLED BEFORE ANNEAL, (b) HOLE DRILLED AFTER ANNEAL.

19-066-1733/ORD-61

FIGURE 14

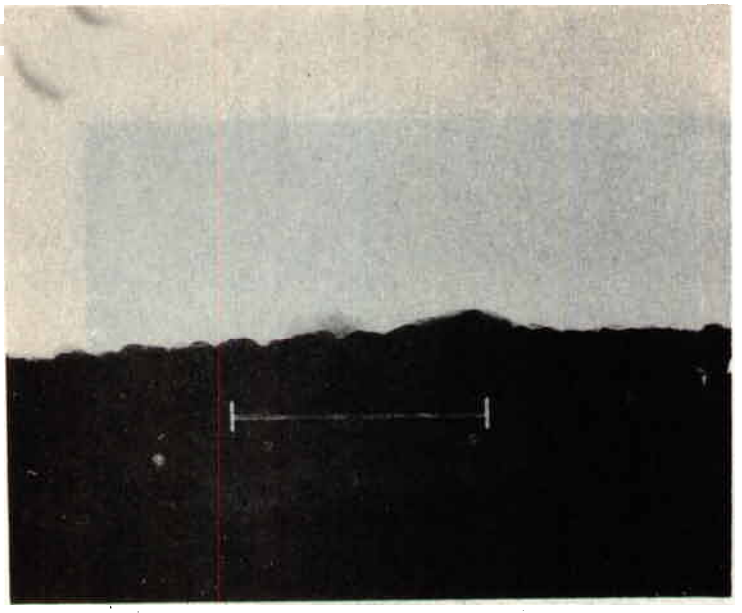

a

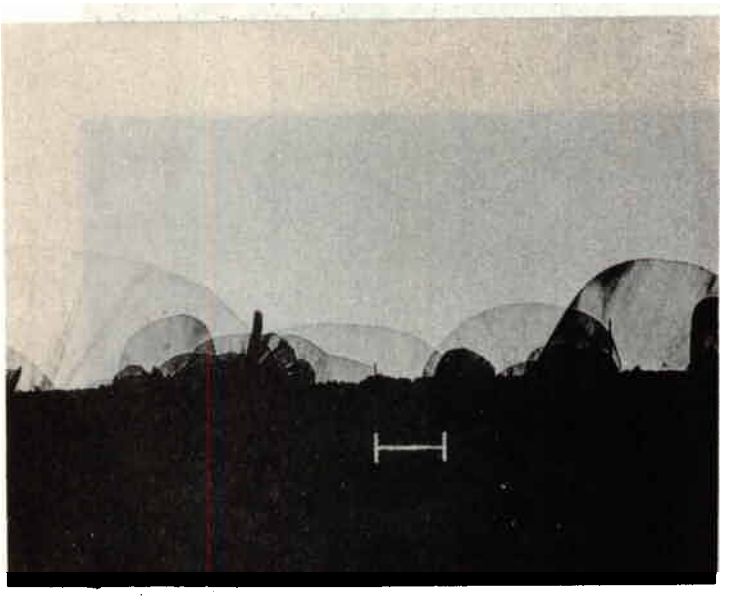

b

EFFECT OF TENSILE STRESS ON CRYSTAL HABIT OF OXIDE FILM FORMED ON 304 STAINLESS STEEL. OXIDIZED 24 HOURS 0.1 ATMOSPHERE OF OXYGEN AT 600°C. (a) NO APPLIED STRESS, (b) 44,000 p.s.i.

19-066-1734/ORD-61

FIGURE 15

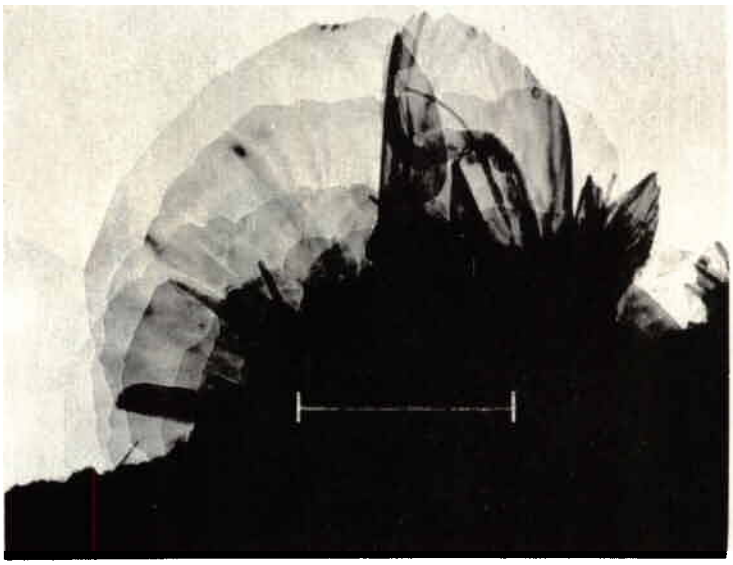

OXIDE PLATELET GROWTH 304 STAINLESS STEEL.
OXIDIZED 24 HOURS 600°C, 0.1 ATM. OXYGEN.
STRESS OF 44,000 P.S.I.

19-066-1735/ORD-61

FIGURE 16

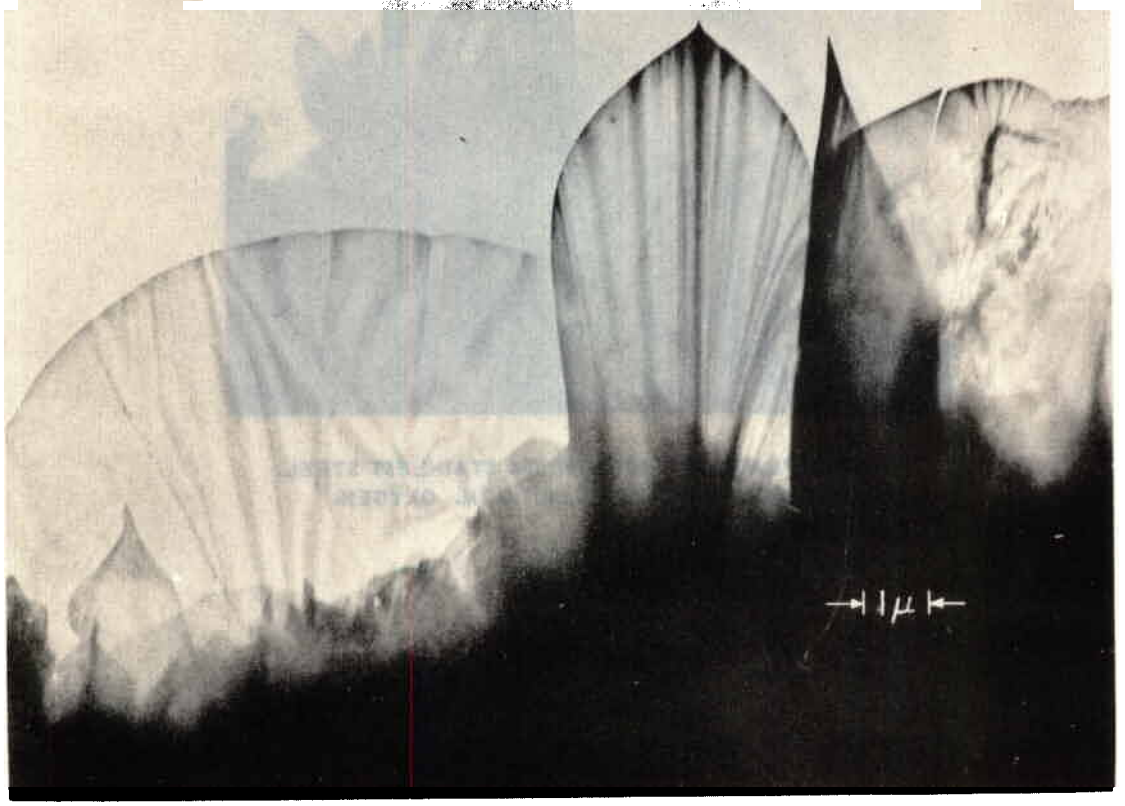

CRYSTAL HABIT OF OXIDE FORMED IN THE OXIDATION OF 18-8 STAINLESS STEEL AT 600°C IN WET OXYGEN PLUS TRACE OF HCl VAPOR FOR 138 HOURS. PRE-STRESSED TO 59,000 p.s.i.

MAGNIFICATION: 9000 X

19-066-1724/ORD-61

FIGURE 17

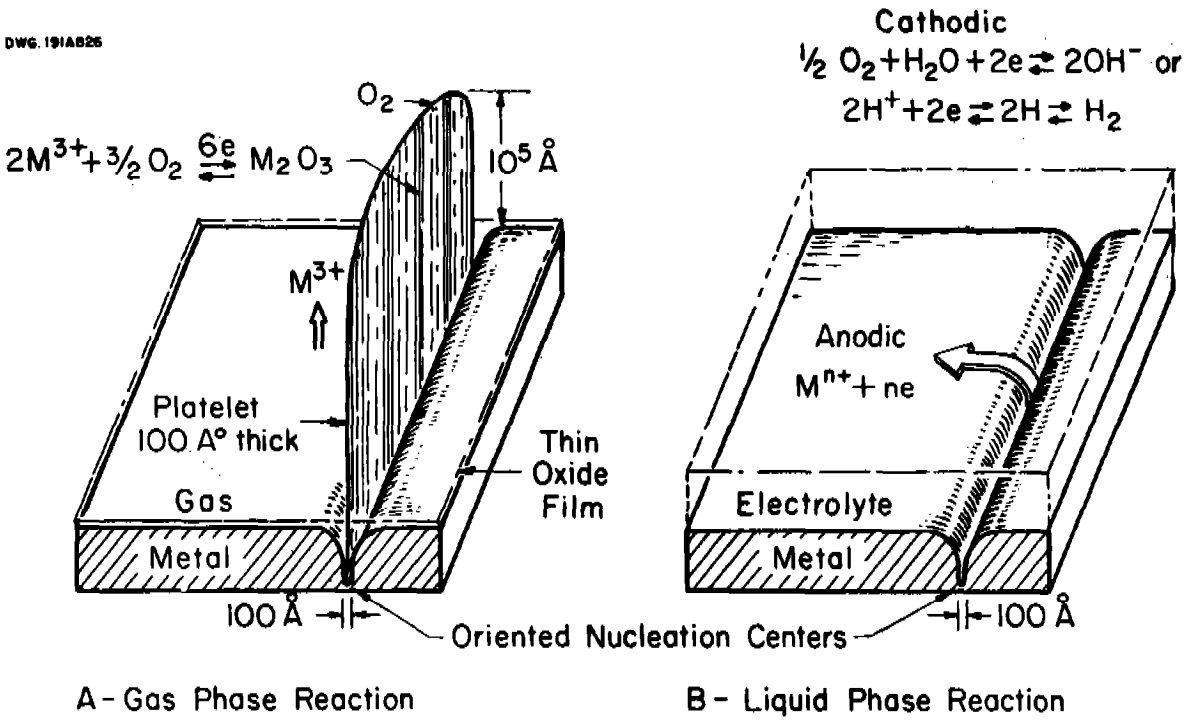

TRENCHING BY LOCALIZED CORROSION

19-066-1694/ORD-61 RM 15105

FIGURE 18

GRAIN BOUNDARY BEHAVIOR IN HIGH TEMPERATURE DEFORMATION AND FRACTURE

by

Dr. Arthur W. Mullendove

and

Dr. Nichols J. Grant

SECTION I. INTRODUCTION

Progress in the past ten years in our understanding of the nature of grain boundaries and boundary processes has been marked, but a great deal has yet to be uncovered, as is evidenced by the volume of research which regularly appears in the literature. Historically, interest in grain boundaries in metals began in the late nineteenth century, when it was noted that the boundaries between crystals exhibited a variety of characteristics which were different from those of the crystals themselves. Thus, Rosenhain[1] was led to regard the metallic structure as consisting of crystals cemented together by a layer of the same material in the amorphous state. This theory was used to explain the apparent difference in the temperature dependencies of the properties of grains and grain boundaries, as evidenced by grain boundary deformation and intercrystalline failure at high temperatures, in contrast to crystalline deformation at low temperatures. Most of the other observed properties of grain boundaries and grain size effects in metals were interpreted in terms of the amorphous grain boundary concept. In 1924, Jeffries and Archer[2] suggested the transition lattice concept of the grain boundary, and this set the stage for much of the recent thinking concerning the nature of the grain boundary.

Several excellent reviews of research on the nature of the grain boundary and grain boundary phenomena in metals have appeared in recent years. These include the works of McLean[3], Weinberg[4], and Amelinckx and Dekeyser[5], who have exhaustively reviewed the important research in this area. Gifkins[6], in addition, has reviewed research in grain boundary sliding and fracture.

It shall not be the purpose of this paper to review with the same thoroughness and detail all of the experimental results in recent years on grain boundary phenomena, but rather to rely on the existing reviews as background and then to select particular items of research (when possible, from the authors' laboratory) to indicate the trends of recent work in this field. We shall further limit the discussion to properties of grain boundaries which relate to the elevated temperature behavior of grain boundaries.

SECTION II. STRUCTURE OF THE GRAIN BOUNDARY

Dislocation Structure of Boundaries

The modern theory of the structure of the grain boundary is dominated by the concept of the transition lattice which supposes that near the boundary the atoms occupy their correct lattice positions except for a layer one or two atoms thick right at the boundary. This concept was evolved into the dislocation structure of the grain boundary by Burgers[8] in 1939, in which he described the pure "tilt" and pure "twist" grain boundaries. With this boundary structure,

a continuous transition between the two lattices is achieved by an array of equally spaced dislocations. The existence of this type of boundary has been well established in subsequent years by direct observation[7], and the dislocation model of the grain boundary has been extended to more general cases involving both tilt and twist, that is, relative rotation of the lattices about an axis lying both in and perpendicular to the grain boundary plane with various combinations of dislocations. The dislocation structure of the grain boundary has been discussed very fully by Amelinckx and Dekeyser[5], and only a brief summary will be given here to relate the structure of the boundary to experimental observations.

The pure tilt boundary, as defined by Burgers[8] is shown in Figure 1, which illustrates the symmetrical disposition of the grains about the grain boundary plane, whose normal is perpendicular to the pure edge dislocation lines and which contains dislocations of just one type. A more general tilt boundary, described by Read and Shockley[9], is shown in Figure 2. Again the grain boundary plane contains only edge dislocations and the orientations of the two grains are related by a simple rotation about an axis perpendicular to the Burgers vector and parallel to the dislocation lines. In this case, however, the boundary plane is no longer a symmetry plane for the bicrystal. The construction of a pure tilt boundary with such characteristics demands that dislocations of more than one kind be used. Two types of edge dislocations with mutually perpendicular Burgers vectors are necessary for the description.

The second type of boundary, the twist boundary, is formed by a rotation of the lattice about an axis perpendicular to the boundary plane. A dislocation structure of this type of boundary consists of two sets of parallel screw dislocations which form a square array in the grain boundary plane, as depicted in Figure 3.

Using these two basic boundaries, it is possible to construct any grain boundary by appropriate combinations of the two; and one can do this without difficulty for low angle boundaries. A difficulty is encountered, however, with high angle boundaries in that the spacing of the dislocations necessary to produce the large angular difference between the adjacent grains is such that the dislocations become unresolvable. Since dislocations have around them a disturbed region called the core, they lose their individuality when separated by less than a certain critical distance. It thus becomes necessary to develop a separate model for high angle boundaries to explain their properties.

Boundary Energy

The dislocation model of grain boundaries has been well established for boundaries of low angular misorientation both by direct observations of the dislocation density in boundaries of a given misorientation (see Figure 4) and by measurements of grain boundary interfacial energy, comparing the experimental results with the Read-Shockley equation for the energy of a grain boundary. Direct observations of etch pit densities on low angle boundaries are limited to very small angular misorientations because the resolution of the etch pit method is low. However, the dislocation model of the grain boundary at angles less than 1 degree has been closely checked by this method. Studies of the energy of grain boundaries in a number of materials have been made either by measurement of dihedral angles formed by intersectiong boundaries of tricrystals, or of the angle of the trough formed at the intersection of a grain boundary with a surface after thermal etching. Chalmers[16] and Weinberg[4] have summarized investigations in this area.

Read and Shockley have shown that the energy, E, of the boundary is given by the equation

$$E = E_0 \theta (A - \ell n \theta \qquad (1)$$

where E_o and A are constants for a given material and θ is the angular misorientation of the boundary. The equation applies to pure twist or pure tilt symmetrical boundaries. If the boundary is not symmetrical, E_o and A become variables where E_o is linearly proportional to the total density of dislocations, and A varies in a complicated way with the orientation of the grain boundary[9]. The Read and Shockley equation can be put into a universal form[3], applying to any material, by differentiating the grain boundary energy with respect to θ, which gives

$$\frac{\partial E}{\partial \theta} = E_o (A - \ell n \theta) - E_o \tag{2}$$

and since the curves of E versus θ level out at a maximum value, E_m, at some value θ_m, one sets $\partial E/\partial \theta$ equal to zero and obtains $\ell n \theta_m = A\text{-}1$ when $E = E_m$. Substituting these values into (1) and dividing the result into (1), we obtain:

$$\frac{E}{E_m} = \frac{\theta}{\theta_m} \ell n \frac{\theta}{\theta_m} \tag{3}$$

Data from a number of investigations on the energy of tilt boundaries in various materials are presented in Figure 5. The solid line indicates the theoretical curve of equation (3) fitted to the data. It is seen that there is good experimental agreement with the Read-Shockley equation up to and beyond $\theta = \theta_m$ which occurs at various misorientations for different materials, from 12 to 30°. More recent data for silver[13] show that the value of θ_m occurs at even higher values (35°) than for lead and tin, and the Read-Shockley equation holds up to θ of about 35°. Wagner and Chalmers[14] have determined relative boundary energies for <100> tilt boundaries in germanium for θ up to 46° and found no sharp discontinuity of energy values for orientation differences above that for which the Read-Shockley equation applies, and cusps in the relative energy boundary curve which might be associated with twin type interfaces are rare (See Figure 6). In silver chloride[15], when tilt boundaries with various crystallographic axes of tilt are examined, it is found that different curves are obtained for the grain boundary energy as a function of orientation difference (Figure 7).

It should be emphasized that dihedral angle measurements yield only a boundary energy relative to that of a large angle randomly oriented boundary of the same material. Thus, it is quite possible that the matching of the data with the form of the Read-Shockley equation at fairly large values of θ may be fortuitous. Absolute values of boundary energy are necessary for a true test of the equation. Gjostein and Rhines[17] have determined such values for copper and find that the equation holds for misorientations up to 5 or 6 degrees (dislocation spacings of 10 atom diameters). Above this (up to 16°) other treatments of grain boundary energy, such as van der Merwe's[18], which account for the non-Hookian elastic stress-strained behavior near the core of dislocations, agree better with the data.

Grain Boundary Melting

The grain boundary melting experiment is another which has been used to obtain some idea of whether or not the transition from the relatively low angle boundaries, which obey the Read-Shockley equation, to high angle boundaries with more or less constant grain boundary energy is delineated in any clear way. Weinberg[4] has summarized the melting behavior of grain boundaries as follows:

(1) Large angle grain boundaries melt preferentially, at essentially the same melting temperature as crystalline material.

(2) Small angle boundaries and coherent twin boundaries do not melt preferentially.

(3) A transition between melting and non-melting takes place relatively sharpely at $\theta = 12^{o}$ for tin, and $\theta = 14^{o}$ for aluminum, independent of the type of boundary.

(4) In zinc, boundaries melt preferentially in the range of θ from 27^{o} to 108^{o}. The melting transition angle depends on the orientation of the boundary plane.

(5) The melting transition is assumed to delineate small angle boundary structures conforming with the Burgers' model, and large angle structures which are irregular.

Grain Boundary Segregation

It has long been supposed that solute atoms should segregate to grain boundaries under equilibrium conditions, and various experimental confirmations of this supposition have been made. Grain boundary segregation has been detected by etching effects, by radioactive tracer techniques, by indirect evidence such as is found in bubble model experiments, and in measurement of certain grain size effects. The reason for expecting segregation at grain boundaries is that large solute atoms should be able to lower their energy by moving into regions of tension which exist in the grain boundary, while small solute atoms can lower their energy by moving into regions of compression. McLean[3] has considered the subject of grain boundary segregation observations in detail. Thomas and Chalmers[29] measured the segregation of polonium to the boundaries in bicrystals of lead as a function of relative orientation of the grains and obtained the results shown in Figure 8. The results are similar to those mentioned for grain boundary melting in that a sharp transition in the relative concentration of the solute element in the grain boundary occurs at misorientations greater than 15^{o}, but is a relatively minor effect at angles below 15^{o}. Thus, solute segregation would be expected to have a marked effect on grain boundary migration and hence should have in turn an effect on grain boundary sliding and fracture in creep.

Large Angle Grain Boundaries

Several models exist for large angle grain boundaries which attempt to show a relationship to the observed properties of these boundaries. These include the models of Kê[10], Mott[11], and Freidel, Cullity and Crussard[12]. In considering these models of large angle grain boundaries, it may be significant to remember that two of them, Kê's and Mott's models, were conceived to predict the behavior of grain boundaries under dynamic conditions, that is, during strain, while the model of Freidel et al has been compared against grain boundary properties under static conditions. There may be certain changes in the structure of the grain boundary under stress, and particularly during deformation, and it would not be expected necessarily that a model which is successful in predicting properties during deformation is similarly successful in predicting static properties of the grain boundary.

The Mott "island" model for large angle grain boundaries was advanced to explain grain boundary sliding and migration, and the temperature dependence of the velocity of these phenomena. Mott considers that a grain boundary consists of regions or "islands" where a good matching of the atomic lattices of the two grains exists, separated by regions of poor matching. The regions of good match are considered to be more or less uniformly sized areas

spaced regularly on a plane grain boundary. The transition from good to bad regions is rather well defined instead of showing a continuous gradation. It was considered that the islands of good-fit offered little resistance to sliding, whereas the bad-fit regions resisted shear; thus, the action of sliding necessitated a thermal agitation in the bad-fit region around the islands in order for the resistance to shear to decrease locally. This would explain the viscous nature of grain boundary sliding, and is related to Kê's observation that the rate of sliding, when extrapolated to the melting point of the metal, corresponded to that which might be expected for crystals separated by a layer of liquid a few atoms thick.

Mott obtained an expression for the free energy of disordering of the atoms surrounding an island of good fit by considering that at the melting temperature, T_m, the free energy of melting is zero, and at absolute zero it is nL, where L is the latent heat of melting and n is the number of atoms surrounding an island of good fit. The free energy of melting at intermediate temperatures is assumed to vary in a linear fashion with temperature between these two points. On application of a shear stress, σ, to a boundary, disordering results from slip over a distance b corresponding to the atomic diameter of the group of n atoms, and the work done by the stress is σnb^3. The following expression is obtained for the velocity, ν, of grain boundary sliding as a function of temperature:

$$\nu = \frac{2\nu b^4 \sigma n}{KT} e^{\frac{nL}{RT_m}} e^{-\frac{nL}{RT}} \qquad (4)$$

where ν is the frequency of atomic vibration and K is Boltzmann's constant.

Kê[11] was one of the first to observe that the activation energies for grain boundary sliding of metals, for which the appropriate data were available, were nearly equal to the activation energies for self-diffusion. He reasoned that the grain boundary consisted of an assembly of the same types of lattice faults which were responsible for grain diffusion, namely, lattice vacancies, or disordered groups. He showed that the rate of sliding was governed by an equation of the form

$$\nu = A \frac{\sigma}{KT} e^{-\frac{Q}{RT}} \qquad (5)$$

where A is constant and Q is the activation energy for sliding.

This result was criticized by Mott on the basis of experimentally determined values for the activation energy for sliding, and he was able to show that the constant in the above equation according to Ke's reasoning would be 6×10^{-5}, whereas the measured value was of the order of unity. A distinction between Kê's formula for grain boundary sliding and Mott's is that Mott's formula contains a figure for the size of the islands of misfit which offers a possible comparison between grain boundaries of differing orientation.

The Freidel, Cullity and Crussard[12] model of the grain boundary makes possible a calculation of grain boundary energy for particular orientation differences between grains. The technique involves assigning bond energies from an assumed law relating the energy of the bond to the distance of separation of the atoms. Nearest and next neighbors were considered. The energy total was worked out for special orientations and it was assumed that the atoms would occupy their normal lattice sites unless it was found that when an atom was removed from the aggregate, that the one extended bond resulting has less energy than the two short

ones which existed before. As in the Kê equation, they assumed that the free energy of bonding vanishes at the melting point and that a linear extrapolation of the grain boundary free energy could be used.

SECTION III. CREEP AND GRAIN BOUNDARY SLIDING

Grain boundary sliding experiments have been reviewed numerous times in the past years, the most recent articles being those of Gifkins[6], Weinberg[4], McLean[3], and Grant and Chaudhuri[24]. Because the investigations of grain boundary sliding have been reviewed often and well elsewhere, in this section we shall treat the recent observations of grain boundary sliding, primarily from the authors' laboratory, and simply show how these relationships relate to the measurements of others.

Sliding in Polycrystalline Metals and Alloys

The general features of grain boundary sliding are well known. Displacement takes place on grain boundaries tested at elevated temperatures in amounts which vary widely with temperature and stress. In general, high temperatures and low stresses favor large offsets on the grain boundary; but as will be shown later, this is not always true. The sliding often produces a region of heavy deformation in the grain opposite the sliding boundary which we term a fold, and is also often accompanied by extensive migration of the grain boundaries. Intercrystalline cracking is often associated with the grain boundary sliding, but again there are notable exceptions to this; in particular, in high purity aluminum, grain boundary fractures are not observed.

Quantitative measurements of grain boundary sliding from the displacement of reference scratches across grain boundaries, or from surface offsets during creep, have been made by numerous investigators, and equations for the translation of these data into values of the contribution of the grain boundary to the total extension of the specimen have been made by McLean[19], Fazan, Sherby and Dorn[20], and Brunner and Grant[21]. The technique of calculating the contribution of internal grain boundaries to elongation from measurements of grain shape following creep deformation have been developed by Rachinger[22]. A brief description of one of the methods of Brunner and Grant is as follows: assume a long, narrow strip on the surface of the specimen along the axis between two gauge lines. On this narrow strip, grain boundaries can be approximated by straight lines intersecting the strip at arbitrary angles. Grain boundary sliding causes the displacement of the transverse marker lines at the grain boundary. The axial component of the grain boundary displacement is called Δu_s. The amount of displacement varies widely from grain to grain boundary. Δu_s has to be averaged statistically to give a good quantitative value. From 50 to 100 determinations of Δu_s are ordinarily considered necessary to give good results. If the grain size is sufficiently small, it is only necessary to sum these contributions over the gauge length, as indicated by the following equation:

$$E_{GB} = \frac{1}{\ell_0} \sum_{\text{length}} \Delta u_s \qquad (6)$$

If, however, the grain size is large, this operation must be repated numerous times and the average of the values of E_{GB} taken. In this equation, E_{GB} is the grain boundary contribution to total elongation and ℓ_0 is the distance between gauge markers before the test starts. The total elongation, E_T, and the relationship between total elongation, grain boundary elongation and grain elongation are given by

$$E_T = \frac{\ell - \ell_0}{\ell_0} \qquad (7)$$

$$E_T = E_{GB} + E_G \quad (8)$$

where E_G is the contribution of the grains to total elongation and ℓ is the gauge length at any given time.

Before considering the total contribution of all the grain boundaries in a polycrystalline specimen to elongation, let us examine the nature of sliding on single grain boundaries, as shown by Chang and Grant[23] for pure aluminum. It is seen in Figure 9 that a coarse grained polycrystalline specimen (which yielded the usual smooth total creep curve) displays grossly non-homogeneous deformation of individual consecutive grain boundaries in the gauge length. The grain boundary displacement curves are characterized by alternate periods of relatively rapid and very slow creep. Chang and Grant related this behavior to alternate periods of grain boundary sliding (resulting in strain hardening) and periods of recovery (associated with grain boundary migration).

The variation of E_{GB} versus total elongation for all grain boundaries of Al-1.9% Mg specimens is indicated by the curves of Figure 10. In this case, because the tests were performed at a constant strain rate, the abscissa also corresponds to a linear time scale. The variation of E_{GB} with time for the total specimen gives a smooth curve which is quite similar to the overall creep curve in its character.

Brunner and Grant's[26] results for E_{GB}/E_T as a function of temperature for aluminum, aluminum-2% magnesium, and aluminum-5% magnesium (solid solution alloys at test temperature) are shown in Figure 11. These are data from specimens strained in creep at a minimum creep rate of 2.7 percent/hour. All the alloys show increasing grain boundary sliding with increasing temperature in the lower temperature range, which passes through a maximum, and thereafter decreases slightly with increasing temperature. The position of this maximum is not well defined and apparently varies with alloy content in an as yet undetermined fashion. The maximum values of E_{GB}/E_T are rather similar for the three alloys, falling between 13 and 15 percent.

Figure 12 shows the dependence of E_{GB}/E_T on stress for the alloys tested by Brunner and Grant, and for McLean's data on pure aluminum. It has been indicated by Harper, Shepard and Dorn[27] that the ratio of grain boundary sliding to total strain should be independent of temperature, but dependent on stress. Since the stress for a value of E_{GB}/E_T of 10 percent is not single valued for pure aluminum, the data cast doubt on this conclusion. McLean's[19] data on this plot fall at somewhat higher stresses than the data of Brunner and Grant for pure aluminum; however, if McLean's[28] values are corrected for an error which Brunner and Grant detected in their measuring technique, the values fall very well in line with those of Brunner and Grant.

Regarding grain size, the first and most interesting observation was to the effect that coarse slip bands are observed, with a minimum of grain boundary sliding, as long as the grain diameter is at least twice the minimum slip band spacing[44] at any given stress. Fine slip, as observed by a number of investigators, of course takes place at all deformation stresses.

The second observation is that the effect of grain size on grain boundary sliding is such that the larger the grain size the greater the grain boundary displacement on the average grain boundary. This is shown in Figure 13 for the results of Brunner and Grant[26], and Mullendore and Grant[25] for aluminum-magnesium. A semi-logarithmic plot is used in this case because of the wide range of grain sizes; however, since the slope of the experimental line is 1, a linear

relationship would be observed on a rectilinear plot. McLean and Gifkins indicate the same sort of trend for data of various investigators in pure aluminum[30], see Figure 14. These data do not, however, represent an increase in the ratio of E_{GB}/E_T as a function of grain size. The dotted line in this figure indicates the values of average grain boundary sliding displacement necessary to give a value of E_{GB} equal to E_T, in other words, E_{GB}/E_T of 100 percent. The line representing constant E_{GB}/E_T values of 50 percent would be a straight line extending from the origin with the lower slope, and zero percent contribution to elongation would be, of course, a straight line of zero slope. Since the experimental points would intersect these radii of constant E_{GB}/E_T at decreasing values of E_{GB}/E_T with increasing grain size, the data indicate a decreasing contribution of the grain boundary to elongation with increasing grain size. Perhaps the differing purity of the aluminum used for the values in this figure has an important effect on the data, for Brunner and Grant[26] did not observe the same variation of E_{GB}/E_T with grain size. Their data for aluminum-2% magnesium is indicated in Figure 15 by a plot of E_{GB}/E_T versus E_T. At a value of E_T of 10 percent, it can be seen that the data for grain sizes from 25 microns to 460 microns for aluminum - 1.9% magnesium all fall in the range between 8 and 11 percent for E_{GB}/E_T, indicating an approximate constancy of this value with grain size.

The effect of orientation of the grain boundary with respect to the tensile axis on polycrystals of aluminum-magnesium has been investigated by Mullendore and Grant[25], who find, in agreement with others[20], that the orientation of the grain boundary with respect to the tensile axis has no systematic effect on the observed grain boundary sliding magnitude. This is shown in Figure 16, where magnitude of sliding of individual grain boundaries in a single polycrystal are plotted versus the resolved shear stress on the grain boundary. Often grain boundaries with very low resolved shear stress give large amounts of sliding, and it was even observed that two grain boundaries gave negative values of sliding, indicating sliding in a direction opposite to that which would produce elongation of the specimen.

There was, however, an indication that the relative orientation of the grains across their mutual grain boundary did have an important effect on the observed magnitude of sliding. This is indicated in Figure 17 where grain boundary displacements are plotted versus an orientation factor $\cos\theta s$ in ω, where θ is the angle between maximum resolved shear stress slip directions in the two grains, and ω is the angle measured on the grain boundary between the intersection of the slip planes of the two grains with the grain boundary[25].

One of the most controversial observations of grain boundary sliding has been that of Rachinger[22], who obtained a figure for the contribution of interior grain boundaries to elongation of polycrystalline specimens by measurements before and after creep of the ratio of the length to width of grains. In principle, this gives an indication of the amount of the elongation contributed by grain deformation, and the grain boundary sliding contribution can be obtained by difference from the measured total elongation. He obtained values of E_{GB}/E_T as high as 95 percent; his results have not yet been satisfactorily explained by investigators working strictly on surface measurements. There is, of course, the possibility that preferred direction of grain boundary migration with respect to the tensile axis could maintain equiaxed grains, even in the presence of considerable grain elongation, but this has not yet been established experimentally.

Recent studies of grain boundary sliding in aluminum-3% copper, two-phase alloys by Ishida[33] have shown the remarkable differences in grain boundary sliding produced by variations in the size and distribution of second phase in the material. Four different heat treatments of the alloy were used to produce the structures shown in Figure 18. Following solution treatment at 900°F, the aging treatments were as follows;

1. Heat treatment Q5 - water quenched, aged at 500°F for 72 hours

2. Heat treatment F5 - furnace cooled to 500°F, aged 72 hours

3. Heat treatment Q7 - water quenched, aged at 700°F for 38 hours, stabilized at 500°F for 72 hours

4. Heat treatment F7 - furnace cooled to 700°F, aged 38 hours, stabilized 72 hours at 500°F.

All tests were performed at 500°F over a range of stresses from 2000 to 6000 psi. Figure 19 shows representative creep curves for these materials; Figure 20 shows grain boundary contribution to total elongation versus total elongation for the same materials.

Table I shows the variation in performance of the alloys for the various heat treatments.

TABLE I

Data on Creep Performance for Four Heat Treatments

Heat Treatment	Decreasing Particle Size and Interparticle Spacing	Increasing Creep Resistance	E_{GB}/E_T %	Increasing Ductility
F-7	↓	↓	0.2-0.6	↑
Q-7			1 - 3	
F-5			12 - 23	
Q-5			13 - 25	

It is interesting and expected that creep resistance increases with decreasing particle size of precipitate and decreasing interparticle spacing, while total ductility increases in the reverse direction. It was unexpected, however, to find that the ratio E_{GB}/E_T increased with increasing creep resistance. While the grain boundary creep rate could not be compared directly for all four heat treatments because of the large differences in strength, nevertheless it was possible to observe that the grain boundary creep rate at a given stress increased in the order Q5 to F7, parelleling the trend of increasing total ductility.

Bicrystal Sliding Experiments

Bicrystal sliding experiments fall into two groups, categorized according to the type of specimen used. One group involves the use of tensile specimens with an inclined grain boundary so that one obtains considerable grain deformation along with grain boundary sliding. The second type of test is that in which one attempts to subject the grain boundary to pure shear and to avoid, to whatever extent possible, deformation in the grains.

Gifkins[6] has summarized the forms of grain boundary sliding versus time curves which have been observed in various investigations. These are shown in Figure 21. The general curve observed is similar to the normal creep curve[35] and is indicated by curve X (see also Figures 10 and 20). Tension-type specimens have been shown by Rhines, Bond and Kissel[34] to produce curves of the type Y_1 or Y_2 with an incubation period for sliding, and a cyclical

variation in sliding rate. This has also been occasionally observed in pure shear type specimens. Types Z_1 and Z_2 have also been observed in shear specimens[35]. In addition to the varying observations on the shape of the sliding curve, conflicting results have also been reported on other aspects of the bicrystal sliding experiments. In particular, the presence or or absence of grain boundary migration, the existence of subgrain formation adjacent to sliding boundaries, the nature of the zone of sliding, and whether or not sliding actually takes place on the grain boundary. Many of these conflicting results may be due in part to differences in purity of the materials investigated.

An area of basic agreement between investigators is that grain boundary sliding is profoundly influenced by relative orientation of the crystals making up the boundary. Rhines, Bond and Kissel[34] find that the magnitude of grain boundary sliding is a function of misorientations for randomly oriented bicrystals. Tung and Maddin[35], who systematically varied the relative orientation of their bicrystals found that the activation energy for sliding varied from 8.5 to 39.5 kilocalories per mole as angular misorientation changed from 20 to 88°. These data are shown in Figure 22. Similarly Adsit and Brittain[36] have observed a marked dependence of grain boundary sliding on angular misorientation in zinc bicrystals. Their results indicate that the variation in sliding they note cannot be attributed to variations in grain boundary migration, as has been indicated by Couling and Roberts[37].

Recent studies of grain boundary sliding in aluminum-2% magnesium bicrystals[25], all tested at 500°F, indicate that the magnitude of grain boundary sliding can be rationalized on the basis of continuity of shear requirements. This is thought to constitute one important factor in the variation of grain boundary sliding with relative orientation of grains, although it is probably not the only orientation dependent factor, for it does not explain the orientation dependence of the activation energy for sliding[35]. It is clear from the observations of Ogilvie[38] that in a polycrystalline aggregate the relative orientation of a large fraction of the grains across their mutual grain boundaries is such that slip can propagate readily from one grain into the adjacent grain, even in the absence of grain boundary sliding. At elevated temperatures, where grain boundary sliding presents another degree of freedom, it is even more likely that most grain boundaries will be penetrated by dislocations from the grains. When a dislocation is forced into the vicinity of the grain boundary by the applied stress, it must, in order to maintain the continuity of shear, cause the activation of at least two slip systems in the opposite grain. A component of unresolved shear remains from this operation which can appear as sliding on the grain boundary.

A two-dimensional representation of slip induced sliding is shown in Figure 23. In the schematic, slip in the top grain which crosses the grain boundary into the bottom grain, produces a shear offset on the grain boundary as indicated by the displacement of the dotted reference line on the left hand side of the specimen. It should be noted that the reference line on the right hand side of the specimen suffers no offset at the grain boundary. If one now imagines a whole series of parallel slip planes to operate across the specimen, it can be seen that the displacement of the reference line at the grain boundary on the far right hand side of the specimen would still be zero, and that the displacement as one moves across the grain boundary to the left would increase to a maximum on the far left hand side. In the three-dimensional case, slip on one plane in one grain would have to be accompanied in general by grain boundary sliding, and, in the absence of grain rotation, by slip on two planes in the second grain. The magnitude of grain boundary sliding would still go to zero at some point on the circumference of the specimen, and in general, this would be at one corner of the specimen. The grain boundary displacement would rise to a maximum at the opposite corner of the specimen. This, of course, assumes that there is no contribution to grain boundary displacement

by independent grain boundary sliding. This is substantially the behavior noted in the bicrystal tests performed, as shown in Figure 24. Assuming uniform distribution of slip across the diameter of the specimen, one would expect a linear increase in grain boundary displacement in going from the low corner to the high. The observed grain boundary displacements depart to a small extent from this behavior, but this is not unexpected. The ideal case assumes perfectly uniform slip across the diameter of both grains, and does not allow for changes which would result from closeness to an exterior surface, or from the operation of additional slip systems in different parts of the specimen. In addition, the experimentally determined grain boundary displacements do not go to zero at a corner, but simply to a minimum value, indicating a contribution by independent grain boundary sliding. An approximate relationship between sliding and orientation factors based on this model indicates that the change of grain boundary displacement with distance along the boundary should, at a given stress, strain, and temperature vary as $\cos\omega\ (1 - \tan\beta/\tan\alpha)$ where ω is the angle between intersections of the primary slip planes with the grain boundary, α is the angle between the primary slip direction in one grain and the normal to the boundary, and β is the angle between the primary slip direction in the other grain in the normal to the grain boundary. The experimental data based on this relationship are shown in Figure 25 and are seen to agree quite well with the model.

This model, when applied to polycrystalline materials, would predict that in the absence of secondary effects, E_{GB}/E_T would be a constant with changing E_T in a given test, as has been observed by McLean[19]. It further predicts that E_{GB}/E_T would be a constant for varying grain size, or that the average grain boundary displacement in a polycrystal would vary linearly with increase of grain size. This has been shown to be true[26]; see Figure 13. It is felt that the temperature variation of grain boundary sliding might then be explained on the basis of the tendency of dislocations to penetrate the grain boundary, and this would in part depend on the shear strength of the grain boundary.

Crussard and Freidel[39] presented a model for the driving force for grain boundary migration which, if applied to sliding, is rather similar to the above model and should produce the same results. They consider that when a dislocation is forced into a grain boundary along part of its length that, because the boundary is unable to stand large tangential stresses, the dislocation line will spread by diffusion into a larger zone, which can be formally described as a splitting into several dislocations with small Burgers' vectors. The sum of these partial Burgers' vectors is equal to the Burgers' vector of the original dislocation, and have a tendency to be almost parallel to the boundary. If indeed these partial grain boundary dislocations have Burgers' vectors essentially parallel to the boundary, then Crussard and Freidel must assume that the component of shear perpendicular to the boundary has been transmitted into the opposite grain. The spreading of the grain boundary dislocation is then to be associated with grain boundary sliding.

Rhines[40] has interpreted his bicrystal sliding results in an entirely different way. He concluded that observed grain boundary displacements do not represent sliding on the grain boundary plane at all, but rather represent crystal slip in a zone close to the grain boundary. The alternate periods of rapid and slow grain boundary sliding which he observed are attributed to alternate periods of work hardening and recovery in this grain boundary zone. The recovery process which he calls upon is polygonization, and it is this process which is thought to be rate controlling.

McLean[41] offers another explanation for the relationship between grain shear and grain boundary shear. He supposed that grain boundary sliding occurs to the extent necessary to

accommodate the lattice bending, which occurs prior to polygonization adjacent to the grain boundary. This polygonization of course is dependent on the amount of dislocation pile up at the grain boundary. The implication is that this in turn is related to the misorientation of the shearing element in the two grains.

Gifkins[6] has proposed a model for grain boundary sliding which is designed to allow for the effect on grain boundary sliding of dislocations reaching the grain boundary, and to allow interpretation of the temperature and stress effects. He suggests that the number of dislocations which reach the vicinity of the boundary is dependent on the subgrain size adjacent to the grain boundary. Assuming the subgrain walls to be effective barriers to slip, the number of piled up dislocations on the grain boundary for a given strain would be proportional to the subgrain size. These dislocations then affect the grain boundary sliding through their effect on the vacancy concentration at the boundary (via climb), and by their effect on the migration of the grain boundary.

It is believed that experimental results of different investigators on grain boundary sliding are sufficiently contradictory that it is not possible at this time to conclude with any certainty which model of grain boundary sliding is more exact. Carefully controlled experiments are necessary, which are specifically designed to test out the various models.

SECTIONS IV AND V. GRAIN BOUNDARY RECOVERY PROCESSES

In the study of grain boundary deformation and fracture processes, one can never completely separate the characteristics of grain boundary sliding from the effects of grain boundary migration and subgrain formation. In deformation studies of polycrystalline materials, one rarely, if ever, observes grain boundary sliding occurring without some grain boundary migration taking place at the same time. It is quite probable that grain boundary sliding cannot continue unless there is a certain amount of migration. When grain boundary migration is restricted, either by solid solution alloying, impurity effects, or a second phase existing on grain boundaries, grain boundary fractures often occur at rather small amounts of deformation.

Several causes of boundary migration have been listed by Grant and Chaudhuri[24]. These are summarized as follows:

1. Grain boundary sliding causes departures from equilibrium at grain boundary junctures. The non-equilibrium configuration of the grain boundary juncture which results from an offset on the sliding grain boundary gives an excess surface free energy which constitutes a driving force for migration.

2. Interaction of slip with grain boundaries during creep results in the formation of subgrains along the grain boundary. The difference in intensity of the dislocation structure on the two sides of the boundary creates an unbalanced pull and causes the grain boundary to migrate in a more or less uniform manner to one side or the other of its original position.

3. Grain boundary migration in creep is also affected by the same factors which control grain boundary growth, namely, the tendency to decrease excess surface free energy. In addition to these, it is known that small angle boundary migration can be stress induced. This has been demonstrated by Washburn and Parker[42]. In this case, the boundary migration results in shear and thus occurs in a direction which allows the applied stress to do work on the specimen. Brunner and Grant have demonstrated that this kind of migration of subgrain boundaries occurs during grain boundary sliding.

It is to be expected that alloying will markedly influence the rate of grain boundary migration. It will have its effect both by changing the energy of the grain boundary, which alters the driving force for minimization of surface free energy, and by affecting diffusion rates. Figure 26 shows the effect of alloying lead with tin on the mobility of both random grain boundaries and specially oriented grain boundaries. This work[43] was done on bicrystals of lead and lead-tin alloys which contained a lineage structure which gave the driving force for migration. An addition of 0.006 weight percent tin was found to reduce the rate of grain boundary migration more than a thousand-fold for random grain boundaries. Specially oriented low energy grain boundaries were less strongly affected by the alloying additions.

Subgrain formation has also been shown to be intimately associated with the process of grain boundary sliding. During sliding, a zone of intense polygonization almost invariably occurs along the sliding grain boundary[31], as shown in Figure 27. The role of this layer of subgrains along the grain boundary in relation to sliding has been variously described in the models for grain boundary sliding discussed in the previous section; certainly it must have an important effect of influencing the nature and degree of grain boundary migration.

In grain boundary sliding studies of aluminum and aluminum-magnesium alloys, it is found that the grain boundary becomes roughened during the course of creep and that this roughening of the grain boundary is related to the subgrain structure along the boundary. Figure 28 shows a micrograph of the serrated structure of the grain boundary in aluminum - 1.9% magnesium. Because of the relationship of this structure with the formation of intercrystalline voids during creep, it has been studies in some detail by Mullendore and Grant[32]. Measurements of the wave length of the grain boundary serrations in aluminum-magnesium alloys reveals the dependence on alloy content, stress, and temperature as indicated in Figure 29. The factor which appears to have the greatest effect on the wave length of the serrations is the stress. The higher the stress the smaller the serration. It has been found that the serrations represent intersections of subgrain boundaries with the grain boundary.

To reveal the nature of the serrated structure of the grain boundary, in three dimensions, sequential pictures were taken of a grain boundary as successive layers of the surface of the specimen were removed by electropolishing. Figure 30 shows the topographical map of the grain boundary which was built up in this way, and reveals that the serrations in two dimensions actually represent elongated ledges on the grain boundary when viewed in three dimensions. This structure of the grain boundary of course has a marked influence on the behavior of the boundary during subsequent sliding; and, as will be shown in the succeeding section, it also strongly influences the nature of fracture in these materials.

SECTION VI. VOID FORMATION AND INTERCRYSTALLINE FAILURE IN CREEP

The volume of observations on the nature of intercrystalline fracture and void formation during creep has, in recent years, reached massive proportions; and a number of fundamental treatments of the mechanisms of crack initiation and growth have appeared in the literature. In brief, two schools of thought exist; those who regard the formation and growth of cracks strictly as the result of stress concentrations exceeding the cohesive strength of the material, and those who prefer vacancy condensation on existing nuclei as the growth mechanism. In addition to examination of these two viewpoints, one must also consider the question of whether or not any or all intercrystalline cracks result from void formation. Because the general characteristics of intercrystalline failure have been reviewed adequately elsewhere[24], a summary of observations is sufficient for our purposes.

Almost all metals and alloys, at temperatures low relative to their melting point, display ductile transcrystalline failures; at some higher temperature they usually undergo a transition to intercrystalline failure provided that the strain rates are suitable. The onset of intercrystalline cracking is in general associated with decreased strength of the metals, as measured by rupture life or minimum creep rate, the onset of grain boundary sliding, and usually a decrease in elongation at rupture of the specimen. The transition from transgranular to intergranular failure is a function not only of temperature, but of stress or strain rate, grain size, and metallurgical structure, including purity. Figure 31 is a plot of rupture life versus stress for a vacuum melted 80Ni - 20 Cr alloy showing the transition to intercrystalline failure (high stress discontinuities) as a function of stress and temperature. The numbers on the diagram indicate the reduction of area values at failure. In the vicinity of the transition the ductility starts to decrease and accelerates with decreasing strain rate. Figure 32 compares the reduction of area values at three temperatures as a function of rupture time for the same 80Ni - 20 Cr alloy, one air melted (3A) and one vacuum melted (2V). The very much lower ductility of the air melted alloy illustrates the profound effect which purity and cleanliness have on fracture characteristics[45].

Some metals do not undergo intercrystalline cracking (high purity aluminum) or intercrystalline failure (although intercrystalline cracks may be present in significant amount). In other cases, for example 2S aluminum and high purity solid solution alloys, such as aluminum-magnesium, intercrystalline cracking disappears at high temperatures and long rupture times (very slow strain rates).

A typical example of a material which failed by intercrystalline cracking at high temperatures[45] is shown in Figure 33. The failure results from the joining of numerous grain boundary cracks across the width of the specimen. Although the total fracture is approximately normal to the stress axis, it can be seen that the individual facets of the fracture surface are at various angles to the stress axis. It is also obvious that in spite of the brittle appearance of the fracture, considerable elongation (85%) prior to failure has taken place in the specimen. Chang and Grant[46] have categorized intercrystalline cracks as shown in Figure 34. It is interesting to note that types (a) and (b) show intercrystalline cracks resulting from sliding on an adjacent boundary, but occurring on boundaries which themselves do not slide, while type (c) shows the formation of intercrystalline cracks on sliding boundaries. More complex intercrystalline crack configurations were noted by Chang and Grant, and two examples are shown in Figure 35. These, however, are merely combinations of variations of the three types indicated in the previous figure.

The formation of voids along grain boundaries during elevated temperature deformation occurs in many metals and alloys and the relationship of these voids to intercrystalline failure has been the subject of many investigations. Among the first observations of intercrystalline cavitation were those of Jenkins, Bucknall and Jenkinson[47], working with copper base alloys. The first systematic study of the phenomenon was that of Greenwood[48], and Greenwood, Miller and Suiter[49], who observed the formation of numerous small voids at grain boundaries in brass, copper and magnesium. They related the incidence of cavitation as temperature or strain rate was varied to the start of grain boundary sliding and to a drop of ductility. A vacancy precipitation mechanism was proposed as a possible origin for the voids. Ultimate intercrystalline failure was though to result from growth of the voids to the point where they coalesced into a continuous crack. Subsequent to the work of Greenwood et al, many investigators had studied void formation. The work has been carefully reviewed by Gifkins[6]. Davis and Dennison[50] have also given an excellent review of current theories of intergranular fracture processes.

Relation of Void Formation to Intercrystalline Failure

In discussing the relationship of voids and intercrystalline cracks, Gifkins[6] has found it useful to distinguish between the type of wedge-shaped crack often associated with triple point cracking, and the small isolated rounded cavities in the grain boundary by terming the first a "w" cavity, and the latter an "r" cavity. Greenwood, Miller and Suiter[49] working in copper and alpha brass, observed "r" type cavities distributed along grain boundaries usually transverse to the applied stress, with a spacing of as little as 1 micron at lower temperatures. Their observations indicated that the voids linked up to form continuous intercrystallined cracks. The "r" type cavities were spaced farther apart on the boundaries at higher temperatures of testing.

Other pertinent observations are that the incidence of cavity formation coincided with the beginning of grain boundary sliding, and that cavity formation was associated with a decrease in ductility, indicating that this process was closely associated with all intercrystalline cracking in creep. McLean[51], in examining the fracture characteristics of several commercial high temperature alloys, found that the type of cavity or crack observed was dependent upon stress and temperature. He found that at relatively high stresses and low temperatures "w" type cracks were predominant; at intermediate temperatures and stresses, mixtures of "w" and "r" types were observed; and at still lower stresses and higher temperatures only "r" types cracks formed. In aluminum-magnesium alloys, Mullendore and Grant observed a variety of grain boundary cavities[31] and the observations correspond closely to those of McLean's in commercial alloys. Examples of the cavities are shown in Figures 36 and 37. Wedge-type cracks were observed in aluminum-5% magnesium tested at 500°F, and at a stress which would give a rupture life of 0.53 hour. Figure 36 (a) shows an example of this type of crack which has been impregnated with lucite and mechanically polished (not etched) to preserve the details of the crack edge. Upon light electropolishing of this same structure, view (b), numerous small voids along the grain boundaries which had been smeared over are revealed. Thus it appears that the wedge-type crack may be formed by joining of these small voids along the grain boundary. It is not, however, clear whether this is a case of growth of the voids until they touch one another, or whether the sections of grain boundary separating the voids shear off to create the crack. With the same alloy, tested at the same temperature but at lower stresses, there was observed a decrease in the numbers of voids and fewer "w" type cracks. The large cavities which do form are rounded and give the appearance of having been formed by the joining of small voids (Figure 37a). Again it is not known whether the joining of the voids took place by shear or by vacancy growth of voids from the appearance of the photomicrograph. Aluminum - 1.9% magnesium showed less tendency toward "w" type cracks. Figure 37b shows an example of the specimen tested at 700°F with a 0.25 hour rupture life. Well separated voids are observed on the grain boundaries, and, although the voids are fairly large, there was no tendency for voids to join to form intercrystalline "w" type cracks. At still higher tester temperatures, the amount of voids formation decreased further. At testing temperatures of 700° and above, all fractures in this alloy were transcrystalline in nature. At high temperatures and low stresses, it was often observed that the grain boundaries would migrate completely away from the voids (which were few in number) and hence one would observe in the ruptured specimens voids existing within the grains. In high purity aluminum, voids were not observed either at grain boundaries or in grains, but grain boundary migration was very extensive.

One can conclude from the previous observations that under high temperature - low stress conditions, voids can form without leading to intercrystalline failure. At somewhat lower temperatures and higher stresses, voids are sufficiently numerous on the grain boundaries to join either by shear or growth processes into "w" type cracks, which have nearly straight

sides. In commercial alloys, wedge-type cracks are observed without any indication of void formation at relatively low temperatures and still higher stresses. It thus appears that the same conditions which favor the formation of brittle wedge-type cracks also favor the formation of voids, but, since these same conditions undoubtedly also favor the rapid propagation of "w" type cracks, it is possible for a long brittle crack to grow from the first formed crack nucleus, thus promoting failure before many voids are formed.

Origin of Voids

Voids have been observed to occur at triple points, along apparently straight grain boundaries[49], at the intersection of sub-boundaries and grain boundaries[32], and at precipitates along grain boundaries[52]. Although Greenwood et al[49] observed a preponderence of void formation along transverse boundaries, Gifkins[6] in examining the work of various investigators in the field has found that they are observed on grain boundaries at all angles to the stress axis (see also Figures 36b and 37a), except those which are parallel to it. In compression tests, voids are also observed on the longitudinal boundaries. There is an indication that the relative orientation of grains constituting a boundary is important to the formation of voids since in some instances voids were absent on a particular grain boundary only along that part of the boundary where one of the grains was twinned.

Gifkins[53] and Chen and Machlin[54] have developed models for void initiation at grain boundaries based on the experimental observation that the spacing of voids along grain boundaries is about the same as that of optically visible slip, in some cases. Gifkin's model for the opening of a void on a grain boundary is shown in Figure 38. Slip crossing the sliding grain boundary creates a jog in the grain boundary which, due to sliding and the action of the stress field of the piled up dislocations, causes a loss of cohesion at the jog. Chen and Machlin add that the tensile stresses across the jog, which result from boundary sliding, should aid the formation of the jog, and McLean[3] has indicated that this stress by itself may be sufficient to open the cavity. Gifkins pointed out that the operation of the mechanism may be precluded by grain boundary migration, and relates the orientation dependence for void formation on sliding boundaries to differences in the stress at the jog from piled up dislocations in one grain. Another orientation factor involved is the direction of the shear with respect to the jog. If, in Figure 38, the shear direction were reversed, compressive stresses would develop along the jog and there would not be the same tendency for opening.

In aluminum-magnesium alloys where voids still form under conditions of temperature and stress where discrete slip bands are no longer visible and where even at low temperatures the migration rate of the boundary is probably sufficient to prevent the formation of voids by Gifkins' mechanism, it appears that voids nucleate in a somewhat different manner. Voids are associated with the grain boundary serration peaks noted in Figure 28. Figure 39 shows a grain boundary which is serrated and contains voids on one side of the grain boundary associated with the serration peaks[31]. These peaks, as mentioned before, represent the intersection of a subgrain boundary with the grain boundary. The location of the voids to one side of the grain boundary was established by sectioning the grain boundary at a low angle and electropolishing down to it, at the same time noting the location of the voids. The voids were found to occur to one side of the boundary, and always on the same side. These voids probably do touch the grain boundary, but this was difficult to establish with certainty. It is felt that the configuration of the serrated grain boundary and subgrain boundary junction is a modification of the grain boundary triple point configuration and hence one may apply the Zener mechanism for intercrystalline cracking at a triple point to this situation.

Weaver[52], studying Nimonic alloys, found that voids were often associated with carbide precipitates in the grain boundary. It would appear that this nucleation site for voids as well as that of the serrated grain boundary, the jogged grain boundary, and the grain boundary triple point site, all represent point of discontinuities in grain boundary sliding and slip in the grains, either in direction or in magnitude of the shear. Thus, in each case stress concentrations develop which may exceed the cohesive strength of the material. In the case of the serrated grain boundary, the rupture occurs on a subgrain boundary at the intersection with the grain boundary; and in all other cases the rupture occurs on the grain boundary.

We must conclude that if the foregoing viewpoint is correct, the sites of voids also represent points of low cohesive strength of the material since similar discontinuities in shear also occur within the grains. The lower cohesive strength of the grain boundaries or the subgrain boundaries may be affected by the segregation of impurities or alloying elements at these points. Bleakney's[55] experiments with copper indicate that the segregation of impurities such as oxygen may cause loss of cohesion at grain boundaries at certain temperatures. Similarly, Resnick and Siegle[56] found that the tendency towards cavitation in alpha brass was dependent on oxygen content. The impurity effect may be two-fold in that it affects grain boundary migration rates as well as the cohesive strength of the boundary. Ivanova and Oding[57] believe that void formation occurs on pre-existing micropores that are present in materials both in the cast form and the completely recrystallized state.

The site of formation of void nuclei is extremely important to the theory based on the growth of voids by vacancy condensation. It is important from the standpoint of the conditions for supply of vacancies to the nucleus for growth, as well as from the standpoint that without a critical size nucleus, precipitation of vacancies will not occur. Several investigators have shown on a theoretical basis that a very large supersaturation of vacancies is necessary to form a stable cluster, hence it is unlikely that void formation originates by the precipitation of vacancies. Hull and Rimmer[58] have shown that the critical size of a nucleus which is necessary for growth by vacancy precipitation is given by:

$$\rho_0 > \frac{2\gamma}{\sigma - P} \tag{9}$$

where ρ_0 is the critical radius of the void nucleus, γ is the surface energy of the material, σ the applied tensile stress, and P the superimposed hydrostatic pressure. If void nuclei are smaller than this critical size, they tend to sinter and disappear. For a stress of 1500 psi (10^8 centimeters^{-2}) and a surface energy of 1,000 ergs/cm^2, the critical void size is 2×10^{-5} cm, which is at the limit of the resolving power of a light microscope.

McLean[3] has applied Stroh's[64] equation for the stress at the end of a slip band, consisting of a pile-up of edge dislocations which will initiate a crack perpendicular to the Burger's vector, to situations involving grain boundary sliding, such as the jogged grain boundary, or the triple point crack. Stroh suggests that a crack will form when the stress at the end of a slip band satisfies the Griffith condition that the energy of the new surfaces created is less than the elastic strain energy released. This gives:

$$n b \sigma_0 > 12 \lambda \tag{10}$$

where σ_0 is the applied shear stress, and λ is the energy per centimeter^2 of the crack surfaces, and n is the number of dislocations in the pile up. Since n depends on the length of the shear interface at the applied stress, according to the Eshelby, Frank and Nabarro[65] relationship:

$$a = \pi L (1 - \nu) \frac{\sigma_o}{Gb} \tag{11}$$

where L is the slip distance and substitution into equation (10) gives

$$L \sigma_o^2 > \frac{12 \lambda G}{\pi (1 - \nu)} \tag{12}$$

McLean applied this equation to the situation at a triple point with the assumption that the grain boundary sliding is equivalent to the passage of dislocations. Thus, the surface energy term now becomes the difference in surface energy of the grain boundary and the surface free energy, and L is associated with the length of the sliding grain boundary. For a grain size of .1 mm, he finds the critical applied tensile stress for crack formation to be about 8×10^8 cm^2 (10,000 psi) for copper. This figure seems high for intercrystalline fracture in copper when compared to experimental data, however, the equation might give quite reasonable stress if applied to stronger materials, such as high temperature nickel base alloys. In addition, solute segregation at grain boundaries could decrease the difference of surface and interfacial energy and hence give a lower value for the critical applied tensile stress.

Growth of Voids

A suggestion by Greenwood et al[49] that the growth of voids occurs by condensation of vacancies would lead one to the conclusion that the best way to verify the mechanism is by a study of the rate of growth of voids. Such a study, however, requires that one have a reasonable model for the process. One needs to know the source of the voids, how they nucleate, and the rate of the transport process. Machlin[59] evaluated the rate of growth of voids, assuming that the source of vacancies was the grain, the necessary vacancies being generated during creep by the migration of suitable dislocation jogs.

Baluffi and Seigle[60] suggested that it is more reasonable to assume that the vacancies for void growth arise from the grain boundaries due to the tensile stresses on the boundary, as in the Nabarro and Herring expression for creep by diffusion of vacancies. This course of vacancies agrees better with the observation that greater numbers of voids occur on transverse grain boundaries in tension tests, whereas they occur on longitudinal grain boundaries in compression tests. McLean used this model in developing an expression for the volume of cavities which results from vacancy precipitation. He found that the rate of growth of cavities in nickel-base high temperature alloys was in reasonable agreement with his calculations. Hull and Rimmer examined the relative contributions to void growth by lattice diffusion and grain boundary diffusion, using the equation:

$$\frac{D_\ell \cdot \rho}{D_g \cdot \delta_z} \tag{13}$$

where D_ℓ and D_g are respectively the lattice and grain boundary diffusion coefficients, ρ is the void radius, and δ_z is the grain boundary width. This ratio gives the number of atoms transferred from a void to the boundary by lattice diffusion to that by grain boundary diffusion. Substituting appropriate values for copper at the temperatures of testing (400 to 500°C), they found that the contribution from lattice diffusion was only 6 percent of the total, and therefore set up a relationship for void growth based on grain boundary diffusion. This was then related to the time to rupture for creep specimens by assuming that rupture takes place as soon as the

voids in the assumed square array go to the point where they touch one another. The expression for rupture time is as follows:

$$t_r \sim \frac{K T a^3}{4(D_g \delta_z)(\sigma - P)\Omega} \qquad (14)$$

where K is the Boltzmann constant, T the temperature, a the spacing of the square array of void nuclei, σ the applied tensile stress, P the superimposed hydrostatic pressure, and Ω the atom volume. If the spacing of void nuclei and the initial size of the void nuclei were as constant as the equation presumes, then the rupture time would vary only as $(\sigma - P)$. Although the experimental determinations of the curve of rupture time versus tension stress at various values of hydrostatic pressure did agree in form with the equation developed, it was found that it was necessary to use different values of void spacing in order to superimpose the curves for different values of $(\sigma - P)$. In the tensile stress range investigated, 4,730 to 6,000 psi, it was necessary to use values of a = 2.1 - 1.1 microns. In other respects, the equation agreed quite well with the experimental data. The observed activation energy for void formation was 25,000 ± 3000 cal/mol, which is a reasonable figure for the activation energy for grain boundary diffusion in copper. A test in which the value of $(\sigma - P)$ was zero gave no evidence of any void formation in the creep specimen.

Boettner and Robertson[61] recently studied the growth of voids in copper during creep by measuring the change of density of such specimens. Their results, shown in Figure 40, indicate that the volume of voids produced during creep is a function of the total strain and is different for different values of the applied stress. They also obtain an activation energy for the growth of voids equal to 29,000 cal/mole, which is in good agreement with the results of Hull and Rimmer. They conclude that growth of voids does occur by a vacancy condensation mechanism.

Kramer and Machlin, on the other hand, have measured the fraction of total grain boundary area occupied by cracks and voids by lineal analysis, and have found that this measurement is a linear function of percent elongation in creep[62]. They suggest this linear response, using McLean's[19] observation that the amount of grain boundary sliding is proportional to the amount of creep elongation, to be dependent on the magnitude of grain boundary sliding. They contend that their results confirm the generation of cracks by shear, and argue against the vacancy condensation mechanisms.

Seigle[63] had subsequently criticized the conclusions drawn from these data from the standpoint that neither of the crack growth mechanisms has yet been developed to a sufficient extent to say whether the linear relationship between crack grain boundary area and total elongation would exist.

Mullendore and Grant have examined the change in volume of aluminum - 5% magnesium specimens in creep at 500°F, and find that the rate of growth of void volume in the second and third stages of creep is approximately linear, as shown in Figure 41b. The size distribution of voids under these testing conditions is indicated in Figure 41b. Application of the Hull and Rimmer formula to these data indicates that the observed rate of growth of voids cannot be explained solely by vacancy condensation and a certain large amount of the void growth must be due to a shear mechanism.

SUMMARY

It is perhaps obvious to the reader, even without comment from the authors, that the past fifteen years have witnessed a major advance in our understanding of high temperature deformation, even though the results of the large amount of work cannot be neatly packaged into a set of conclusions. High temperature fracture, on the other hand, while definable from a mechanistic point of view, is very much more poorly understood.

There obviously remains much to be done. Additional work is necessary to settle a number of disagreements, however, the areas of disagreement can be sharply defined and the necessary experiments and calculations planned. A number of new approaches and areas of interest must be initiated to take advantage of the progress already made.

In particular, these items or areas can be selected for continuing, or for future research:

1. A check on Rachinger's high value of internal grain boundary sliding.

2. Does sliding take place on the grain boundary, or near the grain boundary?

3. The interplay of strain hardening and recovery on the creep process.

4. The role of solute segregation on boundary sliding and migration, and the change of grain boundary energy with solid solution alloying.

5. A more positive check of intercrystalline crack initiation and the mechanism of crack growth and propagation. This work should be done in pure metals or simple solid solution alloys for the time being, since it will serve as a basis for studies in complex alloys (see below).

6. Does fracture occur in the grain boundary, in one grain, or does it encompass both grains? Grain boundary serrations would indicate a preference for the third case.

7. The study of deformation and fracture should be extended immediately to two-phase alloys, including solid solution mixtures and precipitation or dispersion hardened alloys. The very large variation in the ratio E_{GB}/E_T for aluminum - 3% copper alloys, as a function of heat treatment (structure) point to very interesting and useful studies. Fracture in these systems has been looked at only in a very preliminary manner.

8. An extension of the studies to body-centered-cubic and hexagonal metals is long overdue.

Finally, it is expected that such studies will, over the near term, permit tailoring alloys for optimum creep resistance with a maximum safety factor of high fracture ductility. The data should permit, for example, alloy development in which the grain boundary is pinned by large precipitates and the grains strengthened by a fine precipitate, once the desired formula is known.

Recommended Research Activities

1. The interplay of strain hardening and recovery during high temperature deformation. Because strain rate as well as temperature are important variables, along with considerations of the structure of the material, the interplay of strain hardening and recovery must be better understood. The balance of these two forces determines the interplay of local processes, expecially the balance between grain and grain boundary behavior. The inbalance between these two phenomena has an extremely important bearing on the initiation and propagation of fracture.

2. The role of solute segregation on the grain boundary as well as along sub-boundaries, and the effect of such segregation on boundary sliding and migration. Consideration should be given to changes in grain boundary energy, surface energy, recrystallization phenomena, and fracture characteristics.

3. A detailed investigation of the initiation of intercrystalline cracking. Because of the extensive disagreement regarding the initiation of intercrystalline cracks, and the role that vacancy condensation plays in modern theory, this subject deserves much greater attention. Once crack initiation is better understood, it should be possible to devote more time to crack propagation. For the time being, this work should be concerned with the behavior of pure metals and in simple solid solution alloys, avoiding for the moment two phase alloys.

4. Does sliding take place on the grain boundary, or near the grain boundary? Parallel with this problem is the question of intercrystalline fracture. Does the fracture follow the grain boundary, does it include the grain boundary and one grain, or does it encompass the grain boundary and both grains? The recent observation of grain boundary serrations would indicate a preference for the third case.

5. A check should be made of Rachinger's very high values of the contribution of grain boundary sliding as measured internally, in contrast to the more extensive work based on surface measurements.

6. An initial effort should be undertaken to start looking at commercial alloys, or at tailored two-phase or multi-phase alloys to see how both grain boundary sliding and grain boundary fracture differs in these more complex alloys in contrast to pure metals and simple solid solutions. A few recent observations have indicated a very large span of values of grain boundary contribution to total deformation as a function of heat treatment (therefore structure). There is enough background of test work, theory, and experimental techniques to permit a good start in this direction.

BIBLIOGRAPHY

1. W. Rosenhain and J. C. W. Humphrey, J. Iron Steel Institute, 1913, *87*, 219.
2. Z. Jeffries and R. S. Archer, "Science of Metals", McGraw-Hill, 1924, p. 73.
3. D. McLean, "Grain Boundaries in Metals", Clarendon Press, Oxford, 1957.
4. S. Weinberg, "Progress in Metal Physics", *8*, 1959, Pergamon Press.
5. S. Amelinckx and W. Dekeyser, "Solid State Physics", *8*, 1959.
6. R. C. Gifkins, "Fracture", Edited by B. L. Averbach, D. S. Felbeck, G. T. Hahn, and D. A. Thomas. The Technology Press and John Wiley and Sons, Inc., 1959.
7. F. L. Vogel, W. G. Pfann, H. E. Corey and E. E. Thomas, Phys. Rev., *90*, 1953, 489.
8. J. M. Burgers, Proc. Koninkl. Med. Akad. Wetenschop, *42*, 1939, 293, 378.
9. W. Shockley and W. T. Read, Jr., Phys. Rev., *75*, 1949, 692; *78*, 1950, 275.
10. N. F. Mott, Proc. Phys. Soc., *60*, 1948, 391.
11. T. S. Ke, J. Apply. Phys., *22*, 1949, 274.
12. J. Friedel, B. D. Cullity and C. Crussard, Acta Met., *1*, 1953, 79.
13. K. T. Aust, Trans. AIME, *206*, 1956, 1026.
14. R. S. Wagner and B. Chalmers, J. Apply. Physics, *31* (3), 1960, 581.
15. K. A. McCarthy and B. Chalmers, Canad. J. Phys., *36*, 1958, 1645.
16. B. Chalmers, "Progress in Metal Physics", *3*, 1952, 293.
17. N. A. Gjostein and F. N. Rhines, Acta Met., *7*, 1959, 319.
18. J. H. van der Merwe, Proc. Phys. Soc., *A63*, 1950, 616.
19. D. McLean, J. Inst. Metals, *81*, 1952-53, 293.
20. B. Fazan, O. D. Sherby, and J. E. Dorn, Trans. AIME, *200*, 1954, 920.
21. H. Brunner and N. J. Grant, Trans. AIME, *215*, 1959, 48.
22. W. A. Rachinger, J. Inst. Metals, *81*, 1952, 33.
23. H. C. Chang and N. J. Grant, Trans. AIME, *197*, 1953, 1175.
24. N. J. Grant and A. R. Chaudhuri, "Creep and Recovery", ASM, 1957, 284.

25. A. W. Mullendore and N. J. Grant: to be submitted to AIME.

26. H. Brunner and N. J. Grant, Trans. AIME, *218*, 1960, 122.

27. J. G. Harper, L. A. Shepard and J. E. Dorn, Acta Met., *6*, 1958, 509.

28. D. McLean, J. Inst. Metals, *80*, 1951, 507.

29. W. R. Thomas and B. Chalmers, Acta Met., *3*, 1955, 17.

30. D. McLean and R. C. Gifkins, J. Inst. Metals, Tech. Note, *89*, 1960-61, 29.

31. A. W. Mullendore and N. J. Grant, WADD Report TR 60-340.

32. A. W. Mullendore and N. J. Grant, Joint symposium on Structural Processes in Creep, Iron and Steel Institute and Inst. of Metals, London, May, 1961. To appear in J. Inst. Metals.

33. Yoichi Ishida: private communication.

34. F. N. Rhines, W. E. Bond and M. A. Kissel, Trans. ASM, *48*, 1956, 919.

35. S. K. Tung and R. Maddin, Trans. AIME, *209*, 1957, 905.

36. N. R. Adsit and V. O. Brittain, Trans. AIME, Tech. Note, *218* (4), 1960, 765.

37. S. L. Couling and C. S. Roberts, Trans. AIME, *209*, 1957, 1252.

38. G. J. Ogilvie, J. Inst. Metals, *81*, 1952-53, 491.

39. C. Crussard and J. Friedel, NPL Symposium on Creep and Fracture of Metals at High Temperatures, HMSO, 1956, 243.

40. F. N. Rhines, NPL Symposium on Creep and Fracture of Metals at High Temperatures, HMSO, 1956, 47.

41. D. McLean, NPL Symposium on Creep and Fracture of Metals at High Temperatures, HMSO, 1956, 73.

42. J. Washburn and E. R. Parker, Trans. AIME, *194*, 1952, 1076.

43. K. T. Aust and J. W. Rutter, Trans. AIME, *215*, 1959, 119.

44. I. S. Servi and N. J. Grant, Trans. AIME, *191*, 1951, 919.

45. R. Widmer and N. J. Grant Trans. ASME, Jour. Basic Eng., Dec., 1960, p. 829.

46. H. C. Chang and N. J. Grant, Trans. AIME, *206*, 1956, 544.

47. C. M. H. Jenkins, E. H. Bucknall, and E. A. Jenkinson, J. Inst. Metals, *70*, 1944, 57.

48. J. C. Greenwood, J. Iron Steel Inst., *171*, 1952, 380.

49. J. N. Greenwood, D. R. Miller, and J. W. Suiter, Acta Met., *2*, 1954, 250.

50. P. W. Davis and J. P. Dennison, J. Inst. Metals, *4*, 1958-59, 119.

51. D. McLean, J. Inst. Metals, *85*, 468, 1957.

52. C. W. Weaver, J. Inst. Metals, *87*, 1958, 126.

53. R. D. Gifkins, Acta Meta., Tech. Note, 1956, 98.

54. C. W. Chen and E. S. Machlin, Acta Met., Tech. Note, *4*, 1956, 655.

55. H. H. Bleakney, Canad. J. Tech., *30*, 1952, 340.

56. R. Resnick and L. L. Seigle, Trans. AIME, *209*, 1957, 87.

57. V. S. Ivanova and L. A. Oding, Dok. Akad. Nank, USSR, *103*, 1955, 77.

58. D. Hall and D. E. Rimmer, Phil. Mag., *4*, 1959, 673.

59. E. S. Machlin, Trans. AIME, *206*, 1956, 106.

60. R. W. Balluffi and L. L. Seigle, Metallurgia, *5*, 1957, 449.

61. R. C. Boettner and W. D. Robertson, Trans. AIME, *221*, 1961, 613.

62. D. Kramer and E. S. Machlin, Acta Met., Tech. Note, *6*, 1958, 454.

63. L. L. Seigle, Acta Met., Tech. Note, *7*, 1959, 421.

64. A. N. Stroh, Proc. Roy. Soc., *A 218*, 1953, 391.

65. J. D. Eshelby, F. C. Frank and F. R. N. Nabarro, Phil. Mag., *42*, 1951, 351.

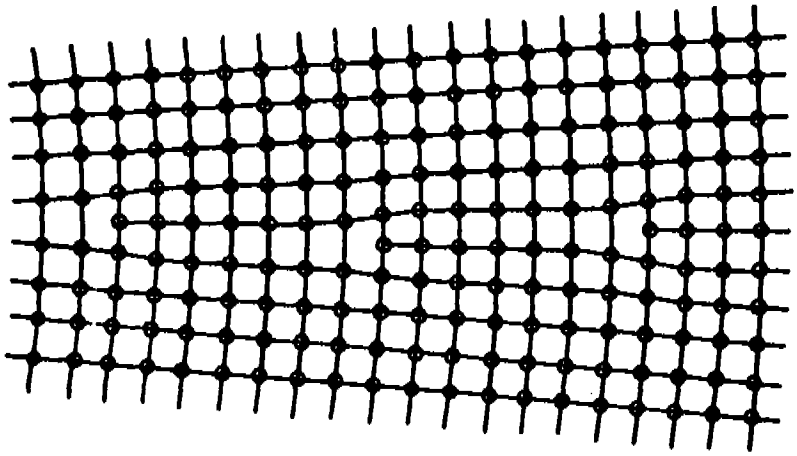

FIGURE 1

BURGERS' MODEL OF A SYMMETRICAL PURE TILT BOUNDARY (5)

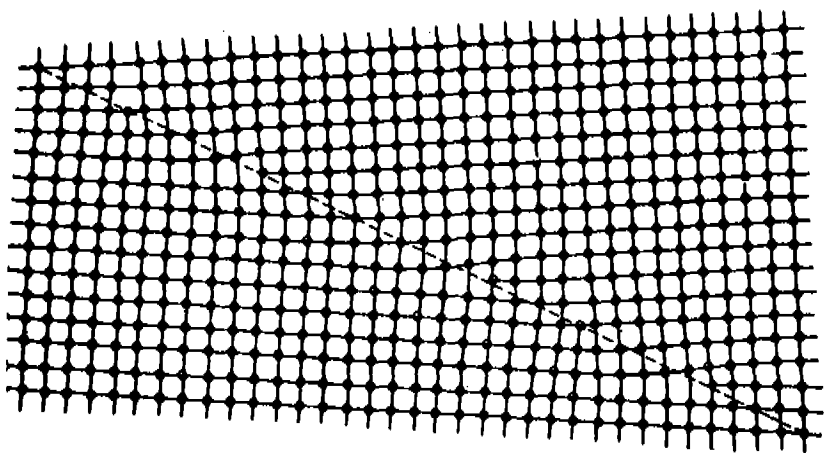

FIGURE 2

ASYMMETRICAL PURE TILT BOUNDARY CONTAINING TWO SETS OF EDGE DISLOCATIONS, ACCORDING TO THE MODEL OF READ AND SHOCKLEY (9)

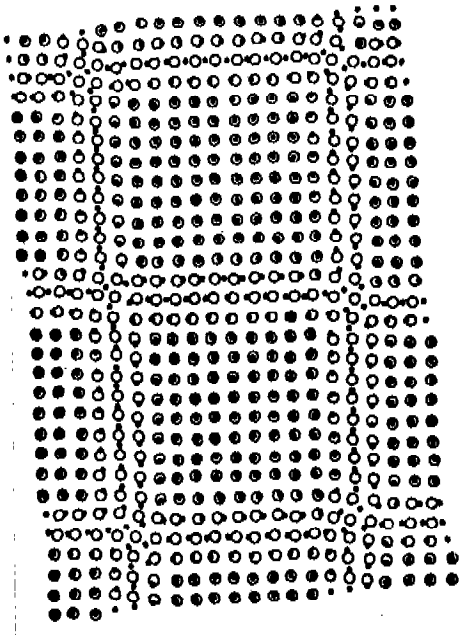

SQUARE GRID OF SCREW DISLOCATIONS FORMING A PURE TWIST BOUNDARY. SOLID CIRCLES REPRESENT ATOMS UNDER THE PLANE OF THE DRAWING; OPEN CIRCLES ATOMS ABOVE IT (5)

FIGURE 3

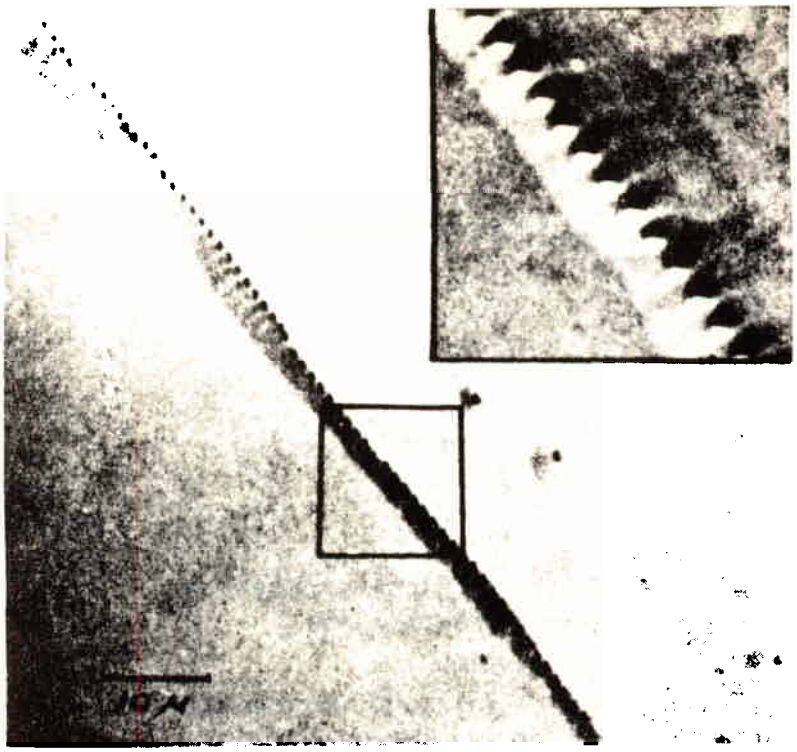

FIGURE 4

DISLOCATIONS IN A SMALL ANGLE BOUNDARY IN GERMANIUM REVEALED BY ETCHING (7)

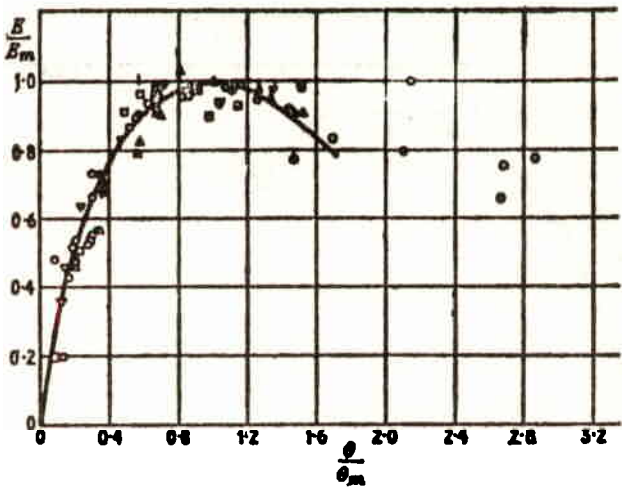

FIGURE 5

COMPARISON OF THEORETICAL ENERGY OF DISLOCATION BOUNDARIES (CURVE) WITH MEASURED ENERGIES OF GRAIN BOUNDARIES (POINTS) (AFTER READ AND SHOCKLEY) (9)

- o Dunn Silicon iron (110) series, θ_m = 26.6
- Δ Dunn silicon iron (100) series, θ_m = 29.8
- ▭ Aust and Chalmer's tin, θ_m = 12.2
- ▽ Aust and Chalmer's lead, θ_m = 25.7

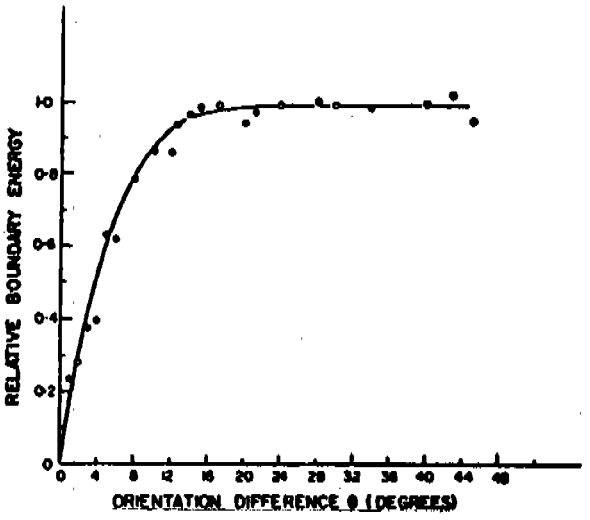

FIGURE 6

RELATIVE BOUNDARY ENERGY OF <100> TILT BOUNDARIES IN GERMANIUM, AS A FUNCTION OF BOUNDARY ANGLE (14)

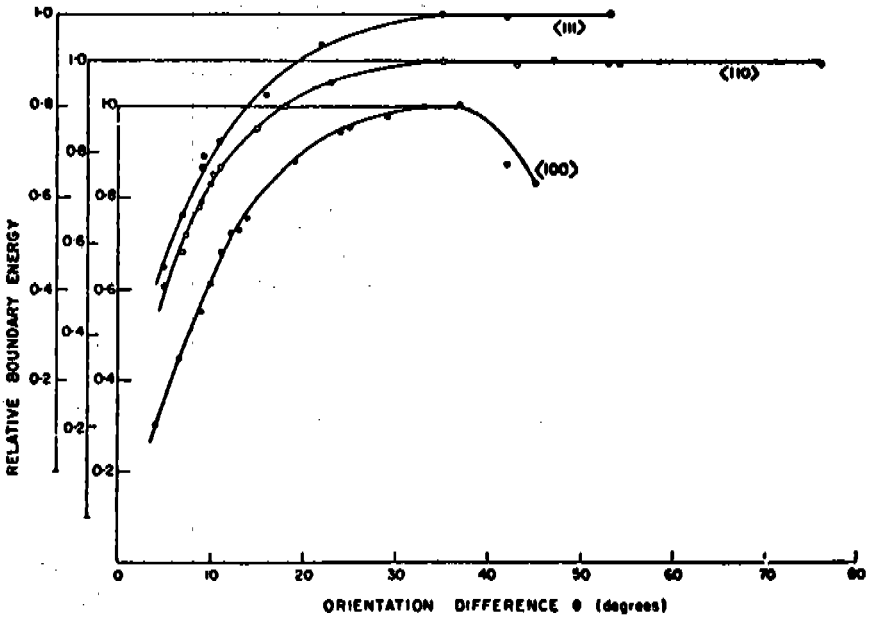

FIGURE 7

RELATIVE BOUNDARY ENERGY AS A FUNCTION OF ORIENTATION DIFFERENCE FOR SILVER CHLORIDE TRICRYSTALS OF <100>, <110>, AND <111> ISOAXIAL ORIENTATION (15)

FIGURES 6 & 7

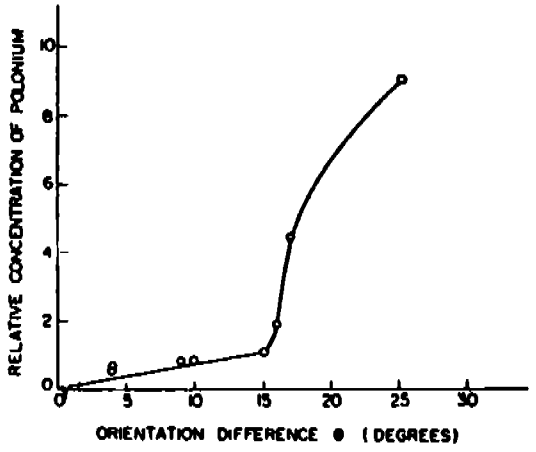

FIGURE 8

RELATIVE GRAIN BOUNDARY CONCENTRATION OF POLONIUM, AS A FUNCTION OF BOUNDARY ANGLE IN A LEAD - 5% BISMUTH ALLOY (29)

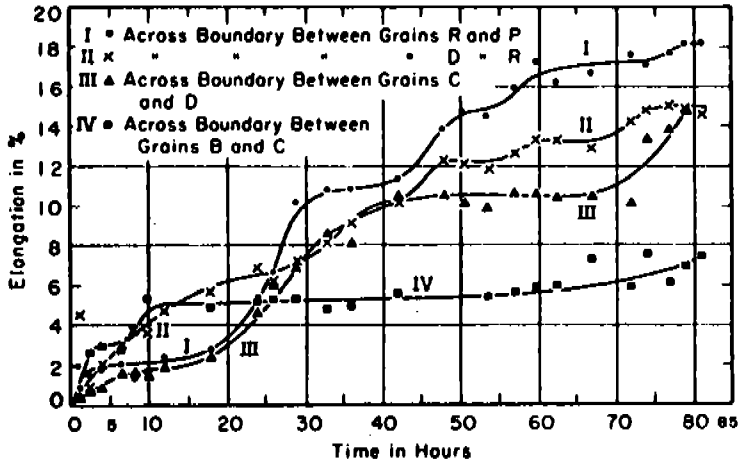

FIGURE 9

COMPONENT CREEP CURVES ACROSS GRAIN BOUNDARIES OF AN ALUMINUM POLYCRYSTAL TESTED AT 700°F (23)

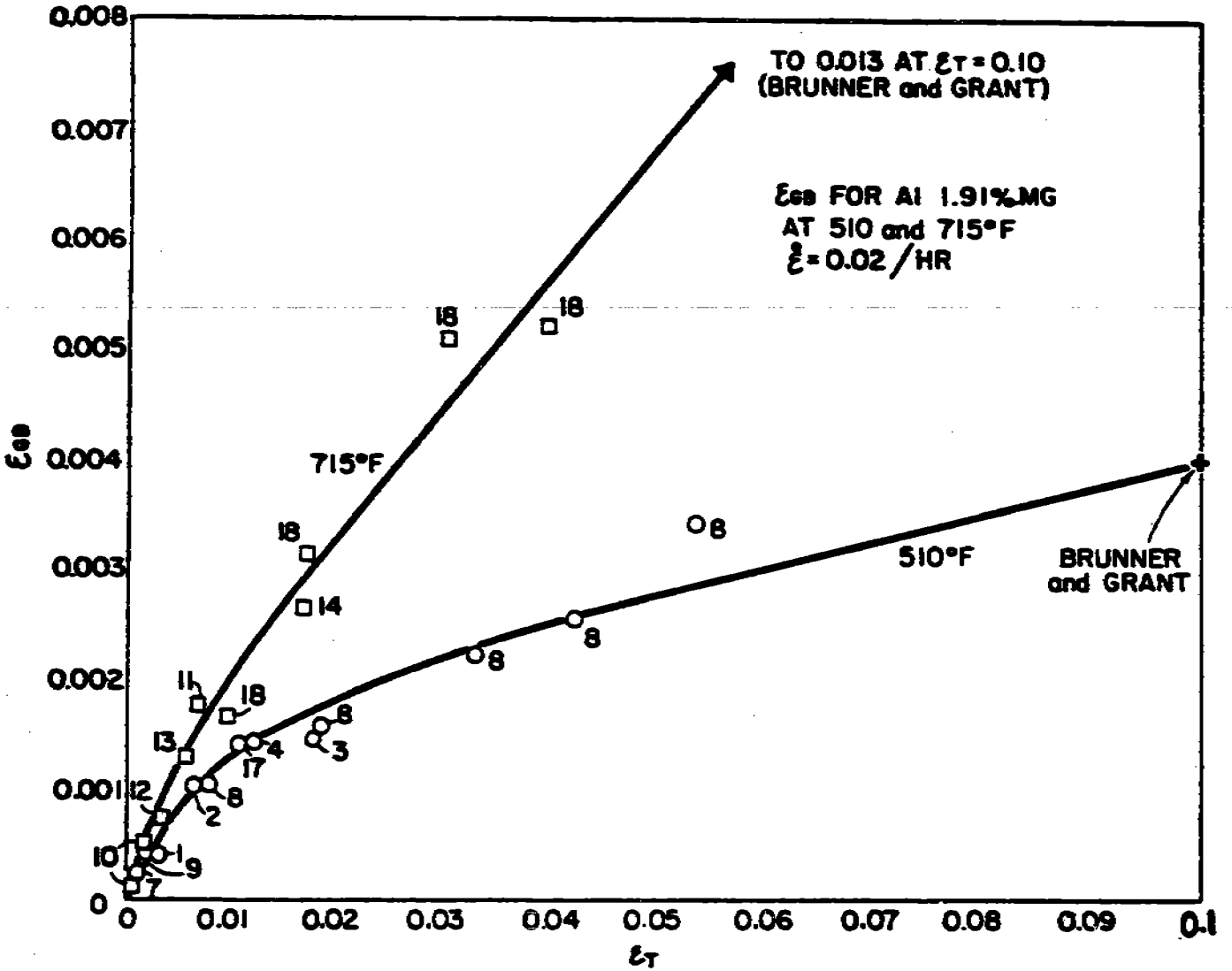

E_{GB} VERSUS E_T FOR CONSTANT STRAIN RATE TESTS OF Al-1.9 PERCENT MG (25)

FIGURE 10

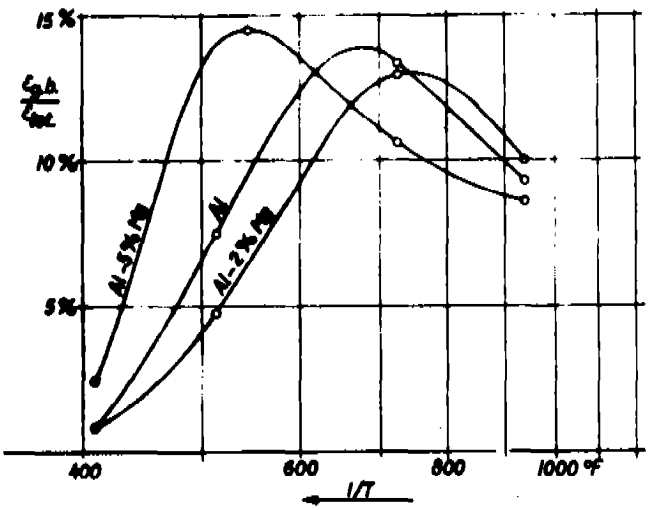

FIGURE 11

CONTRIBUTION OF GRAIN BOUNDARY SLIDING TO TOTAL ELONGATION, IN PERCENT, FOR PURE ALUMINUM AND TWO ALLOYS, AFTER ABOUT 10 PERCENT STRAIN (21)

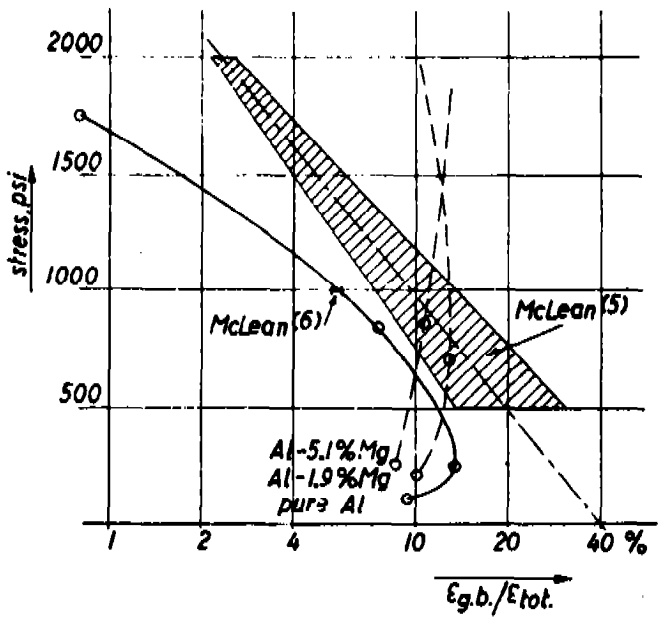

FIGURE 12

COMPARISON OF THE PRESENT TEST RESULTS WITH THE PUBLISHED DATA OF MCLEAN (21)

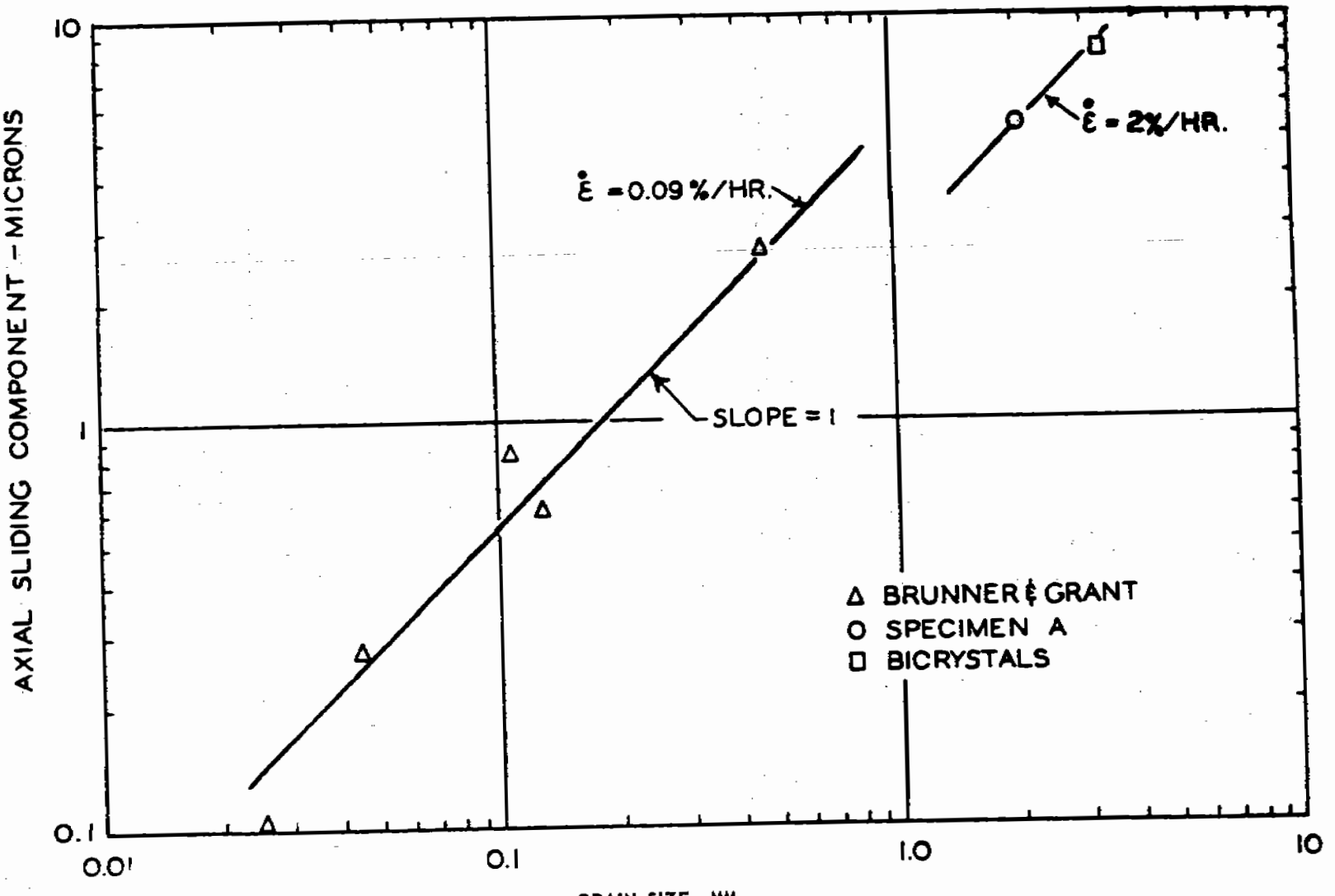

AVERAGE AXIAL COMPONENT OF GRAIN BOUNDARY SLIDING IN A1-1.9% MG VERSUS GRAIN SIZE (26)

FIGURE 13

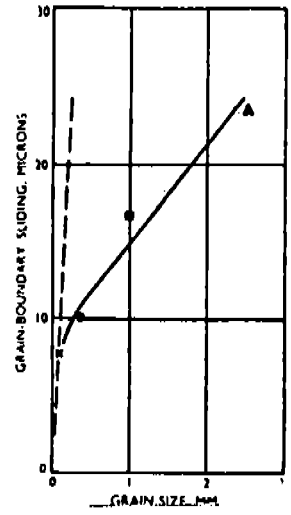

FIGURE 14

GRAIN BOUNDARY SLIDING PLOTTED AGAINST GRAIN SIZE (30)

	Curve	Material and Treatment
✕	1	99.95% Al; 10-12 grains/mm; ϵ = 0.1% hr.
●	2	99.98% Al; 2-73 grains/mm; ϵ = 0.1% hour
■	3	99.994% Al; 1-0 grain/mm; stress probably 250 lb/in^2
▲	4	99.99% Al; 0-4 grain/mm; stress 250 lb/in^2; ϵ ranged from 0.2%/hr at 337°C to 73%/hr at 474°C

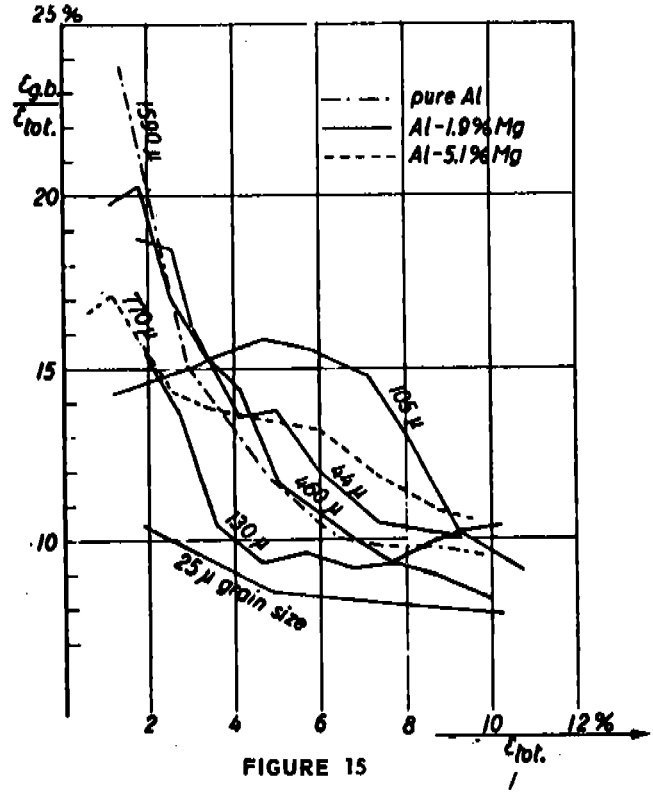

FIGURE 15

CONTRIBUTION OF GRAIN BOUNDARY SLIDING TO TOTAL DEFORMATION VERSUS STRAIN FOR PURE Al AT 940°F (STRAIN RATE 3.4%/HR); Al-1.9% MG ALLOY AT 500°F STRAIN RATE 0.9%/HR); AND Al-5.1% MG (STRAIN RATE 2.6%/HR). LISTED FIGURES ARE GRAIN DIAMETERS (26)

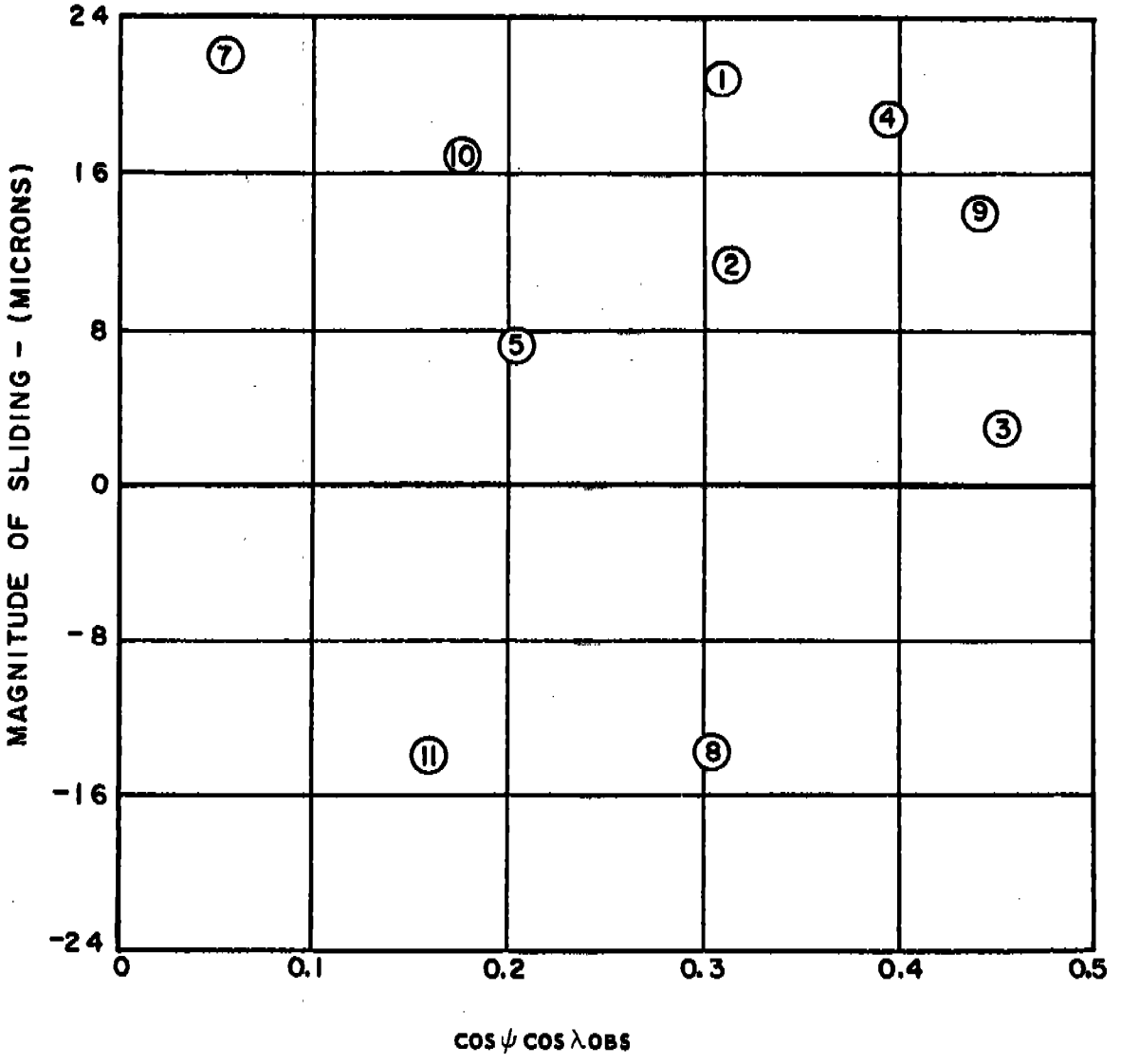

MAGNITUDE OF GRAIN BOUNDARY SLIDING VERSUS RESOLVED SHEAR STRESS ON THE GRAIN BOUNDARY FOR AN Al-1.9% MG POLYCRYSTALLINE SPECIMENS (31)

FIGURE 16

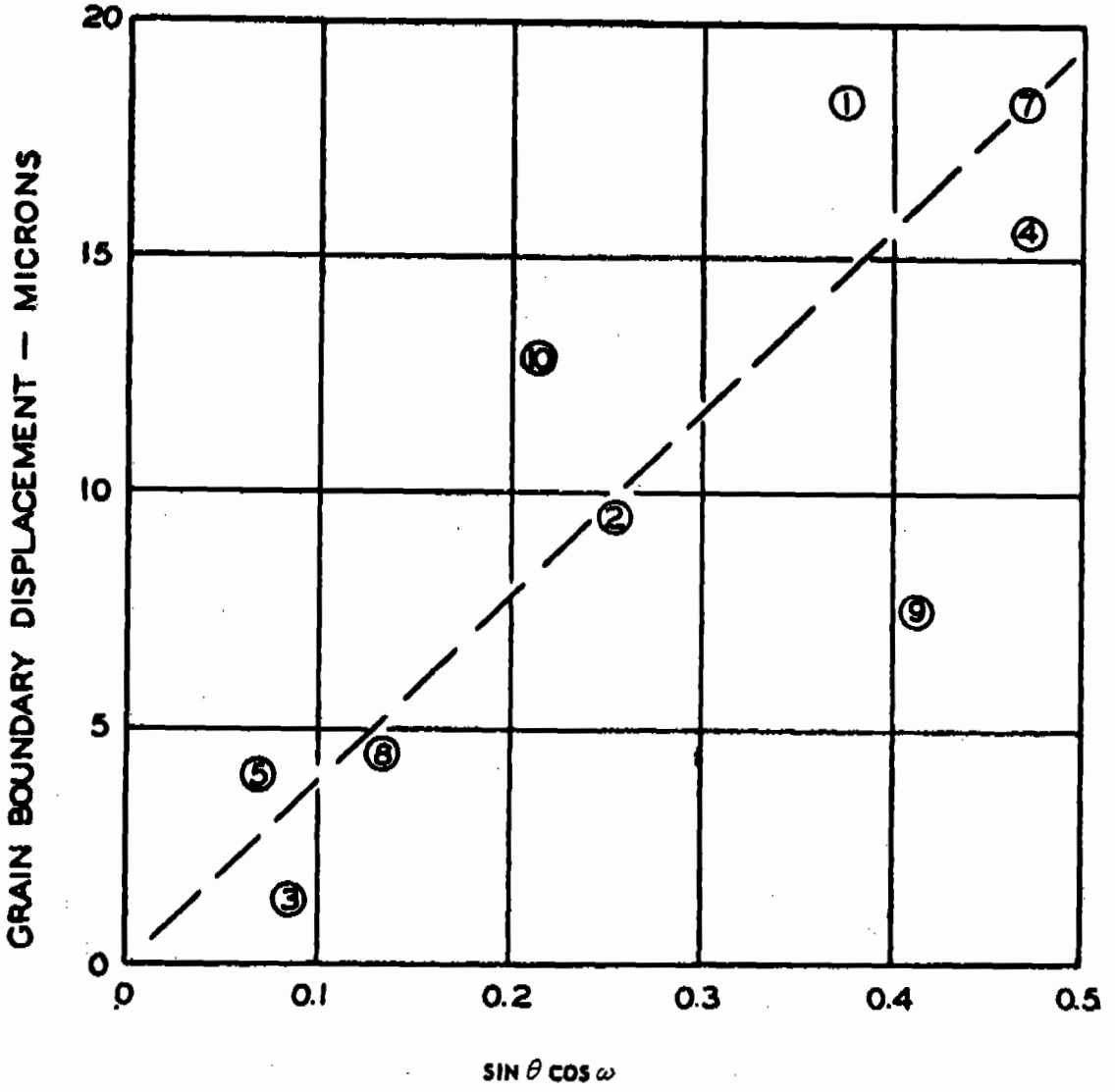

GRAIN BOUNDARY DISPLACEMENTS AFTER 5-1/2% ELONGATION VERSUS SIN θ COS ω, A GRAIN ORIENTATION FACTOR, FOR A1-1.9% MG POLYCRYSTALLINE SPECIMENS AT 500°F, ϵ = 2%HOUR (25)

FIGURE 17

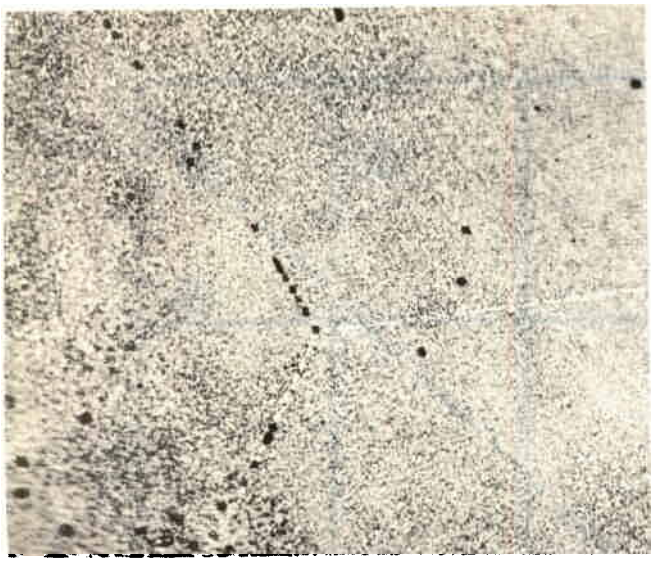

Q5

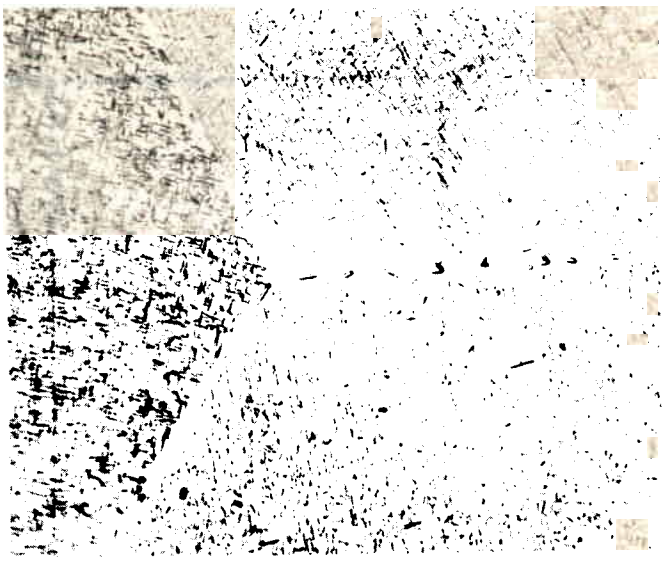

P5

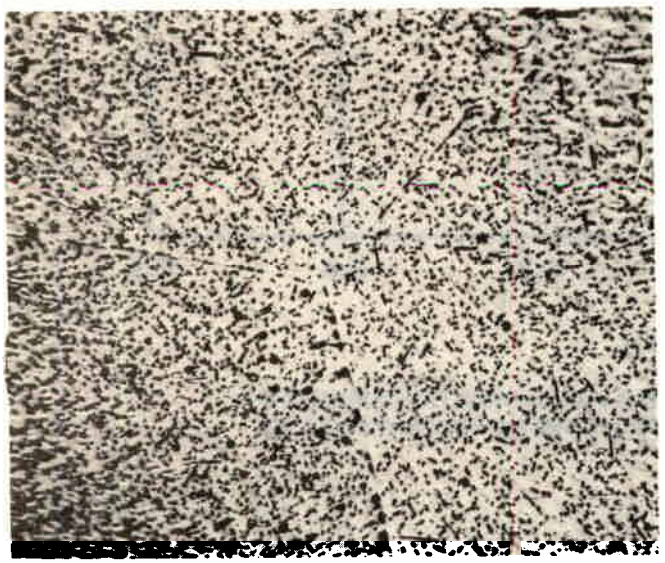

Q7

F7

STRUCTURES PRODUCED BY DIFFERENT HEAT TREATMENTS OF Al-3% Cu (33) 500X

FIGURE 18

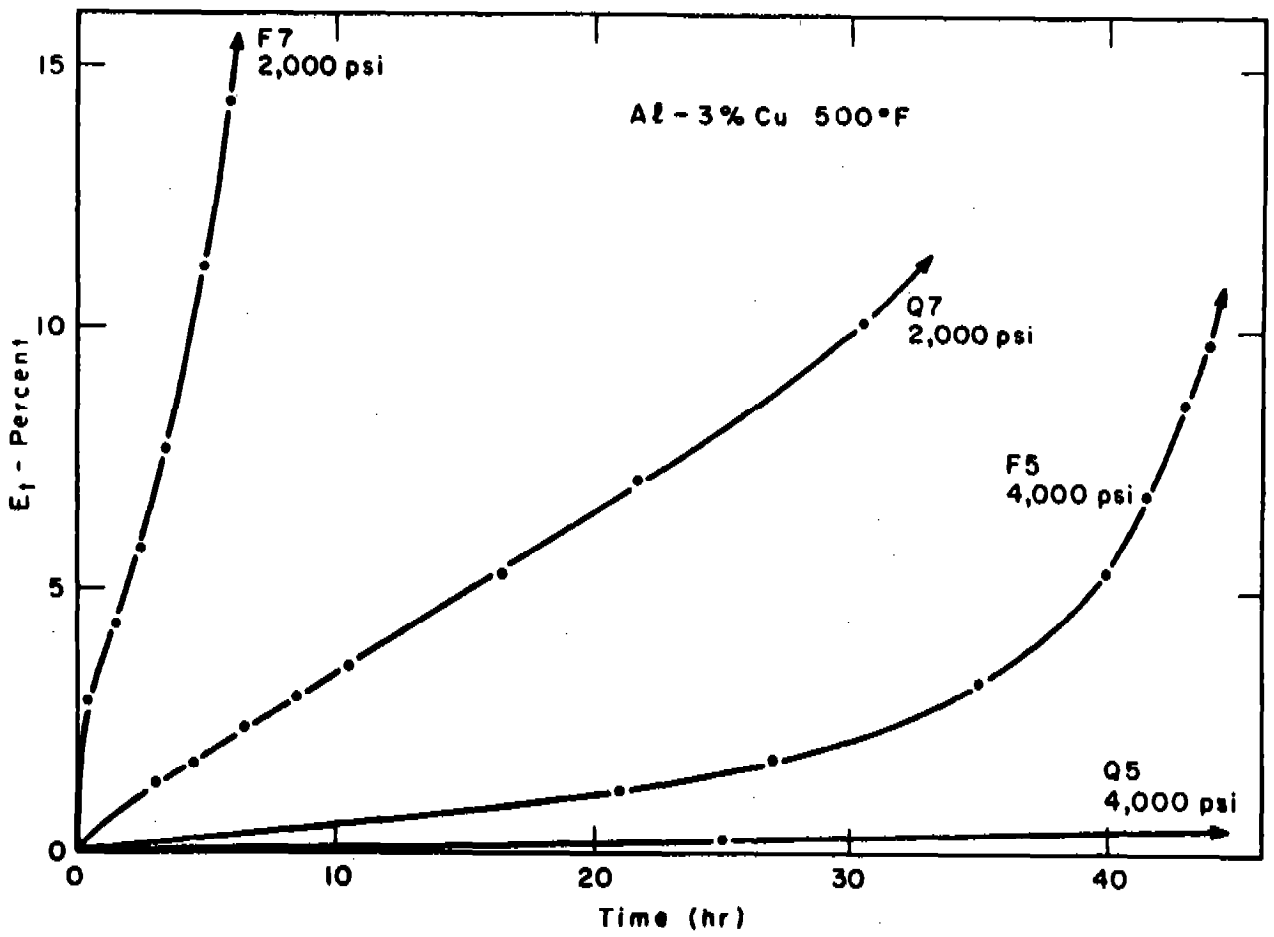

TYPICAL CREEP CURVES FOR A1-3% CU (33)

FIGURE 19

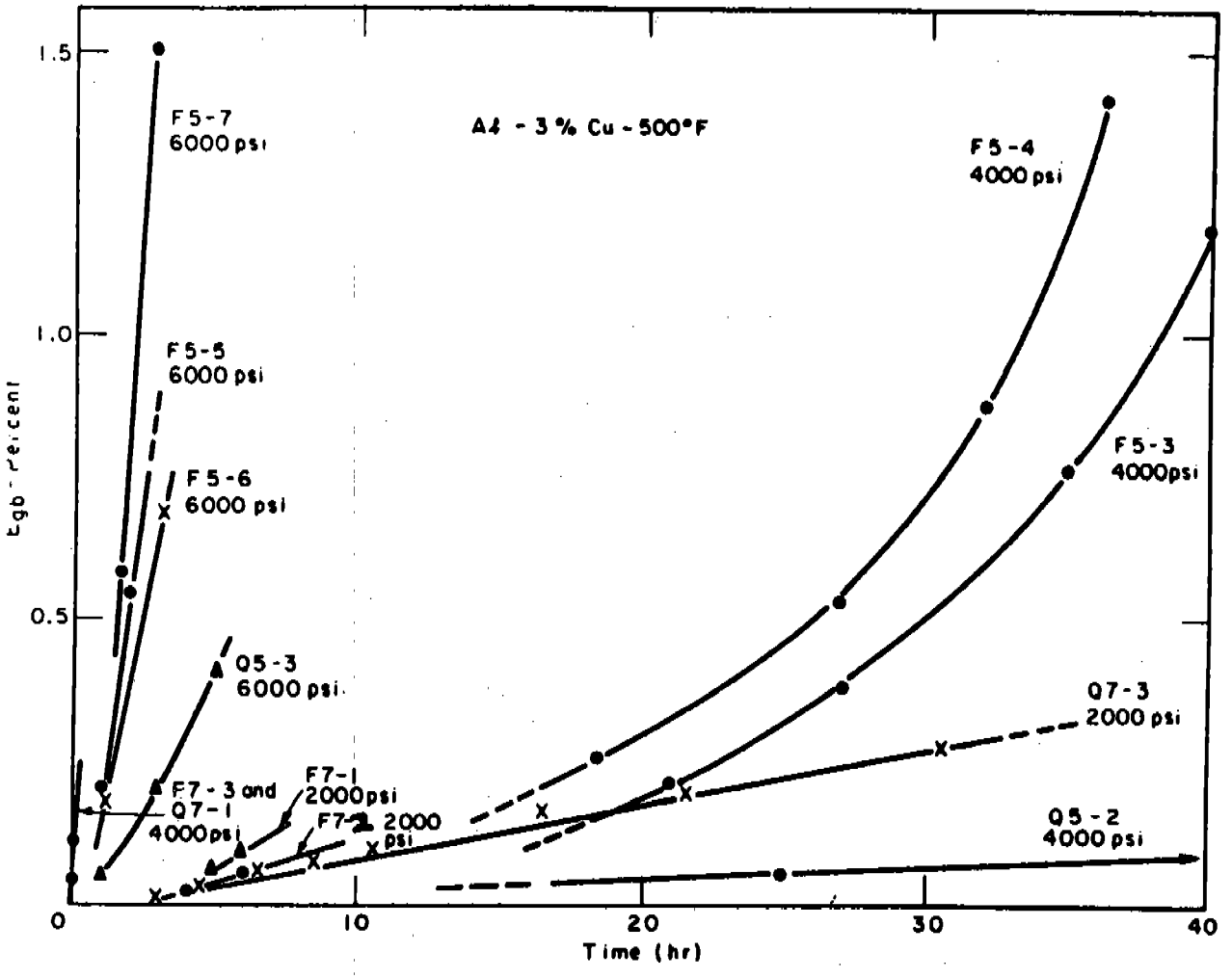

FIGURE 20

GRAIN BOUNDARY SLIDING CONTRIBUTION TO ELONGATION VERSUS TIME FOR Al-3% CU AS A FUNCTION OF HEAT TREATMENT (33)

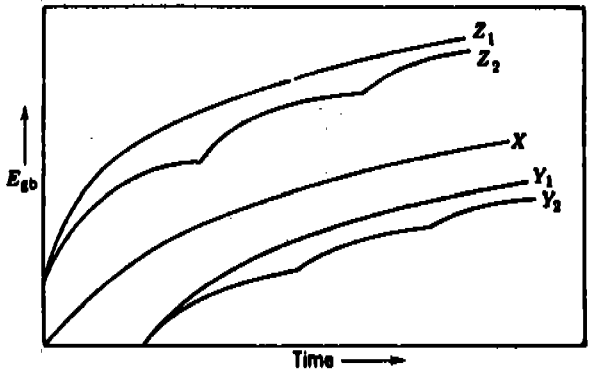

FIGURE 21

GENERAL TYPES OF SLIDING-TIME CURVES FOUND FOR BICRYSTALS[6]

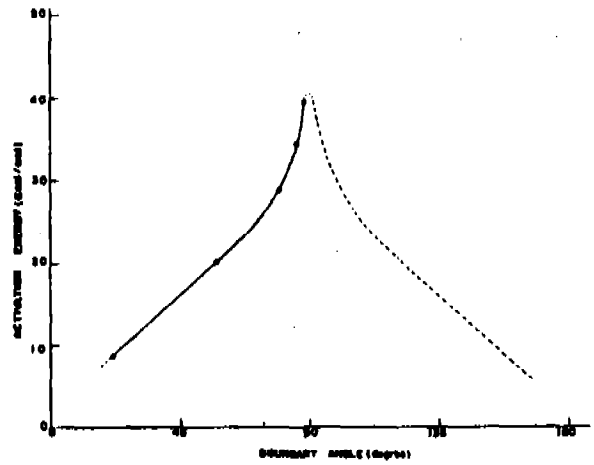

FIGURE 22

PLOT OF ACTIVATION ENERGY FOR GRAIN BOUNDARY SHEAR VERSUS BOUNDARY MISORIENTATION ANGLE θ (35)

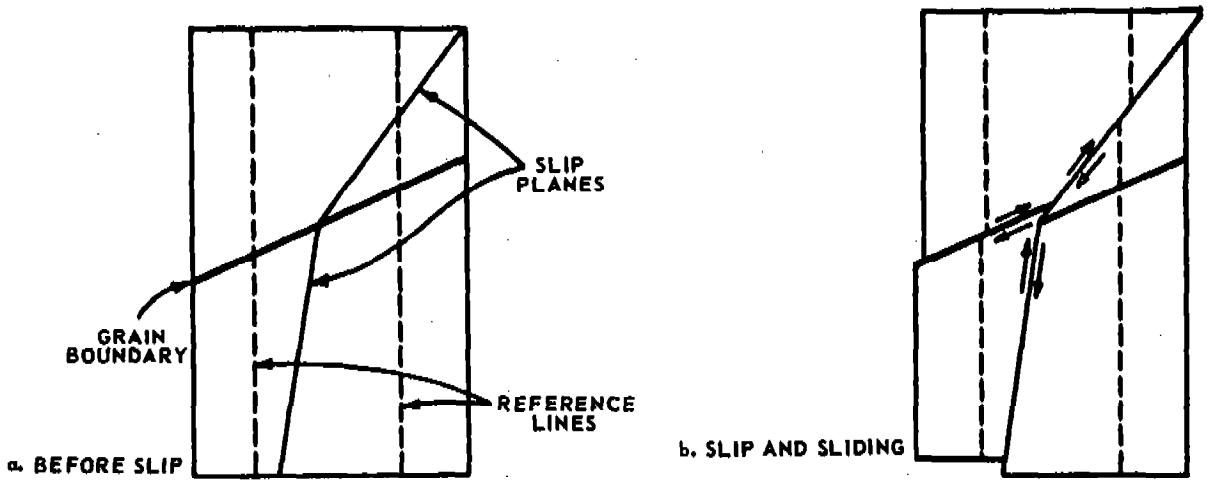

a. BEFORE SLIP b. SLIP AND SLIDING

FIGURE 23

SCHEMATIC OF SLIP INDUCED SLIDING (25)

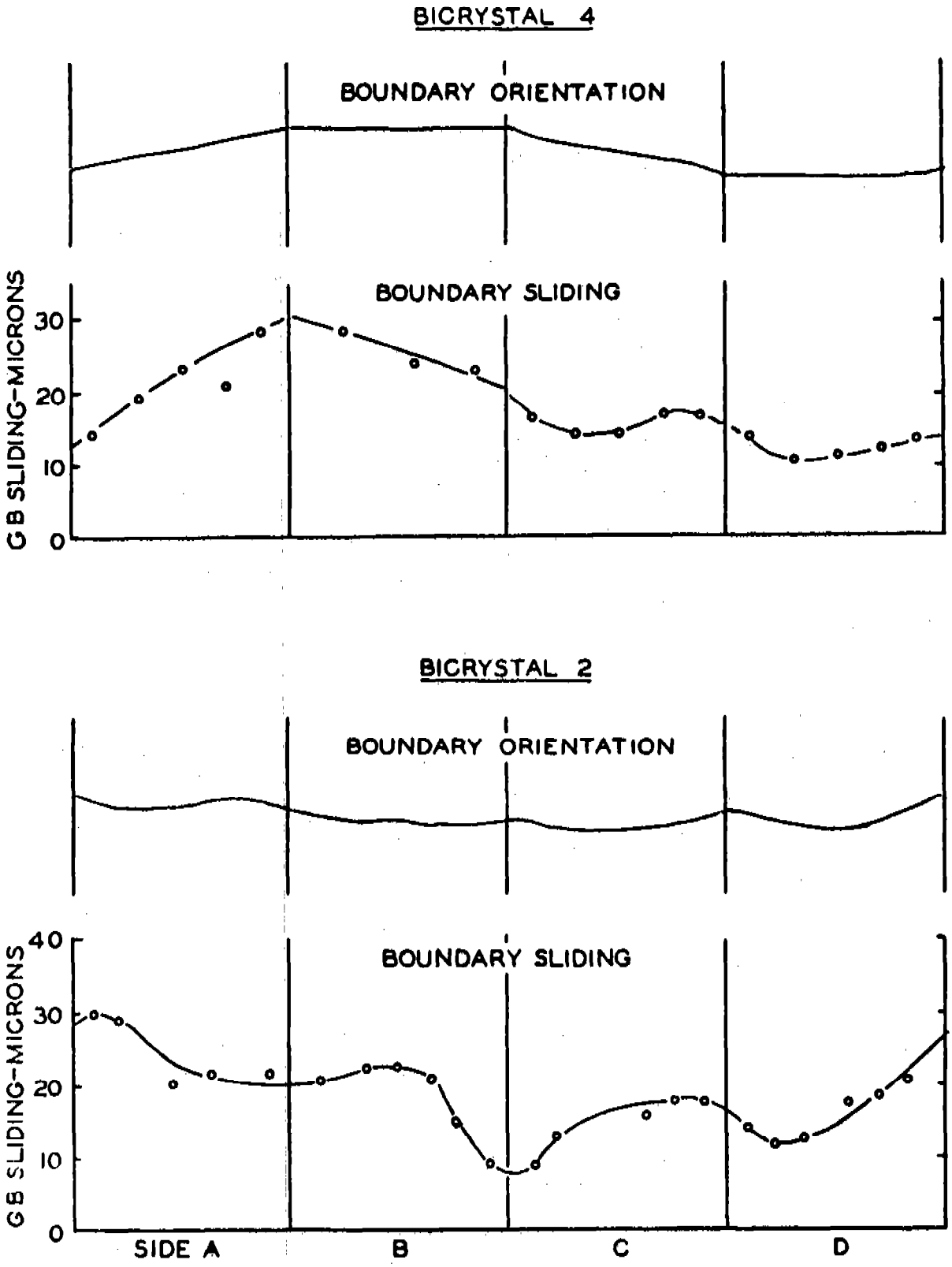

GRAIN BOUNDARY DISPLACEMENTS AROUND THE CIRCUMFERENCE OF A1-1.9% MG BICRYSTALS AFTER CREEP AT 500°F. ϵ = 2%/HOUR, $E_T \simeq$ 5% (25)

FIGURE 24

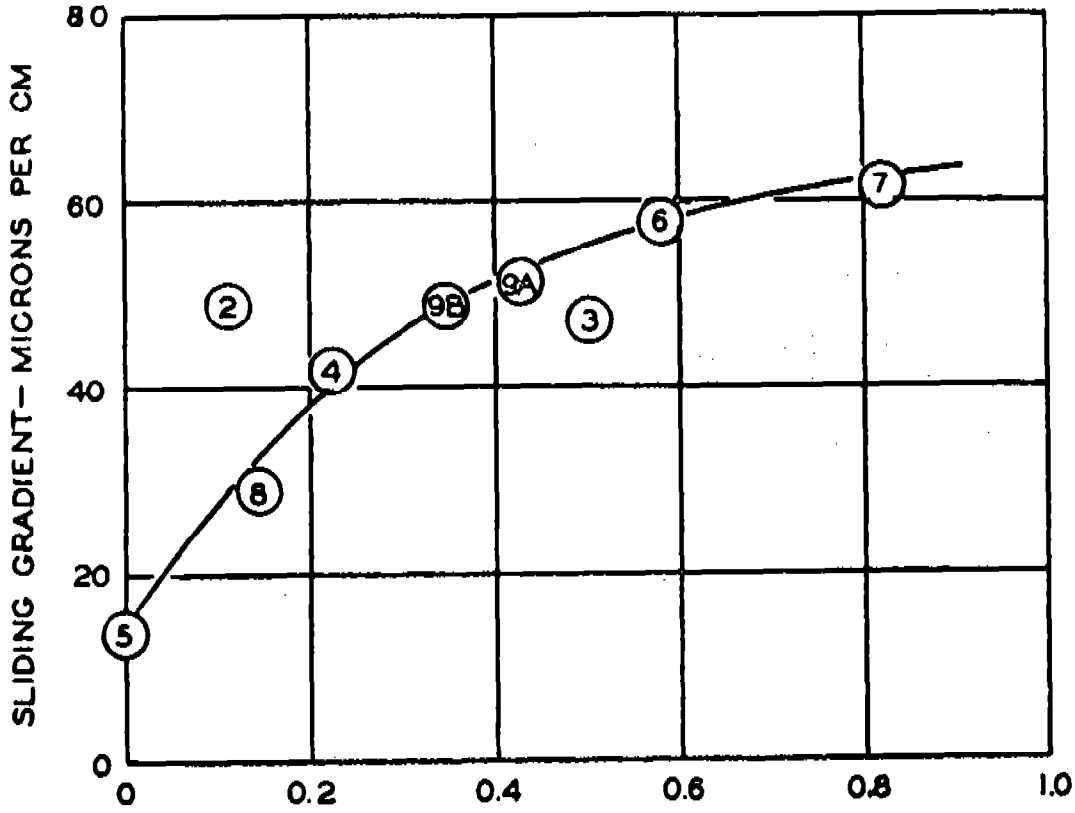

FIGURE 25

$$\left|\cos\omega\left(1-\frac{\tan\beta}{\tan\alpha}\right)\right|$$

GRADIENT OF GRAIN BOUNDARY SLIDING VERSUS A RELATIVE ORIENTATION FACTOR FOR A1-1.9% MG BICRYSTALS (25)

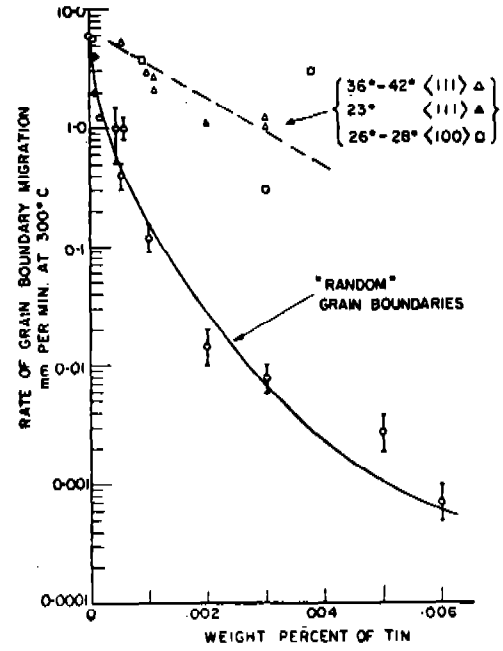

FIGURE 26

THE RATE OF GRAIN BOUNDARY MIGRATION OF ZONE-REFINED LEAD AS A FUNCTION OF THE WEIGHT PERCENT OF ADDED TIN FOR "RANDOM" AND "SPECIAL" GRAIN BOUNDARIES. ANNEALING TEMPERATURE 300°C (43)

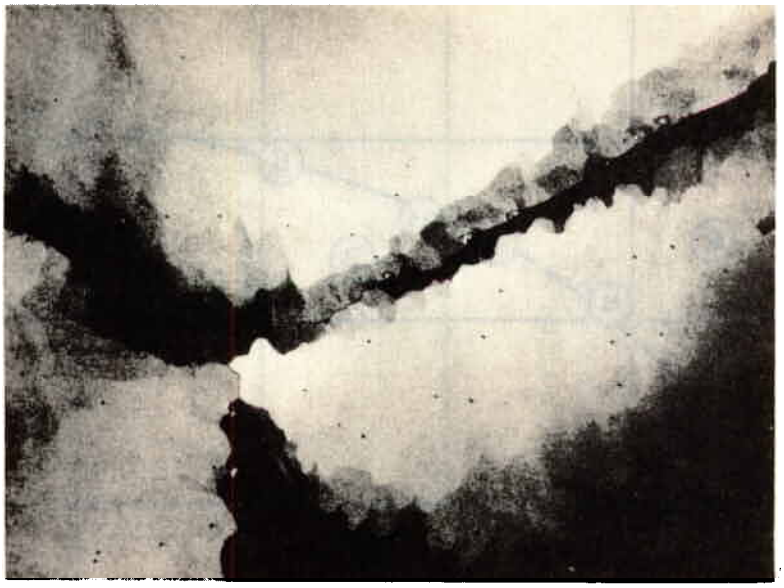

FIGURE 27

SUBSTRUCTURE NEAR SERRATED BOUNDARY. POLARIZED LIGHT. 100X
A1-1.9% MG (31)

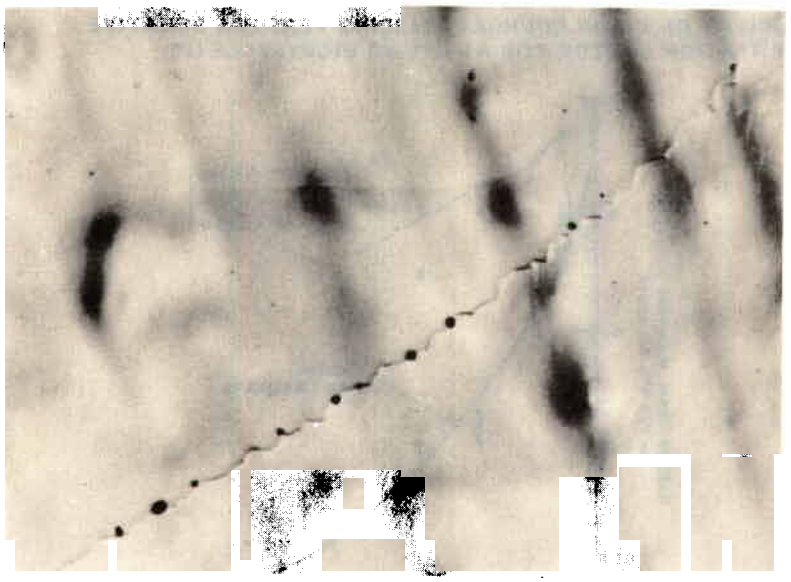

FIGURE 28

EXAMPLE OF SERRATED GRAIN BOUNDARY WITH VOIDS. 100X.
A1-1.9% MG (31)

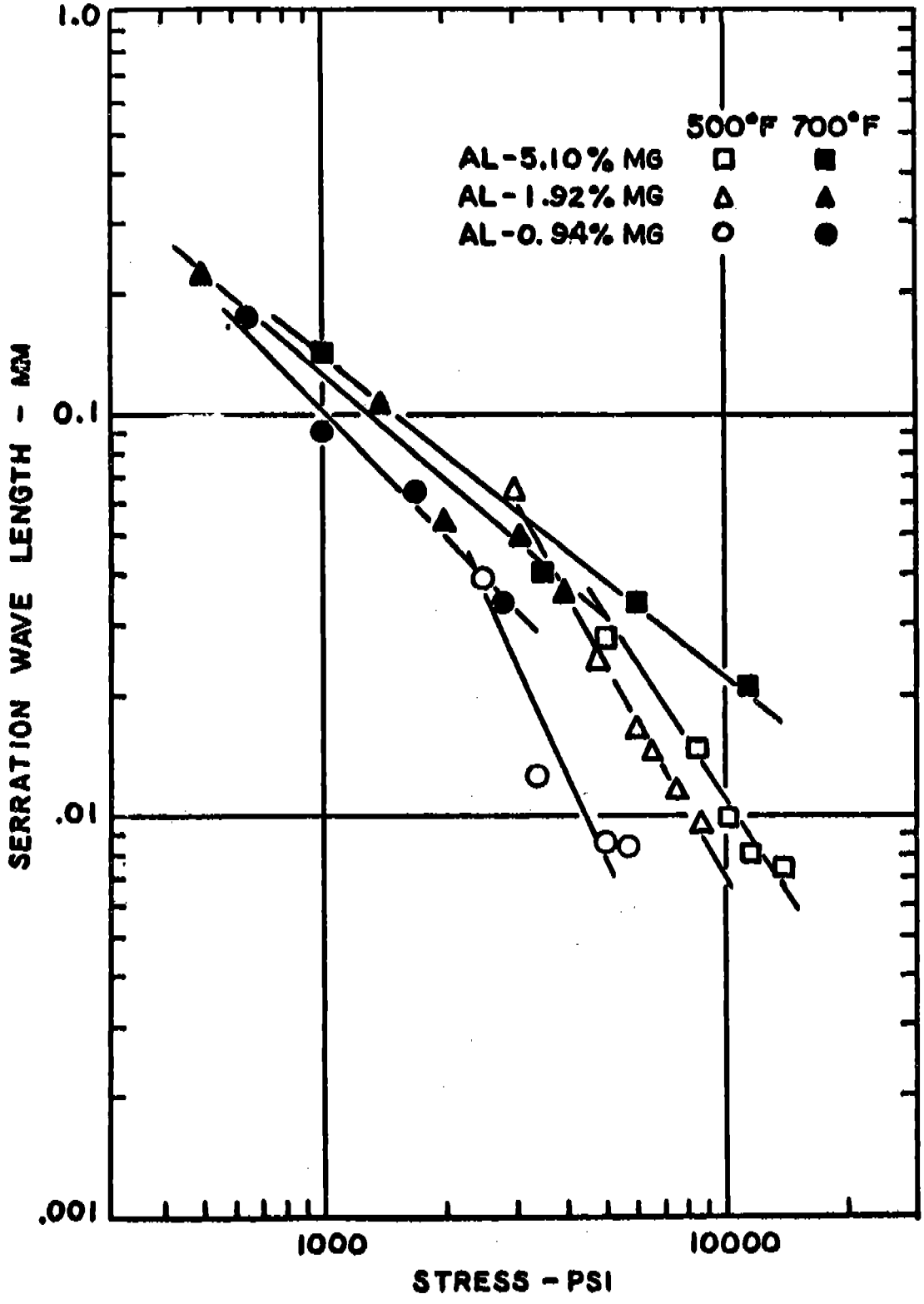

SERRATION WAVE LENGTH VERSUS STRESS FOR RUPTURE CREEP SPECIMENS OF A1 - 1.9% MG (32)

FIGURE 29

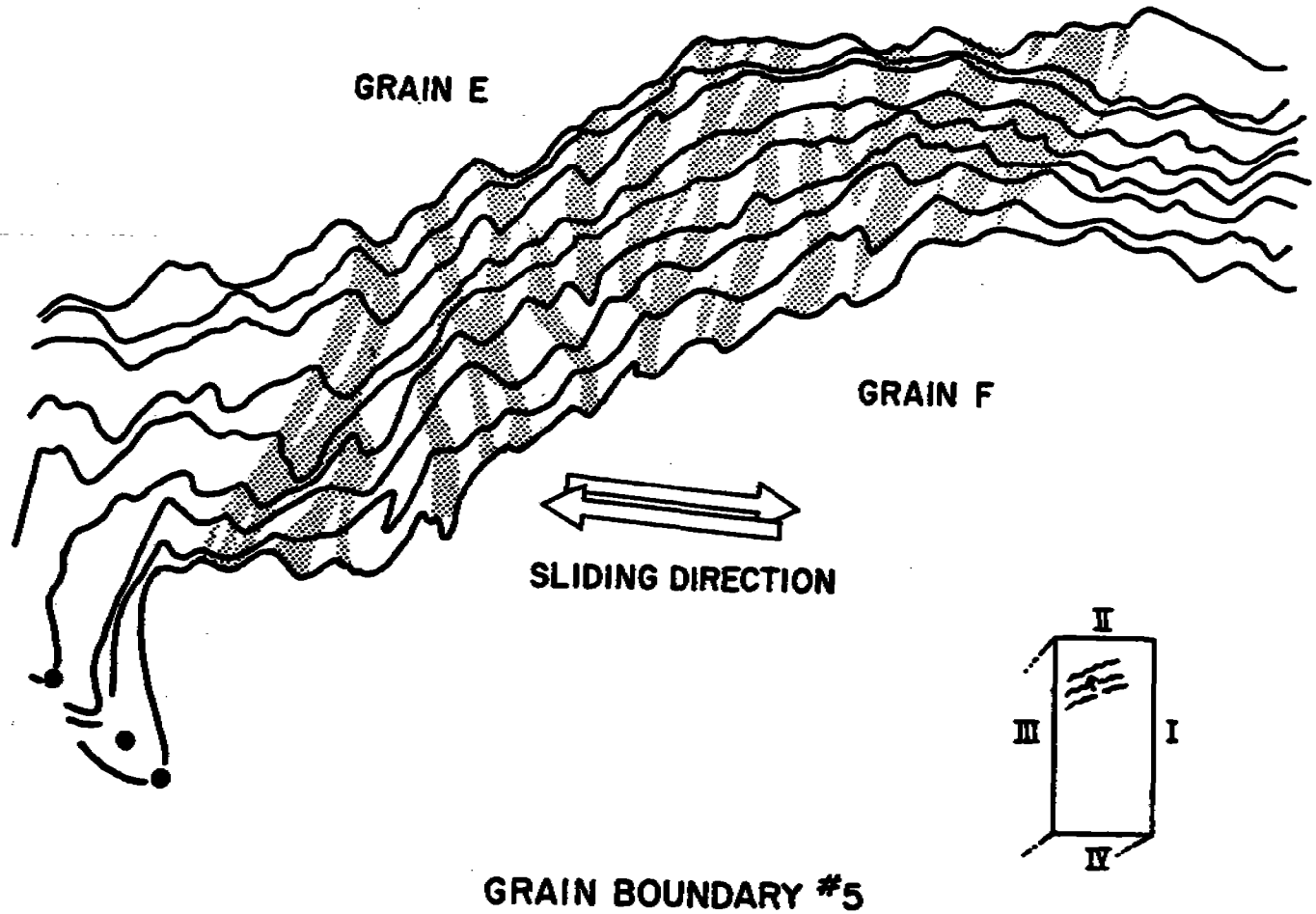

FIGURE 30

TOPOGRAPHY OF GRAIN BOUNDARY 5. A1-1.9% MG POLYCRYSTAL; 500°F, 12-1/2% ELONGATION, ϵ = 1%/HR, 400X (32)

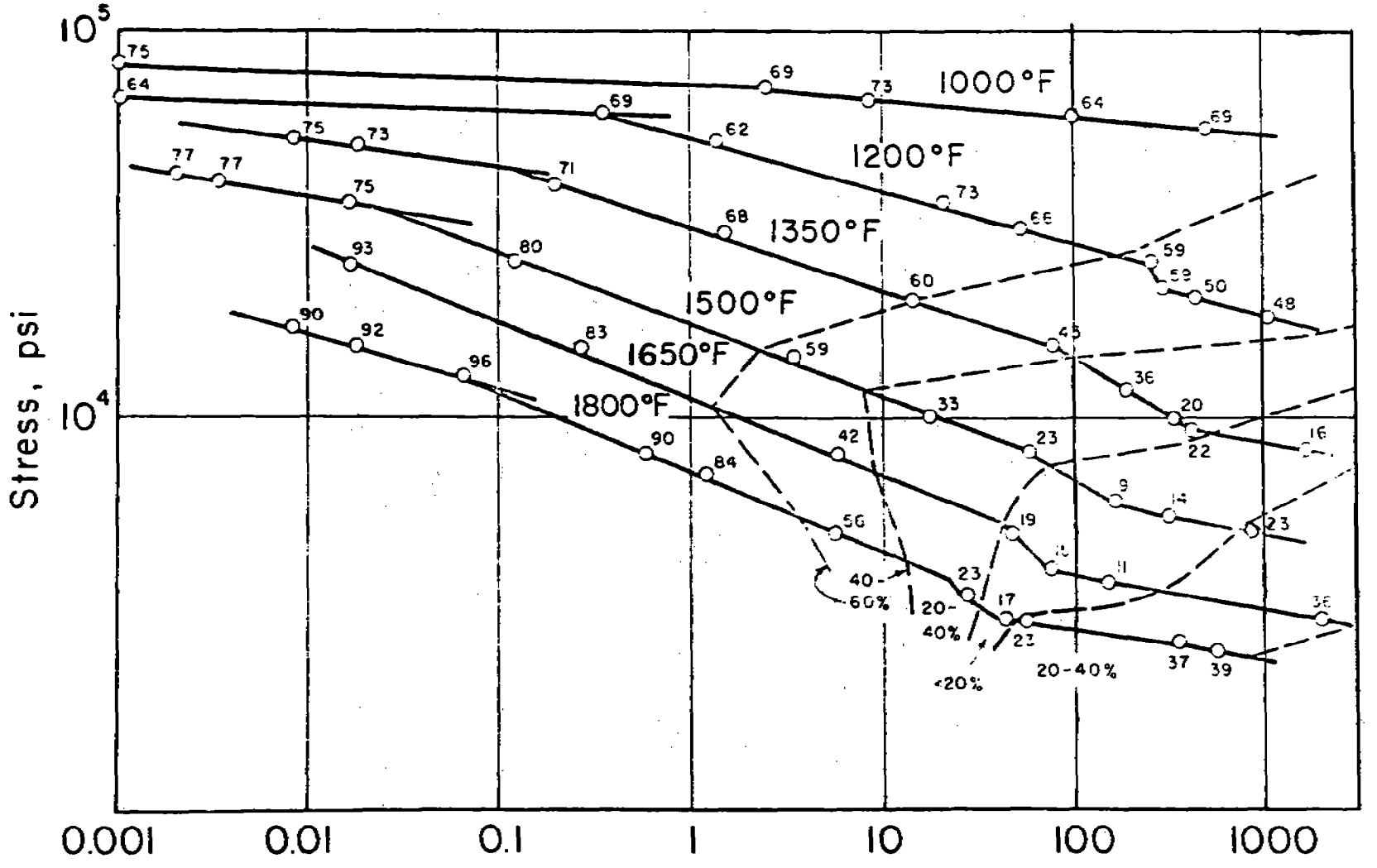

FIGURE 31 LOG STRESS VERSUS LOG RUPTURE LIFE PLOT OF AN 80NI-20CR ALLOY SHOWING DUCTILITY IN TERMS OF REDUCTION OF AREA AS A FUNCTION OF STRESS AND TEMPERATURE (45)

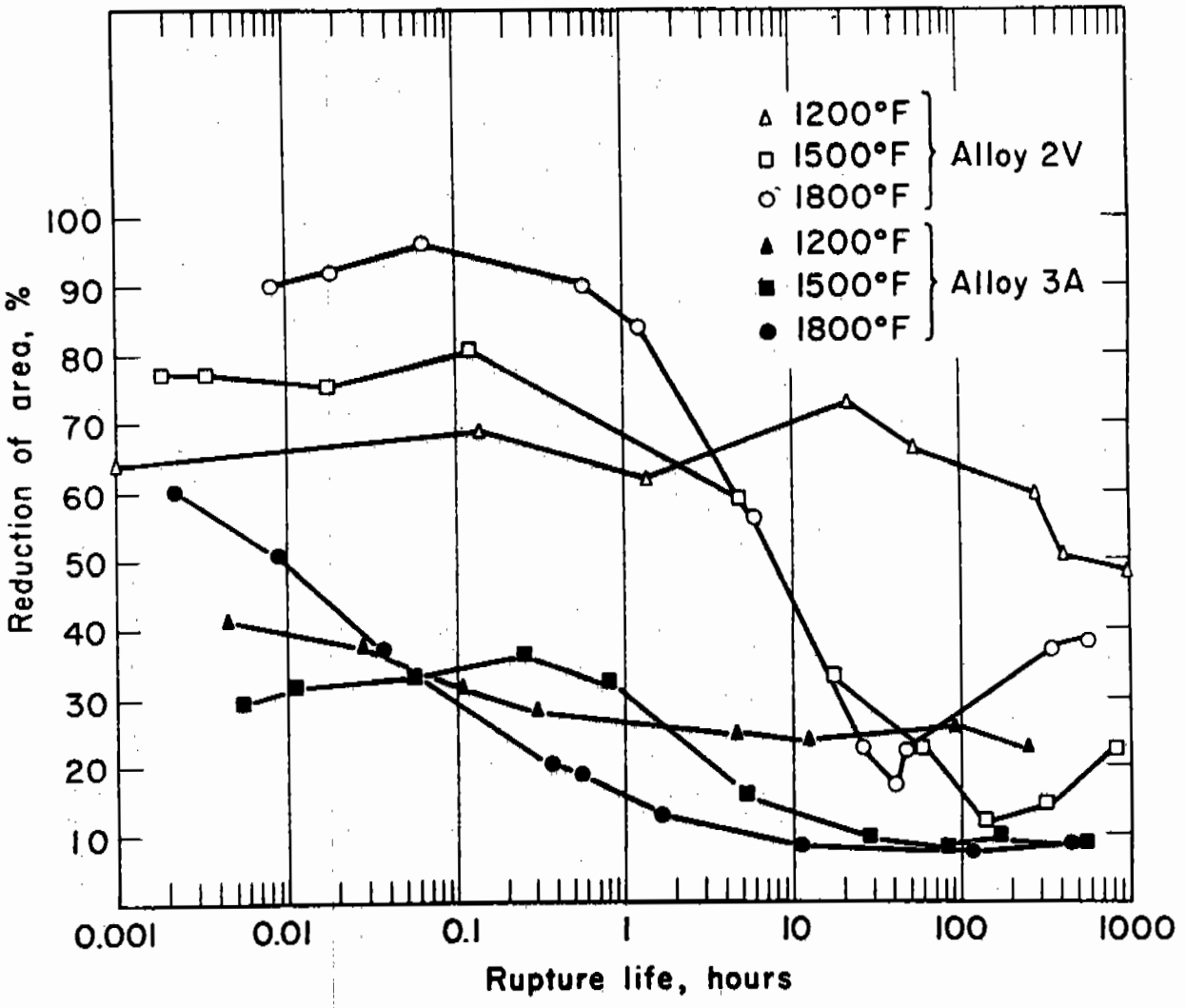

REDUCTION OF AREA AS A FUNCTION OF RUPTURE LIFE FOR 80 NI-20 CR ALLOYS (2V IS VACUUM MELTED) AND (3A IS AIR MELTED), TESTED AT 1200°, 1500°, AND 1800°F (45)

FIGURE 32

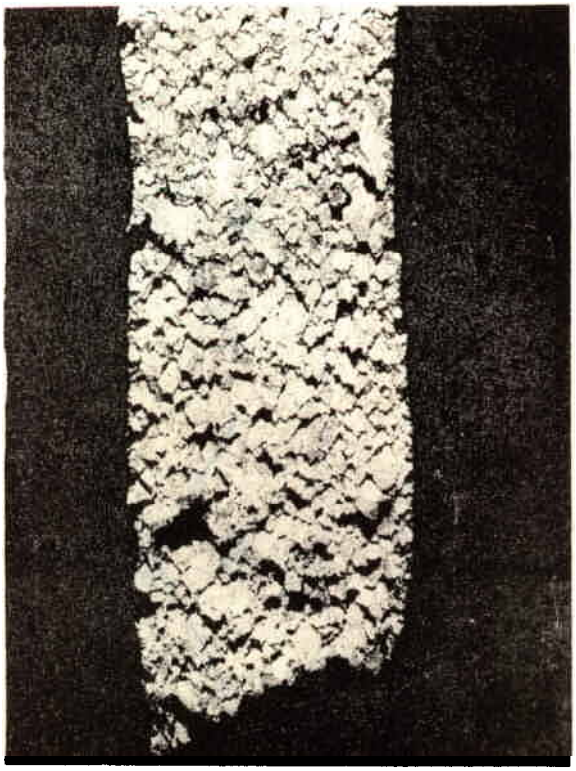

80 NI-20 C R VACUUM MELTED, TESTED AT 1800°F, 2750 PSI. RUPTURE LIFE - 347 HOURS, TOTAL ELONGATION - 85% 10X (45)

FIGURE 33

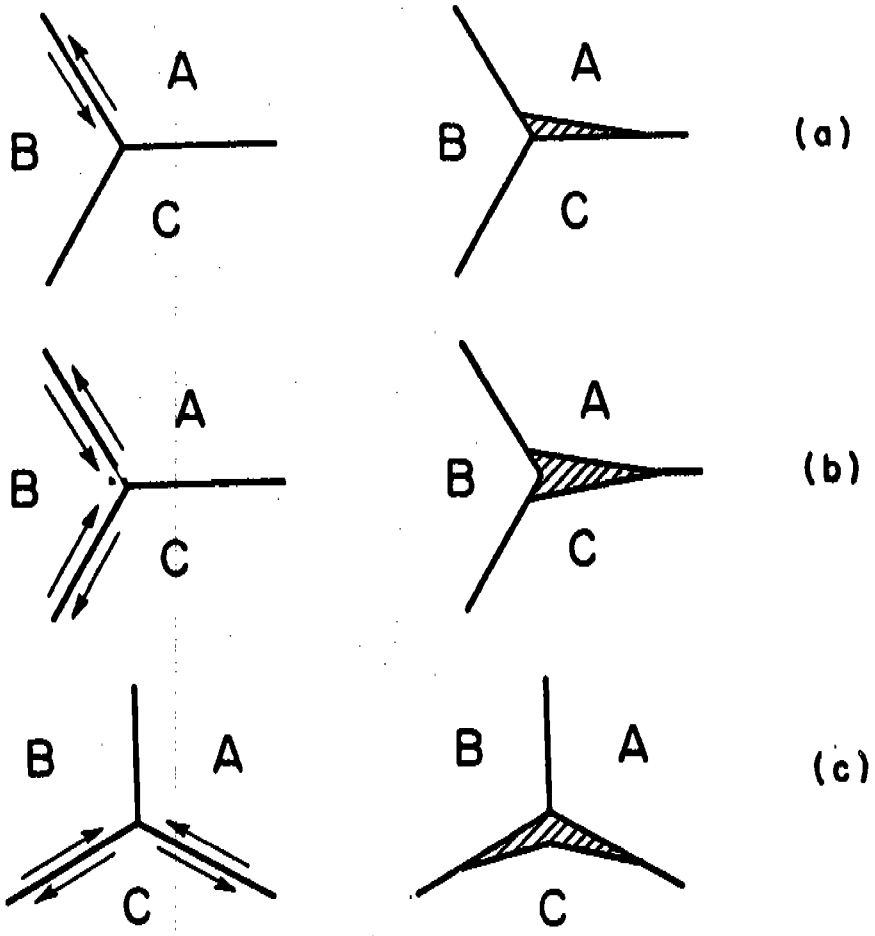

SCHEMATIC VIEWS SHOW THREE OF THE SIMPLE BASIC MEANS OF INITIATING INTERCRYSTALLINE CRACKS DUE DIRECTLY TO GRAIN BOUNDARY SLIDING. THE ARROWS ALONG A GRAIN BOUNDARY INDICATE THAT THIS BOUNDARY UNDERWENT SLIDING (46)

FIGURE 34

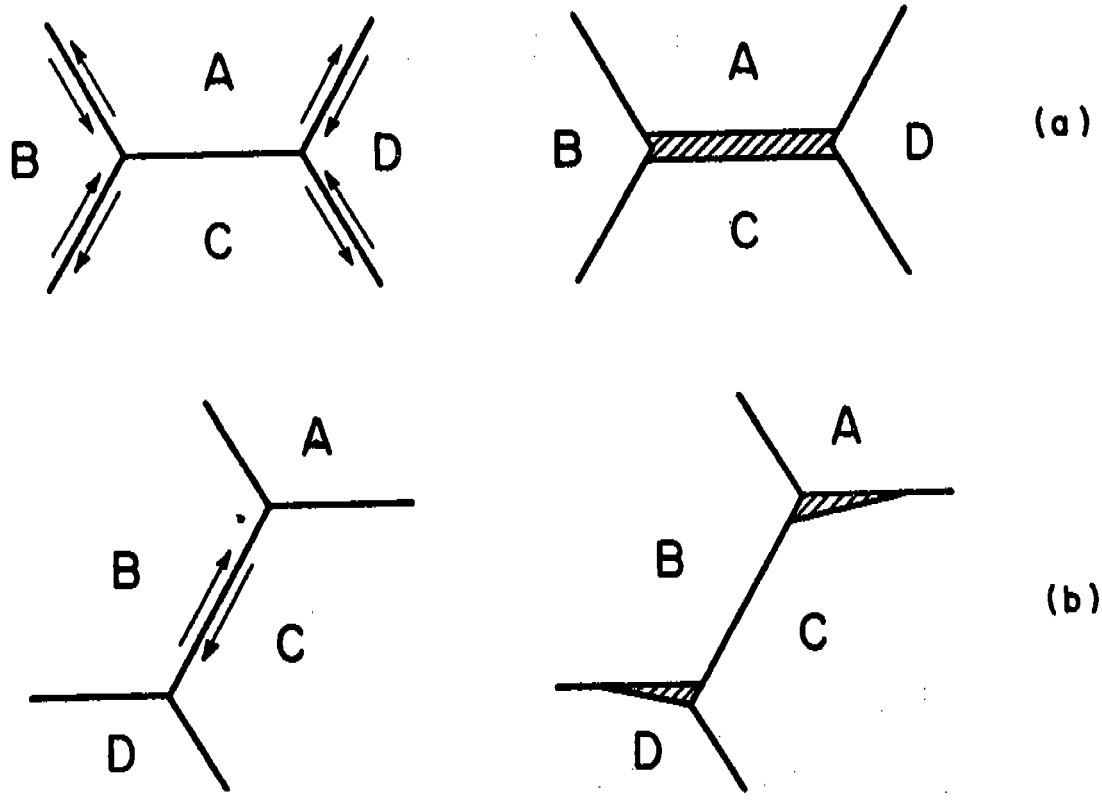

SCHEMATIC VIEWS SHOW THE MORE COMPLEX INITIATION OF INTERCRYSTALLINE CRACKS WHICH ARE BASED ON THE SIMPLE CASES SHOWN IN FIGURE 34 (46)

FIGURE 35

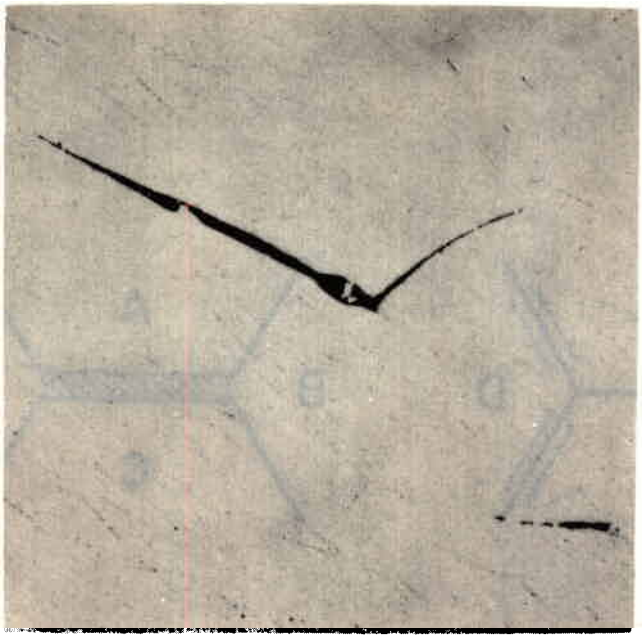

a

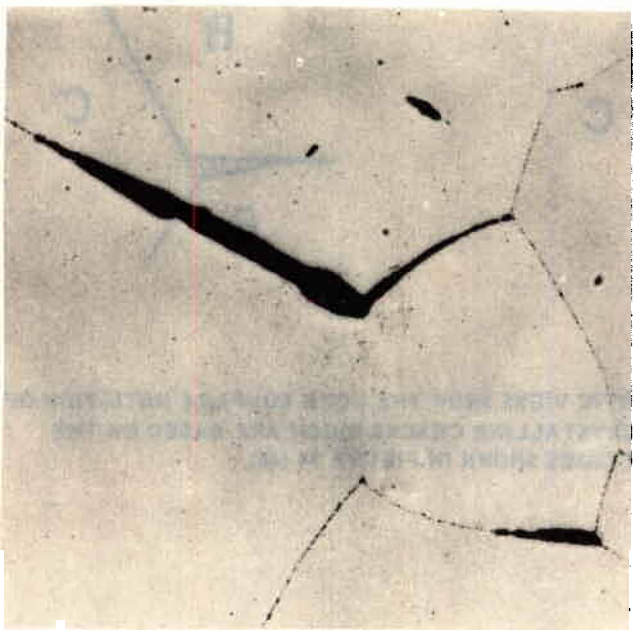

b

CRACKS AND BOIDS IN A1-5.10% MG TESTED AT 500°F, 0.53 HOUR RUPTURE LIFE, 100X. (31)
(a) LUCITE IMPREGNATED AND MECHANICALLY POLISHED
(b) SAME AREA ELECTROLYTICALLY POLISHED

FIGURE 36

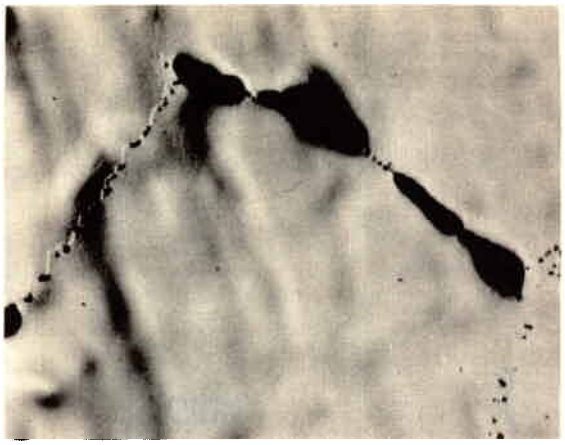

a

b

GRAIN BOUNDARY SERRATIONS AND VOIDS. 100X (31)
(a) 5.10% MG, 500°F, 5000 PSI
(b) 1.9% MG, 700°F, 4000 PSI

FIGURE 37

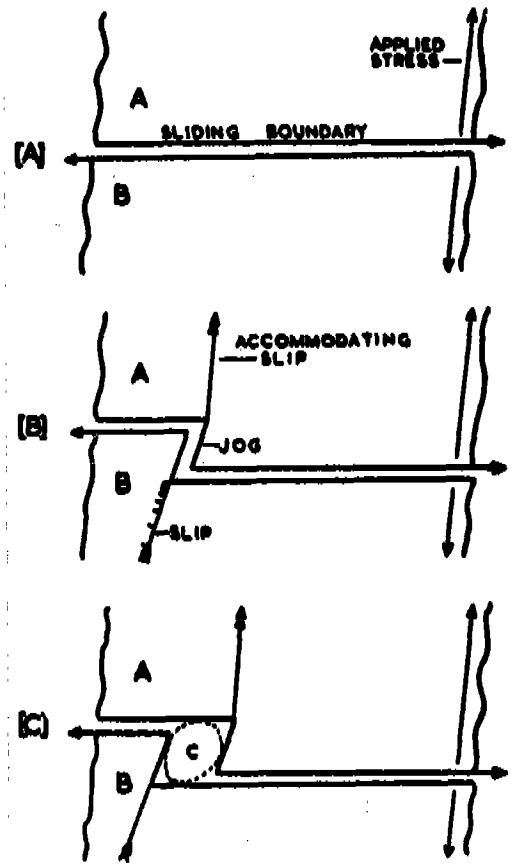

MECHANISM FOR VOID INITIATION ON A JOGGED GRAIN BOUNDARY (53)

FIGURE 38

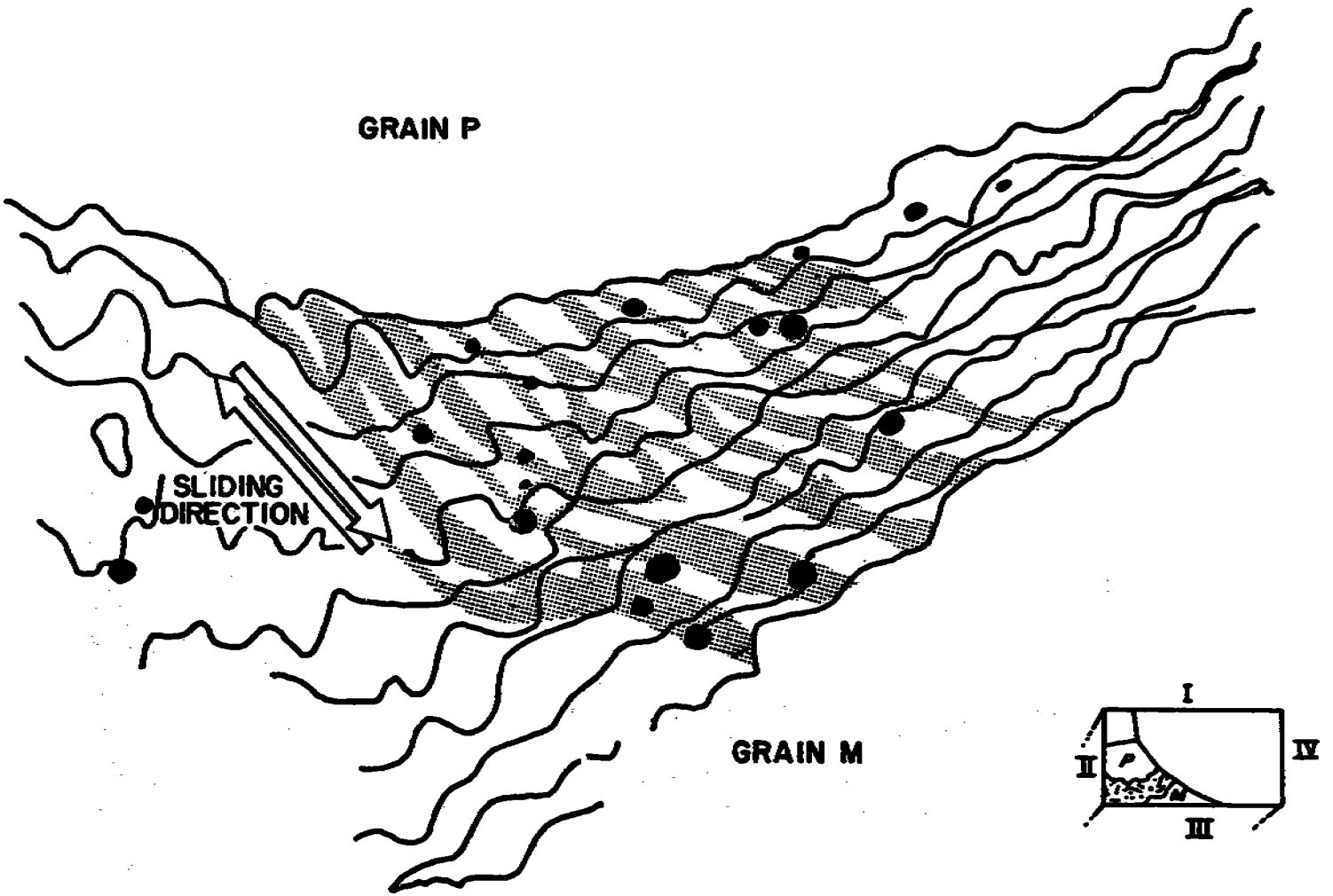

GRAIN BOUNDARY #11

FIGURE 39 TOPOGRAPHY OF GRAIN BOUNDARY 11. Al-1.9% MG POLYCRYSTAL, 500°F, 12-1/2% ELONGATION, ϵ = 1%/HR. 400X (31)

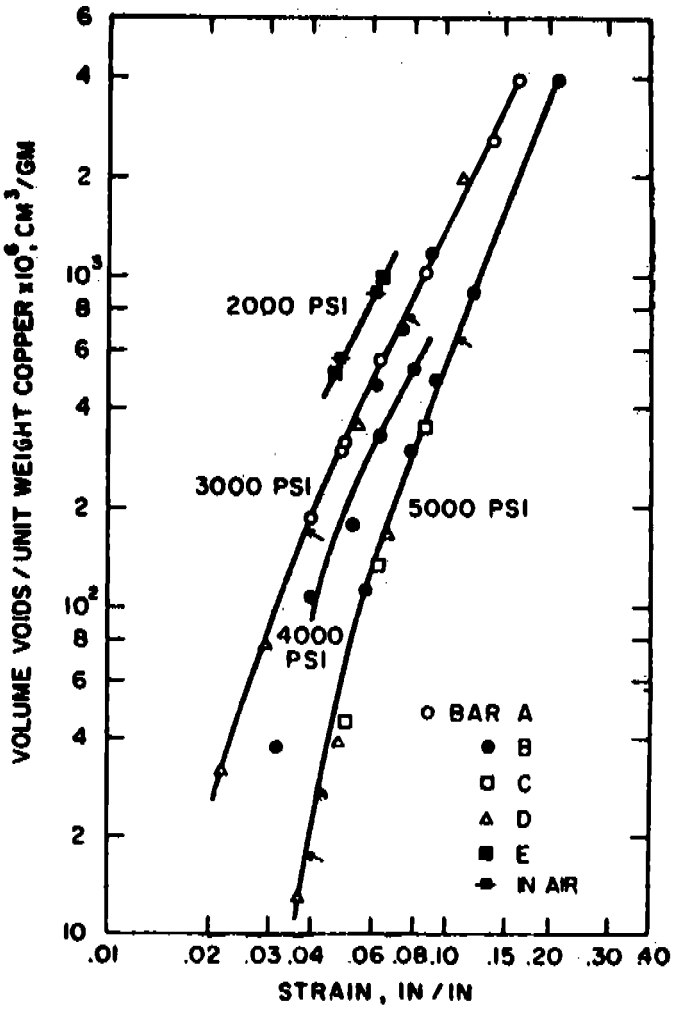

VOID VOLUME AS A FUNCTION OF CREEP STRAIN AT 500°C IN ARGON FOR SPECIMENS FROM FIVE BARS OF OFHC COPPER. AT 200 PSI SPECIMENS WERE TESTED IN ARGON AND IN AIR (61)

FIGURE 40

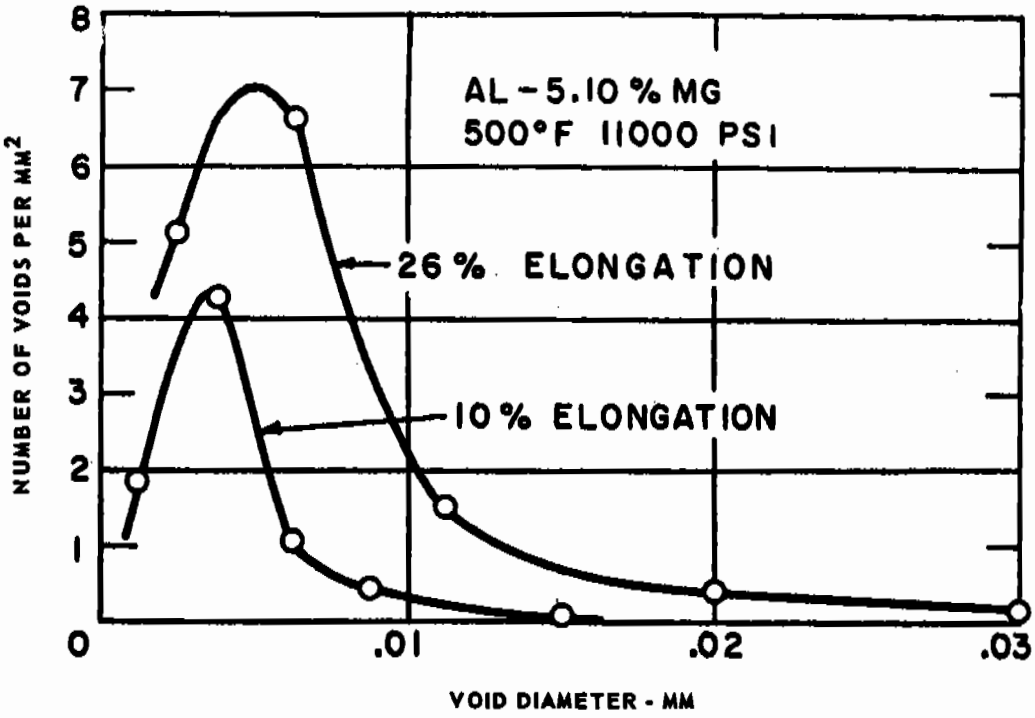

a

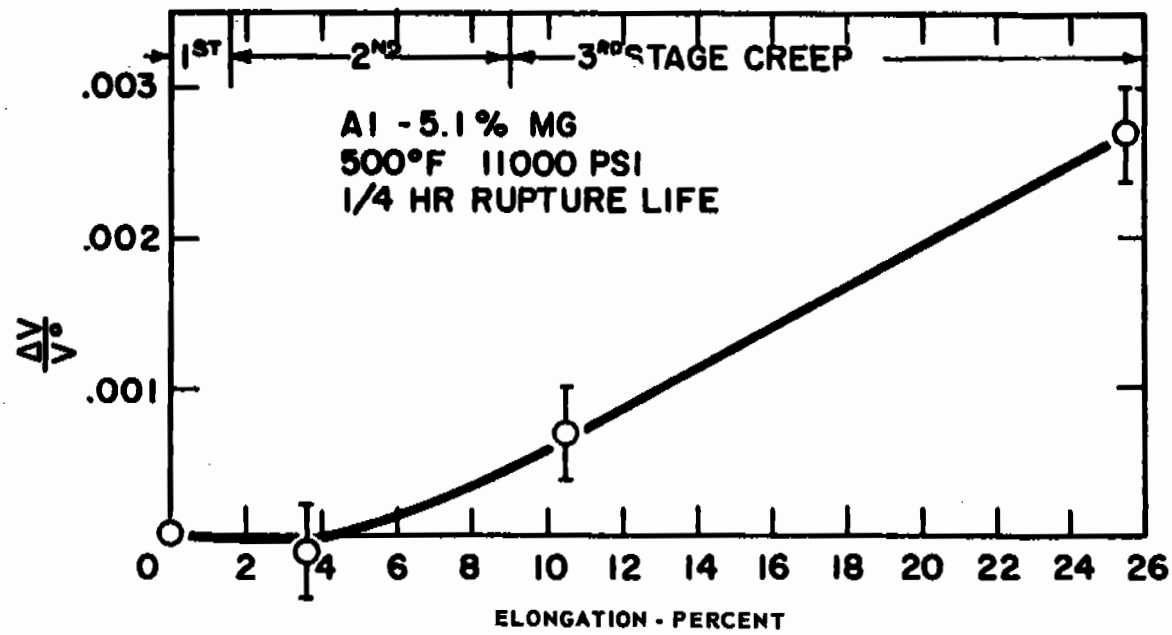

b

INCREASE IN THE NUMBER OF VOIDS AND VOID VOLUME WITH ELONGATION IN CREEP OF A1-5, 1% MG AT 500°F (31)

FIGURE 41

LIST OF ATTENDEES

Abrahamson II, E. P.	Watertown Arsenal, Watertown, Mass.
Alexander, J. A.	Watertown Arsenal, Watertown, Mass.
Avery, D. H.	MIT, Cambridge, Mass.
Backofen, W. A.	MIT, 35-238 MIT, Cambridge 39, Mass.
Barrett, J. C.	Office of Director Defense Research & Eng., Pentagon, Washington, D.C.
Bechtold, J. H.	Westinghouse Electric, Research Labs. Beulan Rd., Pittsburgh 35, Pa.
Bhat, G. K.	Mellon Institute, 4400 Fifth Avenue, Pittsburgh 13, Pa.
Birchenall, C. E.	University of Delaware, Dept. of Chem. Eng. Newark, Del.
Brittain, John	Northwestern University, Evanston, Illinois
Burke, J. J.	OMRO, Watertown Arsenal, Watertown, Mass.
Chang, W. H.	General Electric, Flight Propulsion Lab. Dept. Cincinnati 15, Ohio
Cornthwaite, C. R.	DA, OCO, Washington 25, D.C.
Cuff, Jr., F. B.	Advanced Metals Research, 625 McGrath Highway, Somerville, Mass.
Cupp, C. R.	International Nickel Co., 8 Cartier Circle (P.O. Box 236) Deep River, Ontario
Darcy, G. A., Jr.	OMRO, Watertown Arsenal, Watertown, Mass.
Davis, R. S.	A. D. Little, Inc., 15 Acorn Park, Cambridge 40, Mass.
Decker, R.	International Nickel Co., Bayonne, New Jersey
Dulis, E. J.	Crucible Steel Co. of America, 234 Atwood St., Pittsburgh, Pa.
Elbaum, C.	Brown University, Providence 12, R. I.
Farnsworth, H. E.	Brown University, Providence 12, R. I.
Galbraith, R. A.	Syracuse University, Bldg. 6, Campus, Syracuse 10, N. Y.
Grant, N. J.	MIT, 8-305 MIT, Cambridge, Mass.
Grewal, K. S.	Syracuse University, Bldg. D-6, Collendale, Syracuse 10, N. Y.
Gulbransen, E. A.	Westinghouse Research Labs., Churchill Borough, Pittsburgh, Pa.
Hagel, W. C.	General Electric, Research Lab., Schenectady, N. Y.
Hodi, F. S.	OMRO, Watertown Arsenal, Watertown, Mass.

Huminik, Jr., J.	Value Eng. Co., 2320 Jeff Davis Highway, Alexandria, Va.
Inverarity, B.	Adirondack Museum, Blue Mt. Lake
Jacobson, M. M.	Watertown Arsenal, Watertown, Mass.
Jaffe, R. I.	Battelle Memorial Institute, Columbus 1, Ohio
Jones, A. F.	OMRO, Watertown Arsenal, Watertown, Mass.
Kaufman, L.	Manufacturing Lab., 21 Erie St., Cambridge, Mass.
Keller, D. V.	Syracuse University, 344 Hinds Hall, Campus, Syracuse 10, N. Y.
Kleppinger, D. H.	Frankford Arsenal, Philadelphia, Pa.
Kula, E.	Watertown Arsenal, Watertown, Mass.
Latorre, J. V.	Syracuse University, Bldg. D-6, Collendale, Syracuse 10, N. Y.
Leslie, W. C.	U.S. Steel Corp., E.C. Bain Lab. for Fundamental Research, Research Center, Monroeville, Pa.
Levitt, A. P.	Watertown Arsenal, Watertown, Mass.
Lowrie, R.	Union Carbide Research Institute, P. O. Box 278, Tarryton, N. Y.
Maltz, J.	Bureau of Naval Weapons, Navy Dept., Washington 25, D. C.
Markus, H.	Frankford Arsenal, Tacony & Bridge St., Philadelphia, Pa.
Moran, Jr., J. J.	International Nickel Co., N.Y. 5, N.Y.
Newkirk, J. B.	Cornell University, Olin Hall, Ithaca, N. Y.
Packman, P.	Syracuse University, Bldg. D-6, Collendale, Syracuse 10, N. Y.
Pops, H.	Mellon Institute, 4400 5th Ave., Pittsburgh 13, Pa.
Pschera, K. G.	Marschall Space Flight Center, NASA, Redstone Arsenal, Ala.
Queisser, H. J.	Shockley Transistor, Stanford Industr. Park, Palo Alto, Cal.
Radavich, J. F.	Purdue University, W. Lafayette, Inc.
Reed, N. L.	OMRO, Watertown Arsenal, Watertown, Mass.
Robertson, W. D.	Yale University, New Haven, Conn.
Schaeffer, G. T.	Syracuse University, Bldg. D-6, Collendale, Syracuse 10, N. Y.
Schuetz, A. E.	Sikorsky Aircraft, Div. of United Aircraft Corp. Stratford, Conn.
Sessler, J. G.	Syracuse University, Bldg. D-6, Collendale, Syracuse 10, N.Y.
Shepheard, R. G.	Elec. Boat Co., Div. of General Dynamics, Groton, Conn.
Sullivan, J. F.	Watertown Arsenal Lab., Watertown Arsenal, Mass.
Takimoto, A.	Syracuse University, Bldg. D-6, Collendale, Syracuse 10, N. Y.

Tarpinian, A.	Watertown Arsenal Lab., Watertown Arsenal, Mass.
Warmuth, F. J.	Special Metals, Inc., New Hartford, N.Y.
Warnas, Albert	OMRO, Watertown Arsenal, Watertown, Mass.
Weddeling, F. K.	U.S. Army Research Office (Durham), Box CM, Duke Station, Durham, N. C.
Weigle, R. E.	Watervliet Arsenal, Watervliet, N. Y.
Weinberg, F.	Govt. of Canada, Dept. of Mines and Technical Surveys, 568 Booth St., Ottawa, Canada
Weiss, V.	Syracuse University, Bldg. D-6, Collendale, Syracuse 10, N. Y.
Werner, F. E.	Westinghouse Electric, Research Labs., Beulen Rd., Pittsburgh, Pa.
Wilsdorf, H. G. F.	Franklin Institute, Philadelphia 3, Pa.
Wimmer, A.	Syracuse University, Bldg. D-6, Collendale, Syracuse 10, N. Y.
Wong, A.	Watertown Arsenal, Watertown, Mass.
Wyman, L. L.	National Bureau of Standards, Dept. of Commerce, Washington, D. C.
Widmer, R.	New England Materials Lab., Medford, Mass.
Zwilsky, K	New England Materials Lab., Medford, Mass.
Jaffe, H.	ARDE - Portland, Paramus, N. J.